# Improved Determination of Nitrate Concentrations and Flow Rates in Freshwater using 'Diffusive Gradients in Thin-films'

---

Thesis submitted in partial fulfilment of the requirements for the degree of

Doctor of Philosophy in Earth Sciences at The University of Waikato

**Thomas D W Corbett**

*Supervisors: Louis Schipper, Adam Hartland, William Henderson, and Gerald Rys*

2021

THE UNIVERSITY OF WAIKATO

*Te Whare Wānanga o Waikato*

# Abstract

Nutrient pollution, particularly by nitrate, is a persistent issue in waterways. Numerous mitigation strategies have been developed to address this pollution, such as denitrifying bioreactors. The monitoring, however, of nutrient concentrations and mitigation strategy performance has relied on infrequent grab sampling, or expensive on-site equipment. There are numerous challenges with these techniques, such as sample preservation and transport, operational expense, and the ability to account for temporal changes in concentration. Diffusive Gradients in Thin Films (DGT) are capable of overcoming many of the challenges, however, to date their use has mainly been research based, and they are not widely used by monitoring authorities or communities. Diffusive Gradients in Thin Films are passive accumulative chemical monitoring devices, designed to be analyte specific. This thesis sought, firstly, to establish the efficacy of a modified DGT for the monitoring of nitrate, following deployment in chemically and physically complex denitrifying bioreactors. Secondly, the extension of the DGT methodology through (A) incorporation of colour reagents into the binding layer for rapid in-field analysis of nitrate concentrations, (B) developing a DGT method for the determination of flow rates, and (C) understanding the potential biases inherent in DGT methodology for determining concentrations and loads.

The first study focused on the utility of DGT for the determination of denitrifying bioreactor performance – via deployment in two denitrifying bioreactors. DGT overcame many of the challenges of grab sampling, such as more easily accounting for temporal nitrate concentration variation, and reduced analytical requirements. Diffusive Gradients in Thin Films determined nitrate concentrations and removal rates were in strong agreement with high frequency grab sampling, and data collection via DGT was considerably easier than high frequency grab sampling. The DGT, however, still required in-lab analysis for nitrate.

Development of colourimetric binding layers, as a hydrogel or liquid binding layer, might allow infield determination of analyte concentrations easily and accurately. Here, a chitosan-stabilised AuNP

suspension, as a liquid binding layer was developed and tested for the colourimetric determination of nitrite concentrations (0 to 1000 mg $L^{-1}$) and masses (145 µg) in lab based colour development studies. Nitrate reduction to nitrite was achieved through the development of an Fe(0) impregnated poly-2-acrylamido-2-methyl-1-propanesulfonic acid/acrylamide copolymer hydrogel. The developments lay the foundations for further development of the colourimetric-DGT concept.

A novel bromide selective DGT ($Br^-$-DGT) was developed, using the Purolite Bromide Plus anion exchange resin, which provided stream flow rates when combined with the constant rate tracer-injection method. The $Br^-$-DGT flow method was tested infield at the Mangaharakeke Stream. Flow rates determined by DGT were between -14.7 and 6.5 % of the flow independently monitored weir flow rate. In comparison, grab sample flow rates diverged by 5.5 to 58.9 % from the weir flow rate.

Dynamic and coordinated changes in temperature, flow, and concentration, as potential sources of bias in concentration and load calculations using DGT and grab sampling were modelled. Large, dynamic, and highly correlated to concentration, temperature changes have minimal effect on the calculated DGT concentration. In contrast, as the correlation between concentration and flow increases the bias in calculated DGT loads becomes significant. This means that in systems where there is a high correlation of concentration and flow DGT may not be appropriate for determining loadings.

This thesis had important implications for the use of DGT for determining nutrient concentrations and loads, and stream flow rates – and the monitoring of nutrient pollution. Firstly, it demonstrated that DGT were a useful tool for the determination of nitrate removal rates in the chemically and physically challenging denitrifying bioreactor systems. Secondly, it established the foundation for the in-field determination of nitrate concentrations. Lastly, it extended the DGT methodology for the determination of bromide concentrations and stream flow rates, and provided a greater understanding of the issues when using DGT to determine nitrate loads. This research opened the possibility of DGT for large-scale nutrient monitoring and determination of nutrient mitigation strategy performance, given the quality of DGT data and ease-of-use compared to grab sampling.

# Acknowledgements

The number of people who have helped and supported me through my PhD has been great and varied. The contribution of each individual and group have been a major reason I was able to complete my PhD. The list of those who enabled and supported me is long, but it only seems reasonable to start at the beginning, my family, especially Mum and Dad. Thank you does not really do it justice – but thank you, for everything! An immense thank you to my partner Tiffany, for being so understanding when an 18-month masters turned into a 3-year PhD instead. For the months you spent here working, in between your own studies, supporting me – I love you.

To my supervisors, Louis, Adam, Bill, and Gerald. Working with you has been a privilege. Louis for those fateful words, 'why don't you do a PhD instead of masters?' Thank you for your help and guidance to becoming a scientist. The technical staff at Waikato University have also been incredible. Annie has always been ready to help – 'no' does not seem to be in Annie's vocabulary. My co-authors Hannah and Bryan – it was a pleasure working alongside you.

The WaiBER and WEG research groups for the varied and engaging discussions. Amir and Huma your help with learning to make DGT and with fieldwork were invaluable. Dori and Aaron for your help procuring the many reagents and equipment. Dave, Louis and Adam, for maintaining supportive, and cooperative groups. It was a pleasure to be a part of WaiBER and WEG.

Last but not least, the CSC. Jacob, Ingrid, Yanan, Jessie, Nyssa, and Greer. Your friendships have been an absolute privilege – tea breaks, quizzes, cathartic complaints, adventures, and games, kept me sane. Jacob and Jessie (and Mickey and the little munnas), thank you for taking me into your home.

To everyone, thank you!

# Table of Contents

# List of Abbreviations

| | |
|---|---|
| $A_{eff}$ | Effective exposure window area |
| $A_B$ | Blue effective intensity |
| $A_G$ | Green effective intensity |
| $A_R$ | Red effective intensity |
| $A_x$ | Effective intensity |
| a.u. | Atomic units |
| Ag | Silver |
| (aq) | Aqueous |
| Au | Gold |
| AuNP | Gold Nanoparticles |
| AuNP-chitosan | Chitosan stabilised gold nanoparticles |
| AuNP-rGO | Reduced graphene oxide supported gold nanoparticles |
| $B_b$ | Blank blue intensity |
| $B_g$ | Sample blue intensity |
| $C_b$ | Free concentration of ions in the bulk solution |
| $C_{DGT}$ | Diffusive Gradient in Thin-Films determined concentration |
| $C_f$ | Analyte concentration at membrane filter surface |
| $C_g$ | Analyte concentration at diffusive gel surface |
| $C_{in}$ | Concentration of the injected tracer |
| $C_r$ | Analyte concentration at binding layer |
| C’ | Free concentration of the ion in the resin layer (binding layer) |
| $C_0$ | Concentration of tracer in stream before tracer injection |
| $C_1$ | Concentration of the tracer downstream of injection point |
| Cd | Cadmium |
| Ce | Cerium |
| Cl | Chlorine |
| Cr | Chromium |
| Cu | Copper |
| Cu(II) | Divalent Copper |
| DBL | Diffusive Boundary Layer |
| DET | Diffusive Equilibrium in Thin Films |
| DGT | Diffusive Gradients in Thin Films |
| $D_f$ | Filter membrane diffusion coefficient |

| | |
|---|---|
| $D_{gel}$ | Diffusive gel diffusion coefficient |
| $D_{mdl}$ | Material diffusion layer diffusion coefficient |
| $D_w$ | Water diffusion coefficient |
| DNA | Deoxyribonucleic Acid |
| Fe(III) | Trivalent Iron |
| Fe(III)-p(AMPS/AMA) | Iron (III) impregnated poly-2-acrylamido-2-methyl-1-propanesulfonic acid/acrylamide copolymer hydrogel |
| Fe(0)-p(AMPS/AMA) | Iron (0) impregnated poly-2-acrylamido-2-methyl-1-propanesulfonic acid/acrylamide copolymer hydrogel |
| FTIR | Fourier-transform infrared |
| $G_b$ | Blank green intensity |
| $G_g$ | Sample green intensity |
| GiO | Graphite oxide |
| GO | Graphene oxide |
| J | Flux |
| M | Mass |
| MDL | Material Diffusion Layer |
| N | Nitrogen |
| $NH_3$ | Ammonia |
| Ni | Nickel |
| $NO_2^-$ | Nitrite |
| $NO_3^-$ | Nitrate |
| $NO_x$ | Nitrogen Oxide (x number of oxygens) |
| Pd | Palladium |
| Pt | Platinum |
| $Q_0$ | Flow upstream of tracer injection |
| $Q_1$ | Flow at Diffusive Gradients in Thin-Films deployment |
| $Q_{in}$ | Flow at tracer injection |
| $R_b$ | Blank red intensity |
| $R_g$ | Sample red intensity |
| RGB | Red, green, blue |
| rGO | Reduced graphene oxide |
| RNA | Ribonucleic Acid |

| | |
|---|---|
| SEM | Scanning electron microscopy |
| $t_{dep}$ | Deployment Time |
| V | Vanadium |
| Zn | Zinc |
| ZVI, Fe(0) | Zero Valent Iron |
| $\Delta f$ | Membrane filter thickness |
| $\Delta g$ | Membrane filter and ion-permeable gel membrane thickness |
| g | Ion-permeable gel membrane thickness |
| $\Delta r$ | Ion-exchange resin layer thickness |
| $\delta$, $\delta_{dbl}$ | Diffusive boundary layer thickness |
| $\delta_{mdl}$ | Material diffusion layer thickness |

# List of Figures

# List of Tables

# Chapter 1 - Introduction, Thesis Aim and Outline

## 1.1 Introduction

The focus of this thesis was the application and development of Diffusive Gradients in Thin-Films (DGT). This thesis sought to provide the basis for using DGT to analyse the movement of nitrate through the wider landscape, to identify point and non-point nutrient sources, for the targeting of nutrient mitigation strategies and the determination of their performance. Diffusive Gradients in Thin Films are passive samplers that are capable of providing time-weighted average concentrations over environmentally relevant time scales and integrating short-term analyte concentration variations (Davison, 2016; Huang et al., 2016b). Diffusive Gradients in Thin Films rapidly and strongly adsorb specific analytes, supplied to an ion exchange resin by diffusion from surrounding water (Davison, 2016; Davison & Zhang, 2012; Zhang & Davison, 1995; Zhang et al., 1998; Zhang et al., 2013). Measurement of the accumulated mass enables the calculation of the average concentration for the deployment period (Davison, 2016; Zhang & Davison, 1995; Zhang et al., 1998).

The DGT technique was based on Fick's first law of diffusion (Menegário et al., 2017; Zhang & Davison, 1995). Due to their random thermal motion, chemical species move in the direction of decreasing concentration resulting in a uniform distribution (King et al., 2013). The DGT probes typically consist of three layers, a filter membrane, a hydrogel diffusion layer, and an analyte specific binding layer (Davison, 2016). The filter membrane and diffusion layer constrain transport of ions to the binding layer, above a threshold level of convection, to diffusion (Davison, 2016). The hydrogel diffusion layer must be of sufficient thickness to ensure the flux of ions to the binding layer is independent of the hydrodynamics in solution (Zhang & Davison, 1995).

DGT overcome many of the methodological limitations of other sampling techniques. For example, grab sampling is limited by transport and storage (S˙liwka-Kaszyńska et al., 2003), while the frequency of sampling often means that the temporal change in concentration is missed (Corbett et al., 2019).

Other methods such as colourimetric test kits and automated sampling systems are limited by operational range and expense (Corbett et al., 2019; Maxwell et al., 2018).

DGT research has been extensive since its conception (Davison, 2016), however, to date DGT had not been used to determine the performance of nutrient mitigation strategies (Corbett et al., 2019), nitrate concentration colourimetrically *in situ* (Chapter 4), or stream flow rate (Corbett et al., 2021a). The potential biases in DGT concentrations and loads, due to dynamic and correlated changes in temperature, concentration and flow, had also not been explored (Corbett et al., 2021b). Diffusive Gradients in Thin Films research has focused on the development of binding layers for the determination of trace metals and phosphate (Price et al., 2013; Søndergaard et al., 2014; Veeken & Leeuwen, 2010; Zhang & Davison, 1995; Zhang et al., 1998), until recently nitrate specific DGT had not been developed (Cai et al., 2017; Huang et al., 2016a; Huang et al., 2016b). It has widely been recognised that there is a need to grow the application of DGT (Li et al., 2003; Liu et al., 2016) , and develop new methods to continue to improve the efficacy of DGT. For example, o-DGT and liquid binding layer DGT are some of the new developments in binding layer development and expansion of the DGT methodology (Chen et al., 2012; Chen et al., 2013; Li et al., 2003; Liu et al., 2016).

### *1.1.1 Utility of DGT for Measuring Nitrate in Freshwaters and Mitigation Strategies*

The increase in environmental nutrient concentrations has necessitated the application of effective mitigation strategies (Christianson & Schipper, 2016; Schipper et al., 2010). Determination of the performance of mitigation strategies has relied on infrequent grab-sampling and expensive on-site continuous samplers. The use of passive samplers such as DGT, to determine the performance of nutrient mitigation strategies not only represents a novel extension of the DGT technique, but due to their affordability, ease-of-use, and ability to capture temporal changes in concentration improves the current capabilities for determining mitigation performance (Corbett et al., 2019).

The importance of nutrient mitigation strategies, particularly for nitrate, is driven in large part by the increase in anthropogenic sources from agricultural and urban systems. Nitrate-N can affect each

system as it moves from the terrestrial sources to the ocean (Galloway et al., 2003). The overabundance of nutrients can lead to eutrophication and hypoxia (Allaby, 2010; Rabalais et al., 2002) – which not only have ecological consequences, but impacts social, cultural, recreational, and economic values of the system (Smith et al., 1999). Tools for the accurate, affordable, and easy measurement of nitrate concentrations in aquatic systems are necessary to meet the monitoring requirements, to redress the effects of nutrient pollution. Diffusive Gradients in Thin Films provide one potential solution to this challenge, but there are several lines of research needed to increase their utility so as to improve uptake by researchers and the wider stakeholder community.

### *1.1.2 Colourimetric DGT*

Presently, the determination of DGT concentrations requires the laboratory measurement of the bound mass. Incorporation of colourimetric techniques into DGT could overcome this limitation, but is yet to be explored.

Standard colourimetric methods for nitrate determination often involve an initial reduction of nitrate to nitrite, utilising zinc, cadmium, and vanadium as electron sources (Morita & Nakamura, 2008; Nydahl, 1976; Schnetger & Lehners, 2014). Zero-valent iron nanoparticles, produced and held within a co-polymeric network (poly(2-acrylamido-2-methylpropanesulfonic acid/acrylamide)), is a stable, less toxic alternative reactor bed for the reduction of nitrate (Muradova et al., 2016; Sahiner et al., 2010; Thoniyot et al., 2015) (Jamshidi & Rabiee, 2014; Su & Okay, 2018).

Colour reactions for the determination of nitrite are commonly based on the Greiss reaction, a two-step reaction involving azo-diazo coupling to produce quantitative colour changes (Knyazev et al., 2002; Tarafder & Rathore, 1988). These reactions are likely unsuitable for the incorporation into DGT, due to the two-step reaction and requirement for close control of pH (Knyazev et al., 2002; Tarafder & Rathore, 1988), and the difficulty of stopping reagents from diffusing out of the binding layer. Chitosan stabilised gold nanoparticle suspensions (Amanulla et al., 2017), as liquid binding layers, might overcome these limitations. Gold nanoparticles have numerous properties which make them

more suitable for incorporation into DGT, over other metallic nanoparticles and colour reactions, such as, their distance dependant optical properties (Lee et al., 2008), well-defined colour change (Gunupuru et al., 2014), and high stability (Zhang et al., 2014). Infield determination of nitrate concentrations would remove the requirement for laboratory analysis, which is a significant barrier to the uptake of DGT for routine monitoring by individuals and communities.

### *1.1.3 DGT for Flow Rate Measurements*

Determination of nitrate concentration alone, however, may not provide the whole picture, in regards to the potential environmental and ecological effects because ecosystem responses can depend on load (Pinckney et al., 2001). Calculation of loading requires the determination of flow rate, expressed as tons of analyte per year, and is calculated by multiplying concentration by discharge or flowrate (Pinckney et al., 2001). The measurement accuracy and frequency of the concentration and flow variables determines the accuracy of the calculated loading rate (Pinckney et al., 2001). While there are numerous methods for the determination of flow, such as time volume, formed constructions (weirs), remote sensing, velocity area, and tracer injection, each of these present challenges such as accuracy and alteration to stream structures, for example (Bonacci et al., 2016; Dobriyal et al., 2017; Moore, 2005).

The combination of a bromide-selective DGT with a constant-rate bromide injection might enable the calculation of time-weighted average flow rate (Corbett et al., 2021a). If successful this new approach might allow determination of loadings, when combined with DGT deployments for nutrient or other contaminants (Corbett et al., 2021a) – where the technique for concentration and flow measurement are the same, potentially simplifying monitoring requirements whilst providing accurate concentrations, flows and loads. This requires an understanding of the challenges for using DGT to determine concentration and load.

### *1.1.4 Potential Sources of Bias in DGT Concentration and Load Calculations*

Understanding the sources of potential bias in DGT determined concentrations and loads, is critical for the large-scale use of DGT for environmental monitoring (Corbett et al., 2021b). The analyte accumulation on DGT is theoretically independent of flow, if the diffusive boundary layer is accounted for, and capable of accounting for changes in temperature (Davison, 2016). The extent to which the DGT concentration and load diverge from the actual solution concentration and load, as concentration and temperature or flow co-vary had not been investigated (Corbett et al., 2021b). The calculation of the DGT concentration requires careful measurement of temperature, because temperature determines that rate at which the target analyte diffuses through the diffusive boundary layer and material diffusion layer (Davison, 2016; Davison & Zhang, 2012). The accuracy and frequency with which concentration (and flow) are made determines the accuracy of the calculated loading rate (Pinckney et al., 2001)

## 1.2 Thesis Aims

This research project can be broken down into two components. Firstly, establishment of the utility and efficacy of Diffusive Gradients in Thin-Films for the measurement of nitrate in freshwaters. Denitrifying bioreactors were selected as a test case because they are chemically and physically challenging systems, with high concentrations of other ions and poor mixing mechanisms due to the restriction of flow by the substrate. Secondly, the extension of the DGT methodology by:

1. Incorporation of colour change mechanisms such that in-field determination of nitrate concentrations may be made;
2. Development of a bromide-specific DGT method for measuring flow, when combined with the trace-dilution method; and,
3. Understanding the potential sources of bias in DGT concentration and load calculations due to dynamic and coordinated changes in temperature, flow, and concentration.

These aims (Figure 1.1) are further developed and addressed in the following chapters.

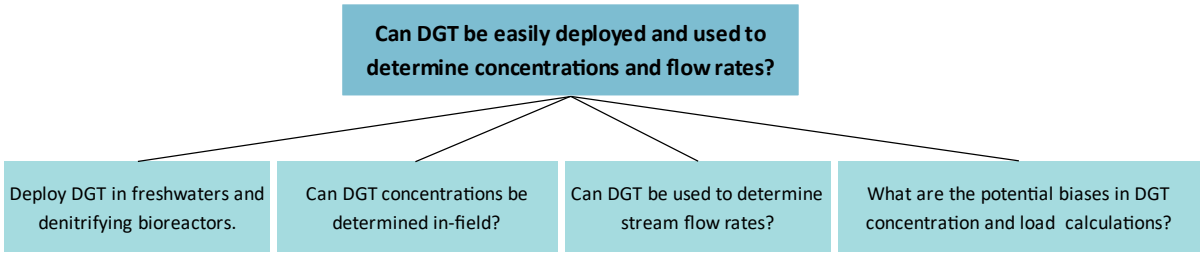


Figure 1.1: PhD Schematic.

## 1.3 Outline

In the subsequent chapter (Chapter 2), a focused literature review of nutrient mitigation strategies (for example, bioreactors), Diffusive Gradients in Thin-Films, polymeric hydrogels, colourimetric nitrate determination, and flow-rate measurement is presented. It is intended for the review to contextualise the research project into the wider literature landscape, address the shortcomings in present nutrient measurement techniques, and provide the theoretical basis for the research. Subsequent chapters (Chapters 3 to 6) detail the research conducted, each addressing a different component of the developments made to the DGT technique. Each of these sections is presented as an independent manuscript, comprised of an abstract, introduction, methodology, results, and discussion. Chapter 7 summarises the research project, the individual results and conclusions, how they address the previously identified shortcomings in our collective understanding of DGT, potential implications of the research, and finally it will provide recommendations for future work.

## References


ALLABY, M. (2010). Eutrophication. In *A Dictionary of Ecology* (4 ed., pp. 141): Oxford University Press.

AMANULLA, B., PALANISAMY, S., CHEN, S.-M., CHIU, T.-W., VELUSAMY, V., HALL, J. M., CHEN, T.-W., & RAMARAJ, S. K. (2017). Selective Colorimetric Detection of Nitrite in Water using Chitosan Stabilized Gold Nanoparticles Decorated Reduced Graphene oxide. *Scientific Reports, 7*(1), 14182. doi:10.1038/s41598-017-14584-6

BONACCI, O., BUZJAK, N., & ROJE-BONACCI, T. (2016). Changes in hydrological regime caused by human intervention in karst: the case of the Rumin Springs. *Hydrological Sciences Journal, 61*(13), 2387-2398. doi:10.1080/02626667.2015.1111518

CAI, C., WILLIAMS, P. N., LI, H., DAVISON, W., WEI, T.-J., LUO, J., ZHU, Y.-G., & ZHANG, H. (2017). Development and Application of the Diffusive Gradients in Thin Films Technique for the Measurement of Nitrate in Soils. *Analytical Chemistry, 89*(2), 1178-1184. doi:10.1021/acs.analchem.6b03609

CHEN, C.-E., ZHANG, H., & JONES, K. C. (2012). A novel passive water sampler for in situ sampling of antibiotics. *Journal of Environmental Monitoring, 14*(6), 1523-1530. doi:10.1039/C2EM30091E

CHEN, C.-E., ZHANG, H., YING, G.-G., & JONES, K. C. (2013). Evidence and Recommendations to Support the Use of a Novel Passive Water Sampler to Quantify Antibiotics in Wastewaters. *Environmental Science & Technology, 47*(23), 13587-13593. doi:10.1021/es402662g

CHRISTIANSON, L. E., & SCHIPPER, L. A. (2016). Moving Denitrifying Bioreactors beyond Proof of Concept: Introduction to the Special Section. *Journal of Environmental Quality, 45*(3), 757-761. doi:10.2134/jeq2016.01.0013

CORBETT, T. D. W., DOUGHERTY, H., MAXWELL, B., HARTLAND, A., HENDERSON, W., RYS, G. J., & SCHIPPER, L. A. (2019). Utility of 'Diffusive Gradients in Thin-Films' for the measurement of nitrate removal performance of denitrifying bioreactors. *Science of The Total Environment*, 135267. doi:https://doi.org/10.1016/j.scitotenv.2019.135267

CORBETT, T. D. W., HARTLAND, A., HENDERSON, W., RYS, G. J., & SCHIPPER, L. A. (2021a). Development of Bromide-Selective Diffusive Gradients in Thin-Films for the Measurement of Average Flow Rate of Streams. *Science of The Total Environment*.

CORBETT, T. D. W., HARTLAND, A., HENDERSON, W., RYS, G. J., & SCHIPPER, L. A. (2021b). The Temperature and Flow Dependence of Nitrate Concentration and Load Estimates based on Diffusive Gradients in Thin-Films. *Journal of Environmental Quality (Under Review)*.

DAVISON, W. (2016). *Diffusive Gradients in Thin-Films for Environmental Measurements*. Cambridge, UNITED KINGDOM: Cambridge University Press.

DAVISON, W., & ZHANG, H. (2012). Progress in understanding the use of diffusive gradients in thin films (DGT) – back to basics. *Environmental Chemistry, 9*(1), 1-13. doi:https://doi.org/10.1071/EN11084

DOBRIYAL, P., BADOLA, R., TUBOI, C., & HUSSAIN, S. A. (2017). A review of methods for monitoring streamflow for sustainable water resource management. *Applied Water Science, 7*(6), 2617-2628. doi:10.1007/s13201-016-0488-y

GALLOWAY, J. N., ABER, J. D., ERISMAN, J. W., SEITZINGER, S. P., HOWARTH, R. W., COWLING, E. B., & COSBY, B. J. (2003). The Nitrogen Cascade. *BioScience, 53*(4), 341-356. doi:10.1641/0006-3568(2003)053[0341:TNC]2.0.CO;2

GUNUPURU, R., MAITY, D., BHADU, G. R., CHAKRABORTY, A., SRIVASTAVA, D. N., & PAUL, P. (2014). Colorimetric detection of $Cu^{2+}$ and $Pb^{2+}$ ions using calix[4]arene functionalized gold nanoparticles. *Journal of Chemical Sciences, 126*(3), 627-635. doi:10.1007/s12039-014-0600-5

HUANG, J., BENNETT, W., TEASDALE, P. R., GARDINER, S., & WELSH, D. (2016a). Development and evaluation of the diffusive gradients in thin films technique for measuring nitrate in freshwaters. *Analytica Chimica Acta, 923*, 74-81. doi:10.1016/j.aca.2016.04.006

HUANG, J., BENNETT, W. W., WELSH, D. T., & TEASDALE, P. R. (2016b). Determining time-weighted average concentrations of nitrate and ammonium in freshwaters using DGT with ion exchange membrane-based binding layers. *Environmental Science: Processes & Impacts, 18*(12), 1530-1539. doi:10.1039/c6em00260a

JAMSHIDI, H., & RABIEE, A. (2014). Synthesis and Characterization of Acrylamide-Based Anionic Copolymer and Investigation of Solution Properties. *Advances in Materials Science and Engineering, 2014*. doi:10.1155/2014/728675

KING, R. C., MULLIGAN, P. K., & STANSFIELD, W. D. (2013). Diffusion. In *A Dictionary of Genetics* (8 ed., pp. 122). Oxford: Oxford University Press.

KNYAZEV, D. A., IVANOV, V. M., SAMOKHVALOV, S. G., ZOLOTOV, Y. A., MARKINA, V. M., & KNYAZEV, V. D. (2002). Blister Drop-Pellet Tests for Nitrates and Nitrites. *Journal of Analytical Chemistry, 57*(1), 75-82.

LEE, J. H., WANG, Z., LIU, J., & LU, Y. (2008). Highly sensitive and selective colorimetric sensors for uranyl (UO2(2+)): development and comparison of labeled and label-free DNAzyme-gold nanoparticle systems. *J Am Chem Soc, 130*(43), 14217-14226. doi:10.1021/ja803607z

LI, W., TEASDALE, P. R., ZHANG, S., JOHN, R., & ZHAO, H. (2003). Application of a Poly(4-styrenesulfonate) Liquid Binding Layer for Measurement of $Cu^{2+}$ and $Cd^{2+}$ with the Diffusive Gradients in Thin-Films Technique. *Analytical Chemistry, 75*(11), 2578-2583. doi:10.1021/ac020658q

LIU, S., QIN, N., SONG, J., ZHANG, Y., CAI, W., ZHANG, H., WANG, G., & ZHAO, H. (2016). A nanoparticulate liquid binding phase based DGT device for aquatic arsenic measurement. *Talanta, 160*, 225-232. doi:https://doi.org/10.1016/j.talanta.2016.06.064

MAXWELL, B. M., BIRGAND, F., SMITH, B., & AVENI-DEFORGE, K. (2018). A small-volume multiplexed pumping system for automated, high-frequency water chemistry measurements in volume-limited applications. *Hydrology and Earth System Sciences, 22*(11), 5615-5628. doi:10.5194/hess-22-5615-2018

MENEGÁRIO, A. A., YABUKI, L. N. M., LUKO, K. S., WILLIAMS, P. N., & BLACKBURN, D. M. (2017). Use of diffusive gradient in thin films for in situ measurements: A review on the progress in

chemical fractionation, speciation and bioavailability of metals in waters. *Analytica Chimica Acta, 983*, 54-66. doi:https://doi.org/10.1016/j.aca.2017.06.041

MOORE, R. D. (2005). Slug Injection Using Salt in Solution. *Streamline Watershed Management Bulletin, 8*(2), 1-6.

MORITA, E., & NAKAMURA, E. (2008). Reduction of Nitrate to Nitrite by Using Zinc Powder for Determination of Total Nitrogen in Sea Water. *Bunseki Kagaku, 57*(10), 777-781. doi:10.2116/bunsekikagaku.57.777

MURADOVA, G. G., GADJIEVA, S. R., DI PALMA, L., & VILARDI, G. (2016). Nitrates Removal by Bimetallic Nanoparticles in Water. *Chemical Engineering Transactions, 47*, 205-210. doi:10.3303/CET1647035

NYDAHL, F. (1976). On the optimum conditions for the reduction of nitrate to nitrite by cadmium. *Talanta, 23*(5), 349-357. doi:https://doi.org/10.1016/0039-9140(76)80047-1

PINCKNEY, J. L., PAERL, H. W., TESTER, P., & RICHARDSON, T. L. (2001). The role of nutrient loading and eutrophication in estuarine ecology. *Environmental health perspectives, 109 Suppl 5*(Suppl 5), 699-706. doi:10.1289/ehp.01109s5699

PRICE, H. L., TEASDALE, P. R., & JOLLEY, D. F. (2013). An evaluation of ferrihydrite- and Metsorb™-DGT techniques for measuring oxyanion species (As, Se, V, P): Effective capacity, competition and diffusion coefficients. *Analytica Chimica Acta, 803*, 56-65. doi:https://doi.org/10.1016/j.aca.2013.07.001

RABALAIS, N. N., TURNER, R. E., & SCAVIA, D. (2002). Beyond Science into Policy: Gulf of Mexico Hypoxia and the Mississippi RiverNutrient policy development for the Mississippi River watershed reflects the accumulated scientific evidence that the increase in nitrogen loading is the primary factor in the worsening of hypoxia in the northern Gulf of Mexico. *BioScience, 52*(2), 129-142. doi:10.1641/0006-3568(2002)052[0129:BSIPGO]2.0.CO;2

S˙LIWKA-KASZYŃSKA, M., KOT-WASIK, A., & NAMIEŚNIK, J. (2003). Preservation and Storage of Water Samples. *Critical Reviews in Environmental Science and Technology, 33*(1), 31-44. doi:10.1080/10643380390814442

SAHINER, N., OZAY, H., OZAY, O., & AKTAS, N. (2010). A soft hydrogel reactor for cobalt nanoparticle preparation and use in the reduction of nitrophenols. *Applied Catalysis B: Environmental, 101*(1), 137-143. doi:https://doi.org/10.1016/j.apcatb.2010.09.022

SCHIPPER, L., ROBERTSON, W., GOLD, A., JAYNES, D. B., & C. CAMERON, S. (2010). Denitrifying Bioreactors — An Approach for Reducing Nitrate Loads to Receiving Waters. *Ecological Engineering, 36*, 1532-1543. doi:10.1016/j.ecoleng.2010.04.008

SCHNETGER, B., & LEHNERS, C. (2014). Determination of nitrate plus nitrite in small volume marine water samples using vanadium(III) chloride as a reduction agent. *Marine Chemistry, 160*, 91-98. doi:https://doi.org/10.1016/j.marchem.2014.01.010

SMITH, V. H., TILMAN, G. D., & NEKOLA, J. C. (1999). Eutrophication: impacts of excess nutrient inputs on freshwater, marine, and terrestrial ecosystems. *Environmental Pollution, 100*(1), 179-196. doi:https://doi.org/10.1016/S0269-7491(99)00091-3

SØNDERGAARD, J., BACH, L., & GUSTAVSON, K. (2014). Measuring bioavailable metals using diffusive gradients in thin films (DGT) and transplanted seaweed *(Fucus vesiculosus)*, blue mussels *(Mytilus edulis)* and sea snails *(Littorina saxatilis)* suspended from monitoring buoys near a former lead–zinc mine in West Greenland. *Marine Pollution Bulletin, 78*(1), 102-109. doi:https://doi.org/10.1016/j.marpolbul.2013.10.054

SU, E., & OKAY, O. (2018). Hybrid cross-linked poly(2-acrylamido-2-methyl-1-propanesulfonic acid) hydrogels with tunable viscoelastic, mechanical and self-healing properties. *Reactive and Functional Polymers, 123*, 70-79. doi:https://doi.org/10.1016/j.reactfunctpolym.2017.12.009

TARAFDER, P. K., & RATHORE, D. P. S. (1988). Spectrophotometric determination of nitrite in water. *Analyst, 113*(7), 1073-1076. doi:10.1039/AN9881301073

THONIYOT, P., TAN, M. J., KARIM, A. A., YOUNG, D. J., & LOH, X. J. (2015). Nanoparticle-Hydrogel Composites: Concept, Design, and Applications of These Promising, Multi-Functional Materials. *Advanced science (Weinheim, Baden-Wurttemberg, Germany), 2*(1-2), 1400010-1400010. doi:10.1002/advs.201400010

VEEKEN, P. L. R. V. D., & LEEUWEN, H. P. V. (2010). DGT/DET Gel Partition Features of Humic Acid/Metal Species. *Environmental Science & Technology, 44*(14), 5523-5527. doi:10.1021/es100861t

ZHANG, H., & DAVISON, W. (1995). Performance Characteristics of Diffusion Gradients in Thin Films for the in Situ Measurement of Trace Metals in Aqueous Solution. *Analytical Chemistry, 67*(19), 3391-3400. doi:10.1021/ac00115a005

ZHANG, H., DAVISON, W., GADI, R., & KOBAYASHI, T. (1998). In situ measurement of dissolved phosphorus in natural waters using DGT. *Analytica Chimica Acta, 370*(1), 29-38. doi:https://doi.org/10.1016/S0003-2670(98)00250-5

ZHANG, Y., MASON, S., MCNEILL, A., & MCLAUGHLIN, M. J. (2013). Optimization of the diffusive gradients in thin films (DGT) method for simultaneous assay of potassium and plant-available phosphorus in soils. *Talanta, 113*, 123-129. doi:https://doi.org/10.1016/j.talanta.2013.03.023

ZHANG, Z., CHEN, Z., WANG, S., QU, C., & CHEN, L. (2014). On-Site Visual Detection of Hydrogen Sulfide in Air Based on Enhancing the Stability of Gold Nanoparticles. *ACS Applied Materials & Interfaces, 6*(9), 6300-6307. doi:10.1021/am500564w

# Chapter 2 - Literature Review

The purpose of this review was to situate the research project in the DGT and bioreactor research fields, and provide the theoretical basis for the research conducted. Comprehensive reviews of denitrifying bioreactors and other mitigation strategies are already available (Addy et al., 2016; Christianson & Schipper, 2016; Schipper et al., 2010a). Excellent reviews of the reviews of DGT use and theory are presented elsewhere also (Davison, 2016; Lehto et al., 2006).

New Zealand has recently recognised our responsibility to improve the health and quality of our freshwater resources with the implementation of the National Environmental Standards for Freshwater in September 2020 (Reddy, 2020). Some of the key requirements, among many others, of the standards include: management of freshwater to give effect to Te Mana o te Wai; improve degraded water bodies, and maintain or improve all others; and avoid further loss or degradation of wetlands and streams (Environment, 2020; Reddy, 2020).

The National Policy Statement for Freshwater Management 2020 outlines the guidelines and values for nutrients and other pollutants (Government, 2020). It establishes a ranking system for rating the levels of nutrients in freshwater systems. The importance of this research is even more apparent given the implementation of the standards, and the necessity widespread for nutrient monitoring (Reddy, 2020).

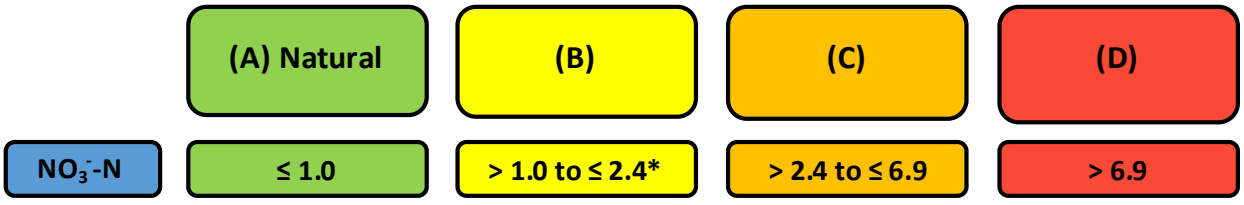


Figure 2.1: Summary of yearly median nitrate-N guidelines from the National Policy Statement for Freshwater Management in mg $L^{-1}$ (Government, 2020). *National bottom line.

## 2.1 Brief Introduction to Environmental Issues of Excess Nutrients

Nutrients, such as nitrate, are necessary inputs to agricultural systems to sustain crop/plant growth. Once they are leached out they become externalities for local waterways as they are transported downstream to lakes, estuaries, coastal ecosystems and the ocean (Rabotyagov et al., 2014). Society has also long used waterways as convenient waste water disposal systems (i.e. direct or indirect sewage disposal), and as such the loading of nitrate is very strongly influenced by human and livestock population density, and land use (Smith et al., 1999).

### *2.1.1 Nitrogen Accumulation and Cascade*

The increase in bioavailable nitrogen can be attributed to four main causes. (1) Widespread cultivation of crops that promote biological nitrogen fixation, converting $N_2$ to organic nitrogen; (2) the conversion to reactive $NO_x$ species through the burning of fossil fuels; (3) the Haber-Bosch process; and (4) the overflow of human waste (Galloway et al., 2003; Huang et al., 2016b).

The cultivation of legumes, rice and other crops that promote nitrogen fixation has increased globally since 1860, and dramatically since 1960 (Galloway et al., 2003). $NO_x$ creation through fossil fuel combustion has increased from 1 Tg N $year^{-1}$ in 1860, to approximately 25 Tg N $year^{-1}$ in 2000 (Galloway et al., 2003). This is unsurprising given the rate at which combustion of fossil fuels has grown since the industrial revolution. In combustion systems which are not highly efficient, $NO_x$ is produced, a significant fraction of which returns to land and water systems via wet and dry deposition (Smith et al., 1999).

The Haber-Bosch process, primarily used for the production of industrial fertilisers, is now responsible for the largest input of nitrogen to the environment. Pre 1910 there was no reactive nitrogen created from the process, however this grew to more than 100 Tg N $year^{-1}$ (Galloway et al., 2003). The removal of nitrogen in farm produce necessitates the addition of nutrients to replenish the depleted soils (Robertson & Vitousek, 2009). New nitrogen must come from outside the plant-soil system as there is no potentially available nitrogen in the rock from which soil is derived (Robertson & Vitousek, 2009).

Applications of nitrogen fertiliser are not particularly efficient – most nitrogen does not reach the intended target, protein in the human diet (Robertson & Vitousek, 2009).

Human waste and animal waste are also strong supplies of nutrients to waterways, both from leaching from terrestrial systems and direct discharge (Smith et al., 1999). Discharge from wastewater contains significant concentrations of ammonium, of which a small fraction is oxidised by conventional treatment (Wakelin et al., 2008). Discharge from treatment plants can therefore deposit large quantities of organic matter and nutrients into receiving waterways (Wakelin et al., 2008).

Each additional reactive nitrogen species added to the environment can have a cumulative effect, known as the nitrogen cascade. The sequential transfer of nitrogen through environmental systems can result in environmental changes in each system as it moves through or is temporarily stored (Galloway et al., 2003). This means that before denitrification back to $N_2$, a single nitrogen atom can have an impact on all biospheres, and the origin of the reactive nitrogen becomes unimportant (Galloway et al., 2003).

### *2.1.2 Eutrophication and Hypoxia*

Nitrogen and phosphorus both contribute to eutrophication and hypoxia (Rabotyagov et al., 2014). Eutrophication refers to the over-availability of nutrients in aquatic systems and the increased productivity that follows (Allaby, 2010). The increase in nutrients stimulates growth of organic matter (e.g. phytoplankton and algae) (Allaby, 2010). The organic matter dies, it falls through the water column, and is decomposed in the bottom water layer and sediment (Rabotyagov et al., 2014). Decomposition of the organic matter consumes oxygen, reducing the availability of oxygen in the waterbody to sustain the ecosystem (Rabalais et al., 2002).

Hypoxia refers to oxygen deficiency, and is defined as water containing less than 2 mg $L^{-1}$ of oxygen (Rabotyagov et al., 2014). Hypoxic zones are created through the process of eutrophication, fundamentally altering the functioning and structure of an ecosystem, often resulting in loss of habitat and reduction in biodiversity (Rabalais et al., 2002).

### *2.1.3 Secondary Effects of Excess Nutrients*

There are numerous secondary effects of excess nitrogen on biology, chemistry, and human use (Smith et al., 1999). These are often deleterious and of concern to users of the resource (Smith et al., 1999).

These effects include: phytoplankton species composition shifting to taxa that may be toxic or inedible (e.g. bloom-forming cyanobacteria – blue green algae); changes in biomass, and species composition; reduced water clarity; decreased aesthetic value; taste, odour, and water supply filtration problems; possible health risks in water supplies; elevated pH; increased short term fish production and harvest; and increased probability of fish kills (Smith et al., 1999). Consumption of nitrates and nitrites has also been associated with gastrointestinal cancer and infant methemoglobinemia (Hord et al., 2009; Knobeloch et al., 2000).

Eutrophication and hypoxia can have substantial economic consequences; therefore there is a trade-off between the benefits from polluting activities and the services of the ecosystem forgone (Smith et al., 1999).

## 2.2 Mitigation Strategies

Constructed wetlands, riparian buffers, saturated buffers and denitrifying bioreactors nutrient mitigation strategies have been developed to remove excess reactive nitrogen species at the source and limit the downstream effects (Tanner et al., 2012, Jaynes and Isenhart, 2019, Chandrasoma et al., 2019).

### *2.2.1 Denitrifying Bioreactors*

Denitrifying bioreactors are simple engineered systems that use a solid carbon substrate to enhance the microbial conversion of dissolved nitrogen species, primarily nitrate, to nitrogen gas (Schipper et al., 2010a) (Figure 2.2). Bioreactors are designed for simple and passive treatment of drainage waters, groundwater, and wastewater dissolved nitrogen species (Addy et al., 2016; Rambags et al., 2016; Schipper et al., 2010a). Denitrifying bioreactors have also been found to consistently and substantially

reduce faecal bacteria (Rambags et al., 2016). Little evidence has been found to support the use of denitrifying bioreactors for the removal of phosphate (Corbett et al., 2019; Schipper et al., 2010a; Schipper et al., 2010b), however because of their reducing conditions bioreactors have been used for the removal of dissolved metal species (Neculita et al., 2008). Sulfate reducing bioreactors have been used for the treatment of contaminated acid mine drainage (Neculita et al., 2008), however sulfate reducing conditions can lead to the production of highly toxic methyl mercury (Shih et al., 2011).

The carbon source has two functions, firstly as a carbon source for denitrification (Rivett et al., 2008). Secondly, the oxidation of organic compounds by aerobic organisms, creating and maintaining the anoxic conditions making it energetically favourable for nitrate to act as an electron acceptor (Rambags, 2019).

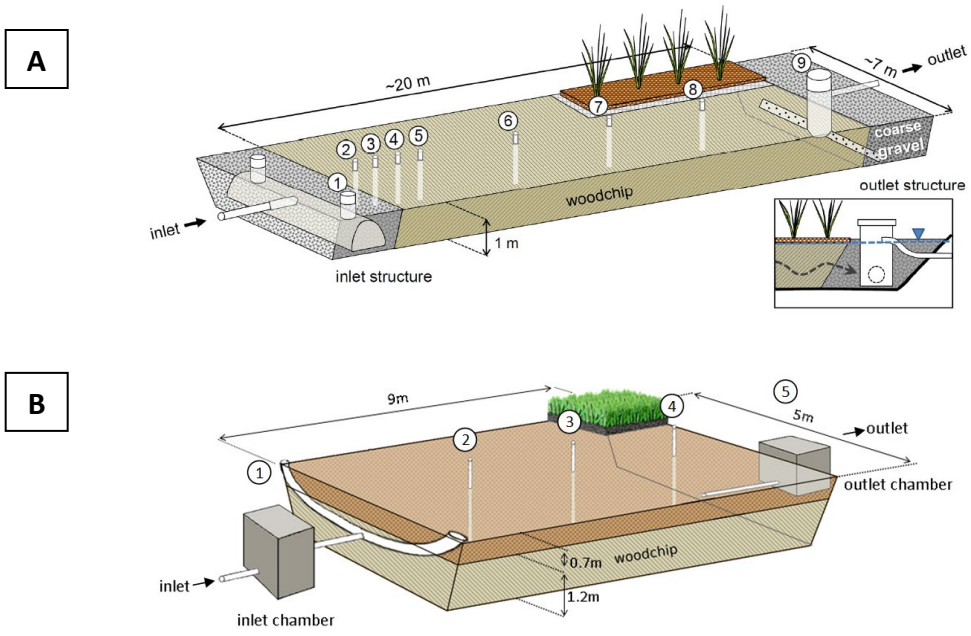


Figure 2.2 (A) Bioreactor treating effluent (Rambags et al., 2016). (B) Bioreactor treating agricultural runoff (Corbett et al., 2019). Diffusive Gradients in Thin Films were deployed at both bioreactors in study 1. The inlet and outlet chambers, and wells where DGT were deployed and grab samples taken are numbered (Corbett et al., 2019).

There are numerous factors influencing denitrification rates. Temperature controls microbial activity, increasing temperature stimulates microbial processes, and has been reported to significantly impact denitrification rates (Addy et al., 2016; Schipper et al., 2010a). The availability of both nitrogen species

and dissolved organic carbon also affects denitrification, the greater the availability of either the greater the denitrification rate, providing one was not limiting (Addy et al., 2016; Schipper et al., 2010a). Dissolved oxygen also influences denitrification rate, aerobic microorganisms may outcompete denitrifiers for available carbon (Rivett et al., 2008). Hydraulic retention time has been reported to significantly influence the denitrification rate, as hydraulic retention time increases as does nitrate removal rate (Hoover et al., 2016). Microbial transformation of nitrate to nitrogen gas produces hydroxyl groups, and pH has also been reported to influence denitrification rates (Peng et al., 2006).

There are many potential applications and approaches for implementing denitrifying bioreactors (Figure 2.3), the design of which is determined by the above factors. The application of bioreactors has focused primarily on watersheds with high non-point source nitrate loads and tertiary wastewater treatment (Christianson & Schipper, 2016).

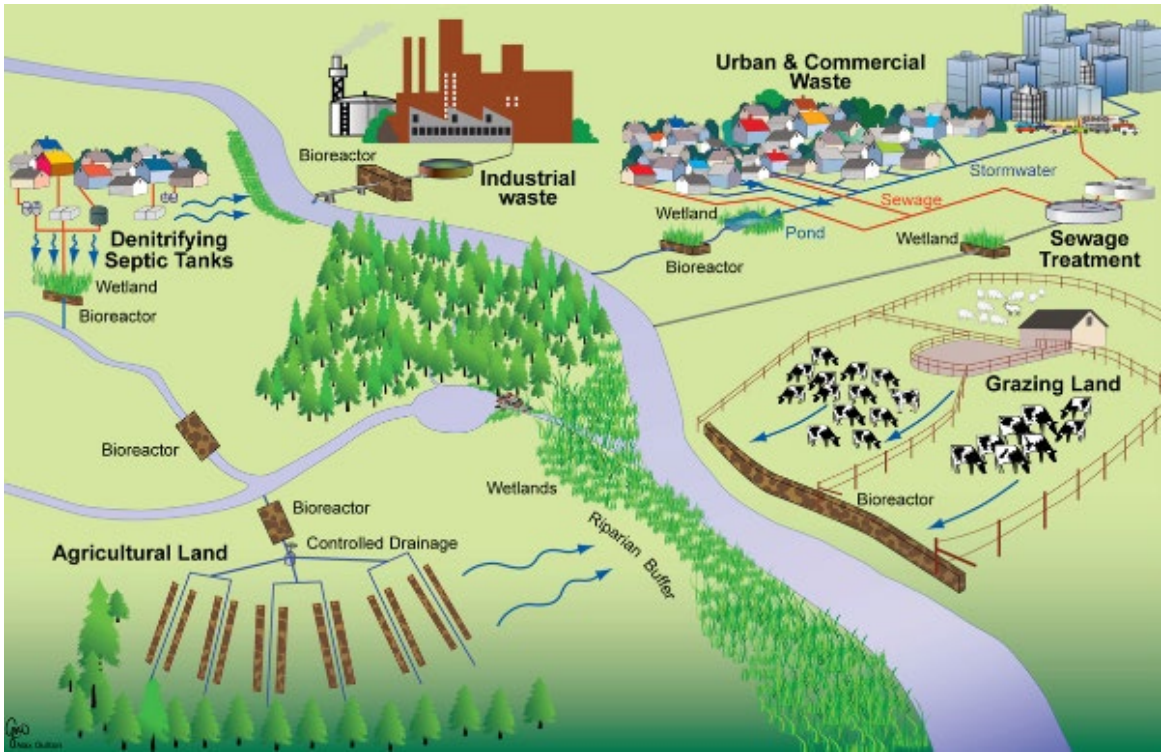


Figure 2.3: Potential sites and approaches for enhancing denitrification to reduce nitrogen movement along the nitrogen cascade (Schipper et al., 2010c).

## 2.3 Water Sampling

Sampling is one of the main complexities in environmental water monitoring (Kianpoor Kalkhajeh et al., 2019). Multiple methods exist to measure nitrate and phosphate in aquatic systems, and each has their advantages and disadvantages. For example, manual grab sampling, automated sampling, passive sampling (such as Diffusive Gradients in Thin-Films), and flow-proportional sampling (Kianpoor Kalkhajeh et al., 2019). A summary of the commonly deployed sampling techniques for the collection of water samples is provided in Table 2.1.

Table 2.1: Summary of the commonly deployed sampling techniques for the collection of water samples (Kianpoor Kalkhajeh et al., 2019).

| **Sample** | **Location** | **Frequency** | **Sampling** | **Recommended** |
|---|---|---|---|---|
| Surface Runoff | Catchment outflow; Chanel outlet. | Based on irrigation or precipitation intensity (seconds to hours). | Manual; Automated; Passive; Flow-proportional. | Automated; Passive. |
| Leachate | Point Samples; Tile drains. | Based on irrigation or precipitation intensity. | Lysimeter; Passive. | Zero-tension lysimeter; Passive. |
| Groundwater | Springs; Alluvial and upland point samples. | Purpose dependant (weekly to yearly). | Well; Piezometer; Passive. | Well; Passive. |
| Rivers/Streams | Upstream; Downstream; River mouth; Along river. | Usually weekly to monthly, or seasonal. | Manual; Automated; Passive; Piezometer; Flow-proportional. | Automated; Passive. |
| Lakes/Ponds | Inlet; Outlet: Within water body. | Usually weekly to monthly, or seasonal. | Manual; Passive. | Manual; Passive. |
| Wetlands/ Estuaries | Inlet; Outlet; Within wetland. | Usually weekly to monthly, or seasonal. | Manual; Passive; Water column; Flow-proportional. | Water column; Flow-proportional; Passive (Corbett et al., 2019). |

Grab sampling is the predominant method for measuring analyte concentrations in aquatic systems, because it is quick and simple (Huang et al., 2016b), and requires little investment in sampling equipment. They are however unlikely to provide representative nutrient concentration data due to the infrequency of sampling, and high temporal variability in concentration (Corbett et al., 2019; Huang et al., 2016b). Continuous automated sampling can more accurately capture temporal changes in nutrient concentrations, but require significant investment in on-site equipment (Audet et al., 2014). To achieve the same temporal resolution via grab sampling is time consuming, requiring extended periods on-site (Corbett et al., 2019). The large number of samples, associated with grab and automated sampling, for analysis can be expensive (Corbett et al., 2019).

Microbial and chemical transformations during transport and storage of grab samples, necessitates chemical or physical preservation (S˙liwka-Kaszyńska et al., 2003). Physical preservation is preferential, as preservatives such as mercuric chloride can be toxic and have matrix effects, and sample dilution must be considered (S˙liwka-Kaszyńska et al., 2003). Standard physical preservation techniques include immediate filtering to 0.45 µm, and freezing to -20 $^{o}$C, however, these temperatures are difficult to maintain in-field and during transport (S˙liwka-Kaszyńska et al., 2003).

Development of in-situ continuous monitoring and measurement systems overcome many of the limitations of grab and automated sampling systems (Kianpoor Kalkhajeh et al., 2019). For example, an automated multiplexed pumping system and UV-VIS field spectrophotometer coupled system (MPS UV-VIS) was found to provide high resolution accurate nitrate concentration data in a range of denitrifying bioreactors (Maxwell et al., 2018). These systems are limited, as with automated sampling systems, by capital and operational expense (Corbett et al., 2019; Kianpoor Kalkhajeh et al., 2019; Maxwell et al., 2018). Systems such as the MPS UV-VIS are limited by spectrophotometer data storage, cuvette fouling, and battery power and require careful calibration (Corbett et al., 2019; Maxwell et al., 2018). In-field analyses using colorimetric test kits, are simple and relatively easy to use, however they are of low precision, and are limited by their operational range and by the skill of the user in

determining the colour change (Corbett et al., 2019). Diffusive Gradients in Thin-Films are able to overcome many of the methodological limitations of other sampling techniques, as discussed in the following section.

## 2.4 Diffusive Gradients in Thin-Films

Passive techniques, such as DGT, are capable of providing time weighted average concentrations of environmentally relevant time scales and integrating short term analyte concentration variations (Huang et al., 2016b). The DGT Technique enables the *in situ* measurement of labile species in aqueous systems (Zhang & Davison, 1995). The following sections detail the theoretical background on which DGT is based, comprehensive reviews of the DGT use and theory are presented elsewhere (Davison, 2016; Lehto et al., 2006).

### *2.4.1 Fick's First Law of Diffusion*

DGT is based on Fick's first law of diffusion (Zhang & Davison, 1995). Diffusion is the tendency of chemical species to move in the direction of decreased concentration as to make concentration uniform, the flux, due to the random heat motion of molecules (King et al., 2013). Diffusive Gradients in Thin Films directly measures a flux, i.e. the rate of supply of material in a given time (Zhang & Davison, 1995). Due to the dependency of the rate on the solution exchange kinetics, DGT measures the labile fraction of species in solution (Zhang & Davison, 1995).

Equation (2.1 details how the diffusion flux (J, mg $cm^{-2}$ $s^{-1}$) of chemical species is determined by the diffusion coefficient (D, $cm^2$ $s^{-1}$) and concentration (C, mg $cm^{-3}$), divided by the position (x, cm) (Schaschke, 2014). Flux is driven in the direction of increasing position, denoted by the negative sign (Schaschke, 2014). The diffusion coefficient varies for species and solutes, and is dependent on temperature, fluid viscosity, and particle size (Schaschke, 2014).

$$\boldsymbol{J = \frac{-D\partial C}{\partial x}} \tag{2.1}$$

### *2.4.2 DGT Assembly*

There are two essential parts to DGT, the analyte specific binding layer and the material diffusion layer consisting of a diffusive hydrogel and filter membrane (Davison, 2016; Zhang & Davison, 1995), illustrated in Figure 2.4. The hydrogel and filter constrain transport of ions to the binding layer, enabling the application of Fick's First Law. The filter is incorporated to protect the hydrogels from microbial decomposition and stop clogging by particles in solution (Davison, 2016).

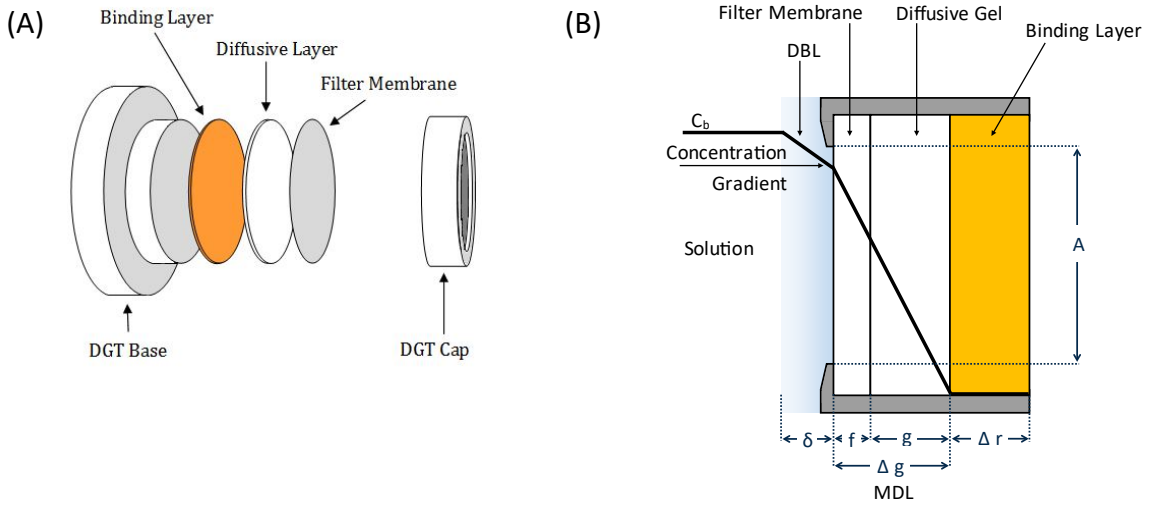


Figure 2.4: (A) Exploded Diffusive Gradient in Thin-Films (DGT) piston assembly schematic (Corbett et al., 2019). (B) Cross-sectional view of concentration gradient through material diffusion layer (MDL) and diffusive boundary layer (DBL) (discussed in section 2.4.10) to the binding layer at steady state (Davison, 2016; Davison & Zhang, 2012). Where A = exposure window area; Δr, Δg, g, f and δ = binding layer, MDL, diffusive gel, filter membrane and DBL thicknesses respectively; and, $C_b$ = bulk concentration (Davison & Zhang, 2012; Zhang & Davison, 1995).

### *2.4.3 Derivation of the DGT Equation*

As described above, an ion-exchange resin layer (binding layer) is separated from the bulk solution by an ion-permeable gel membrane, illustrated in Figure 2.4, such that transport of ions to the binding layer is constrained to diffusion, above a threshold level of convection (Zhang & Davison, 1995). If the thickness of the diffusive boundary layer (DBL, δ) (discussed in section 2.4.10) is negligibly small compared to Δg, flux (J) can be expressed by Equation (2.2), where $C_b$ is the concentration of ions in the bulk solution, and C' is the concentration of the ion in the resin layer (Zhang & Davison, 1995).

$$\boldsymbol{J = \frac{D(C_b - C')}{\Delta g}} \tag{2.2}$$

Providing the resin is not saturated and the free ions are in rapid equilibrium with the resin, with a large binding constant, C' is effectively zero and Equation (2.2) can therefore be simplified to Equation (2.3) (Zhang & Davison, 1995).

$$\boldsymbol{J = \frac{DC_b}{\Delta g}} \tag{2.3}$$

Combining Equations (2.3) and (2.4) gives Equation (2.5), and because the mass of ions that have diffused into the resin (M) can be determined analytically, $C_b$ can be quantified by Equation (2.6) (Zhang & Davison, 1995).

$$\boldsymbol{J = \frac{M}{At}} \tag{2.4}$$

$$\boldsymbol{M = \frac{DC_bAt}{\Delta g}} \tag{2.5}$$

$$\boldsymbol{C_b = \frac{M\Delta g}{DAt}} \tag{2.6}$$

The use of the simple DGT equation is based on the following assumptions (Davison, 2016; Davison & Zhang, 2012):

(1) Before steady state is achieved the accumulated mass is negligible;

(2) Initial transient period to achieve steady state is negligible with respect to deployment time;

(3) Diffusion through the device is planar;

(4) Negligible interactions such as charge effect and binding to material diffusion layer (MDL);

(5) Rapid and non-penetrative interaction of analyte with binding layer;

(6) Exposure area and Δg geometric values apply with a negligible DBL; and

(7) Accurate measurement of accumulate mass, MDL thickness, diffusion coefficient, and deployment time.

### *2.4.4 Steady State*

At steady state, flux in and out of each layer is constant and equal to the flux through the adjoining layer (Equation (2.7) (Davison, 2016). Where $D_{gel}$, $D_f$, $D_w$ = diffusion coefficients of diffusive gel, membrane filter, and water; g, $\Delta_f$, δ = diffusive gel layer, membrane filter, and DBL thicknesses; and $C_g$, $C_f$, $C_r$ = analyte concentration at the diffusive gel, membrane filter, and binding layer surfaces respectively (Davison, 2016).

$$\boldsymbol{J = \frac{D_{gel}(C_g - C_r)}{g} = \frac{D_f(C_f - C_g)}{\Delta_f} = \frac{D_w(C_b - C_f)}{\delta}} \quad (2.7)$$

The period before steady state is met is termed the transient period. During this period the flux is lower than in the steady state (Lehto et al., 2006). The time to reach the steady state is dependent upon the diffusion coefficient and the MDL thickness – among others (Lehto et al., 2006). All previously derived equations assume a steady state has been met, however during the transient period several processes occur (Davison, 2016).

Upon immersion solutes diffuse between the solution and diffusive layer (Davison, 2016). Solutes which do not bind to the binding layer tend towards chemical equilibrium, i.e. concentration in each diffusion layer of the DGT is equal to that in the bulk solution (Davison, 2016). Binding solutes never reach equilibrium due to continual removal of the solute from solution by the binding layer, thereby maintaining a negligible concentration at the binding layer and MDL interface (Davison, 2016). Under these conditions $C_r$ is effectively zero (Davison, 2016). Binding solute progressively enters the MDL until steady state is achieved; where the concentration profile in the MDL is linear, with a constant gradient throughout (Figure 2.4) (Davison, 2016).

As stated earlier, use of the simple DGT equation assumes that before steady state is achieved the accumulated mass is negligible (Davison, 2016), and the initial transient period is negligible with respect to the deployment time (Davison & Zhang, 2012). For valid application the actual mass accumulated cannot be significantly different from the accumulated mass if there was no transient

period (Davison & Zhang, 2012). These two assumptions are intrinsically related. Potential error cannot be expressed solely as percentage of time to steady state of deployment time, it must also account for accumulated mass (Davison & Zhang, 2012). The extent to which total mass accumulated is overestimated depends on total deployment time (Lehto et al., 2006), as the total deployment time increases the influence of the transient period proportionally decreases.

The difference between the accumulated masses when neglecting the transient period, expressed as percentage error, can to a good approximation be calculated using Equation (2.8), adapted from Equation (2.9), where coefficient y = 6 and $t_{dep}$= deployment time (Davison & Zhang, 2012).

$$\boldsymbol{Percentage\ error} = \frac{\boldsymbol{\Delta g^2}}{\boldsymbol{6D}} \times \frac{\boldsymbol{100}}{\boldsymbol{t_{dep}}} \tag{2.8}$$

$$\boldsymbol{Time\ to\ reach\ steady\ state} = \frac{\boldsymbol{\Delta g^2}}{\boldsymbol{yD}} \tag{2.9}$$

### *2.4.5 Diffusion Layer*

As discussed above, DGT samplers rely on diffusion through a permeable diffusion layer of known thickness for *in situ* measurement of ions in natural waters (Larner & Seen, 2005). Controlling the mode of transport to diffusion enables the use of Fick's First Law to back calculate the solution concentration from the accumulated mass. As such, a sufficiently thick hydrogel is required to ensure the flux of ions to the binding layer, above a threshold level of convection, is independent of the hydrodynamics in solution (Zhang & Davison, 1995). The principal diffusion layer utilised is based on polyacrylamide hydrogels (Larner & Seen, 2005), however agarose is also widely utilised (Davison, 2016). Polyacrylamide is cross-linked with either an agarose derivative, or with bis-acrylamide (Davison, 2016). Commercially available chromatography paper has also been investigated as an alternative diffusion layer (Larner & Seen, 2005).

Hydrogels are typically soft, flexible and elastic, they can range from fragile to quite strong and viscous fluid to fairly rigid solid depending on their composition (Davison, 2016). Hydrogel formation and selection will be discussed subsequently. The hydrogel structure consists of three-dimensional

polymer networks, which are water insoluble and highly hydrophilic (Davison, 2016). The water is bound to the hydrogel via hydrogen bonding or dipole interactions, *in situ* they can contain over 95% water and ensures the hydrogel structure does not collapse, the free water in the hydrogel has the same properties as normal water (Davison, 2016).

DGT makes two assumptions regarding the diffusive gel, and MDL as a whole: (1) diffusion through the device is planar; and (2) negligible interactions such as charge effect and binding to MDL (Davison, 2016; Davison & Zhang, 2012).

The assumption that diffusion through the device is planar does not stand. Measurements of Cd distribution in a DGT resin, using laser ablation inductively coupled plasma mass spectrometry, found that the effective sampling window was larger than the geometric diameter of the sampling window (Warnken et al., 2006). Diffusion through the centre of the exposure window is planar, while diffusion close to the edges of the window can also occur laterally (in both MDL and DBL), thereby enabling analyte to accumulate over an area of binding gel greater than the area of the exposure window, and enhancing the flux to the binding layer (Davison, 2016). Taking lateral diffusion into account gives the effective area of diffusion ($A_{eff}$), and increased the effective surface area of the device by approximately 20% (Warnken et al., 2006). The full DGT equation accounts for this (Equation (2.15).

Analyte binding and charge effect interactions within the MDL are not always negligible, at least not under low ionic strength solutions (Davison, 2016). Charge on the diffusive layer/MDL can modify the interfacial concentration and therefore the concentration gradient through the MDL (Davison, 2016). For example, anions will become electrostatically enhanced at the gel surface if the diffusive gel is positively charged (Davison, 2016).

Previous studies have found that diffusion coefficients in APA (agarose crosslinked polyacrylamide) gels were erratic at low ion strengths (Davison & Zhang, 2012). This is attributable to the degree of washing, when the gel is not exhaustively washed it has a partial negative charge due to the presence

of unreacted polymerisation reactants, while under exhaustive washing there was a net positive charge (Warnken et al., 2005). Polyacrylamide crosslinked with bis-acrylamide gels had a slight negative charge after washing (van der Veeken et al., 2010; Veeken & Leeuwen, 2010; Yezek et al., 2008). Charges on gels appear to have no effect on DGT measurements when utilising APA gels at ionic strengths of 1mM or above (Davison & Zhang, 2012).

In many cases it is incorrect to assume that there are no binding interactions between solutes and the MDL (Davison & Zhang, 2012). Ions enter the diffusive layer, bind to it, and accumulate until the binding capacity (usually low) is reached, thereby lengthening the transitional period before steady state is reached (Davison & Zhang, 2012). The final stage of the APA diffusive hydrogel washing procedure is therefore the charge neutralisation of the gel by storage in a 0.01 mol $L^{-1}$ NaCl solution, at room temperature.

### 2.4.5a Hydrogel Formation

Hydrogels are water-swollen, and cross-linked polymeric network produced by the reaction of one or more monomers, they do not dissolve in water, instead exhibit the ability to swell and retain a significant fraction of water within their structure (Ahmed, 2015). Protection from dissolution arises from cross-links between network chains (Ahmed, 2015). In the swollen hydrogel, the mass fraction of the water in the hydrogel is considerably larger than the polymer (Ahmed, 2015). High degrees of swelling are commonly achieved by using monomers which are water soluble when in non-crosslinked form (Ahmed, 2015).

$-SO_3H$, -COOH, $-CONH_2$, -OH and $–NH_2$ functional groups within the polymeric network provide the hydrophilic character (Sahiner et al., 2010). Negatively charged functional groups, $SO_3^-$ and $COO^-$ can also be formed, and via electrostatic interactions absorb metal cations (Sahiner et al., 2010). While the impacts of pH changes can be offset by the formation of carboxyl functional groups (-COOH, $-COO^-$) which can react with hydroxyl and hydronium ions (Liu & Wang, 2019).

Hydrogels can be classified into numerous groups based on source (natural or synthetic), composition (homo, co, or multi polymer, or double network), configuration (amorphous to crystalline), crosslinking, appearance, and electrical charge (Ahmed, 2015; Chen et al., 2015a; Iizawa et al., 2007; Maolin et al., 2000; Yang et al., 2002). In general, hydrogels are prepared from natural or synthetic polymers, or an optimised combination depending on the intended hydrogel properties (Ahmed, 2015; Tabata, 2009). Any technique that can be used to crosslink polymers can be used to produce hydrogels (Ahmed, 2015). These include bulk polymerisation, solution polymerisation/crosslinking, suspension or inverse suspension polymerisation, grafting to a support, and irradiation polymerisation (Ahmed, 2015).

Hydrogels are predominantly prepared utilising monomers, gel initiators and accelerators, and then cured (Thoniyot et al., 2015), as via solution polymerisation. The standard DGT procedure for the formation of hydrogels involves the radical solution polymerisation of acrylamide and agarose, using Ammonia peroxydisulfate (APS) and N,N,N',N'-tetramethylethylenediamine (TEMED) as redox initiators (Zhang & Davison, 1995). Alternative crosslinking agents such as bis-acrylamide have been used (Davison, 2016), and, as discussed above, the standard diffusive gel has been replaced by commercially available chromatography paper (Larner & Seen, 2005).

As discussed in Section 2.5 however, the colourimetric determination of nitrate requires the reduction of nitrate to nitrite. For the purposes of utilising colour change DGT to determine solution nitrate concentrations this must be done within the diffusive layer. The incorporation of a reductant within the binding layer is, in principle, like the synthesis of binding layer (discussed in section 2.4.6c).

The strategy adopted in this research was the formation of zero-valent metal nanoparticles within the hydrogel network, by swelling the dried hydrogel in a high concentration solution of Fe(III) (Chapter 4). The reduction of 4-nitrophenol and 2-nitrophenol by Co(0) nanoparticles formed in a poly- 2-acrylamido-2-methyl-1-propanesulfonic acid, N,N'-methylenebisacrylamide crosslinked (PAMPS)

hydrogel has been reported (Sahiner et al., 2010). PAMPS hydrogels are however limited by their low mechanical strength (Gong et al., 2003).

Hybrid cross-linked PAMPS hydrogels have been reported to have excellent mechanical properties, due to the strengthened interactions between chemically cross-linked PAMPS chains and incorporated nanoparticles (Su & Okay, 2018). Alternatively, double network hydrogels consist of contrasting interpenetrating polymer networks (Chen et al., 2015a). Classically the first polymer network is formed, which is subsequently immersed and swelled in the precursors to the second polymer (Chen et al., 2015a). It requires however a large excess of the second monomer, to form the strong intertangled network (Chen et al., 2015a).

PAMPS/Acrylamide copolymer hydrogels consisting of varying mole ratios have been reported (Jamshidi & Rabiee, 2014). The AMPS sulfonate group provides ionic exchange capability, electrical conductivity, and resistance to divalence and salinity (Sheng, 2010). Acrylamide shields the copolymer, by providing resistance to hydrolysis, acidity and alkalinity (Sheng, 2010). The rigid side chains, large chains, and chains of ring structures provide good thermal stability, and further shielding effects (Sheng, 2010). The formation and protection of nanoparticles in hydrogels helps overcome many of the challenges associated with using nanoparticles for the reduction on nitrate, discussed in Section 2.5.1 of this review.

#### 2.4.5b Filter Membrane

Filter membranes are an important component of the material diffusion layer. Membrane filters provide an average cut-off for filtration, and protect the inner diffusive gel and binding layer (Davison, 2016). They consist of polymers fabricated to have a network of pores, generally of 0.45 µm pore size, with thickness typically varying from 0.13 to 0.15 mm (Davison, 2016).

Membrane filters are commonly made from polyethersulphone, however cellulose acetate and nitrate membranes have also been utilised (Davison, 2016). Due to its resistance to microbial attack, polyethersulphone is preferred for *in situ* deployment in natural waters (Brandl & W. Hanselmann,

1991). Microbial attack can weaken and reduce mechanical stability and alter membrane permeability or block membrane pores (Brandl & W. Hanselmann, 1991). If microorganisms were metabolically stimulated by a digestible membrane polymer false analyte concentration would be determined (Brandl & W. Hanselmann, 1991).

### *2.4.6 Binding Layer*

The binding layer rapidly and strongly removes specific analytes transported to it through the diffusion layer from solution, necessary to maintain the concentration gradient through the diffusive layer. Enabling the application of Fick's First Law to back calculate the solution concentration once the adsorbed mass is determined.

For DGT to provide accurate measurement of solutes, the binding layer must strongly interact with the analyte (Davison, 2016). Rapid and strong reaction of the analyte with the binding layer reduces the concentration of the labile analyte at the binding layer surface to effectively zero, thereby creating a steady-state linear diffusion gradient in the diffusive gel (Zhang & Davison, 1995), illustrated in Figure 2.4. Enabling the application of Fick's First Law to back calculate the solution concentration once the adsorbed mass is determined.

Typically binding layers are near-homogenous, and consist of solid resins or powders incorporated into a gel matrix (e.g. polyacrylamide) (Davison, 2016). The particle size of the incorporated solid must be sufficiently small to allow simple and even incorporation into the gel matrix (Davison, 2016). It is recommended that the diameter of the incorporated solid particles should be <100µm, significantly smaller than the standard thickness of binding layers (250µm un-hydrated and ≈400µm hydrated) (Davison, 2016).

Numerous investigations have been undertaken into alternative DGT binding phases (Li et al., 2003). Li et al., (2003) detailed the use of a liquid binding phase of poly(4-styrenesulfonate) for the determination of cadmium and copper. Dialysis membranes, of known molecular weight cut-off, were used to stop diffusion of the liquid binding phase to bulk solution (Li et al., 2003; Liu et al., 2016).

Liquid binding layer DGT are a continuation of the development of liquid collection phases developed for *in situ* equilibrium dialysis samplers (peepers) (Teasdale et al., 1995). The use of liquid binding phases opens the possibility for a wide range of colourimetric reactions, especially those that require greater mobility and cannot be incorporated into hydrogel frameworks (Chapter 4).

The suitability of a binding layer depends on the deployment conditions; numerous binding layers are only applicable in systems with low concentrations of potential competing ions (Davison, 2016). For example, the measurement of dissolved reactive phosphorus in synthetic freshwater and seawater comparing Metsorb and ferrihydrite binding layers, found that the ferrihydrite method underestimated dissolved reactive phosphorus by 23-30% for deployments longer than 2 days (Panther et al., 2010).

When choosing a binding, three characteristics must be considered (Davison, 2016). (1) Binding strength, higher binding strength means the binding layer is more suited for measurement in diverse systems. (2) The intrinsic binding capacity, a greater binding capacity enables use of lower binding strength binding layers or deployment in higher competition systems. (3) The competition effects rising from the presence of ions with similar or greater binding strengths, thereby decreasing the concentration of binding sites available to the measured analyte, potentially leading to non-ideal adsorption.

The ability of binding layers to adsorb the desired analyte and the recoverability of the adsorbed mass is also an important consideration. Experiments are often conducted in simple solutions, containing the binding gel, analyte and ionic strength adjuster (Huang et al., 2016a). The uptake efficiency, or the ability of the binding gel to uptake the analyte, is quantified as the proportion of the analyte removed from solution. The elution efficiency, ability to desorb the bound mass, is quantified using the elution procedure for that analyte and binding layer. Elution procedures are designed and selected to have the greatest elution efficiency. These factors are applied to the measure mass adsorbed to the binding layer, prior to incorporation into the $C_{DGT}$ equations (Equations (2.6) and (2.15)).

A detailed list of potential binding layers for this research, and their efficiencies, is given in the subsequent subsections. There are numerous other binding layers available to various analytes, comprehensive lists are provided elsewhere (Davison, 2016).

### 2.4.6a Background Mass and Adsorption Maximum

The background mass, and adsorption maximum are important binding layer characteristics, that should be defined for binding layers. It is best practice to determine adsorption and background mass for each binding layer formation protocols. Differences in protocols, for the same binding gel have been reported (Corbett et al., 2019; Huang et al., 2016a).

The background mass is the analyte mass present on the binding layer before the DGT are deployed. This should be determined for each set of gels made, to monitor and account for possible contamination during the experimental process (Cai et al., 2017). The method detection limit is commonly calculated as three times the standard deviation of the blank value (Cai et al., 2017). The lower background mass and the greater the reproducibility, the better the binding gel is at determining low concentrations. Diffusive Gradients in Thin Films is an accumulative technique, therefore the material detection limit varies with both time and solution concentration (Cai et al., 2017).

Adsorption maximum, saturation point or intrinsic binding capacity, the total mass capable of being bound to the binding layer, also determines the ability of a binding layer to accurately determine solution concentration. This must be sufficiently large, such that it the binding layer does not become saturated during DGT deployment. If it becomes saturated, as stated earlier, the concentration gradient through the hydrogel is no longer maintained and therefore the DGT theoretical requirements are no longer met (Davison, 2016). It may be the case that adsorption is not linear up until saturation, as the number of binding sites available decreases with adsorption and the rate of adsorption decreases (Corbett et al., 2019).

### 2.4.6b Available Binding Layers

There are numerous binding layers available for use in DGT. The binding layers considered in this research for nitrate are detailed below Table 2.2. A bromide selective binding was developed over the course of this research project, based on Purolite Bromide Plus, for the determination of flow rates (Corbett et al., 2021). This is the first reported bromide selective DGT.

Table 2.2 Available Binding Layers for Nitrate.

| Analyte | Binding Layer | Uptake Efficiency | Reference |
|---|---|---|---|
| $NO_3^-$ | Purolite A520E | >98% (pH 3.5 - 8.5) | (Huang et al., 2016a) |
| | AMI-7100 | 96.7 ± 3.3% (pH 3.5 - 8.5) | (Huang et al., 2016a) |
| | SIR-100-HP | - (pH 3-8) | (Cai et al., 2017) |

Binding layers can be prepared in a multitude of ways, these are detailed in the following section.

### 2.4.6c Hydrogel Binding Layer Formation

As discussed in Section 2.4.5a, DGT hydrogels are generally formed via radical solution polymerisation. The development of binding layers, however, involves the suspension of particles within the hydrophilic network. There are numerous methods for suspending particles in hydrogels: (1) hydrogel formation in a particle suspension; (2) physical incorporation after gelation; (3) reactive formation aided by the hydrogel network; (4) nanoparticles as cross-linkers; (5) and using nanoparticles, polymers and distinct gelators (Thoniyot et al., 2015). The method used depends on the hydrogel, particle used and the desired properties of the composite (Thoniyot et al., 2015).

DGT binding layers are generally formed via hydrogel formation in a particle suspension, because many DGT binding layers are based on the suspension of cationic/anionic exchange resins and metal hydroxides particles, generally < 100 µm, within the hydrogel framework (Davison, 2016). Such as for cation selective Chelex (Zhang & Davison, 1995), phosphate selective ferrihydrite (Zhang et al., 1998), nitrate selective Purolite A520E (Corbett et al., 2019; Huang et al., 2016a), and bromide selective Purolite Bromide Plus binding layers (Corbett et al., 2021).

Liquid binding layers have been reported for arsenic, and cadmium and copper based on nanoparticulate Fe3O4 and poly(4-styrenesulfonate) respectively (Li et al., 2003; Liu et al., 2016). These systems required a change in the design of the DGT solution probe, to include a chamber to hold the solution (Figure 2.5), however it enables the application of a wide range of potential solutions as binding layers.

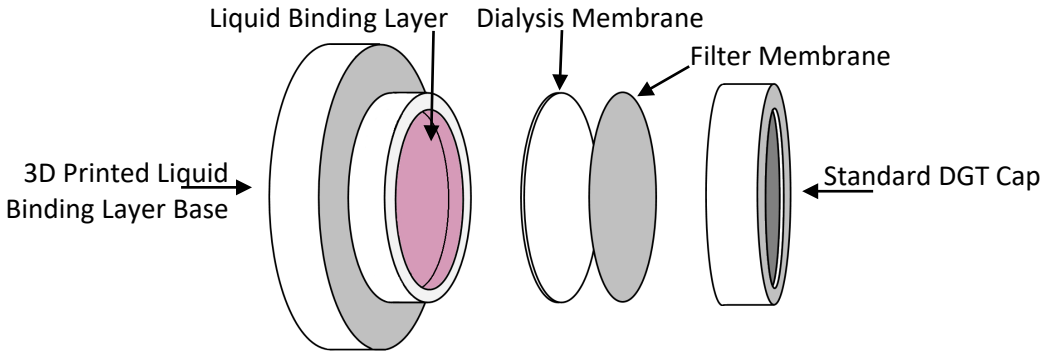


Figure 2.5: Schematic of liquid binding phase DGT (Chapter 4).

### *2.4.8 Diffusion Coefficient*

Analyte diffusion coefficients are temperature dependent (Davison, 2016). The Stokes-Einstein equation (Equation (2.10) links temperature dependence to the viscosity of water (η), the diffusion coefficient (D) and the absolute temperature (T) (Davison, 2016).

$$\frac{D_1\eta_1}{T_1^K} = \frac{D_2\eta_2}{T_2^K} \tag{2.10}$$

The viscosity of water where temperature is given in degrees Celsius is given by Equation (2.11) (Davison, 2016).

$$log\frac{\eta_{25}}{\eta_T} = \frac{1.37023(T-25) + 0.000836(T-25)^2}{109+T} \tag{2.11}$$

The following equation enables correction of the diffusion coefficient at 25°C to any temperature (Davison, 2016).

$$logD_T = \frac{1.37023(T-25) + 0.000836(T-25)^2}{109+T} + log\frac{D_{25}(273+T)}{298} \tag{2.12}$$

The diffusion coefficient of nitrate/nitrite, and bromide through the standard APA DGT diffusive layer are 1.46 x $10^{-5}$, and 1.29 x $10^{-5}$ $cm^2$ $s^{-1}$ (Corbett et al., 2021; Huang et al., 2016a), and 1.49 x $10^{-5}$, and 2.13 x $10^{-5}$ $cm^2$ $s^{-1}$ through water at 25 °C respectively (Lide, 1999; Picioreanu et al., 1997; Yuan-Hui & Gregory, 1974).

### 2.4.8a Determination of Diffusion Coefficient

If the diffusion coefficient through the diffusive layer is unknown there are two commonly deployed methods for determining it: (1) using DGT of different diffusion layer thicknesses in controlled solution; and (2) diffusion cell.

In the first method, multiple sets of DGT with different material diffusion layer thicknesses are deployed concurrently and removed at different time intervals. Temperature is monitored throughout, and the accumulated mass is analysed for each DGT to which the previously determined elution and uptake factors are applied. The concentration determined by DGT ($C_{DGT}$), if the binding layer meets the theoretical requirements (discussed above), is the same as the concentration of the bulk solution (Davison, 2016). The relationship between the accumulated mass and $C_{solution}$ provides a calibration curve with the following slope equation, where $A_{eff}$ = effective area due to lateral diffusion ($cm^2$), t = time/length of deployment (s), $D_{mdl}$, $D_w$ = material diffusion layer and water diffusion coefficients respectively ($cm^2$ $s^{-1}$), and $\delta_{mdl}$, $\delta_{dbl}$ = material diffusion layer and diffusive boundary layer thicknesses respectively (cm) (Davison, 2016). The equation can be rearranged to solve for $D_{mdl}$.

$$\boldsymbol{Slope} = \boldsymbol{A_{eff}t}\left(\frac{\boldsymbol{D_{mdl}D_w}}{\boldsymbol{\delta_{mdl}D_w} + \boldsymbol{\delta_{dbl}D_{mdl}}}\right) \quad (2.13)$$

The second method utilises a diffusion cell (Figure 2.6). Two chambers are connected through a window of known diameter (Zhang et al., 1998). A hydrogel of thickness δ is secured in the window with area A, by clamping the two chambers together. In one chamber (X) a high concentration solution of the analyte, in the other (Y) milliQ water (Zhang et al., 1998). The solutions should be held at a constant temperature and vigorously stirred throughout (Davison, 2016). Transport between the two chambers is restricted to diffusion, and calculation of the diffusion coefficient is based on Fick's First

Law (Equation (2.1) (Davison, 2016; Zhang et al., 1998). Sub-samples, representing a very small fraction of total volume, are periodically taken for analysis, and used to calculate the mass diffused from X to Y (Davison, 2016). The concentration (C) in Equation (2.1) represents the concentration difference between the source and receiving solutions, however if there is negligible change in the concentration of the analyte in X during the first few hours, C is effectively constant and equal to the concentration in the source solution (X) (Davison, 2016; Zhang et al., 1998). The slope of the accumulated mass in the receiving solution (Y) plotted against time can be combined with Equation (2.1) to give Equation (2.14), for determining the diffusion coefficient (D) (Davison, 2016; Zhang et al., 1998).

$$\boldsymbol{D = \frac{slope \times \delta}{A\partial C}} \tag{2.14}$$

The experiment should be conducted multiple times using hydrogels of various thicknesses to determine the effect of a diffusive boundary layer at either side of the hydrogel (Scally et al., 2006).

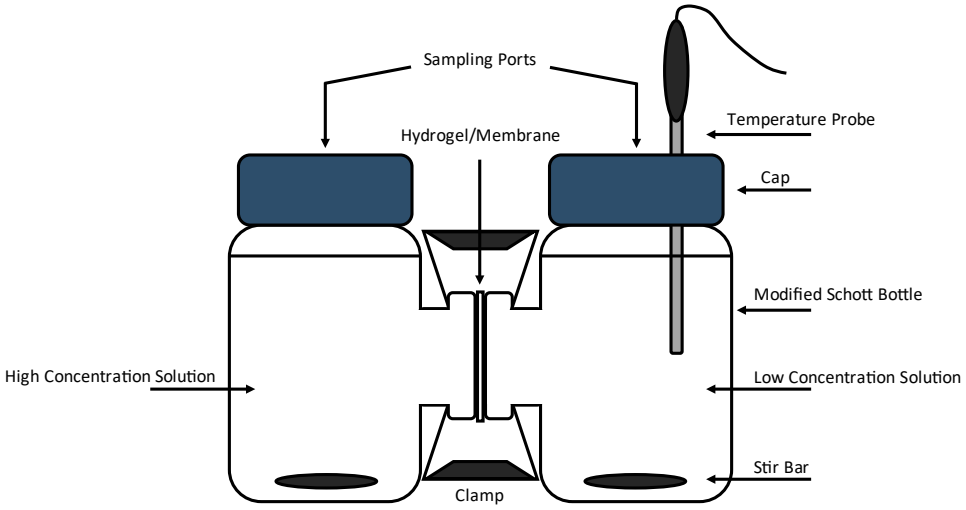


Figure 2.6: Diaphragm diffusion cell schematic.

The diffusion layer through the polyethersulfone filter membrane is often treated as the same as through the APA diffusive layer because they are indistinguishable (Davison, 2016). Monitoring of temperature throughout the deployments is necessary for the temperature correction of diffusion coefficients, using Equation (2.12) (Davison, 2016).

### *2.4.9 Full DGT Equation*

For use of DGT in well-stirred solutions DBL is generally ignored on the assumption that compared to the total thickness of Δg, it is negligibly small (Warnken et al., 2006). Measurements in synthetic solutions utilising different Δg found that the DBL was approximately 0.23 mm in well and moderately stirred solution, but substantially larger in poorly and unstirred solutions (Corbett et al., 2019; Warnken et al., 2006).

Measurements using 0.80 mm diffusive gel in well-stirred solutions found that neglecting the DBL and the effective geometric area offset each other, producing an error <±10% (Warnken et al., 2006). Implicitly, the standard DGT equation (Equation (2.6) corrects for DBL induced decrease in flux and increased flux due to lateral diffusion not accounted for, as they tend to cancel each other out (Kreuzeder et al., 2015; Warnken et al., 2006).

It is best practice, however, to utilise the full DGT equation (Equation (2.15), because although the even if the effects of the DBL and lateral diffusion (discussed in Section 2.4.5 Diffusion Layer) cancel each other out, their measured uncertainties do not and must still be accounted for (Kreuzeder et al., 2015). Lastly, the binding gel layer does not need to be considered, as it is adjacent to the diffusive gel, and is therefore unlikely to contribute significantly to Δg (Warnken et al., 2006).

The expanded DGT equation (Equation (2.15) is given below: where, M = accumulated mass on binding layer; $A_{eff}$ = effective exposure window area; t = length of deployment; Δg, f, and δ = diffusive gel, filter membrane and DBL thicknesses respectively; $D_{gel}$, $D_f$, $D_w$ = diffusive gel, filter membrane and water diffusion coefficients respectively (Kreuzeder et al., 2015).

$$\boldsymbol{C = \frac{M}{A_{eff}t}\left(\frac{\Delta g_{gel}}{D_{gel}} + \frac{\Delta_f}{D_f} + \frac{\delta}{D_w}\right)} \quad (2.15)$$

$D_{gel} \approx D_f$ in commonly used DGT devices, therefore $\Delta_f$ and $\Delta g_{gel}$ can be treated singularly as Δg (Kreuzeder et al., 2015; Scally et al., 2006). If a small pore size diffusive gel (restricted gel) and a filter

membrane is utilised the diffusion coefficients may differ enough that it is necessary to take into account the difference in diffusion between them (Scally et al., 2006).

### *2.4.10 Diffusive Boundary Layer Calculation*

The Diffusive Boundary Layer (DBL), introduced earlier, is the area of solution at the filter/solution interface with reduced analyte concentration in relation to the rest of solution (Corbett et al., 2019). As stated earlier, it is necessary to include the DBL in $C_{DGT}$ calculations due to the associated error, because it increases the effective diffusive pathway length, increasingly as flow decreases (Corbett et al., 2019).

The DBL can be calculated by plotting 1/M for different gel thicknesses versus δ, and by combining the slope and intercept (Equations (2.16) and (2.17) to give Equation (2.18) (Levy et al., 2011; Zhang et al., 1998).

$$\boldsymbol{slope(s)} = \frac{\mathbf{1}}{\boldsymbol{C_{DGTe}A_{eff}D^{mdl}t}} \tag{2.16}$$

$$\boldsymbol{intercept(y)} = \frac{\boldsymbol{\delta}}{\boldsymbol{C_{DGTe}A_{eff}D^{w}t}} \tag{2.17}$$

$$\boldsymbol{\delta} = \frac{\boldsymbol{yD^{w}}}{\boldsymbol{sD^{mdl}}} \tag{2.18}$$

δ is unlikely to be of constant thickness due to variations in the convective regime during deployment in natural waters (Davison, 2016). A mean value can be calculated for the deployment period by using a set of devices with a range of material diffusion layer thicknesses and plotting 1/M for different gel thicknesses versus δ, as stated above (Davison, 2016; Levy et al., 2011; Zhang et al., 1998). Assuming that each device experiences the same flow regime, and thus same convective regime and effective DBL (Davison, 2016). The analyte must also be fully labile, so that the measurement of δ is not affected by kinetic effects (Davison, 2016).

## 2.5 Colourimetric Determination of Nitrate

Nitrate and bromide solution concentrations, in this research, were analysed alongside commercial anion standards (Dionex Seven Anion Standard) using a Dionex ICS-200 Ion Chromatograph (Dionex,

California, United States) (Corbett et al., 2019). A gradient concentration method was used to give optimal peak resolution, ensuring that the chloride binding gel eluent peak does not overlap the other peaks (Corbett et al., 2019). Concentration values were converted to mass and the appropriate elution and uptake factors applied (Corbett et al., 2019), for inclusion into the full DGT equation (Equation (2.15) (Davison, 2016).

The following section is intended to detail the many available colourimetric analysis procedures, and the advantages of incorporating reagents into hydrogels. It is not however an exhaustive list, instead it is intended to provide an understanding of the methods available and outline the rational for the methods chosen to develop for incorporation into hydrogels for use in DGT. Incorporation of colourimetry into the nitrate-DGT method provides an opportunity to overcome the need for laboratory analysis of nitrate-DGT.

### *2.5.1 Nitrate*

For the determination of nitrate determination in water samples nitrate has customarily been reduced to nitrite (Equation (2.19) and reacted with colour reagents (Section 2.5.1a) (Nydahl, 1976). A list of potential reducing agents is provided in Table 2.3.

$$\boldsymbol{NO_3^- + 2H^+ + 2e^- \rightarrow NO_2^- + H_2O} \qquad (2.19)$$

Reduction efficiency is dependent on the reductant composition, its effective surface area, and the incident time/flow rate (Hydes & Hill, 1985; Nydahl, 1976). Reduction, however, does not necessarily terminate at $NO_2^-$, it can also proceed to $NH_3$ and $NH_4^+$, and $NO_x$ gaseous species (Hydes & Hill, 1985; Nydahl, 1976)(Chapter 4).

Table 2.3: Potential reductants for incorporation into the diffusive layer.

| Reductant | Reduction Pairs | $E^0$ (volts) | Reference |
|---|---|---|---|
| Cadmium | $Cd^{2+} + 2e^- \rightarrow Cd$ | -0.4025 | (Bard et al., 1985) |
| Amalgamated Cadmium | $Cd^{2+} + Hg + 2e^- \rightarrow Cd(Hg)$ | -0.3515 | (Bard et al., 1985) |
| Copperised Cadmium | $Cd^{2+} + Cu + 2e^- \rightarrow Cd(Cu)$ | -0.743 | (Hydes & Hill, 1985) |
| Silverised Cadmium | $Cd^{2+} + Ag + 2e^- \rightarrow Cd(Ag)$ | -1.202 | (Bard et al., 1985; Nydahl, 1976) |
| Iron | $Fe^{2+} + 2e^- \rightarrow Fe$ | -0.44 | (Bard et al., 1985) |
| | $Fe^{3+} + e^- \rightarrow Fe^{2+}$ | 0.771 | (Bard et al., 1985) |
| | $Fe^{3+} + 3e^- \rightarrow Fe$ | -0.037 | (Bard et al., 1985) |
| Zinc | $Zn^{2+} + 2e^- \rightarrow Zn$ | -0.7626 | (Bard et al., 1985) |
| Hydrazine Copper | $Cu^{2+} + 2e^- \rightarrow Cu$ | | (Bard et al., 1985; Nydahl, 1976) |
| Vanadium(III) | $VO^{2+} + 2H^+ \leftrightarrow V^{3+} + H_2O$ | 0.359 | (Hendrix & Braman, 1995) |
| | $VO^{2+} + H^+ + e^- \leftrightarrow VOH^{2+}$ | 0.164 | (Hendrix & Braman, 1995) |
| | $VO^{2+} + e^- \leftrightarrow VO^+$ | -0.44 | (Hendrix & Braman, 1995) |
| Nitrate Reductase | $NADH + NO_3^- \rightarrow NAD^+ + OH^- + NO_2^-$ | 0.74 | (Campbell, 1999) |

The reduction of nitrate to nitrite has commonly used zinc (Morita & Nakamura, 2008), and various forms of cadmium (precipitated, pure filings, or amalgamated) (Nydahl, 1976), as the electron source. Alternative reduction reactions can involve vanadium (III) (Schnetger & Lehners, 2014), and nitrate reductase (Campbell, 1999). Zero-valent iron (ZVI), ferrous ion, sulphur and hydrogen have also been reported for the determination and remediation of nitrate (Zhu & Getting, 2012). Bimetallic nanoparticles based on zero-valent iron such as Cu, Pd, Pt, Ni and Ag (Muradova et al., 2016), and magnetite doped ZVI have also been reported (Cho et al., 2015).

Nanoparticles provide greater reduction rates in comparison to their macro-particle counterparts due to their greater surface area, however, the increased oxidation of the metal reductants poses stability and shelf life challenges (Liu & Wang, 2019; Muradova et al., 2016). There are procedures for the enhancement of iron stability and therefore enhance redox performance catalytically, such as the introduction of noble metals onto the nano-ZVI surface (Muradova et al., 2016).

Hydrogel supports help overcome the aggregation, oxidation and inactivation challenges facing the use of metal nanoparticles (Sahiner et al., 2010). As discussed above suspension of particles in hydrogels can also improve mechanical strength (Thoniyot et al., 2015). Hydrogel composites have been reported to provide superior functionality to the composite materials, including bio-sensing, nano-medicine, and environmental remediation (Thoniyot et al., 2015). Halting aggregation increases nanoparticle surface area, and decreases the total mass of nanoparticle required to achieve complete nitrate reduction within the diffusive gel (Liu & Wang, 2019). Electron transfer can be mediated by the support matrix, nucleating product phase growth (Liu & Wang, 2019). Additionally, suspension of zero-valent metal nanoparticles (nZVM) in hydrogels increases the stability and shelf-life of the nanoparticles (Sahiner, 2013). Hydrogels can also resolve many of the environmental concerns associated with using zero-valent metal nanoparticles by encapsulating the often toxic metal nanoparticles (Sahiner, 2013). Toxicity of the reductants should also be considered, because if the DGT system is lost it could be a source of toxic metals (Chapter 4).

### 2.5.1a Azo-coupling and Diazotisation

Colourimetric determination of nitrate, as discussed above, typically involves the reduction to nitrite followed by the reaction with diazotisation and azocoupling reagents. Diazotisation and azocoupling reactions produce coloured azo compounds when reacted with nitrite (Knyazev et al., 2002). Commonly referred to as the Griess reaction (Figure 2.7), many modifications have been made to reduce toxicity and simplify the methodology.

The Griess reaction involves diazotisation of an aromatic ring with nitrite followed by the coupling with an aromatic amine or phenol (Tarafder & Rathore, 1988). These reactions have shown to be sensitive and selective, however they require long coupling times and, during diazotisation, close control of pH and temperature (Tarafder & Rathore, 1988), reagent concentration and reaction time also require optimisation (Irandoust et al., 2013).

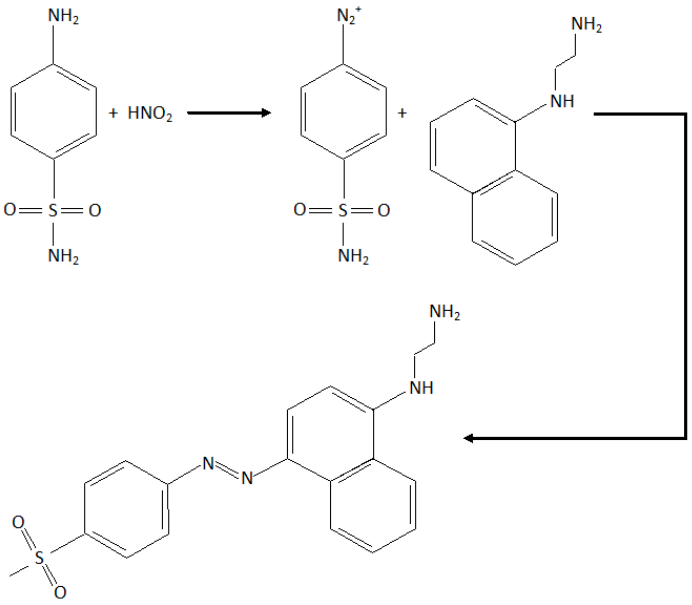


Figure 2.7: Two-step azo-dye formation - diazotisation of nitrite (as a conjugate acid) with sulphanilamide followed by coupling with N-(1-naphthyl)ethylenediamine (Griess reaction).

The standard Griess reaction (sulfanilamide diazotisation and N-(1-naphthyl)ethylenediamine coupling) has two major disadvantages: (1) diazotisation and azo-coupling reactions require different acidity conditions and low temperatures; and (2) N-naphthylamine azo coupling reagent is readily oxidised and strongly carcinogenic (Knyazev et al., 2002). These disadvantages have resulted in extensive research into alternative reagents to simplify the methodology and reduce toxicity, summarised in Table 2.4.

Table 2.4: Summary of reagents for the colourimetric determination of nitrite.

| Reagents | Determination Range (mg/L) | Detection Limit (mg/L) | Reference |
|---|---|---|---|
| Sulfanilamide and N-naphthylethylenediamine | - | - | (Davison, 2016) |
| Sulfanilamide, sulfamethizole and sulfadimidine with sodium 1-naphthol-4-sulfonate | 0.002-0.04 | 0.001 | (Wang et al., 1998) |
| Sulphanilamide with N-(1-naphthyl)ethylenediamine dihydrochloride | 0.02-1.6 | 0.01 | (López Pasquali et al., 2007) |
| Sulphanilamide with N-(1-naphthyl)ethylenediamine dihydrochloride | 0.05-1.6 | 0.02 | (Pasquali et al., 2010) |
| m-Nitroaniline with 1-naphthylamine | 0.01-1.7 | 0.0005 | (Irandoust et al., 2013) |
| p-Nitroaniline with 1-naphthol into thin layer of polyurethane foam | - | 0.005 | (Abbas & Mostafa, 2000) |
| p-Nitroaniline and sulfanilamide with ethyl acetoacetate | 0.05-6.0, 0.2-3.0 | - | (Sreekumar et al., 2003) |
| p-Nitroaniline chromotropic acid | ≤0.0375 | 0.0006 | (Ivanov et al., 2004) |
| p-Nitroaniline with acidified diphenylamine and Triton X-100 micellar media | 0.05-0.08 | 0.01 | (Afkhami et al., 2004) |
| Phloroglucinol (1,3,5 trihydroxybenzene) and phenolic compound | 0.03-0.3 | 0.003 | (Burakham et al., 2004) |
| Sulfanilic acid with 1-naphthol | 4.0-20.0 | - | (Kiso et al., 2006) |
| p-Aminophenylmercaptoacetic acid and N-naphthylethylenediamine | 0.02-0.80 | - | (Tarafder & Rathore, 1988) |
| p-Aminophenylmercaptoacetic acid and 8-hydroxyquinoline | - | - | (Tarafder & Rathore, 1988) |
| p-Aminophenylmercaptoacetic acid and 1-naphthol | - | - | (Tarafder & Rathore, 1988) |
| 4-Amino-5-hydroxynaphthalene-2,7-disulphonic acid monosodium salt | 0.1-1.6 | 0.008 | (Nagaraja et al., 2010) |
| Safranin O and pyrogallol | 0.23 | 0.005 | (Filik et al., 2011) |
| Safranin O | 0.0001-3.00, 0.03-4 | 0.0005, - | (Kazemzadeh & Ensafi, 2001; Mousavi et al., 1998) |
| Safranin O bound to cellulose acetate film | 0.005-2.00 | 0.001 | (Ensafi & Kazemzadeh, 2002) |
| Aza-BODIPY | - | 0.02 | (Adarsh et al., 2013) |
| Phosphomolybdenum blue complex | 0.05-1.15 | 0.01 | (Monser et al., 2002) |

While sensitivity has been improved and toxicity reduced from the standard Greiss system they remain two step reactions which require the close control of pH or temperature, and in some cases pre-concentration. These requirements largely preclude the incorporation of Greiss reagents into the DGT system, however as discussed later the reagents have been incorporated in optical sensing film and gold nanoparticle systems.

### 2.5.1b Optical sensing films

Optical sensing films, based on the immobilisation of Greiss reagents onto transparent supports for the colourimetric determination of nitrite in freshwater (Adarsh et al., 2013; Ensafi & Kazemzadeh, 2002). They are designed to overcome many of the methodological limitations of solution Greiss reagents (discussed above), however limitations, such as reaction conditions, preclude the incorporation of optical sensing films into DGT for *in situ* determination of nitrite. Two example systems are detailed below.

Ensafi et al. (2002) describe a Safranin O based sensor for the direct determination of nitrite in acidic media (Ensafi & Kazemzadeh, 2002). Safranin O is immobilised through covalent bonding to an optically transparent acetyl-cellulose membrane, which has been hydrolysed and activated using thiourea and polyvinyl alcohol (Ensafi & Kazemzadeh, 2002).

An aza-BODIPY based nitrite sensor, developed by Adarsh et al. (2013), selectively recognises nitrite ions to 20 ppb, with a visible detection limit of 1ppm, providing a distinct colour change from bright blue to intense green. A dipstick was created by coating a glass support with the aza-BIDOPY alumina slurry, and protonating it by exposing it to HCl gas (Adarsh et al., 2013). Negligible changes in the absorption spectra were observed during titration experiments with high concentrations of potentially competing biologically relevant anions ($SO_4^{2-}$, $Cl^-$, $HSO_3^-$, $CO_3^{2-}$, $CH_3COO^-$, $NO_3^-$, $S_2O_3^{2-}$, and $N_3^-$) (Adarsh et al., 2013).

### 2.5.1c Gold Nanoparticles

The properties of gold nanoparticles, make their use advantageous over other metallic nanoparticles, such as, their distance dependant optical properties (Lee et al., 2008), well defined colour change (Gunupuru et al., 2014), and high stability (Zhang et al., 2014). AuNP strongly absorb in the visible light region due to surface plasmon resonance, producing strong absorption peak at about 520nm in the Au-NP UV-vis spectra (Nam et al., 2014). The incident electromagnetic field frequency is resonant with the coherent oscillation of Au-NP surface electrons (Nam et al., 2014).

Colour change methods based on cross-linking/aggregation, de-protection, and anti-aggregation have been reported. Cross-linking produces a colour response when the target molecule decreases interparticle distances, causing aggregation (Tsogas et al., 2018). Free specific aptamers weakly bound to the gold nanoparticle surfaces are detached by the target compound thereby producing a colour change, in de-protection methods (Chen et al., 2015b; Liu et al., 2018). During anti-aggregation physiochemical interactions between the target analyte and nanoparticle cross-linking agents inhibits pre-existing cross-linking thereby creating a colour response (Liu et al., 2018).

Gold and silver nanoparticles with varying degrees of selectivity for nitrite have been reported (Amanulla et al., 2017; Daniel et al., 2009; Ibrahim et al., 2019; Nam et al., 2014; Perez-Coronado et al., 2017). Three Au-NP systems are reported below, as examples of potential systems for adaptation in this research.

Isotopically functionalised polyvalent gold nanoparticles with thiolated Greiss reaction precursors, produced a distinct colour change (from red to colourless) upon reaction with nitrite (Daniel et al., 2009). A kinetically controlled end point provided nitrite concentration (Daniel et al., 2009). The nanoparticle probes are interconnected covalently, turning colourless, via two processes: (1) diazotisation of the aniline AuNP under acidic conditions; and (2) coupling with naphthalene AuNP (Daniel et al., 2009). The system is highly sensitive for nitrite, no response was elicited from testing potentially interfering anions ($NO_3^-$, $F^-$, $SO_4^{2-}$, $Br^-$, $ClO^{4-}$, $CH_3COO^-$, $S_2O_3^{2-}$, $C_2O_4^{2-}$, $N_3^-$ and $HCO_3^-$) (Daniel et al., 2009). The system is designed to identify nitrite concentrations above 0.998ppm at 95$^oC$ with a 25 minute incubation period, above ~1.4ppm nearly all functionalised AuNP react and precipitate, producing a clear solution (Daniel et al., 2009).

Nam et al. (2014) developed an Au-NP system, based on 1-(2-mercaptoethyl)-1,3,5-triazinane-2,4,6-trione (thiol-functionalised cyanuric acid) bound to gold nanoparticles via ligand-exchange reaction. The nitrite ion appears to act as a molecular bridge, forming hydrogen bonds with the NH groups of the 1-(2-mercaptoethyl)-1,3,5-triazinane-2,4,6-trione AuNP, reducing the inter-particle distance and

inducing aggregation which results in a colour change from wine-red to purple-grey (Nam et al., 2014). The detection sensitivity improved in acidic solution, and was optimal at pH = 5.0 (Nam et al., 2014). Reaction times were inversely proportional to concentration; at nitrite concentrations of 1, 2, 3, 4, and 5 ppm the respective reaction times are 100, 70, 50, 35, 30 min (Nam et al., 2014). All testing was undertaken at room temperature (Nam et al., 2014).

Amanulla et al. (2017) report a chitosan stabilised gold nanopatricle decorated reduced graphene oxide (AuNP-rGO/CS), used in this research. Aggregation of the chitosan-stabilised gold nanopatricles, arising from their closer formation, produced a wine red to purple colour change (Amanulla et al., 2017). The sensor detected a linear nitrite response from 1 to 20 µmol $L^{-1}$, with a 0.1 µmol $L^{-1}$ detection limit (Amanulla et al., 2017). The sensor displayed high selectivity towards nitrite due to the specify of chitosan amines within the AuNP-rGO/CS to nitrous acid, addition of relevant environmental ions (20 µmol $L^{-1}$ of F-, Br-, CN-, SO42-, PO43-, C2O42-, CO32-, NH4+ and NO3-) did not affect the colour at room temperature and natural pH (Amanulla et al., 2017).

### *2.5.2 Analysis of Hydrogel Colour Change*

Colourimetric determination typically utilises spectrophotometer, measuring the absorbance or transmittance of a solution at a specific wavelength. The concentration is solved for against a calibration curve. Raman and UV-vis spectroscopy have been utilised to quantify colour changes of gold nanoparticles (Amanulla et al., 2017). These are not practical solutions for the in-field determination of colour (Chapter 4).

The colour change gels and liquid binding layers can be photographed and the RGB (red, green, blue) composition analysed (Chapter 4). Colour intensity can be determined relating the RGB values to the mass of analyte bound to the binding layer (Chapter 4).

The effective intensity ($A_x$) can be calculated using the following equations, where $R_s$, $G_s$ and $B_s$ are the sample RGB values, and $R_b$, $G_b$ and $B_b$ are the blank RGB values (Das & Sarkar, 2016)(Chapter 4).

$$\boldsymbol{A_R = -\log\left(\frac{R_s}{R_b}\right)} \tag{2.20}$$

$$\boldsymbol{A_G = -\log\left(\frac{G_s}{G_b}\right)} \tag{2.21}$$

$$\boldsymbol{A_R = -\log\left(\frac{B_s}{B_b}\right)} \tag{2.22}$$

## 2.6 Determination of Flowrates and Nutrient Loadings

Nitrate DGT provide a useful understanding of concentrations of the major limiting nutrients in water ecosystems, however it is important to consider the loading of the system. Loading is the rate of supply of a particular entity to receiving waters, and is important because ecosystem responses depend on the export and import of nutrients (Pinckney et al., 2001).

Loading is often expressed as tons of X per year, and is calculated by multiplying concentration by discharge or flowrate (Pinckney et al., 2001). The measurement accuracy of these two variables and the frequency of the measurements over the course of the measurement time determines the accuracy of the calculated loading rate (Pinckney et al., 2001).

These factors are especially important in episodic events, due to the large volumes of water added to the system (Pinckney et al., 2001). Nutrient loading during these events can exceed the total loading for the rest of the year, and although the increased volume may dilute nutrient concentration the total load may still be high (Pinckney et al., 2001). The advantage of using DGT is their robustness, if properly secured the sensors can continue to operate under these conditions. In contrast, traditional measurement instrumentation is frequently damaged and water samples are not collected due to the risk to personnel safety (Pinckney et al., 2001). The loading events are therefore missed or approximated to low accuracy (Pinckney et al., 2001).

### *2.6.1 Trace Dilution Flowrate*

There are numerous methods for determining flowrate, such as the float, dilution gauging, flume, and acoustic doppler methods. It is the intention of this section to introduce the tracer dilution method, comprehensive reviews of methods for determining flowrate are provided elsewhere (Dobriyal et al., 2017).

Tracer analysis via salt dilution is a commonly used technique for gauging stream flow, particularly where other measurement techniques are unreliable or not possible (Moore, 2004). A schematic of how tracer dilution field experiments are undertaken is provided below (Figure 2.8).

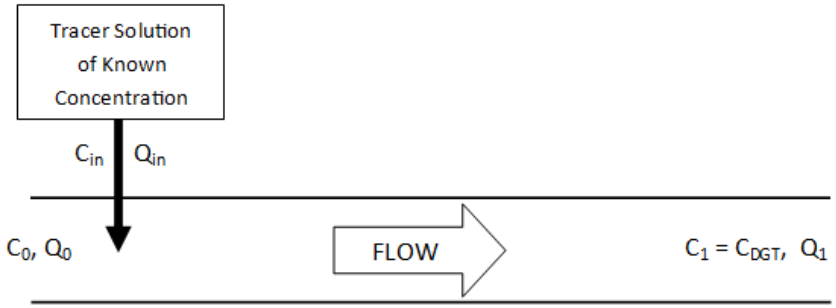


Figure 2.8: Schematic of a theoretical tracer experiment. Where C = concentration, and Q = flow of the tracer solution, and points 0 and 1 respectively.

When water with a flow rate of $Q_0$ (flow before tracer injection) with tracer concentration $C_0$, and a tracer with concentration $C_i$ is injected with flow rate $Q_{in}$, the sum is the mixed flow rate $Q_1$ and concentration $C_1$ downstream (Equations (2.23) and (2.24) (Lee et al., 2007). Importantly this assumes complete mixing of the injected tracer, such that at the downstream measurement location the concentration is uniform (Lee et al., 2007).

$$\boldsymbol{C_0 Q_0 + C_{in} Q_{in} = C_1 Q_1} \tag{2.23}$$

$$\boldsymbol{Q_0 + Q_{in} = Q_1} \tag{2.24}$$

By combining and rearranging these two equations, the following equation for $Q_0$ is obtained (Lee et al., 2007).

$$\boldsymbol{Q_0 = \frac{C_1 - C_{in}}{C_0 - C_1} \times Q_{in}} \tag{2.25}$$

There are three criteria that must be met for the equation to stand for the use of DGT: (1) $Q_{in}$ and $C_{in}$ must be constant; (2) DGT deployment must be after the tracer has begun to flow past the deployment site; and (3) the time must be accurately known, for accurate calculation of $C_{DGT}$ and therefore $Q_0$ (Lee et al., 2007).

Sodium chloride is often used for salt tracer analysis because it is inexpensive and environmentally benign as long as the concentration remains below thresholds associated with ecological impacts (Moore, 2004). In such analyses conductivity is measured, however conductivity can vary considerably between sites due to dissolution and precipitation, adding uncertainty (Moore, 2004). It is preferential to measure the concentration of a known species, which if present are of very low concentration and are environmentally benign. Diffusive Gradients in Thin Films is ideally suited to this application, because it is accumulative and can be used to determine very low concentrations.

Bromide tracers have been widely used for characterisation of streams, rivers, groundwater, and aquifer flow conditions (Ma et al., 2012). Bromide tracers have proven useful for characterising and modelling highly dynamic flow fields (Ma et al., 2012).

# References


ABBAS, M. N., & MOSTAFA, G. A. (2000). Determination of traces of nitrite and nitrate in water by solid phase spectrophotometry. *Analytica Chimica Acta, 410*(1), 185-192. doi:https://doi.org/10.1016/S0003-2670(00)00736-4

ADARSH, N., SHANMUGASUNDARAM, M., & RAMAIAH, D. (2013). Efficient Reaction Based Colorimetric Probe for Sensitive Detection, Quantification, and On-Site Analysis of Nitrite Ions in Natural Water Resources. *Analytical Chemistry, 85*(21), 10008-10012. doi:10.1021/ac4031303

ADDY, K., GOLD, A. J., CHRISTIANSON, L. E., DAVID, M. B., SCHIPPER, L. A., & RATIGAN, N. A. (2016). Denitrifying Bioreactors for Nitrate Removal: A Meta-Analysis. *Journal of Environmental Quality, 45*(3), 873-881. doi:10.2134/jeq2015.07.0399

AFKHAMI, A., MASAHI, S., & BAHRAM, M. (2004). Spectrophotometric Determination of Nitrite Based on Its Reaction with p-Nitroaniline in the Presence of Diphenylamine in Micellar Media. *Bulletin of the Korean Chemical Society, 25*(7), 1009-1011.

AHMED, E. M. (2015). Hydrogel: Preparation, characterization, and applications: A review. *Journal of Advanced Research, 6*(2), 105-121. doi:https://doi.org/10.1016/j.jare.2013.07.006

ALLABY, M. (2010). Eutrophication. In *A Dictionary of Ecology* (4 ed., pp. 141): Oxford University Press.

AMANULLA, B., PALANISAMY, S., CHEN, S.-M., CHIU, T.-W., VELUSAMY, V., HALL, J. M., CHEN, T.-W., & RAMARAJ, S. K. (2017). Selective Colorimetric Detection of Nitrite in Water using Chitosan Stabilized Gold Nanoparticles Decorated Reduced Graphene oxide. *Scientific Reports, 7*(1), 14182. doi:10.1038/s41598-017-14584-6

AUDET, J., MARTINSEN, L., HASLER, B., DE JONGE, H., KARYDI, E., OVESEN, N. B., & KRONVANG, B. (2014). Comparison of sampling methodologies for nutrient monitoring in streams: uncertainties, costs and implications for mitigation. *Hydrology and Earth System Sciences, 18*(11), 4721-4731. doi:10.5194/hess-18-4721-2014

BARD, A. J., PARSONS, R., JORDAN, J., INTERNATIONAL UNION OF, P., & APPLIED, C. (1985). *Standard potentials in aqueous solution*. New York: New York : M. Dekker.

BRANDL, H., & W. HANSELMANN, K. (1991). Evaluation and application of dialysis porewater samplers for microbiological studies at sediment-water interfaces. *Aquatic Sciences, 53*, 55-73. doi:10.1007/BF00877075

BURAKHAM, R., OSHIMA, M., GRUDPAN, K., & MOTOMIZU, S. (2004). Simple flow-injection system for the simultaneous determination of nitrite and nitrate in water samples. *Talanta, 64*(5), 1259-1265. doi:https://doi.org/10.1016/j.talanta.2004.03.059

CAI, C., WILLIAMS, P. N., LI, H., DAVISON, W., WEI, T.-J., LUO, J., ZHU, Y.-G., & ZHANG, H. (2017). Development and Application of the Diffusive Gradients in Thin Films Technique for the Measurement of Nitrate in Soils. *Analytical Chemistry, 89*(2), 1178-1184. doi:10.1021/acs.analchem.6b03609

CAMPBELL, W. H. (1999). Nitrate Reductase Structure, Function and Regulation: Bridging the Gap between Biochemistry and Physiology. *Annual Review of Plant Physiology and Plant Molecular Biology, 50*(1), 277-303. doi:10.1146/annurev.arplant.50.1.277

CHEN, Q., CHEN, H., ZHU, L., & ZHENG, J. (2015a). Fundamentals of double network hydrogels. *Journal of Materials Chemistry B, 3*(18), 3654-3676. doi:10.1039/C5TB00123D

CHEN, W., CAO, F., ZHENG, W., TIAN, Y., XIANYU, Y., XU, P., ZHANG, W., WANG, Z., DENG, K., & JIANG, X. (2015b). Detection of the nanomolar level of total Cr[(III) and (VI)] by functionalized gold nanoparticles and a smartphone with the assistance of theoretical calculation models. *Nanoscale, 7*(5), 2042-2049. doi:10.1039/C4NR06726F

CHO, D.-W., SONG, H., SCHWARTZ, F. W., KIM, B., & JEON, B.-H. (2015). The role of magnetite nanoparticles in the reduction of nitrate in groundwater by zero-valent iron. *Chemosphere, 125*, 41-49. doi:https://doi.org/10.1016/j.chemosphere.2015.01.019

CHRISTIANSON, L. E., & SCHIPPER, L. A. (2016). Moving Denitrifying Bioreactors beyond Proof of Concept: Introduction to the Special Section. *Journal of Environmental Quality, 45*(3), 757-761. doi:10.2134/jeq2016.01.0013

CORBETT, T. D. W., DOUGHERTY, H., MAXWELL, B., HARTLAND, A., HENDERSON, W., RYS, G. J., & SCHIPPER, L. A. (2019). Utility of 'Diffusive Gradients in Thin-Films' for the measurement of nitrate removal performance of denitrifying bioreactors. *Science of The Total Environment*, 135267. doi:https://doi.org/10.1016/j.scitotenv.2019.135267

CORBETT, T. D. W., HARTLAND, A., HENDERSON, W., RYS, G. J., & SCHIPPER, L. A. (2021). Development of Bromide-Selective Diffusive Gradients in Thin-Films for the Measurement of Average Flow Rate of Streams. *Science of The Total Environment*.

DANIEL, W. L., HAN, M. S., LEE, J.-S., & MIRKIN, C. A. (2009). Colorimetric Nitrite and Nitrate Detection with Gold Nanoparticle Probes and Kinetic End Points. *J Am Chem Soc, 131*(18), 6362-6363. doi:10.1021/ja901609k

DAS, J., & SARKAR, P. (2016). A new dipstick colorimetric sensor for detection of arsenate in drinking water. *Environmental Science: Water Research & Technology, 2*(4), 693-704. doi:10.1039/C5EW00276A

DAVISON, W. (2016). *Diffusive Gradients in Thin-Films for Environmental Measurements*. Cambridge, UNITED KINGDOM: Cambridge University Press.

DAVISON, W., & ZHANG, H. (2012). Progress in understanding the use of diffusive gradients in thin films (DGT) – back to basics. *Environmental Chemistry, 9*(1), 1-13. doi:https://doi.org/10.1071/EN11084

DOBRIYAL, P., BADOLA, R., TUBOI, C., & HUSSAIN, S. A. (2017). A review of methods for monitoring streamflow for sustainable water resource management. *Applied Water Science, 7*(6), 2617-2628. doi:10.1007/s13201-016-0488-y

ENSAFI, A. A., & KAZEMZADEH, A. (2002). Monitoring nitrite with optical sensing films. *Microchemical Journal, 72*(2), 193-199. doi:https://doi.org/10.1016/S0026-265X(02)00035-8

ENVIRONMENT, M. F. T. (2020). About the National Policy Statement for Freshwater Management. Retrieved from https://www.mfe.govt.nz/fresh-water/national-policy-statement/about-nps

FILIK, H., GIRAY, D., CEYLAN, B., & APAK, R. (2011). A novel fiber optic spectrophotometric determination of nitrite using Safranin O and cloud point extraction. *Talanta, 85*(4), 1818-1824. doi:https://doi.org/10.1016/j.talanta.2011.07.052

GALLOWAY, J. N., ABER, J. D., ERISMAN, J. W., SEITZINGER, S. P., HOWARTH, R. W., COWLING, E. B., & COSBY, B. J. (2003). The Nitrogen Cascade. *BioScience, 53*(4), 341-356. doi:10.1641/0006-3568(2003)053[0341:TNC]2.0.CO;2

GONG, J. P., KATSUYAMA, Y., KUROKAWA, T., & OSADA, Y. (2003). Double-Network Hydrogels with Extremely High Mechanical Strength. *Adv. Mater., 15*(14), 1155-1158. doi:10.1002/adma.200304907

GOVERNMENT, N. Z. (2020). *National Policy Statement for Freshwater Management 2020*. Wellington: Minister for the Environment.

GUNUPURU, R., MAITY, D., BHADU, G. R., CHAKRABORTY, A., SRIVASTAVA, D. N., & PAUL, P. (2014). Colorimetric detection of $Cu^{2+}$ and $Pb^{2+}$ ions using calix[4]arene functionalized gold nanoparticles. *Journal of Chemical Sciences, 126*(3), 627-635. doi:10.1007/s12039-014-0600-5

HENDRIX, S. A., & BRAMAN, R. S. (1995). Determination of Nitrite and Nitrate by Vanadium(III) Reduction with Chemiluminescence Detection. *Methods, 7*(1), 91-97. doi:https://doi.org/10.1006/meth.1995.1013

HOOVER, N. L., BHANDARI, A., SOUPIR, M. L., & MOORMAN, T. B. (2016). Woodchip Denitrification Bioreactors: Impact of Temperature and Hydraulic Retention Time on Nitrate Removal. *Journal of Environmental Quality, 45*(3), 803-812. doi:10.2134/jeq2015.03.0161

HORD, N. G., TANG, Y., & BRYAN, N. S. (2009). Food sources of nitrates and nitrites: the physiologic context for potential health benefits. *The American Journal of Clinical Nutrition, 90*(1), 1-10. doi:10.3945/ajcn.2008.27131

HUANG, J., BENNETT, W., TEASDALE, P. R., GARDINER, S., & WELSH, D. (2016a). Development and evaluation of the diffusive gradients in thin films technique for measuring nitrate in freshwaters. *Analytica Chimica Acta, 923*, 74-81. doi:10.1016/j.aca.2016.04.006

HUANG, J., BENNETT, W. W., WELSH, D. T., & TEASDALE, P. R. (2016b). Determining time-weighted average concentrations of nitrate and ammonium in freshwaters using DGT with ion exchange membrane-based binding layers. *Environmental Science: Processes & Impacts, 18*(12), 1530-1539. doi:10.1039/c6em00260a

HYDES, D. J., & HILL, N. C. (1985). Determination of nitrate in seawater: Nitrate to nitrite reduction with copper-cadmium alloy. *Estuarine, Coastal and Shelf Science, 21*(1), 127-130. doi:https://doi.org/10.1016/0272-7714(85)90011-3

IBRAHIM, M. H., XUE, Z., ABDU, H. I., SHINGER, M. I., IDRIS, A. M., EDRIS, M. M., SHAN, D., & LU, X. (2019). Sensitive and selective colorimetric nitrite ion assay using silver nanoparticles easily synthesized and stabilized by AHNDMS and functionalized with PABA. *Nanoscale Advances, 1*(3), 1207-1214. doi:10.1039/C8NA00146D

IIZAWA, T., TAKETA, H., MARUTA, M., ISHIDO, T., GOTOH, T., & SAKOHARA, S. (2007). Synthesis of porous poly(N-isopropylacrylamide) gel beads by sedimentation polymerization and their morphology. *Journal of Applied Polymer Science, 104*(2), 842-850. doi:10.1002/app.25605

IRANDOUST, M., SHARIATI-RAD, M., & HAGHIGHI, M. (2013). Nitrite determination in water samples based on a modified Griess reaction and central composite design. *Analytical Methods, 5*, 5977-5982. doi:10.1039/c3ay40913a

IVANOV, V. M., FIGUROVSKAYA, V. N., ERSHOVA, N. I., ALYUKAEVA, A. F., & TSYTSARIN, A. G. (2004). Sorption–Optical Determination of Nitrite Ions in Sea Water with Chromotrope 2B. *Journal of Analytical Chemistry, 59*(6), 541-545. doi:10.1023/B:JANC.0000030874.63843.b9

JAMSHIDI, H., & RABIEE, A. (2014). Synthesis and Characterization of Acrylamide-Based Anionic Copolymer and Investigation of Solution Properties. *Advances in Materials Science and Engineering, 2014*. doi:10.1155/2014/728675

KAZEMZADEH, A., & ENSAFI, A. A. (2001). Sequential flow injection spectrophotometric determination of nitrite and nitrate in various samples. *Analytica Chimica Acta, 442*(2), 319-326. doi:https://doi.org/10.1016/S0003-2670(01)01146-1

KIANPOOR KALKHAJEH, Y., JABBARIAN AMIRI, B., HUANG, B., HENAREH KHALYANI, A., HU, W., GAO, H., & THOMSON, M. L. (2019). Methods for Sample Collection, Storage, and Analysis of Freshwater Phosphorus. *Water, 11*(9), 1889.

KING, R. C., MULLIGAN, P. K., & STANSFIELD, W. D. (2013). Diffusion. In *A Dictionary of Genetics* (8 ed., pp. 122). Oxford: Oxford University Press.

KISO, Y., JUNG, Y.-J., KUZAWA, K., SEKO, Y., SAITO, Y., YAMADA, T., & NAGAI, M. (2006). Visual determination of nitrite and nitrate in waters by color band formation method. *Chemosphere, 64*(11), 1949-1954. doi:https://doi.org/10.1016/j.chemosphere.2006.01.009

KNOBELOCH, L., SALNA, B., HOGAN, A., POSTLE, J., & ANDERSON, H. (2000). Blue babies and nitrate-contaminated well water. *Environmental health perspectives, 108*(7), 675-678.

KNYAZEV, D. A., IVANOV, V. M., SAMOKHVALOV, S. G., ZOLOTOV, Y. A., MARKINA, V. M., & KNYAZEV, V. D. (2002). Blister Drop-Pellet Tests for Nitrates and Nitrites. *Journal of Analytical Chemistry, 57*(1), 75-82.

KREUZEDER, A., SANTNER, J., ZHANG, H., PROHASKA, T., & WENZEL, W. W. (2015). Uncertainty Evaluation of the Diffusive Gradients in Thin Films Technique. *Environmental Science & Technology, 49*(3), 1594-1602. doi:10.1021/es504533e

LARNER, B. L., & SEEN, A. J. (2005). Evaluation of paper-based diffusive gradients in thin film samplers for trace metal sampling. *Analytica Chimica Acta, 539*(1), 349-355. doi:https://doi.org/10.1016/j.aca.2005.03.007

LEE, J. H., WANG, Z., LIU, J., & LU, Y. (2008). Highly sensitive and selective colorimetric sensors for uranyl (UO2(2+)): development and comparison of labeled and label-free DNAzyme-gold nanoparticle systems. *J Am Chem Soc, 130*(43), 14217-14226. doi:10.1021/ja803607z

LEE, S.-K., CHUNG, S.-C., & PARK, S.-K. (2007). Chemical Tracer Method for Measurement of Flow Rates in Closed Conduits. *Journal of Nuclear Science and Technology, 44*(11), 1467-1473. doi:10.1080/18811248.2007.9711394

LEHTO, N. J., DAVISON, W., ZHANG, H., & TYCH, W. (2006). An Evaluation of DGT Performance Using a Dynamic Numerical Model. *Environmental Science & Technology, 40*(20), 6368-6376. doi:10.1021/es061215x

LEVY, J., ZHANG, H., DAVISON, W., & GROBEN, R. (2011). Using diffusive gradients in thin films to probe the kinetics of metal interaction with algal exudates. *Environmental Chemistry, 8*, 517-524. doi:10.1071/en11046

LI, W., TEASDALE, P. R., ZHANG, S., JOHN, R., & ZHAO, H. (2003). Application of a Poly(4-styrenesulfonate) Liquid Binding Layer for Measurement of $Cu^{2+}$ and $Cd^{2+}$ with the Diffusive Gradients in Thin-Films Technique. *Analytical Chemistry, 75*(11), 2578-2583. doi:10.1021/ac020658q

LIDE, D. R. (Ed.) (1999). *CRC Handbook of Chemistry and Physics* (80 ed.). Boca Raton, Florida, USA: CRC Press.

LIU, G., LU, M., HUANG, X., LI, T., & XU, D. (2018). Application of Gold-Nanoparticle Colorimetric Sensing to Rapid Food Safety Screening. *Sensors (Basel, Switzerland), 18*(12), 4166. doi:10.3390/s18124166

LIU, S., QIN, N., SONG, J., ZHANG, Y., CAI, W., ZHANG, H., WANG, G., & ZHAO, H. (2016). A nanoparticulate liquid binding phase based DGT device for aquatic arsenic measurement. *Talanta, 160*, 225-232. doi:https://doi.org/10.1016/j.talanta.2016.06.064

LIU, Y., & WANG, J. (2019). Reduction of nitrate by zero valent iron (ZVI)-based materials: A review. *Science of The Total Environment, 671*, 388-403. doi:https://doi.org/10.1016/j.scitotenv.2019.03.317

LÓPEZ PASQUALI, C. E., FERNÁNDEZ HERNANDO, P., & DURAND ALEGRÍA, J. S. (2007). Spectrophotometric simultaneous determination of nitrite, nitrate and ammonium in soils by flow injection analysis. *Analytica Chimica Acta, 600*(1), 177-182. doi:https://doi.org/10.1016/j.aca.2007.03.015

MA, R., ZHENG, C., ZACHARA, J. M., & TONKIN, M. (2012). Utility of bromide and heat tracers for aquifer characterization affected by highly transient flow conditions. *Water Resources Research, 48*(8). doi:doi:10.1029/2011WR011281

MAOLIN, Z., JUN, L., MIN, Y., & HONGFEI, H. (2000). The swelling behavior of radiation prepared semi-interpenetrating polymer networks composed of polyNIPAAm and hydrophilic polymers. *Radiation Physics and Chemistry, 58*(4), 397-400. doi:10.1016/S0969-806X(99)00491-0

MAXWELL, B. M., BIRGAND, F., SMITH, B., & AVENI-DEFORGE, K. (2018). A small-volume multiplexed pumping system for automated, high-frequency water chemistry measurements in volume-limited applications. *Hydrology and Earth System Sciences, 22*(11), 5615-5628. doi:10.5194/hess-22-5615-2018

MONSER, L., SADOK, S., GREENWAY, G. M., SHAH, I., & UGLOW, R. F. (2002). A simple simultaneous flow injection method based on phosphomolybdenum chemistry for nitrate and nitrite determinations in water and fish samples. *Talanta, 57*(3), 511-518. doi:https://doi.org/10.1016/S0039-9140(02)00057-7

MOORE, R. D. (2004). Introduction to Salt Dilution Gauging for Streamflow Measurement Part 2: Constant-rate Injection. *Streamline Watershed Management Bulletin, 8*(1), 11-15.

MORITA, E., & NAKAMURA, E. (2008). Reduction of Nitrate to Nitrite by Using Zinc Powder for Determination of Total Nitrogen in Sea Water. *Bunseki Kagaku, 57*(10), 777-781. doi:10.2116/bunsekikagaku.57.777

MOUSAVI, M. F., JABBARI, A., & NOUROOZI, S. (1998). A sensitive flow-injection method for determination of trace amounts of nitrite. *Talanta, 45*(6), 1247-1253. doi:https://doi.org/10.1016/S0039-9140(97)00240-3

MURADOVA, G. G., GADJIEVA, S. R., DI PALMA, L., & VILARDI, G. (2016). Nitrates Removal by Bimetallic Nanoparticles in Water. *Chemical Engineering Transactions, 47*, 205-210. doi:10.3303/CET1647035

NAGARAJA, P., AL-TAYAR, N. G. S., SHIVAKUMAR, A., SHRESTHA, A. K., & GOWDA, A. K. (2010). A simple and sensitive spectrophotometric method for the determination of trace amounts of nitrite in environmental and biological samples using 4-amino-5-hydroxynaphthalene-2,7-disulphonic acid monosodium salt. *Spectrochimica Acta Part A: Molecular and Biomolecular Spectroscopy, 75*(5), 1411-1416. doi:https://doi.org/10.1016/j.saa.2010.01.010

NAM, Y.-S., NOH, K.-C., KIM, N.-K., LEE, Y., PARK, H.-K., & LEE, K.-B. (2014). Sensitive and selective determination of NO2− ion in aqueous samples using modified gold nanoparticle as a colorimetric probe. *Talanta, 125*, 153-158. doi:https://doi.org/10.1016/j.talanta.2014.02.030

NECULITA, C.-M., ZAGURY, G. J., & BUSSIÈRE, B. (2008). Effectiveness of sulfate-reducing passive bioreactors for treating highly contaminated acid mine drainage: I. Effect of hydraulic retention time. *Applied Geochemistry, 23*(12), 3442-3451. doi:https://doi.org/10.1016/j.apgeochem.2008.08.004

NYDAHL, F. (1976). On the optimum conditions for the reduction of nitrate to nitrite by cadmium. *Talanta, 23*(5), 349-357. doi:https://doi.org/10.1016/0039-9140(76)80047-1

PANTHER, J. G., TEASDALE, P. R., BENNETT, W. W., WELSH, D. T., & ZHAO, H. (2010). Titanium Dioxide-Based DGT Technique for In Situ Measurement of Dissolved Reactive Phosphorus in Fresh and Marine Waters. *Environmental Science & Technology, 44*(24), 9419-9424. doi:10.1021/es1027713

PASQUALI, C. E. L., GALLEGO-PICÓ, A., HERNANDO, P. F., VELASCO, M., & ALEGRÍA, J. S. D. (2010). Two rapid and sensitive automated methods for the determination of nitrite and nitrate in soil samples. *Microchemical Journal, 94*(1), 79-82. doi:https://doi.org/10.1016/j.microc.2009.09.005

PENG, Y.-Z., SHAO-PO, W., SHU-YING, W., JIAN-GE, H., & HAI-BING, Q. (2006). Effect of denitrification type on pH profiles in the sequencing batch reactor process. *Water Science and Technology, 53*(9), 87-93. doi:10.2166/wst.2006.279

PEREZ-CORONADO, A. M., CALVO, L., BAEZA, J. A., PALOMAR, J., LEFFERTS, L., RODRIGUEZ, J. J., & GILARRANZ, M. A. (2017). Selective Reduction of Nitrite to Nitrogen with Carbon-Supported Pd–AOT Nanoparticles. *Industrial & Engineering Chemistry Research, 56*(41), 11745-11754. doi:10.1021/acs.iecr.7b02944

PICIOREANU, C., VAN LOOSDRECHT, M. C. M., & HEIJNEN, J. J. (1997). Modelling the effect of oxygen concentration on nitrite accumulation in a biofilm airlift suspension reactor. *Water Science and Technology, 36*(1), 147-156. doi:https://doi.org/10.1016/S0273-1223(97)00347-8

PINCKNEY, J. L., PAERL, H. W., TESTER, P., & RICHARDSON, T. L. (2001). The role of nutrient loading and eutrophication in estuarine ecology. *Environmental health perspectives, 109 Suppl 5*(Suppl 5), 699-706. doi:10.1289/ehp.01109s5699

RABALAIS, N. N., TURNER, R. E., & SCAVIA, D. (2002). Beyond Science into Policy: Gulf of Mexico Hypoxia and the Mississippi RiverNutrient policy development for the Mississippi River watershed reflects the accumulated scientific evidence that the increase in nitrogen loading

is the primary factor in the worsening of hypoxia in the northern Gulf of Mexico. *BioScience, 52*(2), 129-142. doi:10.1641/0006-3568(2002)052[0129:BSIPGO]2.0.CO;2

RABOTYAGOV, S. S., KLING, C. L., GASSMAN, P. W., RABALAIS, N. N., & TURNER, R. E. (2014). The Economics of Dead Zones: Causes, Impacts, Policy Challenges, and a Model of the Gulf of Mexico Hypoxic Zone. *Review of Environmental Economics and Policy, 8*(1), 58-79. doi:10.1093/reep/ret024

RAMBAGS, F. (2019). *Microbial contaminat removal and alternative nitogren removal pathways in denitrifying bioreactors.* (Doctor of Philosophy), The University of Waikato,

RAMBAGS, F., TANNER, C. C., STOTT, R., & SCHIPPER, L. A. (2016). Fecal Bacteria, Bacteriophage, and Nutrient Reductions in a Full-Scale Denitrifying Woodchip Bioreactor. *Journal of Environmental Quality, 45*(3), 847-854. doi:10.2134/jeq2015.06.0326

REDDY, P. (2020). *Resource Management (National Environmental Standards for Freshwater) Regulations 2020*. Wellington: Parliamentary Counsel Office.

RIVETT, M. O., BUSS, S. R., MORGAN, P., SMITH, J. W. N., & BEMMENT, C. D. (2008). Nitrate attenuation in groundwater: A review of biogeochemical controlling processes. *Water Research, 42*(16), 4215-4232. doi:https://doi.org/10.1016/j.watres.2008.07.020

ROBERTSON, G. P., & VITOUSEK, P. M. (2009). Nitrogen in Agriculture: Balancing the Cost of an Essential Resource. *Annual Review of Environment and Resources, 34*(1), 97-125. doi:10.1146/annurev.environ.032108.105046

S˙LIWKA-KASZYŃSKA, M., KOT-WASIK, A., & NAMIEŚNIK, J. (2003). Preservation and Storage of Water Samples. *Critical Reviews in Environmental Science and Technology, 33*(1), 31-44. doi:10.1080/10643380390814442

SAHINER, N. (2013). Soft and flexible hydrogel templates of different sizes and various functionalities for metal nanoparticle preparation and their use in catalysis. *Progress in Polymer Science, 38*(9), 1329-1356. doi:https://doi.org/10.1016/j.progpolymsci.2013.06.004

SAHINER, N., OZAY, H., OZAY, O., & AKTAS, N. (2010). A soft hydrogel reactor for cobalt nanoparticle preparation and use in the reduction of nitrophenols. *Applied Catalysis B: Environmental, 101*(1), 137-143. doi:https://doi.org/10.1016/j.apcatb.2010.09.022

SCALLY, S., DAVISON, W., & ZHANG, H. (2006). Diffusion coefficients of metals and metal complexes in hydrogels used in diffusive gradients in thin films. *Analytica Chimica Acta, 558*(1), 222-229. doi:https://doi.org/10.1016/j.aca.2005.11.020

SCHASCHKE, C. (2014). Fick's first law of diffusion. In *A Dictionary of Chemical Engineering* (pp. 144). Oxford: Oxford University Press.

SCHIPPER, L., ROBERTSON, W., GOLD, A., JAYNES, D. B., & C. CAMERON, S. (2010a). Denitrifying Bioreactors — An Approach for Reducing Nitrate Loads to Receiving Waters. *Ecological Engineering, 36*, 1532-1543. doi:10.1016/j.ecoleng.2010.04.008

SCHIPPER, L. A., CAMERON, S. C., & WARNEKE, S. (2010b). Nitrate removal from three different effluents using large-scale denitrification beds. *Ecological Engineering, 36*(11), 1552-1557. doi:https://doi.org/10.1016/j.ecoleng.2010.02.007

SCHIPPER, L. A., GOLD, A. J., & DAVIDSON, E. A. (2010c). Managing denitrification in human-dominated landscapes. *Ecological Engineering, 36*(11), 1503-1506. doi:https://doi.org/10.1016/j.ecoleng.2010.07.027

SCHNETGER, B., & LEHNERS, C. (2014). Determination of nitrate plus nitrite in small volume marine water samples using vanadium(III) chloride as a reduction agent. *Marine Chemistry, 160*, 91-98. doi:https://doi.org/10.1016/j.marchem.2014.01.010

SHENG, J. J. (2010). Polymer Flooding. In *Modern Chemical Enhanced Oil Recovery: Theory and Practice* (pp. 101-206). Burlington, MA, United States of America: Gulf Professional Publishing.

SHIH, R., ROBERTSON, W. D., SCHIFF, S. L., & RUDOLPH, D. L. (2011). Nitrate Controls Methyl Mercury Production in a Streambed Bioreactor. *Journal of Environmental Quality, 40*(5), 1586-1592. doi:10.2134/jeq2011.0072

SMITH, V. H., TILMAN, G. D., & NEKOLA, J. C. (1999). Eutrophication: impacts of excess nutrient inputs on freshwater, marine, and terrestrial ecosystems. *Environmental Pollution, 100*(1), 179-196. doi:https://doi.org/10.1016/S0269-7491(99)00091-3

SREEKUMAR, N. V., NARAYANA, B., HEGDE, P., MANJUNATHA, B. R., & SAROJINI, B. K. (2003). Determination of nitrite by simple diazotization method. *Microchemical Journal, 74*(1), 27-32. doi:https://doi.org/10.1016/S0026-265X(02)00093-0

SU, E., & OKAY, O. (2018). Hybrid cross-linked poly(2-acrylamido-2-methyl-1-propanesulfonic acid) hydrogels with tunable viscoelastic, mechanical and self-healing properties. *Reactive and Functional Polymers, 123*, 70-79. doi:https://doi.org/10.1016/j.reactfunctpolym.2017.12.009

TABATA, Y. (2009). Biomaterial technology for tissue engineering applications. *Journal of the Royal Society Interface, 6*(SUPPL. 3), S311-S324. doi:10.1098/rsif.2008.0448.focus

TARAFDER, P. K., & RATHORE, D. P. S. (1988). Spectrophotometric determination of nitrite in water. *Analyst, 113*(7), 1073-1076. doi:10.1039/AN9881301073

TEASDALE, P. R., BATLEY, G. E., APTE, S. C., & WEBSTER, I. T. (1995). Pore water sampling with sediment peepers. *TrAC Trends in Analytical Chemistry, 14*(6), 250-256. doi:https://doi.org/10.1016/0165-9936(95)91617-2

THONIYOT, P., TAN, M. J., KARIM, A. A., YOUNG, D. J., & LOH, X. J. (2015). Nanoparticle-Hydrogel Composites: Concept, Design, and Applications of These Promising, Multi-Functional Materials. *Advanced science (Weinheim, Baden-Wurttemberg, Germany), 2*(1-2), 1400010-1400010. doi:10.1002/advs.201400010

TSOGAS, G. Z., KAPPI, F. A., VLESSIDIS, A. G., & GIOKAS, D. L. (2018). Recent Advances in Nanomaterial Probes for Optical Biothiol Sensing: A Review. *Analytical Letters, 51*(4), 443-468. doi:10.1080/00032719.2017.1329833

VAN DER VEEKEN, P. L. R., CHAKRABORTY, P., & LEEUWEN, H. P. V. (2010). Accumulation of Humic Acid in DET/DGT Gels. *Environmental Science & Technology, 44*(11), 4253-4257. doi:10.1021/es100510u

VEEKEN, P. L. R. V. D., & LEEUWEN, H. P. V. (2010). DGT/DET Gel Partition Features of Humic Acid/Metal Species. *Environmental Science & Technology, 44*(14), 5523-5527. doi:10.1021/es100861t

WAKELIN, S. A., COLLOFF, M. J., & KOOKANA, R. S. (2008). Effect of Wastewater Treatment Plant Effluent on Microbial Function and Community Structure in the Sediment of a Freshwater Stream with Variable Seasonal Flow. *Applied and Environmental Microbiology, 74*(9), 2659-2668. doi:10.1128/AEM.02348-07

WANG, G. F., SATAKE, M., & HORITA, K. (1998). Spectrophotometric determination of nitrate and nitrite in water and some fruit samples using column preconcentration. *Talanta, 46*(4), 671-678.

WARNKEN, K. W., ZHANG, H., & DAVISON, W. (2005). Trace Metal Measurements in Low Ionic Strength Synthetic Solutions by Diffusive Gradients in Thin Films. *Analytical Chemistry, 77*(17), 5440-5446. doi:10.1021/ac050045o

WARNKEN, K. W., ZHANG, H., & DAVISON, W. (2006). Accuracy of the Diffusive Gradients in Thin-Films Technique: Diffusive Boundary Layer and Effective Sampling Area Considerations. *Analytical Chemistry, 78*(11), 3780-3787. doi:10.1021/ac060139d

YANG, L., CHU, J. S., & FIX, J. A. (2002). Colon-specific drug delivery: New approaches and in vitro/in vivo evaluation. *International Journal of Pharmaceutics, 235*(1-2), 1-15. doi:10.1016/S0378-5173(02)00004-2

YEZEK, L. P., VAN DER VEEKEN, P. L. R., & VAN LEEUWEN, H. P. (2008). Donnan Effects in Metal Speciation Analysis by DET/DGT. *Environmental Science & Technology, 42*(24), 9250-9254. doi:10.1021/es8021232

YUAN-HUI, L., & GREGORY, S. (1974). Diffusion of ions in sea water and in deep-sea sediments. *Geochimica et Cosmochimica Acta, 38*(5), 703-714. doi:https://doi.org/10.1016/0016-7037(74)90145-8

ZHANG, H., & DAVISON, W. (1995). Performance Characteristics of Diffusion Gradients in Thin Films for the in Situ Measurement of Trace Metals in Aqueous Solution. *Analytical Chemistry, 67*(19), 3391-3400. doi:10.1021/ac00115a005

ZHANG, H., DAVISON, W., GADI, R., & KOBAYASHI, T. (1998). In situ measurement of dissolved phosphorus in natural waters using DGT. *Analytica Chimica Acta, 370*(1), 29-38. doi:https://doi.org/10.1016/S0003-2670(98)00250-5

ZHANG, Z., CHEN, Z., WANG, S., QU, C., & CHEN, L. (2014). On-Site Visual Detection of Hydrogen Sulfide in Air Based on Enhancing the Stability of Gold Nanoparticles. *ACS Applied Materials & Interfaces, 6*(9), 6300-6307. doi:10.1021/am500564w

ZHU, I., & GETTING, T. (2012). A review of nitrate reduction using inorganic materials. *Environmental Technology Reviews, 1*(1), 46-58. doi:10.1080/09593330.2012.706646

# Chapter 3 - Utility of 'Diffusive Gradients in Thin-Films' for the measurement of nitrate removal performance of denitrifying bioreactors

*Adapted from:*

CORBETT, T. D. W., DOUGHERTY, H., MAXWELL, B., HARTLAND, A., HENDERSON, W., RYS, G. J. & SCHIPPER, L. A. 2019. Utility of 'Diffusive Gradients in Thin-Films' for the measurement of nitrate removal performance of denitrifying bioreactors. Science of the Total Environment, 135267.

## Highlights

- Diffusive Gradients in Thin-Films (DGT) measured $NO_3^-$ along two bioreactors.
- DGT $NO_3^-$ concentration data were comparable to high frequency grab sampling.
- DGT more easily accounted for temporal variation of $NO_3^-$ than grab sampling.
- DGT enabled the calculation of bioreactor performance.
- $NO_3^-$ removal rates were 1.2 – 30.8 g N $m^{-3}$ $d^{-1}$ for two bioreactors.

## Abstract[1]

The increase in environmental nutrient availability as a result of human activities has necessitated the development of mitigation strategies for nutrient removal, such as nitrate. Current methods for determining the efficiency of different mitigation strategies required measurement of changes in nitrate concentrations, however, these methods can be expensive or do not account fully for the temporal variability of nitrate concentration. This study evaluated the utility of Diffusive Gradients in Thins-Films (DGT) for determining nitrate removal in two denitrifying bioreactors, and compared DGT performance to traditional approaches for determining performance, including high and low

[1] Abbreviations: MPS-UV VIS, automated multiplexed pumping system and UV-VIS field spectrophotometer coupled system; HFGS, high frequency grab sampling; LFGS, low frequency grab sampling.

frequency water grab sampling. The binding layer was produced using the Purolite® A520E anion exchange resin. The uptake and elution efficiencies were 98.8 % and 93.4 % respectively. Diffusive Gradients in Thin Films of three material diffusion layer thicknesses were placed in piezometers along longitudinal transects, to enable calculation of the diffusive boundary layer and provide replicates. These were removed after 16, 24 and 36 hours, and the accumulated nitrate masses were extracted and quantified to calculate nitrate concentration. Concentrations were subsequently utilised to calculate nitrate removal rates in both bioreactors. Grab samples were taken at 30 and 60 minute intervals over those periods, nitrate concentrations were also measured to determine nitrate removal. Diffusive Gradients in Thin Films provided nitrate removal rates at bioreactor site one (controlled flow, wastewater treatment) of 14.83 – 30.75 g N $m^{-3}$ $d^{-1}$, and 1.22 to 3.63 g N $m^{-3}$ $d^{-1}$ at site two (variable flow, agricultural run-off). Diffusive Gradients in Thin Films determined nitrate concentrations and removal rates were in strong accordance with high frequency grab sampling, but data collection via DGT was considerably easier. Utilising DGT for the measurement of bioreactor performance overcame many of the challenges associated with high frequency grab sampling, and other methods, such as accounting for temporal variation in nitrate concentration and reduced analytical requirements.

## Graphical Abstract

DGTs were easier to use and better accounted for $NO_3^-$ temporal variability than traditional grab sampling.

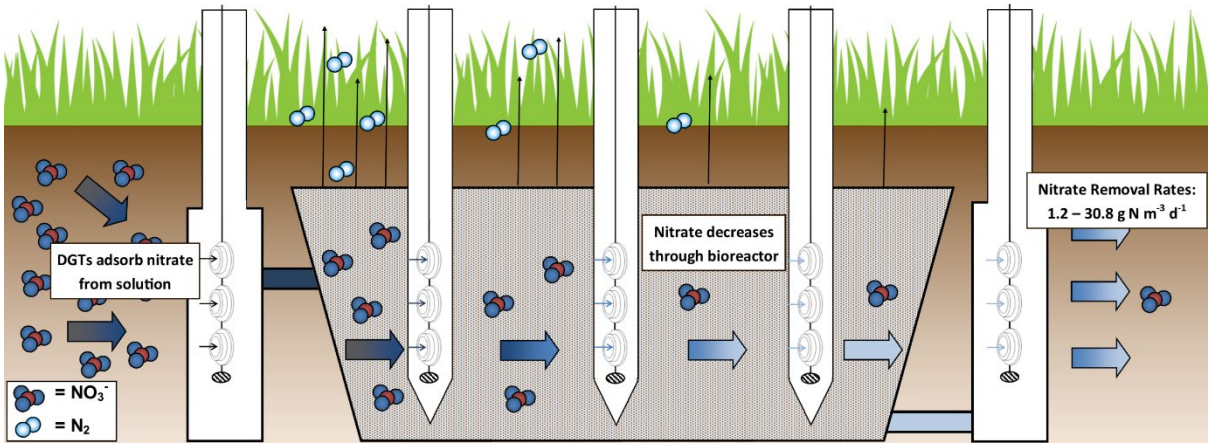

## 3.1. Introduction

Farmers are under ever increasing pressure to produce more food to support an expanding global population. This increase in production has been partially supported by increases in nitrogen fertiliser application, along with other management practices. As a result of increased nitrogen inputs, the sequential transfer of the additional reactive nitrogen from agricultural land to the oceans has resulted in environmental degradation in a range of ecosystems as a single nitrogen atom can impact all biospheres along the nitrogen cascade (Galloway et al., 2003). Excess available nutrients can promote biological growth, and the eventual decomposition of which can lead to eutrophication and hypoxia (Galloway et al., 2003). Ultimately reactive N is transformed back to the atmosphere through microbial denitrification.

To remove excess reactive N species at the source and limit the downstream effects, nutrient mitigation strategies, such as constructed wetlands, riparian buffers, saturated buffers and denitrifying bioreactors, have been developed (Tanner et al., 2012, Jaynes and Isenhart, 2019, Chandrasoma et al., 2019). Bioreactors, in particular, are designed to enhance denitrification, through the simple and passive treatment of drainage waters, groundwater, and wastewater nitrate (Addy et al., 2016, Schipper et al., 2010a). There are different construction designs of bioreactors, but generally these are structures filled with solid organic carbon material (e.g. woodchips) through which nutrient rich water passes (Addy et al., 2016). The carbon acts as an electron donor for denitrifying bacteria (Rivett et al., 2008). The application of bioreactors has been predominantly focused on watersheds with high non-point source nitrate loads and tertiary wastewater treatment (Christianson and Schipper, 2016). To support greater uptake of bioreactors, and other approaches, for the treatment of nutrient rich runoff and wastewater, it is important to quantify nitrate removal rates from water during its passage through the bioreactors to assist with design.

Multiple methods exist to measure nitrate in water samples, each having their advantages and disadvantages. Grab sampling is the most commonly used method for determining nitrate (Huang et

al., 2016c) because it is quick and simple. Grab samples at one time however, may not fully account for the temporal variability of nitrate concentration (Audet et al., 2014). Continuous sampling methods, such as auto samplers, are capable of more accurately capturing this temporal variability in nitrate concentration, however, they require considerable investment in on-site equipment (Audet et al., 2014). Manually performing the high frequency grab sampling required to account for temporal variability is time consuming, and the large number of associated samples for analysis is expensive.

Nitrogen species can also undergo microbial and chemical transformations during transport and storage of grab samples, and so there is a generally a need for preservation. Physical preservation is highly advantageous as there are no added chemical compounds to the sample, for example freezing to -20 $^{o}$C (S˙liwka-Kaszyńska et al., 2003), however, these temperatures can be difficult to maintain in-field and thawing can occur during transport. Chemical preservation, for example using mercuric chloride, is an alternative, however these can be highly toxic (S˙liwka-Kaszyńska et al., 2003), requiring careful handling and subsequent disposal.

In-field analytical methods, such as colorimetric test kits, and the automated multiplexed pumping system and UV-VIS field spectrophotometer coupled system (MPS-UV VIS) (Maxwell et al., 2018), overcome the restrictions of storage and transport. Colorimetric test kits, however, are limited by operational range and by the skill of the user in determining the colour change. Additionally, the precision of these colorimetric measurements is low. Alternatively, the MPS-UV VIS field coupled system is capable of overcoming the temporal limitations of grab sampling (Maxwell et al., 2018) by pumping samples from various sites at variable intervals, analysing them in-field using a UV spectrophotometer and logging the data. This system is limited by spectrophotometer data storage, cuvette fouling, and battery power (Maxwell et al., 2018), and equipment is expensive and requires careful calibration.

In contrast, there have been recent developments in the use of Diffusive Gradients in Thin-Films (DGT) that may overcome many of the limitations of the methods described above. Diffusive Gradients in

Thin Films rapidly and strongly adsorb specific analytes, supplied to an ion exchange resin by diffusion from surrounding water. The DGT technique is based on Fick's first law of diffusion (Menegário et al., 2017, Zhang and Davison, 1995), whereby chemical species move in the direction of decreasing concentration due to their random thermal motion, as to make concentration uniform (King et al., 2013). The DGT probes (Figure 3.1) are constructed to take advantage of this phenomenon. The filter membrane and diffusive layer restrict the transport of ions to the analyte specific binding layer to diffusion, which rapidly and strongly binds the analyte thereby maintaining a concentration gradient through the diffusive layer to the binding layer/diffusive gel interface, at which point the concentration is effectively zero. As such, a sufficiently thick hydrogel is required to ensure the flux of ions to the binding layer, above a threshold level of convection, is independent of the hydrodynamics in solution (Zhang and Davison, 1995). This enables the use of Fick's first law to calculate the time weighted average concentration from the accumulated mass (see full description in methods).

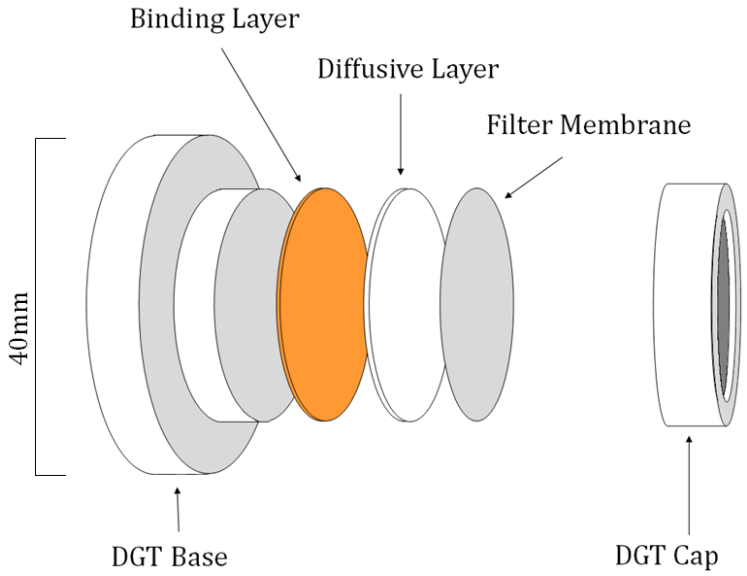


Figure 3.1: Diffusive Gradients in Thin-Films (DGT) solution piston construction, exploded view. Binding layer (A520E resin impregnated APA gel), separated from solution by the diffusive layer (APA gel) and filter membrane (polyethersulfone), all of which are held in place on the base by the cap.

DGT can provide time-weighted average nitrate ($NO_3^-$) concentrations over environmentally relevant time scales and integrate short term analyte concentration variations (Huang et al., 2016c), by *in situ* adsorption of labile species in aqueous systems (Zhang and Davison, 1995). Nitrate-specific Purolite

A520E DGT rapidly and strongly adsorb nitrate (Huang et al., 2016a), thereby removing the need for immediate analysis and resolving the difficulties associated with transport and storage.

DGT have largely been used as a research tool for the environmental measurement of trace metals (Zhang and Davison, 1995) and phosphate (Panther et al., 2010), and only more recently nitrate (Huang et al., 2016a). Huang et al. (2016b) have demonstrated that A520E nitrate-specific DGT could be used for the measurement of nitrate in streams and lakes. Nitrate concentrations determined from DGT compared reasonably with low frequency grab sampling (Huang et al., 2016b), but the frequency of grab sampling and temperature measurements may not have fully captured the extent to which nitrate concentration and temperature varied.

These initial studies by Huang et al. demonstrated the utility of DGT for determining nitrate concentration in streams and lakes, but DGT may also be useful for determining the performance of mitigation strategies, such as bioreactors. Denitrifying bioreactors and other mitigation strategies may not have optimal conditions for the deployment of DGT compared to natural systems, as hydrology and chemistry can differ significantly (e.g. constrained mixing, high competing ion concentrations and pH) which may affect how accurate the concentration determined by DGT is compared to the actual concentration. It is anticipated that if DGT provide quantitative nitrate concentration data along the length of bioreactors, DGT should allow the calculation of nitrate removal rates. If successful in assessing the performance of bioreactors then DGT should also be useful for determining the performance of other mitigation strategies.

As a novel application of this methodology, the use of nitrate DGT for both research and environmental monitoring requires the rigorous demonstration of their performance. The objectives of this study were to (i) assess the efficacy of nitrate measurement by DGT and how it compares to grab sample measurements, and (ii) determine how well DGT measure bioreactor nitrate concentrations and bioreactor N-removal performance. If these DGT are sufficiently sensitive at

demonstrating medium to long-term nitrate concentrations they may provide a simple approach to access the potential of different mitigation strategies.

## 3.2. Materials and Methods

### *3.2.1 Study Sites and DGT Deployment*

DGT solution probes were used to determine nitrate removal at two denitrifying bioreactor sites (Figure 3.2), by measuring nitrate concentration along their length. Bioreactor site 1 (Figure 3.2A) was a controlled flow, saturated bioreactor utilised for wastewater treatment – consisting of grey water and effluent. The bioreactor consisted of a trapezoidal bed 20 m long and 7 m wide along the top, with a 1:1 slope – the volume of the bioreactor was 120 $m^3$ (Rambags et al., 2016). *Carex virgata* and *Cyperus ustulatus* were planted in 150 mm of sand and coconut peat planting media over a geotextile mesh (Rambags et al., 2016). Bioreactor site 2 (Figure 3.2B) was on a dairy farm, where nitrate enriched water was supplied to the inlet via tile drainage from a dairy farm paddock, and included a bypass flow drain for excess water. The bioreactor had a volume of 40.5 $m^3$ consisting of a trapezoidal bed 9 m long and 5 m wide along the top, with a 1.25 to 1.2 slope; and planted with a traditional rye-grass/clover sward. Independent flow measurements were logged at both sites. Both bioreactors were filled with *pinus radiata* woodchips.

At both sites there were pre-existing wells (piezometers), installed along longitudinal transects. At site 1 (Figure 3.2A) the well diameters were initially 30 mm and were replaced with wider wells (50 mm) to allow deployment of the DGT. Two sets of DGT were deployed at the outlet and inlet, and at the 7 centre wells. One set was removed after 16 hours, the second after 36 hours. Grab samples were taken from each well every hour for the first 16 hours, and for hours 24 to 36. The 36 hour DGT deployment was chosen because it was the maximum amount of time that A520E DGT could be deployed before the resins became saturated based on nitrate measurements made by Rambags et al. (2016).

At bioreactor site 2, DGT were deployed for approximately 24 hours alongside a MPS-UV VIS system (described below) in the outlet and inlet, and three centre wells (Figure 3.2B). Each set of DGT consisted of three different material diffusion layer thicknesses, so that the diffusive boundary layer could be calculated (see below) as well as for replication.

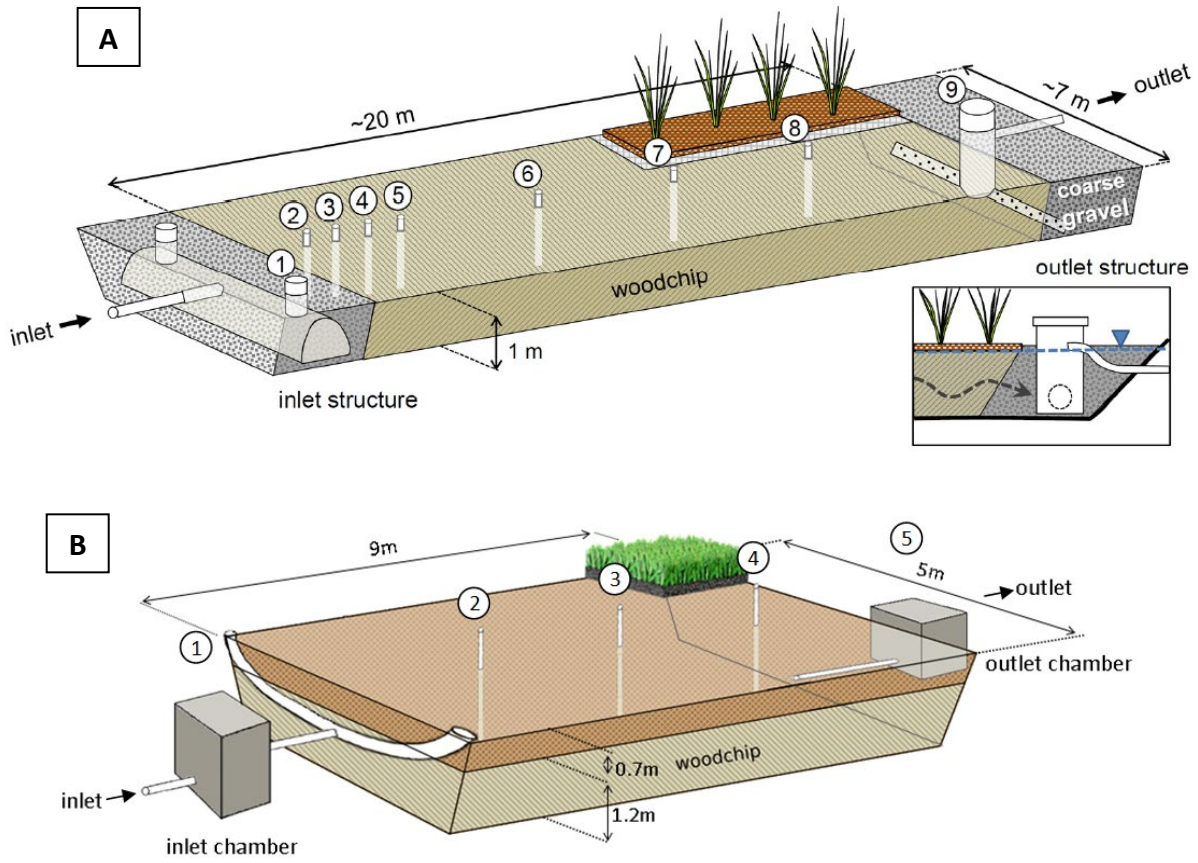


Figure 3.2 (A) Bioreactor site 1 schematic (Rambags et al., 2016). (B) Bioreactor site 2 schematic. The inlet and outlet chambers, and wells where DGT were deployed and grab samples taken are numbered.

At site 1, temperature measurements were made using iButton (iButtonLink, Wisconsin USA) and HOBO (Onset Computer Corporation, Massachusetts USA) temperature data loggers. Temperature measurements at site 2 were taken using an YSI ProODO Optical Dissolved Oxygen Instrument. Temperature values were averaged and used to correct the nitrate diffusion coefficient values used in DGT concentration calculations. Flow rates were independently metred at both bioreactor sites.

### *3.2.2 Gel, Resin, and DGT Preparation*

Deionised water (17.6-18.2 MΩ) was used for solution preparation and all other uses. All plastic and glassware, DGT componentry, and glass plates were washed in 10 % (v/v) HCl for a minimum of 24 hours, before being thoroughly rinsed with deionised water (Huang et al., 2016a). All laboratory experiments were conducted in triplicate.

To minimise contamination in the production of gels and resins, the handling of DGT devices was carried out under clean laboratory conditions (Davison, 2016). Agarose crosslinked polyacrylamide (APA) diffusive gels were prepared as described by Huang et al. (2016). Briefly, the solution was pipetted between glass plates separated by inert 0.4 mm and 0.5 mm spacers and cured at 45 $^{o}$C for 90 minutes. Gels were washed in deionised water six times over 24 hours before being stored at room temperature in approximately 750 mL of 0.01 mol $L^{-1}$ NaCl.

The preparation and storage procedures for the binding layers were based on those developed by Huang et al. (2016). Purolite A520E beads were ground and sieved to ≤125 µm, air dried for 24 hours and stored in a desiccator. Gel-solution (10 mL, 15 % acrylamide, 0.3 % cross-linker) was added to 4 g of ground A520E powder and stirred until the powder was uniformly distributed. Ammonium peroxydisulfate (70 µL of 10 % solution) and N,N,N',N'-tetramethylethane-1,2-diamine (TEMED) (25 µL) were then added. The solution was pipetted between glass plates separated by 0.5 mm inert spacers, and cured at 45 $^{o}$C for approximately 100 minutes. The resin gels were washed 4 times in deionised water over 24 hours before being stored in approximately 750 mL of deionised water at 4 $^{o}$C. Resins were also made using 2.5 g and 5.4 g of A520E to determine the optimal mass of resin for incorporation into the hydrogel. Polyethersulfone membranes (0.15 mm) (Sterlitech, Washington, United States) were cut from sheets and stored in deionised water.

DGT with three different material diffusion layer thicknesses (0.15 mm, 0.79 mm and 0.95 mm) were prepared by cutting the A520E resin and APA gel, and layering onto the DGT piston with the

polyethersulfone membrane. Diffusive Gradients in Thin Films were stored in clean plastic bags immersed in deionised water until deployment.

### *3.2.3 Background Resin $NO_3^-$ Concentrations*

While every effort was made to exclude nitrate during preparation of DGT, residual nitrate remains on resins which needs to be taken into account after use. The background resin nitrate concentration of each batch was subtracted from all proceeding gel concentrations (Davison, 2016).

### *3.2.4 Elution, Uptake Efficiencies and Saturation Point*

To ensure the probes provide quantitative nitrate concentrations the adsorption and elution characteristics need to be quantified. Uptake and elution (the displacement of adsorbed nitrate from the binding resin) efficiencies were measured by immersing the resins in 10 mL $NO_3^-$ solutions of varying concentrations (1 to 50 mg N $L^{-1}$ (milligrams of nitrate-N per litre) and 0.002 mol $L^{-1}$ NaCl), and agitating for 24 hours on a shaker plate (Huang et al., 2016c). As previously reported, resins were eluted in 2 mol $L^{-1}$ NaCl for 24 hours on a shaker plate, however, the volume was increased to 4 mL from the previously reported volume of 2 mL to maintain stoichiometric excess, then diluted to 10 mL (Huang et al., 2016a).

Solution samples were taken before and after the binding resin was added to determine the mass of analyte remaining in solution (Huang et al., 2016c). Uptake efficiency was calculated as the percentage of nitrate removed from solution, while elution efficiency was calculated as the percentage of nitrate in the eluent removed from the resin (Huang et al., 2016c).

Resin gel disks were placed in 1000 mg N $L^{-1}$ solution (10 mL) for 24 hours to measure the intrinsic capacity for adsorption (saturation point).

### *3.2.5 Adsorption Isotherm*

Understanding the adsorption isotherm of A520E DGT was necessary to understand how uptake efficiency changed with decreasing availability of adsorption sites in the resin. Resin disks (area = 3.8

$cm^2$) were deployed in 50 mL of nitrate solution (100 mg N $L^{-1}$) and agitated on a shaker plate, 1 mL grab samples were taken every 10 minutes for the first hour, 20 minutes for the second hour, and every 1 hour for the following 4 hours. A final sample was taken after 10 hours. The removed nitrate mass was accounted for in subsequent calculations of the adsorbed mass (i.e. mass removed from solution).

### *3.2.6 Gel Dehydration*

DGT probes are traditionally stored in a few mL of deionised water to maintain gel hydration, however, this may not always be possible (i.e. lack of deionised water when returning from field deployment), hence it is necessary to quantify the effects of variable transportation and storage conditions (primarily drying). To understand the effects of drying the resin gels on nitrate adsorption and elution, gels were air dried for 24 hours under clean laboratory conditions. Dried blank disks were compared against hydrated blank disks, and gels deployed in 10 mg N $L^{-1}$ nitrate solution were compared to gels dried after and before deployment in 10 mg N $L^{-1}$ nitrate solution.

### *3.2.7 Sample Analysis*

Eluted DGT samples and grab samples were analysed alongside commercial anion standards (Dionex Seven Anion Standard) using a Dionex ICS-200 Ion Chromatograph (Dionex, California, United States). Ion chromatography also provided sulfate and phosphate data. Due to a high chloride concentration, from gel elution, a gradient concentration method was used to give optimal peak resolution. The gradient concentration method ensured that chloride was eluted well before the nitrate was eluted, and that all peaks did not overlap.

Concentration values attained were converted to mass to give total mass taken-up by the resin, after the background mass in the resin was subtracted. Time weighted average concentration (C) was determined using the following equation (Davison, 2016).

$$C_{DGT} = \frac{M}{A_{eff} t}\left(\frac{\Delta g_{gel}}{D_{gel}} + \frac{\Delta_f}{D_f} + \frac{\delta}{D_w}\right) \quad (1)$$

Where C = DGT concentration (i.e. time weighted average nitrate concentration), mg $cm^{-3}$; M = accumulated mass, mg; $A_{eff}$ = effective area, $cm^2$; t = time, length of deployment, s; $D_{gel}$, $D_f$, $D_w$ = diffusion coefficients for the diffusive gel, filter membrane and Diffusive Boundary Layer/water respectively, $cm^2\ s^{-1}$; $\Delta g_{gel}$, Δf, δ = thickness of diffusive gel, filter membrane and Diffusive Boundary Layer respectively, cm (Davison, 2016). The calculation of δ is given in a following section.

The diffusion coefficient of nitrate through the APA gel is 1.46 x $10^{-5}$ $cm^2\ s^{-1}$ at 25 °C (Huang et al., 2016c). The diffusion coefficient through the polyethersulfone filter membrane was treated as the same as the diffusion coefficient through the APA diffusive layer, because it is indistinguishably different (Davison, 2016). As such, the filter and gel components of equation 1 were aggregated to form the material diffusion layer (MDL), providing diffusion coefficient $D_{MDL}$, and diffusion layer thickness Δg.

Diffusion coefficients ($D_{gel}$, $D_f$, $D_w$) were temperature corrected using the following equation, where T = temperature (°C), $D_T$ = diffusion coefficient at temperature T ($cm^2\ s^{-1}$), and $D_{25}$ = diffusion coefficient ($cm^2\ s^{-1}$) at 25°C (Davison, 2016):

$$logD_T = \frac{1.37023(T-25) + 0.000836(T-25)^2}{109+T} + log\frac{D_{25}(273+T)}{298} \quad (2)$$

### *3.2.8 Diffusive Boundary Layer*

The Diffusive Boundary Layer (DBL), is the area of solution at the filter/solution interface with reduced analyte concentration in relation to the rest of solution. It is important to include the DBL in $C_{DGT}$ calculations because it increases the effective diffusive pathway length. The boundary layer decreases

with increased mixing of solution, i.e. at greater flow (Davison, 2016). DBL was calculated by plotting 1/M for different gel thicknesses versus δ, and by combining the slope and intercept equations (Levy et al., 2011, Zhang et al., 1998). As given in the following equation, where $D_W$ = diffusion coefficient through water; $D_{mdl}$ = material diffusion layer diffusion coefficient; y= y intercept; s = slope (Davison, 2016):

$$\boldsymbol{\delta = \frac{yD_w}{sD_{mdl}}} \quad (3)$$

### *3.2.9 Bioreactor Performance*

Bioreactor performances were calculated using nitrate data collected by DGT, high frequency grab sampling (manual at site 1 and via MPS-UV VIS at site 2), and low frequency grab sampling (grab samples only taken at deployment and removal of the DGT). Bioreactor performance was quantified as nitrate removal rate (g N $m^{-3}$ $d^{-1}$), and nitrate removal efficiency (% of nitrate removed) excluding bypass flow. Removal rate enables the comparison between denitrifying bioreactors, while removal efficiency allows for comparison to other nitrate remediation strategies.

Nitrate removal rate ($N_{removal}$ = g N $m^{-3}$ $d^{-1}$) was calculated as the nitrate removed from the inlet to the lowest concentration before nitrate concentration plateaued with distance along the bioreactor.

$$\boldsymbol{N_{removal} = \frac{(N_{inlet} - N_{limited}) \times Q_{average}}{V_{limited}}} \quad (4)$$

Where $N_{Inlet}$ and $N_{Limited}$ = nitrate-N at inlet and at the well where nitrate is limiting (g N $m^{-3}$), $Q_{average}$ = average flow rate ($m^3$ $d^{-1}$), $V_{Limted}$ = volume of bioreactor to the well where nitrate was limiting ($m^3$).

Removal efficiency (R%) was expressed as the percentage of nitrate removed from inlet to outlet, and is given by the following equation ($N_{inlet}$ and $N_{oulet}$ = nitrate-N at the inlet and outlet, mg N $L^{-1}$).

$$\boldsymbol{R\% = \frac{N_{inlet} - N_{outlet}}{N_{inlet}} \times 100} \quad (5)$$

Total organic carbon (TOC) of collected well samples was also measured to estimate the carbon readily available to denitrifying bacteria. Samples collected were analysed using OI Analytical Aurora 1030 TOC analyser (Xylem, New York USA) with carbon standards being made gravimetrically using potassium hydrogen phthalate (Hartland et al., 2012).

## 3.3. Results

### *3.3.1 Nitrate Concentration*

The significant temporal variation in nitrate-N concentration at the inlet of bioreactor site 1 was buffered by the denitrification process within the bioreactor (Figures 3.3A, 3.3B and 3.4), i.e. the fluctuations decreased in magnitude and frequency as a function of distance along the flow path. By three metres (well C3) nitrate-N concentration was effectively zero.

Temporal fluctuations at bioreactor site 2, dairy pasture tile drainage fed, were not as pronounced (Figures 3.3C, 3.3D, and 3.3E).

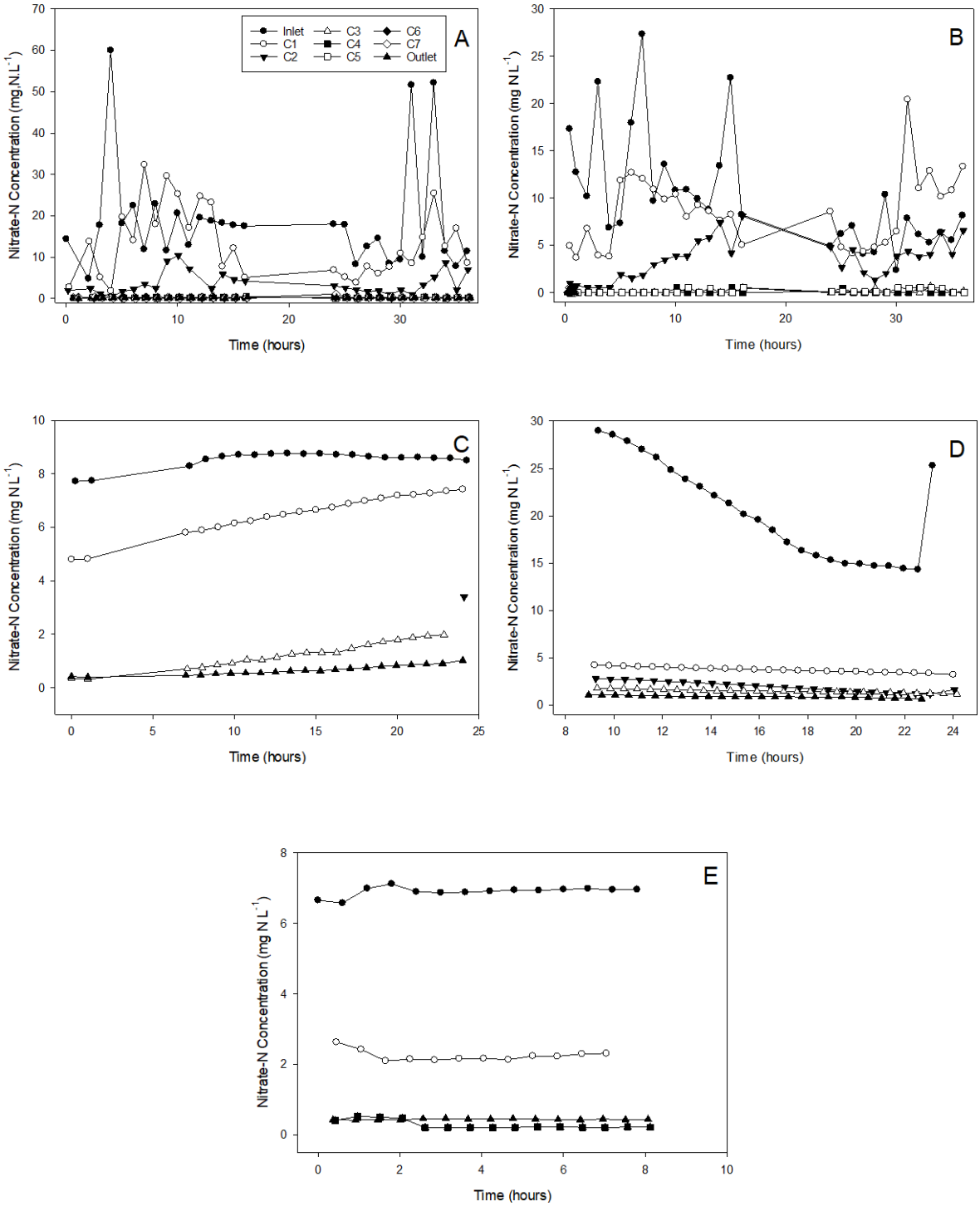


Figure 3.3**:** Temporal variation of nitrate-N concentration for bioreactor site 1, determined by hourly grab samples (A = deployment 1; B = deployment 2), and bioreactor site 2, determined by MPS-UV VIS (C = deployment 1; D = deployment 2; E = deployment 3). C1, C2, C3, C4, C5, C6, and C7 = centre wells 1, 2, 3, 4, 5, 6, and 7 respectively.

There was a strong agreement between nitrate-N concentrations determined by DGT and high frequency grab sampling at site 1 (Figure 3.4). Increasing the frequency of grab sampling might have further reduced discrepancies between DGT and grab sampling concentrations, given there is an hourly variability of up to 40 mg N $L^{-1}$ in inlet concentrations (Figure 3.3A). From 4 metres, DGT provided nitrate-N concentrations of zero, however grab sample measurements show nitrate concentrations to be very low (<0.25 mg N $L^{-1}$). This is likely due to the high concentration (64.6 ± 36.3 mg $L^{-1}$) of chloride, and subsequent competition and *in situ* eluent effects – background nitrate on the binding layer may elute into solution. The A520E DGT consistently provided higher nitrate concentrations at 2 m, possibly due to the grab sampling missing or not fully accounting for nitrate concentration spikes (see discussion).

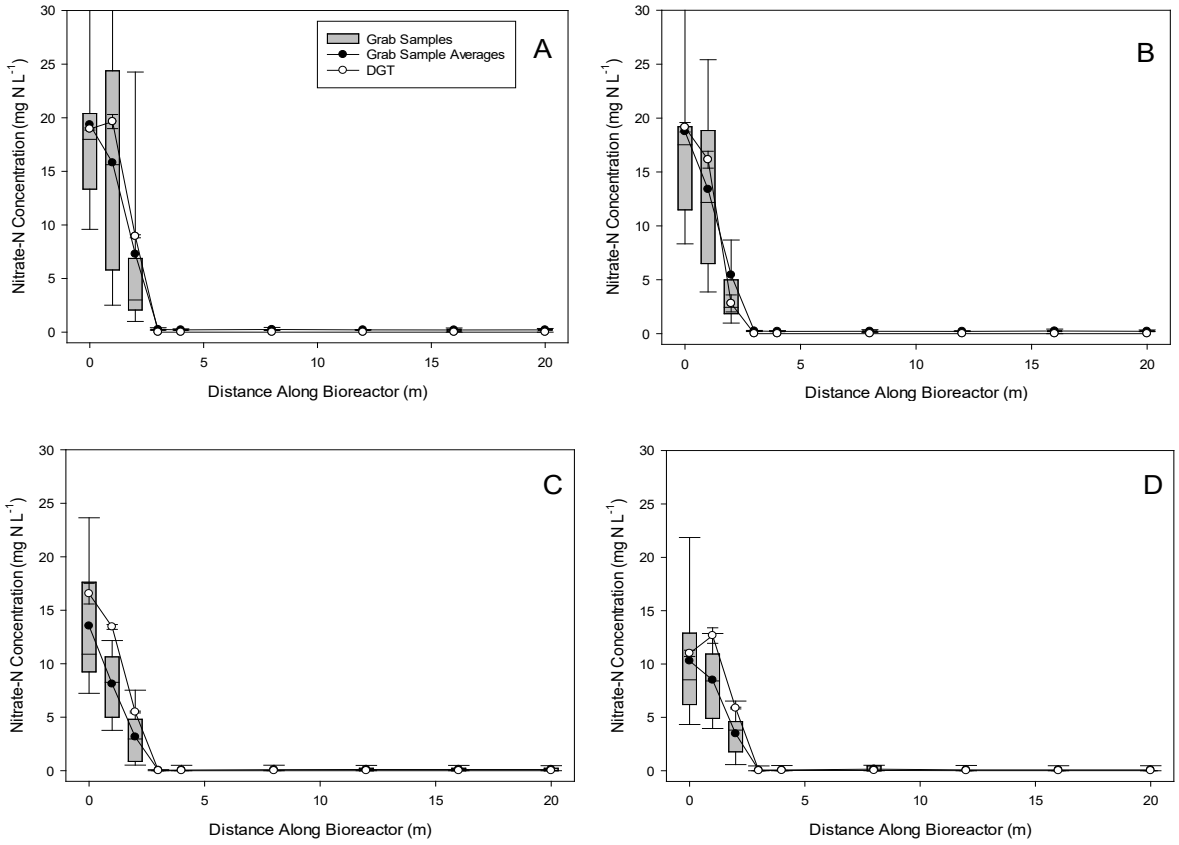


Figure 3.4: Nitrate-N concentration along bioreactor site 1 determined by DGT and high frequency grab sampling (A = deployment 1.1, 16 hours; B = deployment 1.2, 36 hours; C = deployment 2.1, 16 hours; D = deployment 2.2, 36 hours).

There was also a good agreement between DGT nitrate-N concentrations and nitrate-N concentrations determined by MPS-UV VIS at site 2, particularly at lower concentrations found from 2 m into the bioreactor. Up to 2 m along the bioreactor flow length DGT provided nitrate concentrations greater than those determined by MPS-UV (Figures 3.5A and 3.5C). Likely due to the MPS-UV system missing nitrate concentration peaks (due to fouling on the cuvette and the pumping of air), and nitrate concentration was more variable earlier in the bioreactor flow path (Figures 3.3D and 3.5B).

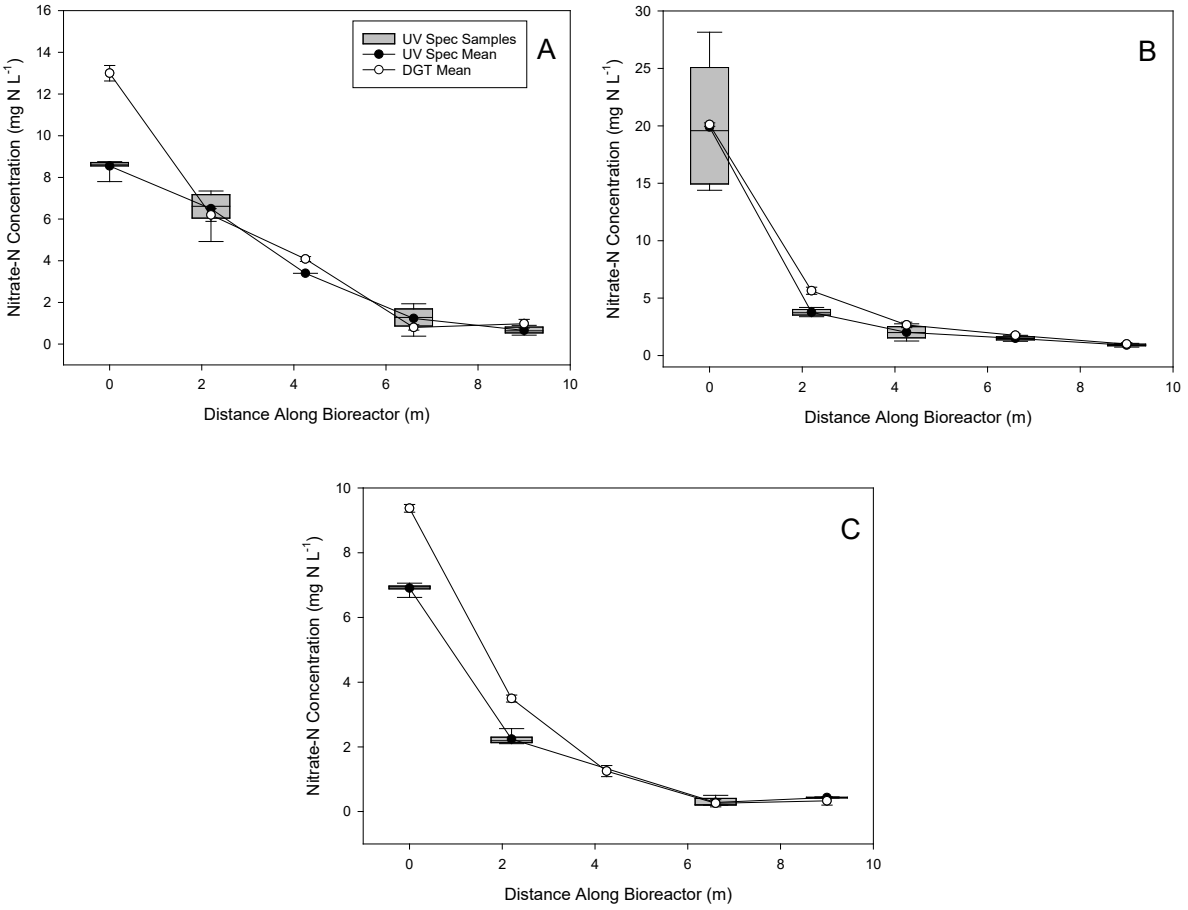


Figure 3.5 Nitrate-N concentration along bioreactor site 2 determined by DGT and MPS-UV VIS (A = deployment 1; B = deployment 2; C = deployment 3).

DGT provide nitrate concentrations of the same magnitude and trend as high frequency grab sampling in bioreactors (Figure 3.6). The magnitude of the difference between the grab sample and DGT concentrations increased as concentration increased. This was likely due to the greater variability in nitrate concentrations at the inlets of the bioreactor, where concentration is highest (Figure 3.3).

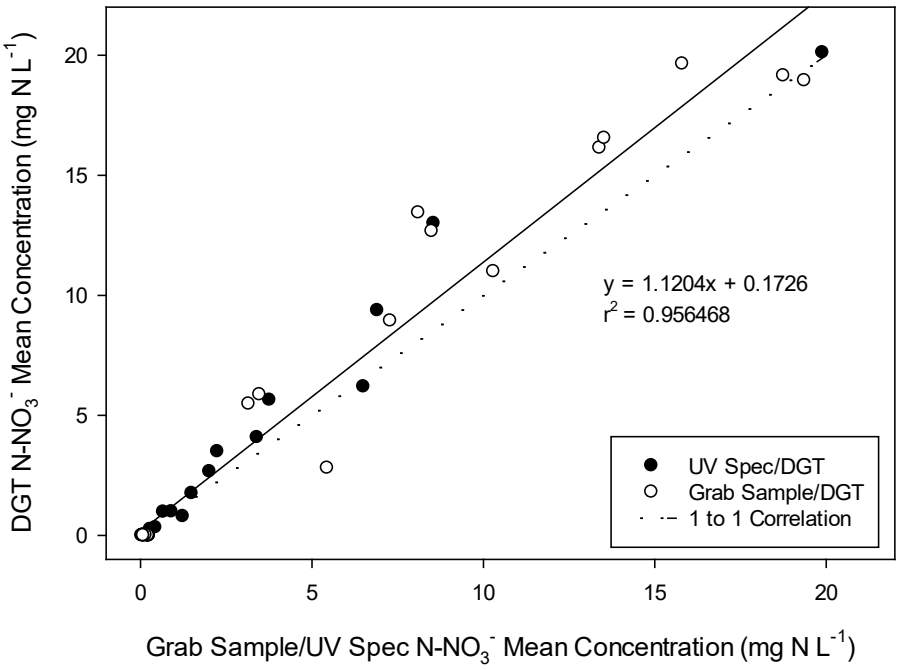


Figure 3.6**:** Mean DGT nitrate-N concentrations versus high frequency sampling nitrate-N concentration for both bioreactor deployments.

Important DGT parameters, such as DBL and resin background mass, are reported below.

### *3.3.2 Bioreactor Performance*

In general, the removal rates of the bioreactors as calculated from DGT and high frequency grab sampling or MPS-UV were in very good agreement (Table 3.1). Removal rates calculated by DGT were generally greater than those determined by high frequency grab sampling. As the frequency of grab sampling increased (from low to high) the calculated removal rates moved towards those calculated by DGT. Increasing the frequency of grab sampling, to better account for temporal variation in nitrate concentration, would likely result in grab sampling removal rates corresponding to those calculated by DGT more strongly. The removal rates at site 2 decreased as flow rate through the bioreactor decreased, i.e. as the total nitrate mass entering the system decreased.

Table 3.1: Removal rates and efficiencies, and average temperatures for bioreactor sites 1 and 2.

| Bioreactor | | Temperature (°C) | Removal Rate (g N $m^{-3}$ $day^{-1}$) | | | Removal Efficiency (%N removed) | | |
|---|---|---|---|---|---|---|---|---|
| Site | Deployment | | DGT | HFGS[a] | Grab Sampling | DGT | HFGS[a] | HFGS |
| 1 | 1.1 | 23.9 ± 0.9 | 30.75 | 29.99 | 22.87 | <99.9 | 98.9 | 99.3 |
| | 1.2 | 23.9 ± 0.9 | 28.07 | 25.16 | 15.60 | <99.9 | 98.8 | 99.2 |
| | 2.1 | 23.0 ± 0.7 | 30.46 | 24.01 | 20.12 | <99.9 | 99.2 | <99.9 |
| | 2.2 | 22.9 ± 0.7 | 14.83 | 13.38 | 16.24 | <99.9 | 99.2 | <99.9 |
| 2 | 1 | 12.3 ± 0.1 | 3.63 | 2.35 | 2.15 | 92.5 | 92.3 | 90.6 |
| | 2 | 12.3 ± 0.2 | 2.47 | 2.54 | 2.02 | 95.1 | 95.5 | 96.0 |
| | 3 | 12.3 ± 0.2 | 1.22 | 1.24 | 1.22 | 96.5 | 93.7 | 93.7 |

[a]HFGS = High Frequency Grab Sampling (site 1), and MPS-UV at bioreactor site 2. Grab Sampling = samples only taken at deployment and removal of DGT. Bioreactor site 1 is a controlled flow effluent system, and bioreactor site 2 is variable flow system fed from agricultural land.

For bioreactor site 1 sulfate removal was also measured (removal rates of 4.8 - 8.2 g $SO_4^{2-}$-S $m^{-3}$ $day^{-1}$, and removal efficiencies of 59 – 74 %) via high frequency grab sampling, as the system became nitrate limited (Figures 3.7A and 3.7B). Sulfate reduction efficiency in this study was significantly lower than the 94 % reduction previously reported for the same bioreactor (Rambags et al., 2016). Mean phosphate concentration marginally increased (4.77 to 5.40 mg $L^{-1}$, 13.3 %), contrary to the mean decrease of 7 % previously reported for this site (Rambags et al., 2016).

TOC provides measurement of the carbon readily available to denitrifying bacteria. For bioreactor site 1, the mean TOC concentrations were relatively high at the inlet (~10 mg C $L^{-1}$), presumably persisting from the effluent wastewater, and decreased by about 5 mg C $L^{-1}$ in the first 4 m along with nitrate reduction (Figure 3.7).

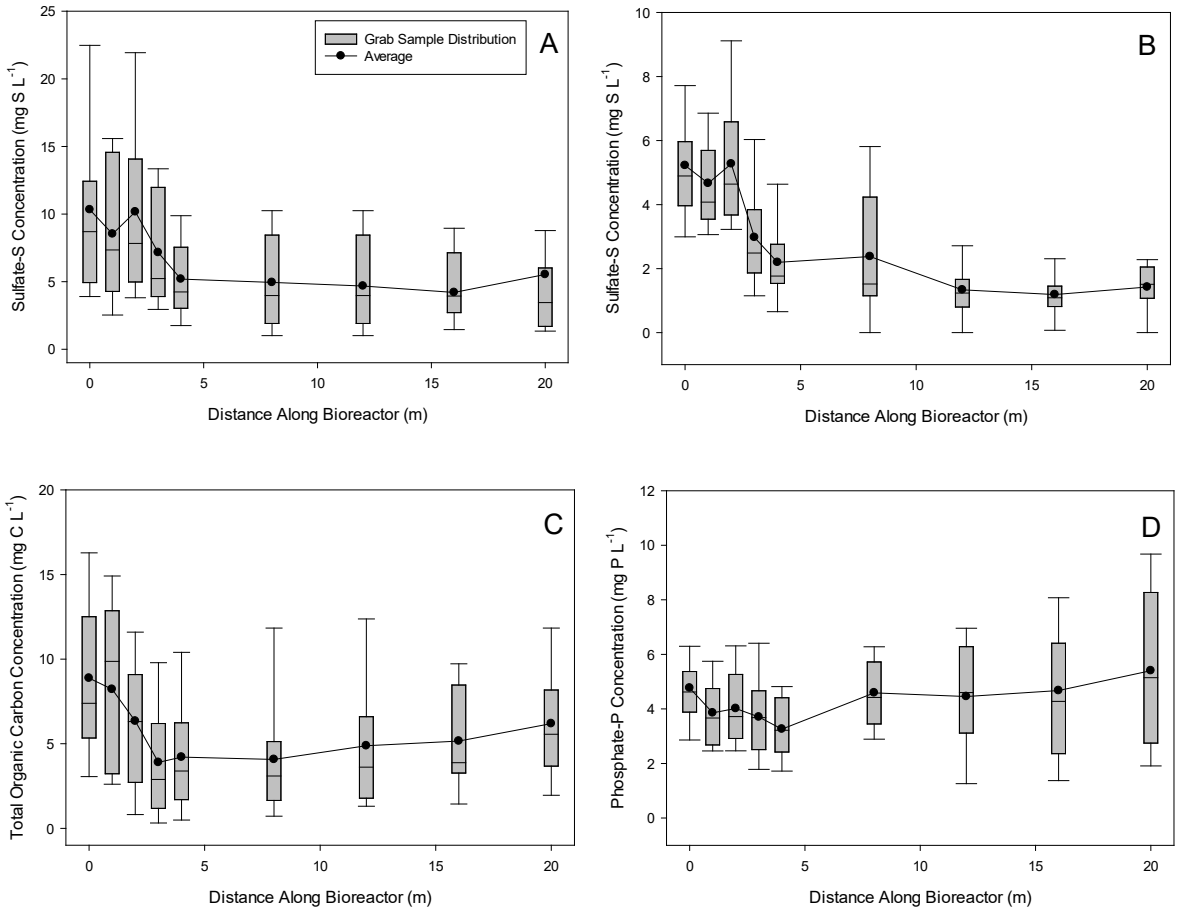


Figure 3.7: Sulfate, Total Organic Carbon (TOC) and phosphate determined by grab sampling. Sulfate-S concentrations at bioreactor site 1 (A = deployment 1; B = deployment 2). (C) TOC through bioreactor site 1 for deployment 2. (D) Phosphate-P concentration for bioreactor site 1 deployment 2.

Temperature at the two sites was both consistent at each well and across the bioreactor as a whole (Table 3.1). Temperature at site 1 ranged from 21-25$^{o}$C and did not change at each well or at the inlet and outlet for the length of each deployment. At site 2, temperatures ranged from 11-13$^{o}$C, and changed <1$^{o}$C at each well over each deployment. Temperature has previously been reported to have a significant impact on denitrification and removal rates (Addy et al., 2016).

### *3.3.3 Diffusive Boundary Layer*

The DBLs at both bioreactor sites were large and differed between the outlet, inlet and centre wells. While the DBLs varied between wells, at each measurement location they were reasonably consistent,

indicating that deployment conditions were reasonably constant in terms of mixing mechanisms. The more constrained (less well mixed) centre wells generally had larger DBLs than the inlet and outlet chambers. At bioreactor site 1, the mean DBL was 0.215 ± 0.092 cm (± standard deviation). From 3 m (well C3) to 20 m (outlet) DGT provided nitrate concentration values of 0, therefore no DBL could be calculated. The mean DBL at 0 m (inlet) was 0.209 ± 0.056 cm, and at the centre wells (1 – 2 m) was 0.218 ± 0.105 cm. At bioreactor site 2, the mean DBL was 0.250 ± 0.188 cm. The mean DBL at the inlet (0 m) was 0.198 ± 0.015 cm, at the centre wells was 0.252 ± 0.231 cm, and at the outlet (9 m) was 0.303 ± 0.025 cm.

### *3.3.4 Background Concentration, Elution and Uptake Efficiencies and Saturation Point*

The background mass of $NO_3^-$-N for 2.5 g A520E gels used at bioreactor site 2 was 0.01065 ± 0.00065 mg N, and for the 4 g A520E gels used at site 1 the background $NO_3^-$-N mass was 0.01675 ± 0.00212 mg N. The relative amount of the total accumulated mass in the resin was dependent on numerous deployment factors (e.g. length of deployment, temperature, and system concentration). There was low variability in blank masses for each set of resin gels made (generally <3 %), however, the variability in background mass of blank resin disks between gel sets was more significant ($NO_3^-$N mass varied by 6 - 16 %), demonstrating that accounting for the background mass specific to the gels of each deployment was essential.

The uptake efficiency was 98.8 %, and the elution efficiency was 93.4 %. The saturation point of the binding gels produced with 2.5, 4.0 and 5.4 g of A520E resin were 0.81 ± 0.042 (equivalent to ± % 5.16), 1.03 ± 0.010 (± % 0.98), and 1.68 ± 0.045 (± % 2.66) mg N, respectively.

### *3.3.5 Adsorption Isotherm*

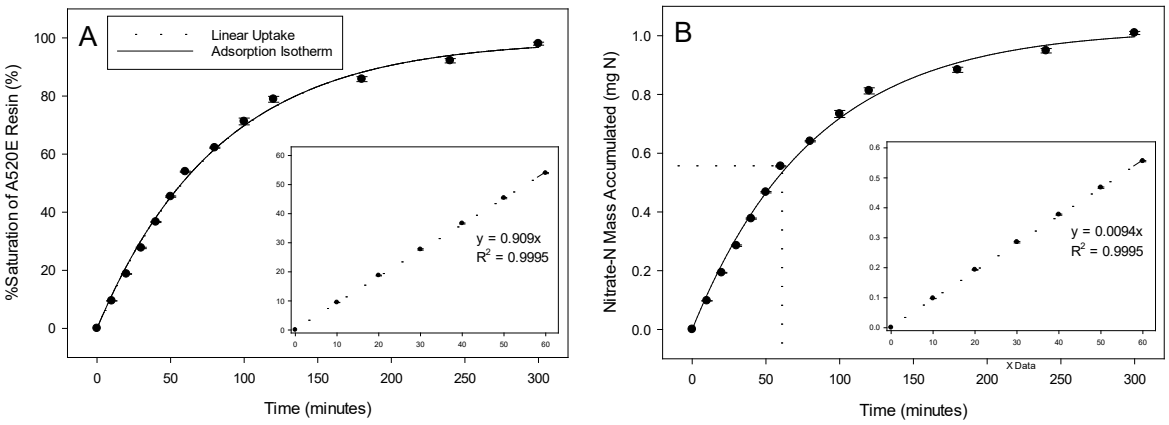


Figure 3.8: Adsorption isotherm as (A) %saturation, and (B) mass accumulated versus time.

Nitrate adsorption to the A520E binding gel was linear up to 55 % saturation of the binding sites (Figure 3.8A). This equates to approximately 0.55 mg N adsorbed or removed from solution (Figure 3.8B). The binding gels, however, continued to adsorb strongly up to 80 % (approximately 0.8 mg N) before adsorption began to tail off and approach 100 % of adsorption sites occupied (100 % saturation).

### *3.3.6 Gel Dehydration*

Drying of gels, under clean laboratory conditions at room temperature, resulted in a decrease in the measured nitrate of <5 % compared to gels which were not dehydrated.

## 3.4. Discussion

### *3.4.1 Bioreactor Nitrate Determination by DGT*

We have demonstrated that DGT were capable of providing environmental nitrate concentration measurements comparable to high frequency grab sampling to demonstrate the performance of denitrifying bioreactors in nutrient mitigation strategies (Figure 3.6). Importantly DGT were easy to use and reduced the analytical requirements associated with high frequency grab sampling. Additionally there was no need for preservation prior to analysis.

A520E DGT adsorbed nitrate continuously during deployment, accounting for fluctuations in nitrate concentration that could be missed by even relatively high frequency grab sampling. Grab sampling at hourly intervals is unlikely to fully capture the temporal variation in nitrate concentration, which fluctuated by up to 40 mg N $L^{-1}$ within 1 hour. These changes are unlikely to be linear between sampling times (Figure 3.3). Consequently, discrepancies between nitrate determined by DGT from that determined by high frequency grab sampling (Figure 3.6) likely reflects the need for higher frequency grab sampling to truly capture the temporal fluctuations. Depending on the frequency of grab sampling it could be easy to miss nitrate peaks and troughs, as such in general it would be expected that DGT determined concentrations to differ from average nitrate concentrations determined by grab sampling.

The difference in nitrate concentration determined using A520E DGT and high frequency grab sampling increased with increasing nitrate concentration. This increasing difference was likely due to the increased nitrate concentration and magnitude of variation in nitrate concentrations at the bioreactor inlets and first wells. As discussed above these variations in nitrate concentrations cannot be easily captured by high frequency grab sampling but are in DGT. Removal rates and efficiencies approached those calculated by DGT as the frequency of grab sampling increased.

While this is the first time DGT have been used to determine mitigation potentials, they have previously been used to monitor nitrate in a variety of freshwater systems (i.e. streams and wetlands) (Huang et al., 2016b). These authors also showed that grab sampling 1-2 times daily resulted in nitrate concentrations that varied dramatically over the 24 and 72 hour deployment times however DGT and grab samples remained in close agreement, with a DGT to grab sample ratio between 1.00 and 1.12 (Huang et al., 2016b). As demonstrated in our research, the required frequency of grab sampling to account for large changes in nitrate concentration was greater than hourly. Consequently discrepancies between DGT and grab sample nitrate concentrations that Huang et al. (2016b) reported could be due to sampling frequency (1-2 times daily).

As demonstrated DGT were useful for determining nitrate concentrations and removal rates, but they have also been utilised to quantify numerous aqueous anionic and cationic species. For example, ferrihydrite binding resins have been widely been reported for the quantitative measurement of dissolved reactive phosphorus (Panther et al., 2010, Saeed et al., 2018). CMI-7000 cationic exchange membranes have successfully been used for determination of ammonium (Huang et al., 2016c). The Chelex-100 resin for *in situ* measurement of trace metals was reported to be capable of measuring metals at extremely low concentrations (4 pmol $L^{-1}$) independently of ionic strength (10 nmol $L^{-1}$ to 1 mol $L^{-1}$) and pH (5 - 8.3) (Zhang and Davison, 1995).

### *3.4.2 Strengths and Weaknesses*

DGT are simple and robust, deployment requires little more than nylon fishing line and a weight to hold the DGT in place. Diffusive Gradients in Thin Films overcome the temporal variability, in-field time, operational range, preservation, and expense limitations of other sampling methods.

DGT not only provide improved nutrient concentration data comparable to high frequency grab sampling, thereby decreasing the number of samples that require analysis and associated time, but also reduce the risk to expensive analytical instruments (e.g. ion chromatographs). Diffusive Gradients in Thin Films are analyte specific, as such they can overcome the matrix effects of analysing water samples which can interfere with optical methods. A520E DGT have a large operational pH range (3.5-8.5) (Huang et al., 2016a). Natural systems, bioreactors and other mitigation strategies can have low pH. The increased reducing conditions increase the solubility of metals such as Fe(II) – which persist in grab samples after filtering. These can precipitate out of solution, when analysing water samples with ion chromatography and hydroxide as the eluent. Precipitation within componentry of analytical instruments can be difficult and expensive to resolve.

One constraint of the use of DGT is the dependence of diffusivity on environmental temperature. As temperature increases so too does the diffusion coefficient due to the increase in the random heat motion of molecules. If temperature changes are large and not fully monitored then diffusivity could

be over/under-estimated resulting in increased error in $C_{DGT}$. However, there was very little variation in temperature in either bioreactor over the deployment periods, as such temperature measurements at DGT deployment and removal suffice. This is because the surrounding thermal mass insulates the water body from short term temporal shifts in weather and air temperature. In contrast the variability of temperature in natural systems (e.g. lakes, rivers and streams), is greater than that of denitrifying bioreactors. Natural streams are more exposed to shading/sunning and other weather events. Huang et al. (2016b) used A520E DGT to monitor seven freshwater systems, and temperature measurements were made at least twice daily, and as stated earlier DGT provided nitrate concentrations in good agreement with low frequency grab sampling. This supported the use of A520E DGT for environmental measurements, although best practice involves temperature measurements throughout.

### *3.4.3 Background Mass, Uptake/Elution Efficiencies, and Saturation*

There was significant and variable background nitrate within the A520E resin; to ensure concentration data were accurate this needs to be quantified for each set of gels made, and subtracted from the total nitrate post deployment. The gels are highly efficient at adsorbing nitrate (uptake efficiency = 98.8 %); Huang et al. (2016a) found uptake efficiencies to be >98 %. Huang et al. (2016a) also reported elution efficiencies of 82.7 %, which was improved in this study to 93.4 %.

The marginal increase in uptake efficiency was likely due to an increase in the surface area of the A520E resin in the binding gels of this research. In the previous study, resin beads were not sieved, which can lead to a greater variation in particle sizes and the presence of larger resin particles. The mass of A520E suspended in the hydrogel was also increased here. Combined, these modifications to the method provide a greater number of sites for nitrate adsorption, evidenced by the increase in saturation point. Bioreactors can experience very high nitrate concentrations, increasing the adsorption maximum increases the total deployable time of the DGT. This in turn increases the length of time $C_{DGT}$ accounts for, and therefore the relevance of the calculated removal rate.

The increase in elution efficiency (9.7 %) was likely due to increasing the volume of 2 mol $L^{-1}$ NaCl eluent utilised from 2 mL to 4 mL. This ensured that the gels were fully submerged during elution and that there remained a significant stoichiometric excess of chloride ions for substitution of nitrate ions bound to the A520E resin.

Determining the saturation point of the A520E resins was necessary to understand the total length of time the resins could be deployed. If the deployed sensors became saturated over the course of the deployment, the calculated concentration would underestimate the actual concentration – no further nitrate can be adsorbed once the resin is saturated.

The optimal mass of dried ground A520E for the preparation of binding gels was found to be 4 g, in 10 mL of gel solution. Even though 5.4 g binding gels provided higher saturation points there were difficulties suspending all of the resin in the gel solution and pipetting the gel suspension between the glass plates.

The 4 g A520E binding resins adsorbed nitrate linearly up to 55 % adsorption site occupation (approximately 0.55 mg N), however they continued to adsorb strongly up to 80 % (approximately 0.8 mg N) (Figure 3.8). Although the DGT continued to adsorb nitrate up to the adsorption maximum it is recommended that deployment times should not exceed those which would provide 80 % adsorption site occupation. As the adsorption moved away from the linearity it was anticipated that the resin would no longer meet the adsorption requirements for equation 1 to be true.

### *3.4.4 Diffusive Boundary Layer*

The Diffusive Boundary Layer, DBL, is the area outside solution with reduced analyte concentration compared to the rest of solution and is effectively the extension of the concentration gradient through the material diffusion layer (Davison, 2016). There is a layer where there is effectively no flow close to the surface of any solid in a fluid, and extends further into solution if mixing mechanisms in the surrounding solution are poor (e.g. low solution flow rates) (Davison, 2016). For use of DGT in well-stirred solutions the DBL is generally ignored on the assumption that compared to the total thickness

of Δg, the DBL is negligibly small (Warnken et al., 2006). Bioreactor wells, and inlet and outlet chambers are not well stirred, and the DBL values determined were large and variable.

It was unsurprising that the DBL values were higher than observed in well mixed systems, as the wells were highly constrained flow environments – the well diameters were 50 mm, little more than the diameter of the DGT 40 mm – and the flow rate through the bioreactors was low. Consequently, it was critical to include the DBL in the full calculation of concentration. This is best practice, and likely necessary for all DGT deployments in piezometers, however, it should also be performed for all DGT deployments. Huang et al. (2016b) also found that $C_{DGT}$ underestimated the concentration determined via grab sampling if DBL was ignored, and when DBL was included $C_{DGT}$ trended towards the concentration determined via grab sampling.

Measuring the DBL can also provide insights as to how well mixed the solution was at the sampling location, providing useful information about solution dynamics when deploying in natural systems (streams, lakes, rivers). Huang et al. (2016b) reported DBLs 0.036 to 0.101 cm, with the creek sampling locations having much smaller DBLs than the slower moving pond sites (Huang et al., 2016b). This was to be expected and is in accordance with the much higher values generally seen in the bioreactors (site 1 = 0.215 ± 0.0917 cm; site 2 = 0.250 ± 0.188 cm) which have greater constrained flows. DBL was also generally smaller in the freer flowing inlet and outlet chambers. If how the DBL changes with flow rate is known it may be possible to calculate/estimate the DBL if flow rate is measured, and vice versa.

### *3.4.5 Nitrogen Removal in Bioreactors*

Simple and accurate methods for measuring nitrate concentrations over extended periods of time will be useful for determining the performance of different mitigation strategies. A major advantage of DGT for assessing N removal rates within mitigation systems is that they obtain time weighted average concentrations, reducing the influence of the temporal variability of instantaneous concentrations on average N removal rates.

Removal rate is generally used for inter-bioreactor comparisons, with reported values generally 2 - 22 g $NO_3^-$-N $m^{-3}$ $d^{-1}$ (Schipper et al., 2010a), however higher removal rates for wastewater have been reported (>39 g N $m^{-3}$ $d^{-1}$) likely due to concurrent inputs of wastewater carbon that support denitrification (Lepine et al., 2016). Nitrate removal rates of the two bioreactor systems used in this study fit at both ends of this range (Table 3.1). Bioreactor site 1 received effluent with high nitrate and organic carbon concentrations at high and constant flow, resulting in increased nitrate reduction. In comparison, site 2 received water leachate from an agricultural field, where the supply of nitrate was determined by rainfall and available nitrate for leaching. Nitrogen limitation has been reported to significantly decrease nitrate removal (Addy et al., 2016).

Nitrate removal rates are also temperature dependent, although even at low temperatures nitrate removal has been reported to be substantial (Addy et al., 2016). This can, in part, explain some of the difference in nitrate removal rates between the two systems. The average temperatures at site 1 (21 - 25 $^oC$) were considerably higher than at site 2 (11 - 13 $^oC$), potentially due to seasonal variation and the upstream wastewater treatment at site 1. The high nitrate removal at site 1 was likely due to the organic carbon input with the effluent (Lepine et al., 2016).

Rambags et al. (2016) report removal rates of ~14 g N $m^{-3}$ $d^{-1}$ calculated to 4 m (equivalent to ~19 g N $m^{-3}$ $d^{-1}$, when calculated to 3 m as in this study) for bioreactor site 1. These rates were generally lower than the removal rates calculated in this study (removal rate range 26 ± 6.5 g N $m^{-3}$ $d^{-1}$). This difference was unlikely due to a change in inputs, and instead the removal rate should decrease with time as the available carbon is consumed and the wood chips deteriorate. It is most probable that the low frequency of sampling in the Rambags et al. (2016) study did not fully account for large short-term changes in nitrate concentration.

Nitrate removal efficiencies (%) do not fully capture the performance of bioreactors because they are dependent on bioreactor characteristics that percentage cannot capture (flow rate and size). They are, however, widely reported in the literature as a bioreactor performance metric and can be utilised for

inter-mitigation strategy comparisons. Bioreactor site 1 was efficient at removing nitrate, achieving removal efficiencies >98.8 % determined by both DGT and high frequency grab sampling. This was in good agreement with previously reported removal efficiencies, Rambags et al. (2016) reported nitrate removal efficiency to be >99.9% for the same bioreactor site, even though grab sample measurements were only made bimonthly. This was unsurprising given that both the DGT and high frequency sampling found nitrate to be completely removed by 3 metres. Bioreactor site 2, similarly achieved high removal efficiencies >90% determined by DGT and grab sampling. Bypass flow at the site was not accounted for and it is expected that the true removal efficiency would decrease as bypass would increase the total mass of nitrate not removed.

In comparison to other nitrate mitigation strategies, the bioreactors studied here compare well in terms of removal efficiencies. Horizontal subsurface-flow wetlands, constructed such that wastewater flow through shallow gravel-filled beds planted with emergent macrophytes, commonly achieve nitrogen reductions of 30-50% (Tanner et al., 2012). Saturated buffers have been engineered to reconnect riparian buffers to the above agricultural land area, otherwise diverted via drainage (Jaynes and Isenhart, 2014), and have reported nitrate removal efficiencies from 8-84% (Jaynes and Isenhart, 2019). Saturated buffers promote nitrate removal via plant uptake, immobilisation and denitrification (Jaynes and Isenhart, 2014). Drainage water is diverted to flow through vegetated buffer soil as shallow groundwater (Chandrasoma et al., 2019). The removal efficiencies of bioreactor site 2, however, are likely overstated, given that bypass flow and the associated nitrate mass was not accounted for.

The complete removal of nitrate resulted in a highly excessive reducing environment that supported sulfate reduction at bioreactor site 1. Sulfate reduction was observed in bioreactor 1 via the high frequency sampling (although not designed for this purpose), with removal rates of 4.8 - 8.2 g $SO_4^{2-}$-S $m^{-3}$ $day^{-1}$, and removal efficiencies of 59 - 74%. Sulfate reduction was initially identified by the smell of hydrogen sulfide at both bioreactors, particularly at the outlets. Sulfate reducing bioreactors have

been used for the treatment of contaminated acid mine drainage, with metal removal rates of 60 – 80 % for Fe and up to 99 % for Cd, Ni and Zn (Neculita et al., 2008), however sulfate reducing conditions have been reported to lead to the production of highly toxic methyl mercury (Shih et al., 2011).

Increased phosphate has been found to stimulate phytoplankton blooms resulting in negative environmental consequences such as eutrophication (Hai et al., 2010). Phosphate removal by denitrifying woodchip bioreactors is not well-documented (Schipper et al., 2010a, Schipper et al., 2010b). Phosphate attenuation does not occur through the path-length of bioreactor 1 (Figure 3.7D), even though it completely removes nitrate and significantly reduces sulfate (Figures 3.7A and 3.7B). Bioreactor amendments, such as the inclusion of iron filters (Guanghui et al., 2016), may be necessary if denitrifying bioreactors are to be used more broadly for the removal of nutrient contaminants.

### *3.4.6 Conclusion*

Bioreactors have been found to be effective methods for treating point and non-point source nitrate enriched water. Diffusive Gradients in Thin Films were useful for determining the performance of bioreactors by integrating short term fluctuations in analyte concentration. As reported in other research, the utility of DGT further extends to analysing the movement of nitrate through the wider landscape, thereby enabling identification of hotspots such that appropriate mitigation strategies or adapted land management practices may be applied. A520E DGT can help target solutions to decrease environmental reactive nitrogen, and as our research shows, are then capable of analysing the performance of implemented mitigation strategies.

## Funding

This study was funded by The University of Waikato, DairyNZ and the Ministry for Primary Industries.

## Acknowledgments

We would like to acknowledge Lincoln Agritech, Aqualink, and Livestock Improvement Corporation for access to the bioreactor sites, and Purolite for the A520E anionic exchange resin. The views expressed in this paper are those of the authors and do not necessarily reflect the views or policies of DairyNZ or the Ministry for Primary Industries.

## References


ADDY, K., GOLD, A. J., CHRISTIANSON, L. E., DAVID, M. B., SCHIPPER, L. A. & RATIGAN, N. A. 2016. Denitrifying Bioreactors for Nitrate Removal: A Meta-Analysis. *Journal of Environmental Quality,* 45**,** 873-881.

AUDET, J., MARTINSEN, L., HASLER, B., DE JONGE, H., KARYDI, E., OVESEN, N. B. & KRONVANG, B. 2014. Comparison of sampling methodologies for nutrient monitoring in streams: uncertainties, costs and implications for mitigation. *Hydrology and Earth System Sciences,* 18**,** 4721-4731.

CHANDRASOMA, J. M., CHRISTIANSON, R. D. & CHRISTIANSON, L. E. 2019. Saturated Buffers: What Is Their Potential Impact across the US Midwest? *Agricultural & Environmental Letters,* 4.

CHRISTIANSON, L. E. & SCHIPPER, L. A. 2016. Moving Denitrifying Bioreactors beyond Proof of Concept: Introduction to the Special Section. *Journal of Environmental Quality,* 45**,** 757-761.

DAVISON, W. 2016. *Diffusive Gradients in Thin-Films for Environmental Measurements,* Cambridge, UNITED KINGDOM, Cambridge University Press.

GALLOWAY, J. N., ABER, J. D., ERISMAN, J. W., SEITZINGER, S. P., HOWARTH, R. W., COWLING, E. B. & COSBY, B. J. 2003. The Nitrogen Cascade. *BioScience,* 53**,** 341-356.

GUANGHUI, H., SALO, M. W., SCHMIT, C. G. & HAY C. H. 2016. Nitrate and phosphate removal from agricultural subsurface drainage using laboratory woodchip bioreactors and recycled steel byproduct filters. *Water Research,* 102, 180-189.

HARTLAND, A., BAKER, A., TIMMS, W., SHUTOVA, Y. & YU, D. 2012. Measuring dissolved organic carbon δ13C in freshwaters using total organic carbon cavity ring-down spectroscopy (TOC-CRDS). *Environmental Chemistry Letters,* 10**,** 309-315.

HAI, X., PAERL, H. W., QIN, B., ZHU, G. & GAO, G. 2010, Nitrogen and phosphorus inputs control phytoplankton growth in eutrophic Lake Taihu, China. *Limnol. Oceanogr.,* 2010, 55, 420-432.

HUANG, J., BENNETT, W., R TEASDALE, P., GARDINER, S. & WELSH, D. 2016a. Development and evaluation of the diffusive gradients in thin films technique for measuring nitrate in freshwaters. *Analytica Chimica Acta,* 923**,** 74-81.

HUANG, J., BENNETT, W. W., WELSH, D. T., LI, T. & TEASDALE, P. R. 2016b. "Diffusive Gradients in Thin Films" Techniques Provide Representative Time-Weighted Average Measurements of Inorganic Nutrients in Dynamic Freshwater Systems. *Environmental Science & Technology,* 50**,** 13446-13454.

HUANG, J., BENNETT, W. W., WELSH, D. T. & TEASDALE, P. R. 2016c. Determining time-weighted average concentrations of nitrate and ammonium in freshwaters using DGT with ion exchange membrane-based binding layers. *Environmental Science: Processes & Impacts,* 18**,** 1530-1539.

JAYNES, D. B. & ISENHART, T. M. 2014. Reconnecting Tile Drainage to Riparian Buffer Hydrology for Enhanced Nitrate Removal. *Journal of Environmental Quality,* 43**,** 631-638.

JAYNES, D. B. & ISENHART, T. M. 2019. Performance of Saturated Riparian Buffers in Iowa, USA. *Journal of Environmental Quality,* 48**,** 289-296.

KING, R. C., MULLIGAN, P. K. & STANSFIELD, W. D. 2013. Diffusion. *A Dictionary of Genetics.* 8 ed. Oxford: Oxford University Press.

LEPINE, C., CHRISTIANSON, L., SHARRER, K. & SUMMERFELT, S. 2016. Optimizing Hydraulic Retention Times in Denitrifying Woodchip Bioreactors Treating Recirculating Aquaculture System Wastewater. *Journal of Environmental Quality,* 45**,** 813-821.

LEVY, J., ZHANG, H., DAVISON, W. & GROBEN, R. 2011. Using diffusive gradients in thin films to probe the kinetics of metal interaction with algal exudates. *Environmental Chemistry,* 8**,** 517-524.

MAXWELL, B. M., BIRGAND, F., SMITH, B. & AVENI-DEFORGE, K. 2018. A small-volume multiplexed pumping system for automated, high-frequency water chemistry measurements in volume-limited applications. *Hydrology and Earth System Sciences,* 22**,** 5615-5628.

MENEGÁRIO, A. A., YABUKI, L. N. M., LUKO, K. S., WILLIAMS, P. N. & BLACKBURN, D. M. 2017. Use of diffusive gradient in thin films for *in situ* measurements: A review on the progress in chemical fractionation, speciation and bioavailability of metals in waters. *Analytica Chimica Acta,* 983**,** 54-66.

NECULITA, C.-M., ZAGURY, G. J. & BUSSIÈRE, B. 2008. Effectiveness of sulfate-reducing passive bioreactors for treating highly contaminated acid mine drainage: I. Effect of hydraulic retention time. *Applied Geochemistry,* 23**,** 3442-3451.

PANTHER, J. G., TEASDALE, P. R., BENNETT, W. W., WELSH, D. T. & ZHAO, H. 2010. Titanium Dioxide-Based DGT Technique for In Situ Measurement of Dissolved Reactive Phosphorus in Fresh and Marine Waters. *Environmental Science & Technology,* 44**,** 9419-9424.

RAMBAGS, F., TANNER, C. C., STOTT, R. & SCHIPPER, L. A. 2016. Fecal Bacteria, Bacteriophage, and Nutrient Reductions in a Full-Scale Denitrifying Woodchip Bioreactor. *Journal of Environmental Quality,* 45**,** 847-854.

RIVETT, M. O., BUSS, S. R., MORGAN, P., SMITH, J. W. N. & BEMMENT, C. D. 2008. Nitrate attenuation in groundwater: A review of biogeochemical controlling processes. *Water Research,* 42**,** 4215-4232.

S˙LIWKA-KASZYŃSKA, M., KOT-WASIK, A. & NAMIEŚNIK, J. 2003. Preservation and Storage of Water Samples. *Critical Reviews in Environmental Science and Technology,* 33**,** 31-44.

SAEED, H., HARTLAND, A., LEHTO, N. J., BAALOUSHA, M., SIKDER, M., SANDWELL, D., MUCALO, M. & HAMILTON, D. P. 2018. Regulation of phosphorus bioavailability by iron nanoparticles in a monomictic lake. *Scientific Reports,* 8**,** 17736.

SCHIPPER, L., ROBERTSON, W., GOLD, A., JAYNES, D. B. & C. CAMERON, S. 2010a. Denitrifying Bioreactors — An Approach for Reducing Nitrate Loads to Receiving Waters. *Ecological Engineering,* 36**,** 1532-1543.

SCHIPPER, L., CAMERON, S., WARNEKE, S. 2010b. Nitrate removal from three different effluents using large-scale denitrification. *Ecological Engineering,* 36, 1552-1557.

SHIH, R., ROBERTSON, W. D., SCHIFF, S. L. & RUDOLPH, D. L. 2011. Nitrate Controls Methyl Mercury Production in a Streambed Bioreactor. *Journal of Environmental Quality,* 40**,** 1586-1592.

TANNER, C. C., SUKIAS, J. P. S., HEADLEY, T. R., YATES, C. R. & STOTT, R. 2012. Constructed wetlands and denitrifying bioreactors for on-site and decentralised wastewater treatment: Comparison of five alternative configurations. *Ecological Engineering,* 42**,** 112-123.

WARNKEN, K. W., ZHANG, H. & DAVISON, W. 2006. Accuracy of the Diffusive Gradients in Thin-Films Technique: Diffusive Boundary Layer and Effective Sampling Area Considerations. *Analytical Chemistry,* 78**,** 3780-3787.

ZHANG, H. & DAVISON, W. 1995. Performance Characteristics of Diffusion Gradients in Thin Films for the in Situ Measurement of Trace Metals in Aqueous Solution. *Analytical Chemistry,* 67**,** 3391-3400.

ZHANG, H., DAVISON, W., GADI, R. & KOBAYASHI, T. 1998. In situ measurement of dissolved phosphorus in natural waters using DGT. *Analytica Chimica Acta,* 370**,** 29-38.

# Chapter 4 - Incorporation of Zero-Valent Metal Reductants and Gold Nanoparticles into Hydrogel Networks for Colourimetric DGT Nitrate Determination

## Abstract

Diffusive Gradients in Thin-Films (DGT) have been established as useful tools for the determination of nitrate, phosphate, trace metals, and organic concentrations. Diffusive Gradients in Thin Films, however, are limited by the requirement for laboratory analysis. To increase the uptake of DGT as a tool for routine monitoring by interest groups, not researchers alone, methods for infield analysis are required. Incorporation of colour reagents into the binding layer, or as the binding layer, can enable the easy and accurate determination of analyte concentrations infield. Here we sought to develop a chitosan-stabilised gold nanoparticles (AuNP) suspension liquid binding layer which developed colour on exposure to nitrite, combined with a Fe(0) impregnated poly-2-acrylamido-2-methyl-1-propanesulfonic acid/acrylamide copolymer hydrogel Fe(0)-p(AMPS/AMA) for the reduction of nitrate. The AuNP-chitosan suspension was housed in a 3D designed and printed DGT base, with volume of 2 mL, for use with the standard DGT solution probe caps. Dialysis membrane with a molecular weight cut-off of <15 kDa was used, as part of the material diffusion layer, to ensure the AuNP-chitosan did not diffuse through to bulk solution. This synthesised AuNP-chitosan provided quantitative nitrite concentrations (0 to 1000 mg $L^{-1}$) and masses (145 µg) in lab-based colour development studies. A Fe(III) impregnated poly-2-acrylamido-2-methyl-1-propanesulfonic acid/acrylamide copolymer hydrogel (Fe(III)-p(AMPS/AMA)) was developed (10 % AMPS, and 90 % AMA), which was treated with $NaBH_4$ to form an Fe(0)-p(AMPS/AMA) hydrogel. The Fe(0)-p(AMPS/AMA) hydrogel quantitatively reduced nitrate to nitrite. The total nitrite mass produced was ~110 µg, from nitrate. The diffusional characteristics of nitrite and nitrate through the Fe(III)-p(AMPS/AMA) and dialysis membrane were 1.40 x $10^{-5}$ and 1.40 x $10^{-5}$, 5.05 x $10^{-6}$ and 5.15 x $10^{-6}$ $cm^2$

$s^{-1}$ at 25 °C respectively. Further research is required to improve the reaction rate of the AuNP-chitosan nitrite binding layer, to operate as a DGT, and for coupling with the Fe(0) hydrogel.

## 4.1. Introduction

The increase in nitrate concentrations in freshwater systems is in part a result of the increased application of nitrogen fertilisers and cultivation of nitrogen fixers in food production and cropping. Discharge of wastewater into the environment has also led to increased environmental concentrations. Importantly, a single nitrogen atom can impact all biospheres before denitrification back to $N_2$, as it is sequentially transferred from agricultural land, through freshwater systems to the ocean (Galloway et al., 2003). Measurement and determination of nitrate concentrations are therefore paramount to understand and reverse the negative effects associated with increased nitrate inputs into nutrient sensitive ecosystems.

Numerous techniques have been deployed for the measurement and determination of nitrate concentration, each having advantages and disadvantages. Grab sampling and the determination via colourimetry or ion chromatography are the most common methods. Determination via colourimtery involves a twostep process. Nitrate is reduced to nitrite and which produces a measureable colour change when further reacted with Griess reagents or one of the many modifications (Nydahl, 1976). While grab sampling is simple and cheap, the temporal variability of nitrate concentrations is difficult to account for via grab sampling (S˙liwka-Kaszyńska et al., 2003). Samples require chemical or physical preservation, due to the potential microbial and chemical transformations nitrate can undergo during transport and storage (S˙liwka-Kaszyńska et al., 2003). Continuous sampling methods more effectively capture the temporal variability of nitrate. They require, however, investment in expensive onsite equipment (Audet et al., 2014), restricting their spatial applications. The in-field determination of nitrate via colourimetric test kits, or the automated multiplexed pumping system and UV-VIS field spectrophotometer coupled system (Maxwell et al., 2018), overcomes transport and storage restrictions. However, these automated multiplexed pumping systems and UV-VIS field

spectrophotometer-coupled systems are expensive and require careful calibration via grab sampling (Maxwell et al., 2018). They are also limited by data storage, cuvette fouling, and battery power (Maxwell et al., 2018).

Diffusive Gradients in Thin-Films (DGT), Figure 1, are capable of overcoming many of the challenges described above. Diffusive Gradients in Thin Films is a passive sampling system which provides time weighted average concentration based on Fick's first law of diffusion (Zhang & Davison, 1995) – due to their random heat motion, molecules and ions move from areas of high concentration as to make concentration uniform (King et al., 2013). The binding layer rapidly and strongly binds a specific analyte, ensuring the concentration is effectively zero at the binding layer/diffusive layer interface, maintaining the concentration gradient through the hydrogel diffusive layer and filter membrane. This enables the back calculation of the average concentration upon measuring the bound mass.

An additional requirement of using DGT for determining nitrate is subsequent laboratory analysis of the mass bound to the binding layer. The nitrate bound to the DGT is stable and does not require immediate analysis, in contrast to grab samples. In-field analysis of DGT would further increase the potential range of users. Incorporation of a colour change mechanism that occurs *in situ* within the binding layer could overcome the necessity for laboratory analysis.

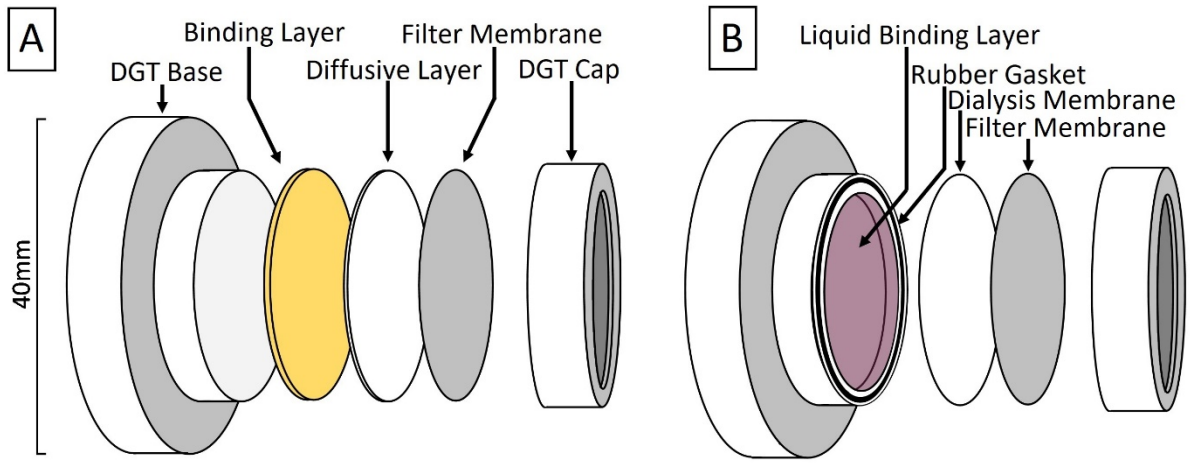


Figure 4.1: (A) Diffusive Gradient in Thin-Films (DGT) solution probe exploded view (Corbett et al., 2019), and (B) the liquid binding phase DGT solution probe (volume = 2 mL) with 1.5 mL of AuNP-chitosan suspension.

DGT make use of hydrogels to both hold analyte-specific resins and constrain transport of ions to the binding layer to diffusion. Hydrogels are polymeric materials with hydrophilic structures which enable them to retain large quantities of water within their three-dimensional network (Ahmed, 2015). Investigations into alternative DGT binding phases have explored the use of liquid binding phases (Li et al., 2003) (Figure 4.1), similar to the set-up utilised by pore water equilibrators (peepers) (Teasdale et al., 1995). The liquid binding phase DGT often make use of commercially available dialysis membranes with tuneable molecular weight cut-offs and high molecular mass soluble polymers (Li et al., 2003; Liu et al., 2016). An $Fe_3O_4$ nano-particulate aqueous suspension has been developed for measurement of arsenic (Liu et al., 2016). Incorporation of a colour change mechanism for nitrate within the DGT probe requires the incorporation of reducing agents into the diffusive layer, to reduce nitrate to nitrite, prior to the colour change reaction in the binding layer whether it is a liquid or a hydrogel.

The reduction of nitrate to nitrite has commonly used zinc (Morita & Nakamura, 2008), and various forms of cadmium (precipitated, pure filings, or amalgamated) (Nydahl, 1976), as the electron source. Alternative reduction reactions can involve vanadium(III) (Schnetger & Lehners, 2014), and nitrate reductase (Campbell, 1999). Zero-valent iron (ZVI), ferrous ion, sulphur and hydrogen have also been reported for the determination and remediation of nitrate (Zhu & Getting, 2012). Numerous bimetallic nanoparticles based on zero-valent iron, have also been suggested, such as Cu, Pd, Pt, Ni and Ag (Muradova et al., 2016), and magnetite doped ZVI (Cho et al., 2015). Due to their greater surface area, nanoparticles provide greater reduction rates in comparison to their macro-particle counterparts, however, the increased rate at which nanoparticle reductants are oxidised poses challenges relating to stability and shelf life of the reductants. Introduction of noble metals onto the nano-ZVI surface has been reported to increase iron stability and therefore enhance redox performance catalytically (Muradova et al., 2016). Reduction in these systems, however, does not necessarily terminate at $NO_2^-$, it can also proceed to $NH_3$ and $NH_4^+$, and $NO_x$ gaseous species (Fanning, 2000). Ongoing reduction beyond $NO_2^-$ would be problematic when the focus is to quantify nitrate.

The utilisation of hydrogel supports helps overcome many of the challenges facing the use of metal nanoparticles, such as aggregation, oxidation and inactivation (Sahiner et al., 2010). Suspension of particles in hydrogels can stop aggregation, and improve mechanical strength (Thoniyot et al., 2015). Hydrogel composites can also provide superior functionality to the composite materials, including bio-sensing, nano-medicine, and environmental remediation (Thoniyot et al., 2015). Halting aggregation often results in increased surface area (Liu & Wang, 2019), thereby decreasing the total mass of nanoparticle required for complete nitrate reduction. The support matrix can also mediate electron transfer, and nucleate product phase growth (Liu & Wang, 2019). In addition to improved activity, suspension of zero-valent metal nanoparticles (nZVM) in hydrogels increases the stability and shelf-life of the nanoparticles (Sahiner, 2013). Most importantly, hydrogels can encapsulate the often toxic metal nanoparticles, resolving many of the environmental concerns associated with using zero-valent metal nanoparticles for the *in situ* reduction of nitrate (Sahiner, 2013).

The major limitation of p(AMPS) hydrogels, used in this research, is their low mechanical strength (Gong et al., 2003), numerous strategies have been developed to improve their mechanical strength while maintaining their chemical properties. Hybrid cross-linked p(AMPS), and double network hydrogels have been reported as methods for improving the mechanical strength of p(AMPS) hydrogels (Chen et al., 2015a; Su & Okay, 2018). P(AMPS/AMA) copolymer hydrogels, as used in this research, consisting of varying mole ratios have also been reported (Jamshidi & Rabiee, 2014). The sulfonate group of AMPS provides ionic exchange capability, electrical conductivity, and resistance to divalence and salinity (Sheng, 2010). Acrylamide shields the copolymer, by providing resistance to hydrolysis, acidity and alkalinity (Sheng, 2010). The rigid side chains, large chains, and chains of ring structures provide good thermal stability, and further shielding effects (Sheng, 2010).

Gold nanoparticles have numerous properties which make their use advantageous over other metallic nanoparticles for the colourimetric determination of nitrite, such as, their distance dependant optical properties (Lee et al., 2008), well defined colour change (Gunupuru et al., 2014), and high stability

(Zhang et al., 2014). Numerous colour change methods have been reported, such as cross-linking, de-protection, and anti-aggregation to name a few. Cross-linking methods produce a colour response when the target molecule decreases inter-particle distances, causing aggregation (Tsogas et al., 2018). In de-protection methods free specific aptamers weakly bound to the gold nanoparticle surfaces are detached by the target compound, inducing a colour change (Chen et al., 2015b; Liu et al., 2018). In anti-aggregation methods physiochemical interactions between the target analyte and nanoparticle cross-linking agents inhibits pre-existing cross-linking (Liu et al., 2018).

Numerous gold and silver nanoparticles have been reported, with varying degrees of selectivity for nitrite (Amanulla et al., 2017; Ibrahim et al., 2019; Perez-Coronado et al., 2017). Amanulla et al. (2017) report a chitosan stabilised gold nanoparticle decorated reduced graphene oxide, for the selective and sensitive detection of nitrite. Aggregation of the chitosan-stabilised gold nanoparticles, arising from their closer formation, produced a wine red to purple colour change (Amanulla et al., 2017).

Although colourimetric determination of nitrite and DGT measurement of nitrate are well established, each has advantages and disadvantages, as discussed above. The objective of this study was to develop and establish a nitrate DGT solution probe that produced a colour change within the binding layer, for the colourimetric determination of nitrate. To achieve this, this research addressed the following: (i) the establishment of a straightforward method for the preparation of zero-valent metal impregnated hydrogel sheets for nitrate reduction to nitrite; and (ii) the incorporation of a nanoparticle into the binding layer that provided a quantitative colour change in the presence of nitrite.

## 4.2. Methods and Materials

The development of the AuNP colour reagents for use as a binding layer in DGT necessitated the development of a nitrate reducing hydrogel. The development of an AuNP-chitosan binding layer and a Fe(0) hydrogel required various strategies and solutions. A schematic of the work undertaken was

supplied in the supplementary material (Figure 4.14) to provide context to the work undertaken. The following section details the methods used in this study.

### *4.2.1 General Procedures*

All reagents were sourced from Merck, New Zealand, unless otherwise stated.

All labware was cleaned with 10 % HCl for 24 hours, before being thoroughly rinsed with deionised water (18.2 MΩ). All solutions were prepared utilising 18.2 mΩ deionised water. Iron(III) solution was prepared with laboratory grade reagent anhydrous $FeCl_3$.

Poly(acrylamide-2-acrylamido-2-methyl-1-propanesulfonic acid) (p(AMA/AMPS)) copolymer hydrogels were prepared using 99 % pure 2-acrylamido-2-methyl-1-propanesulfonic acid, 40 % acrylamide, and 99 % N,N'-methylenebisacrylamide as the monomers and cross-linker respectively, and ammonium persulfate (APS) as the redox initiator (Sigma-Aldrich, New Zealand).

Neutral agarose cross-linked polyacrylamide hydrogels, and Purolite A520E impregnated hydrogels were prepared as detailed in Corbett et al. (2019). The ground and dried Purolite A520E (5 g) resin was preconditioned in 100 mL of 3 mol $L^{-1}$ NaCl however, to remove background nitrate before polymerisation (Huang et al., 2016b).

Dialysis membranes, with a molecular weight cut-off of <15 kDa, were used as the diffusive layer for the liquid binding layer DGT. The membranes were prepared as in previous studies (Li et al., 2003). The membranes were soaked in deionised water (18.2 mΩ) overnight, washed with 80 °C solution of 0.3 w/v % sodium sulphide for a minute, soaked in 60 °C deionised water for 2 minutes, then 0.2 v/v % sulfuric acid, and lastly 60 °C deionised water before being stored in deionised water (Li et al., 2003). The dialysis membrane was then cut into disks (25 mm diameter).

DGT were assembled by layering the diffusion layer and filter membrane over the binding layer on the DGT base, before sealing in place with the DGT cap (Figure 4.1). The volume of the liquid binding layer DGT designed and made here was 2 mL, the 1.5 mL of 5 g $L^{-1}$ AuNP-chitosan suspension was used in

each liquid binding layer DGT. Section 4.2.4 details the preparation of the gold nanoparticle ssuspension.

### *4.2.2 Zero-Valent Iron Hydrogel Preparation*

P(AMPS/AMA) copolymer hydrogels were prepared via radical polymerisation, based on the method developed by Sahiner et al. (2010). Briefly, 0.00789 mol (1.6351 g) 2-acrylamido-2-methyl-1-propansulfonic acid (AMPS), 1 mol % (with respect to the total monomer) of N,N'-methylenebisacrylamide (0.0203 g) were thoroughly mixed in 3.27 mL (0.01841 mol) acrylamide and 6.73 mL of deionised water until completely dissolved. 1 mL of 1 w/v% ammonium persulfate was added and thoroughly mixed. The gel solution was carefully pipetted between glass plates separated by 0.5 mm inert spacers to avoid bubbles, and polymerised at 40 °C for ~100 minutes, or until completely polymerised. Gels were carefully removed from the plates and immersed in 750 mL of 0.12 mol $L^{-1}$ $FeCl_3$ solution for 48 hours. The hydrated Fe(III) impregnated gels were washed in deionised water for 24 hours to remove unreacted reagents and physisorbed Fe(III). The water was changed at least 3 times over that period.

Fe(III) was reduced to Fe(0) with $NaBH_4$ (~30 mL of 0.16 mol $L^{-1}$) under a nitrogen atmosphere for two hours. The sheets were rinsed with $N_2$ splarged 18.2 mΩ water, after which they were cut into disks (diameter = 25 mm) for nitrate reduction studies and incorporation into the DGT devices.

### *4.2.3 Nitrate Reduction*

Determination of the total mass of nitrate reduced to nitrite, and other species ($NH_4^+$/$NH_{3\,(aq)}$, and $NO_{x\,(g)}$, is necessary to ensure enough nitrite is produced to yield colour change in the binding layer. Batch reactor nitrate reduction experiments were performed in triplicate, under atmospheric conditions. Briefly, Fe(0)-p(AMPS/AMA) disks were placed in 100 mL of 20 mg $L^{-1}$ $NO_3^-$ (from $NaNO_3$). Samples (1 mL) were taken at regular intervals which were diluted to 4 mL with deionised water, to meet the required volume for analysis via ion chromatography. Samples were taken at regular intervals and analysed for nitrate and nitrite via ion chromatography, and ammonia/ammonium via

spectrophotometry (EPA, 1993). Discussed in section 4.2.8. Gaseous species were not determined, because they could have no effect on the potential colour reactions, instead a nitrogen balance was performed and the nitrogen unaccounted for by ion chromatography and spectrophotometry was presumed to be $NO_{x\ (g)}$.

To determine whether nitrate reduction could be terminated at nitrite, Fe(0)-p(AMPS/AMA) hydrogels were deployed with the standard A520E nitrate binding layer in a diffusion cell and in the standard A520E-DGT, where the Fe(0)-p(AMPS/AMA) hydrogel made up part of the material diffusion layer (closest to the binding layer).

### *4.2.4 Gold Nanoparticle Preparation*

The synthesis and functionalisation of graphene oxide (GO) commonly involves the treatment of pristine graphite with strong oxidants, producing functionally similar but structurally dissimilar graphite oxide sheets (Khalil et al., 2016). Exfoliation by sonication in the presence of water formed a colloidal suspension of graphene oxide (Paredes et al., 2008; Ye & Feng, 2016) – which was further functionalised with chitosan and Au to produce the reduced GO supported Au nanoparticles (AuNP-rGO). The formation of the chitosan stabilised AuNP (AuNP-chitosan) used largely the same method, excluding the formation and functionalisation of GO. The reaction schematic was provided in Figure 4.2.

Graphite oxide was prepared using a modified Hummers method, as in Amanulla et al. (2017). A mixture of 1 g of $NaNO_3$ and 50 mL $H_2SO_4$ (AR grade), to which 2 g of natural graphite powder (≤44 µm) was added and stirred at 0 $^oC$. 12 g of $KMnO_4$ was slowly added and the solution was continuously stirred for a further 2 hours, and then heated to 35 ± 5 $^oC$ for 30 minutes (Amanulla et al., 2017). Water (150 mL) was added slowly, and the solution heated to 90 $^oC$ under vigorous stirring for 15 minutes. 120 mL of 30 % $H_2O_2$ was added to the suspension until the colour became yellow (Amanulla et al., 2017). The prepared solid sample was allowed to settle and the decanted, before being washed with 5% HCl, and at least three times with milliQ water, following sample settling (Amanulla et al., 2017).

The graphene oxide suspension (50 mL, 1 mg $mL^{-1}$) was formed via the sonication (Soltec Sonica Ultrasonic Cleaner) of 50 mg graphite oxide in 50 mL milliQ (18.2 Ω) water 30 for minutes. 30 minute sonication times have previously been reported to almost completely (97-99 %) form GO sheets of smaller than 1 µm (Ye & Feng, 2016).

Chitosan stabilised gold nanoparticles decorated reduced graphene oxide (Au-rGO) were also prepared as in Amanulla et al. (2017). Briefly, 0.5 g of low molecular weight chitosan (150 kDa) was added to 30 mL of deionised water and stirred, HCl (5 v/v %) was added dropwise until the chitosan was dissolved. Graphene oxide suspension (20 mL of 2.5 mg $mL^{-1}$) was added and the mixture stirred for 30 minutes (Amanulla et al., 2017), to which 0.1 mol $L^{-1}$ succinic acid and 50 mL of 1 mmol $L^{-1}$ $HAuCl_4$ were added simultaneously, and then heated at 60 °C whilst stirring under reflux until the colour turned wine red (Amanulla et al., 2017). NaOH (0.1 mol $L^{-1}$) was added 1 mL at a time to aid in the formation of the AuNP-chitosan. The gold nanoparticle/graphene oxide composite was oven dried at 60 °C. AuNP-chitosan was prepared in the same way; however, there was no graphene oxide added and the chitosan was dissolved in 50 mL of deionised water instead of the graphene oxide suspension.

AuNP suspensions were prepared by adding the dried AuNP to deionised water, and alternately sonicated for 15 minutes and vigorously manual shaken until there were no large AuNP particles in the suspension (determined visually).

The AuNP-rGO hydrogels were prepared using the hydrogel formation in particle suspension method. Briefly, 0.5g of the synthesised AuNP-rGO was added to the agarose/acrylamide gel solution (10 mL), and vigorously stirred. 70 µL of 10 % ammonium persulfate and 25 µL of tetramethylethylenediamine were added to the solution whilst stirring. The solution was quickly pipetted between glass plates separated by 0.4 mm inert spacers, carefully to ensure there were no air bubbles. Polymerisation occurred at 40 °C in an oven for approximately 100 minutes, or until polymerisation was complete.

The prepared AuNP-rGO hydrogels were washed 4 times in 18.2 mΩ water over 24 hours, to remove unreacted hydrogel reagents. The hydrogels were stored in 18.2 mΩ water at 4 °C.

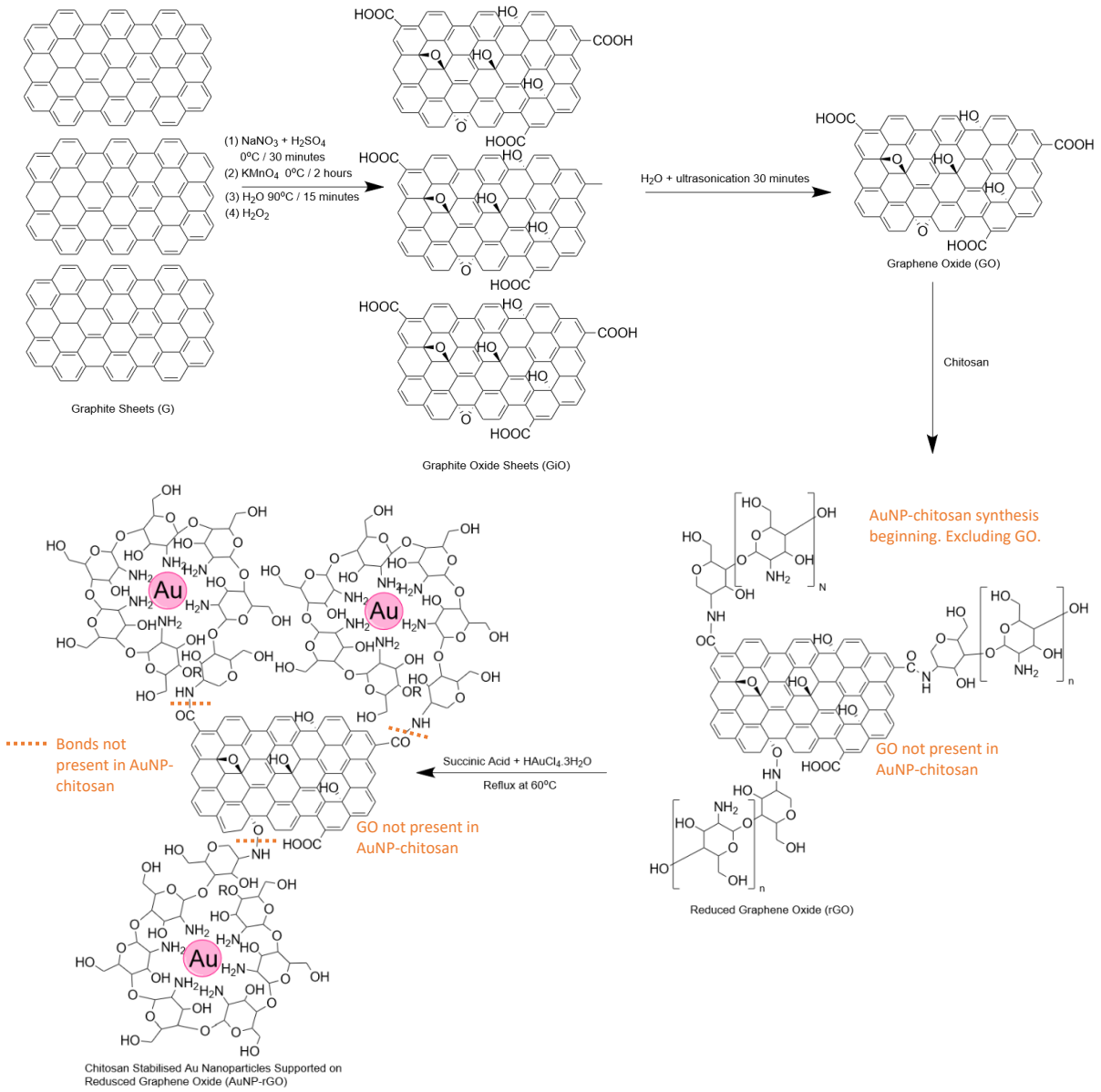


Figure 4.2: Reaction illustration for synthesis of reduced graphene oxide supported Au nanoparticles (AuNP-rGO), and the possible binding modes of the chitosan to graphene oxide and gold (Amanulla et al., 2017; Khalil et al., 2016; Sutirman et al., 2016; Yan et al., 2016). No reduced graphene oxide was used in the synthesis of the AuNP-chitosan, the chitosan stabilised Au nanoparticles (AuNP-chitosan) end product was the same as the AuNP-rGO excluding the amine bond from the chitosan to the reduced graphene oxide (rGO) (red lines).

### *4.2.5 Standard Nitrate Specific and Diffusive Hydrogel Preparation*

Nitrate specific and standard DGT agarose cross-linked polyacrylamide (APA) diffusive gels were prepared as detailed in Corbett et al. (2019). No binding reagent was present in the diffusive gel and inert spacers of 0.25, 0.4, and 0.5 mm thicknesses were used. The AuNP-rGO was substituted for 4 g of ≤125 µm Purolite A520E nitrate specific resin and a 0.5 mm inert spacer was used. Diffusive and

A520E binding gels were washed at least 4 times over 24 hours, before being stored in 0.01 mol $L^{-1}$ NaCl at room temperature and milliQ water at 4 °C respectively.

### *4.2.6 Diffusion Coefficient*

The presence of Fe in the p(AMPS/AMA) hydrogel network, and the use of different monomers to create the hydrogel to the standard APA DGT diffusion layer, means the diffusion coefficients of nitrate through the Fe(0) hydrogels were different. The diffusion coefficient of nitrate/nitrite through the Fe doped p(AMPS/AMA) hydrogels and dialysis membranes were determined by deploying sets of standard Purolite A520E nitrate specific DGT with diffusion layers of varying thicknesses, for 24, 48 and 72 hours. The coefficients were confirmed using a horizontal diffusion cell (area = 3.46 $cm^2$)

The thickness of the dialysis membrane after pre-treatment and the Fe p(AMPS/AMA) hydrogels was measured using a WILD M38 Microscope (Heerbrugg, Switzerland) with a Nikon Digital Sight DS-U1 camera (Tokyo, Japan), and analysed using Image-Pro Plus (Media Cybernetics, Maryland, USA).

### *4.2.7 Colour Determination and Stability*

To determine the optimal AuNP and AuNP concentration for colour development a series of experiments were conducted. Firstly, nitrite solution, prepared from $NaNO_2$, was added to vials of freshly prepared AuNP-chitosan and AuNP-rGO suspensions, to provide $NO_2^-$ masses from 0 – 145 µg and AuNP concentrations of 1, 3, and 5 g $L^{-1}$. The maximum nitrite mass were chosen because it was similar to the previously reported binding capacities of the standard nitrate DGT (Corbett et al., 2019; Huang et al., 2016a). Secondly, the AuNP suspensions were re-analysed 7, 14 and 21 days after the initial analysis to determine the stability of the AuNP suspensions when reacted with nitrite.

Liquid binding layer AuNP-chitosan DGT, Figure 4.1B, were deployed in a range of nitrite solutions (volume = 6 L) to determine whether a colour change could be induced within the DGT probe. Furthermore, the extent to which the AuNP-chitosan liquid binding layer met the theoretical requirements for DGT, of rapid and strong adsorption to maintain the concentration gradient through

the material diffusion layer (MDL) (Davison, 2016), was assessed. AuNP-chitosan DGT were deployed in triplicate for 5 days in nitrite solutions from 0-1000 mg $L^{-1}$ $NO_2^-$ (prepared from $NaNO_2$).

UV-vis spectroscopy was performed on the AuNP-chitosan and AuNP-rGO suspensions, and AuNP-rGO hydrogels to determine the colour intensity, and blue shift when reacted with nitrite. Plastic cuvettes were cut to size, so that when hydrogels were placed on the outside of the cuvette fitted within the instrument.

The AuNP suspensions were photographed using a Samsung S10 mobile phone camera. The RGB (red, green, blue) composition was analysed with using ImageJ. The colour intensity was determined by subtracting the RGB values of the blank. The RGB composition related to the mass of nitrite bound to the colour change binding layer.

The effective intensity ($A_x$) was calculated using the following equations (Das & Sarkar, 2016), where $R_s$, $G_s$ and $B_s$ are the sample RGB values, and $R_b$, $G_b$ and $B_b$ are the blank RGB values (Das & Sarkar, 2016).

$$A_R = -\log\left(\frac{R_s}{R_b}\right) \quad (1)$$

$$A_G = -\log\left(\frac{G_s}{G_b}\right) \quad (2)$$

$$A_B = -\log\left(\frac{B_s}{B_b}\right) \quad (3)$$

### *4.2.8 Analysis*

Scanning Electron Microscope (SEM) images, using a Hitachi S-4700 Field Emission SEM, were taken of the Fe impregnated p(AMA/AMPS) hydrogels, and the AuNP. The Fe hydrogels were imaged pre-reduction to Fe(0), and post nitrate reduction.

SEM, Fourier-transform infrared (Perkin Elmer Spectrum 100), and powder x-ray diffraction (Panalytical Empyrean) spectroscopy of the AuNP-chitosan, AuNP-rGO, rGO, GO, GiO, and graphite

were performed to ensure the desired products were synthesised and to assess the colour response of the AuNP-rGO to nitrite.

Analysis of nitrate and nitrite masses bound to the standard Purolite A520E DGT were performed using a Dionex ICS-200 Ion Chromatograph (Dionex, California, United States), as outlined by Corbett et al. (2019). Analysis of solution nitrate and nitrite concentrations were also performed using ion chromatography as outlined by Corbett et al. (2019). Ammonium/ammonia concentrations were determined using a Spectrophotmeter (Jenway 7300, United Kingdom) (EPA, 1993). Two reagent solutions were prepared for colourimetric determination ammonium/ammonia. Reagent solution 1 was 1 L of 10 g $L^{-1}$ phenol and 50 mg $L^{-1}$ sodium nitroprusside (EPA, 1993). Solution 2 contained 5 g NaOH and 8.4 mL of 5 % NaOCl, which was made to 1 L with deionised water. Both solutions were stored in brown Schott bottles, refrigerated, and aged for 2 days before use. 2 mL of both reagents were added to 2 mL of the sample, which was subsequently heated in a temperature bath (37 °C) for 15 minutes, before being transferred to 5 mL cuvettes for spectrophotometric analysis alongside calibration samples.

Calculation of the time weighted average DGT concentration ($C_{DGT}$, mg $cm^{-3}$) was determined using the full DGT equation (Davison, 2016) (Equation 2), where M = accumulated mass, mg; $A_{eff}$ = effective area, $cm^2$; t = time, length of deployment, s; $D_{mdl}$, $D_{Fe}$, $D_w$ = diffusion coefficients of the material diffusion layer (MDL = APA diffusive gel and polyethersulfone filter membrane), Fe impregnated p(AMPS/AMA) hydrogel), and water respectively, $cm^2$ $s^{-1}$; $\Delta g_{mdl}$, $\Delta g_{Fe}$, $\delta$ = thickness of material diffusion layer, and Diffusive Boundary Layer respectively, cm (Davison, 2016).

$$\boldsymbol{C_{DGT} = \frac{M}{A_{eff} t}\left(\frac{\Delta g_{mdl}}{D_{mdl}} + \frac{\Delta g_{Fe}}{D_{Fe}} + \frac{\delta}{D_w}\right)} \quad (4)$$

The diffusion coefficients through the polyethersulfone filter membrane and APA diffusive layer are indistinguishably different (Davison, 2016), and as such were combined to the material diffusion layer (MDL). The diffusion coefficient through the Fe impregnated gel and dialysis membrane required determination, as discussed above. The diffusion coefficients of nitrate and nitrite were treated as the

same. The diffusion coefficient of nitrate through the APA diffusion layer was 1.46 x $10^{-5}$ $cm^2$ $s^{-1}$ at 25 $^oC$ (Huang et al., 2016b). The diffusion coefficient of nitrate and nitrite through water was 1.70 x $10^{-5}$ $cm^2$ $s^{-1}$ at 25 $^oC$ (Picioreanu et al., 1997). Diffusion coefficients were temperature corrected, and Diffusive Boundary Layer (DBL) calculation were performed as described by Davison (2016) (Equation 3). T = temperature ($^oC$), $D_T$ = diffusion coefficient at temperature T ($cm^2$ $s^{-1}$), and $D_{25}$ = diffusion coefficient ($cm^2$ $s^{-1}$) at 25$^oC$ (Davison, 2016).

$$\boldsymbol{logD_T = \frac{1.37023(T-25)+0.000836(T-25)^2}{109+T} + log\frac{D_{25}(273+T)}{298}} \quad (5)$$

## 4.3. Results

### *4.3.1 AuNP-chitosan Development and Colour Response*

An AuNP-chitosan suspension was developed, which provided a quantitative colour response to varying nitrite masses (0 – 145 µg of nitrite in 1.5 mL of the AuNP-chitosan suspension) (Figures 3-5). The colour response was dependent on the AuNP-chitosan concentration.

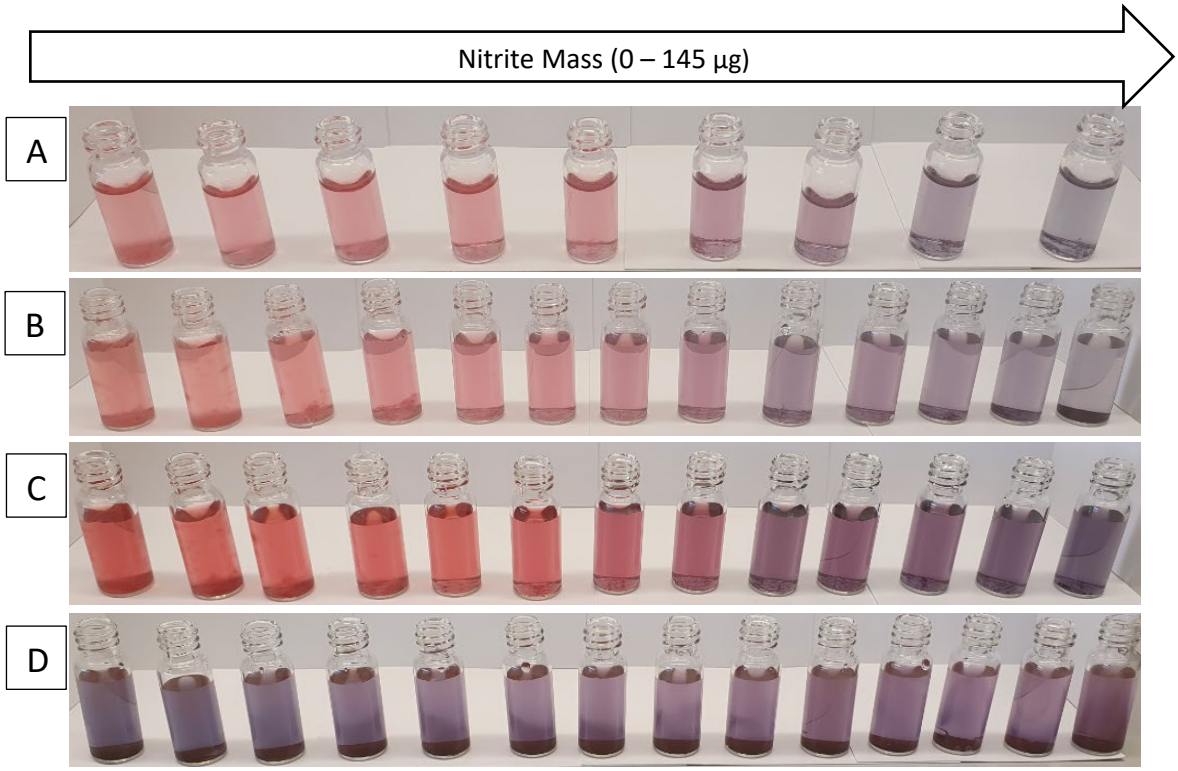


Figure 4.3: Image of the (A) 1 g $L^{-1}$, (B) 3 g $L^{-1}$, and (C) 5 g $L^{-1}$ chitosan stabilised Au nanoparticles (AuNP-chitosan), and (D) 5 g $L^{-1}$ reduced graphene oxide supported Au nanoparticles (AuNP-rGO) reacted with a range of nitrite masses (0 – 145 µg).

Increasing the AuNP-chitosan concentration made visual determination of the colour change easier (Figure 4.3). The colour change was more distinct, providing stronger UV-vis absorption at 523 nm, and 683 nm, as the suspension became blue shifted in the presence of nitrite (Figures 4.5A-C). The higher concentration of AuNP-chitosan also provided stronger UV-vis calibration curves – greater $R^2$ values (Figures 4.3A-C). There was no significant colour change within the AuNP-rGO suspensions (Figure 4.3D) and yielded poorly correlated UV-vis and RGB regression curves (Figures 4.4D and 4.5D). AuNP-hydrogels were also developed, but they did not change colour in the presence of nitrite, determined visually and via UV-vis, as such, they were not pursued.

As the mass of nitrite approached the maximum detection limit, the AuNP precipitated out of solution, accumulating in the bottom of the vials (Figure 4.3). The intensity of the colour of the AuNP suspension decreased, until all AuNP precipitated and the solution became colourless - the UV-vis peaks disappeared (Figure not supplied). Increasing the concentration of the AuNP suspension increased the mass of nitrite required for all AuNP to precipitate out of solution, and therefore the upper detection limit.

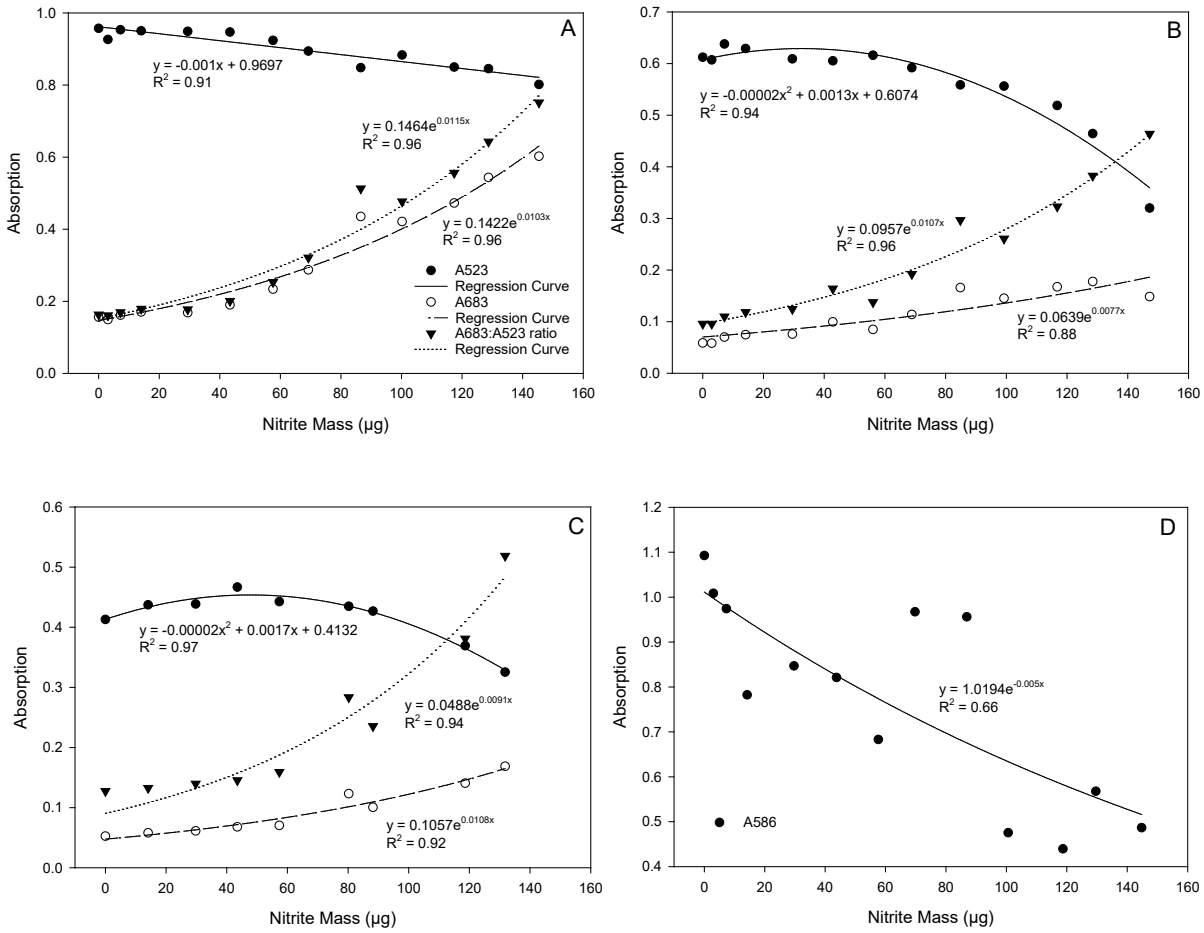


Figure 4.4: UV-vis absorption for (A) 5 g $L^{-1}$, (B) 3 g $L^{-1}$, and (C) 1 g $L^{-1}$ chitosan stabilised Au nanoparticles (AuNP-chitosan), and (D) 5 g $L^{-1}$ reduced graphene oxide supported Au nanoparticles (AuNP-rGO) reacted with a range of nitrite masses (0 – 145 µg). The UV-vis peak for the AuNP-rGO was at 586 nm. Only one curve was presented for the AuNP-rGO because no other peak formed with increasing nitrite mass.

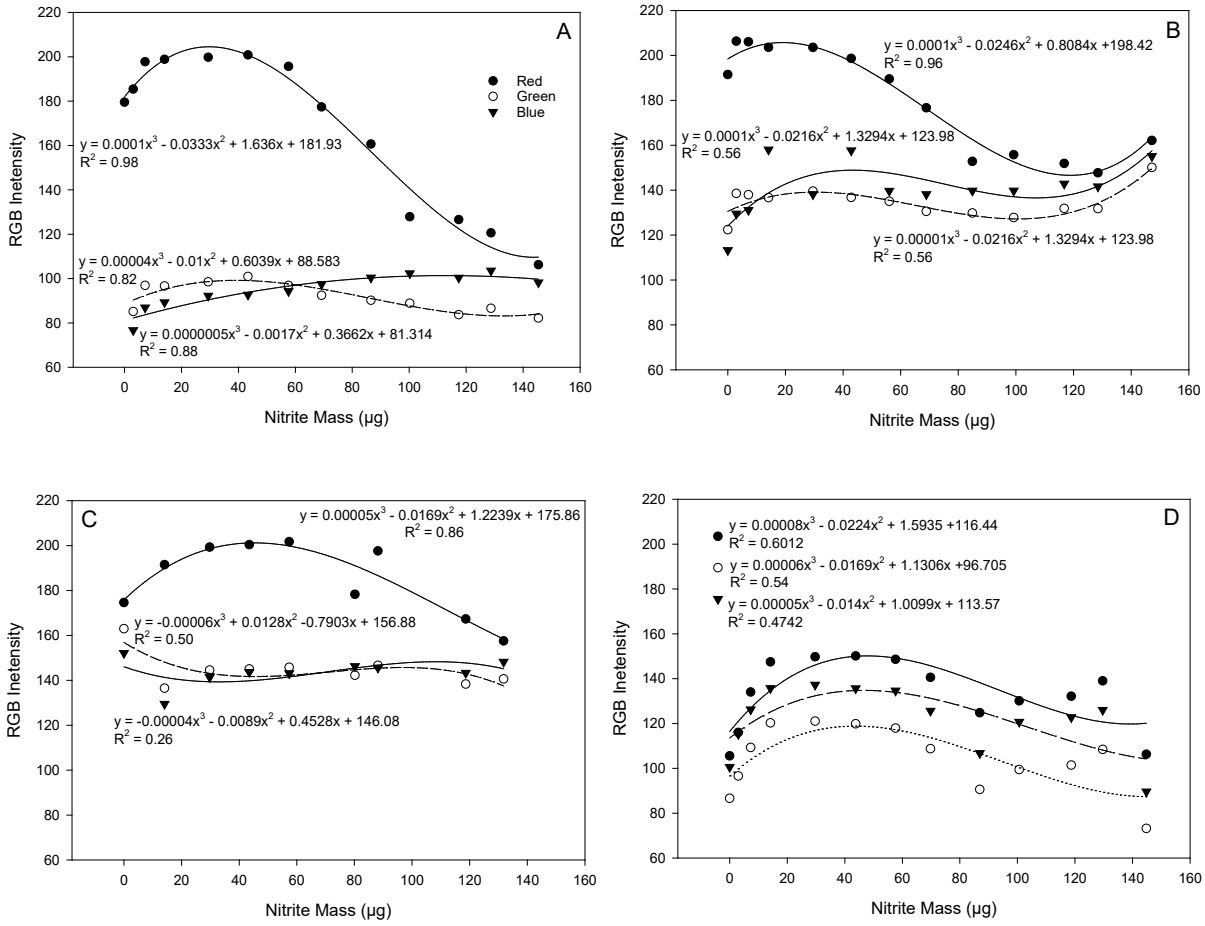


Figure 4.5: The red, green and blue (RGB) intensities versus the nitrite mass for (A) 5 g $L^{-1}$, (B) 3 g $L^{-1}$, and (C) 1 g $L^{-1}$ chitosan stabilised Au nanoparticles (AuNP-chitosan), and (D) reduced graphene oxide supported Au nanoparticles (AuNP-rGO) suspensions.

The formation of layers in the AuNP-rGO system (Figure 4.3D), made consistent sampling for both UV-vis and RGB analysis difficult, resulting in calibration curves with low $R^2$ values (Figures 4.4D and 4.5D). There was little variation in the RGB analysis between data points (Table 4.1), which made accurate determination of nitrite mass more difficult than the AuNP-chitosan systems. The reaction of the AuNP-chitosan with large (> 100 µg) nitrite masses formed a precipitate which settled to the bottom of the vials; however, layers within the suspension were not formed (Figure 4.3A-C). It was, therefore, easier to take consistent samples for UV-vis and RGB analysis, producing regression curves with higher $R^2$ values (Figures 4.4 and 4.5).

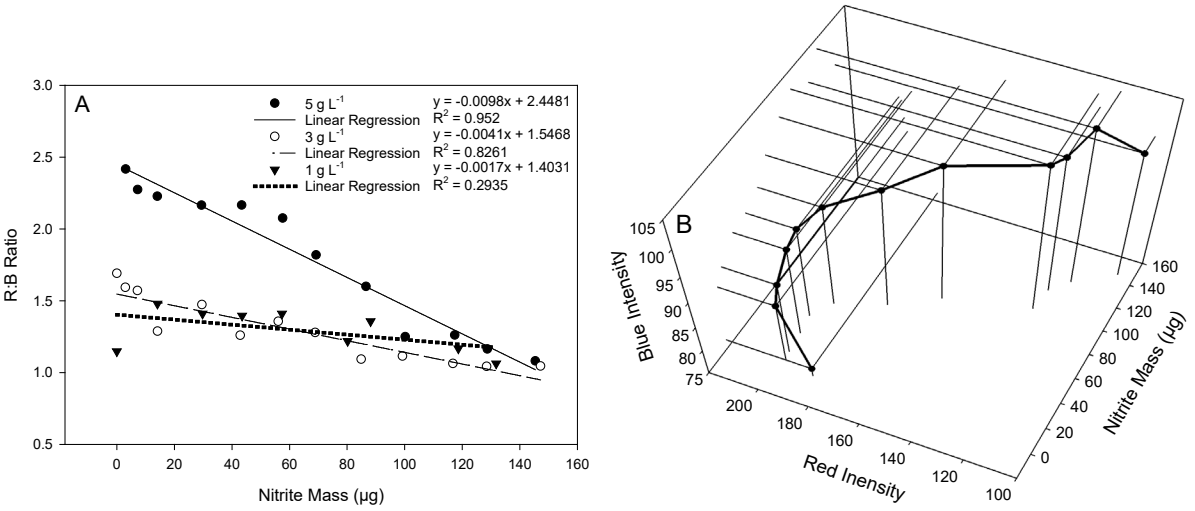


Figure 4.6: (A) The ratio of red to blue intensity for varying concentrations of chitosan stabilised Au nanoparticles (AuNP-chitosan) (1, 3, and 5 g $L^{-1}$) reacted with different masses of nitrite, and the linear regression of the red:blue ratio to nitrite mass. (B) 3-Dimensional plot of the red and blue intensities versus nitrite mass for the 5 g $L^{-1}$ AuNP-chitosan calibration curve.

The best-fit regression curves for the RGB analyses were cubic polynomials (Figure 4.5). RGB analysis therefore required the combination of at least two components, because single components could provide multiple different nitrite masses. The components chosen were red and blue, because they provided the greatest difference in intensity compared to the blank AuNP suspension (Table 4.1), except for 1 g $L^{-1}$ AuNP-chitosan and 5 g $L^{-1}$ AuNP-rGo. The ratio of the red to blue components provided the strongest correlation to mass as the AuNP-chitosan concentration increased (Figure 4.6A). Figure 4.6B illustrates how the red and blue components change in relation to each other as nitrite mass increases.

Table 4.1: RGB Intensities for 5 g $L^{-1}$, 3 g $L^{-1}$, and 1 g $L^{-1}$ chitosan stabilised Au nanoparticles (AuNP-chitosan, and 5 g $L^{-1}$ reduced graphene oxide supported Au nanoparticles (AuNP-rGO) suspensions determined using Equations 1-3. *Note: values determined for nitrite data presented above, 0 – 145 µg).*

| Component | | 5 g $L^{-1}$ | 3 g $L^{-1}$ | 1 g $L^{-1}$ | rGO 5 g $L^{-1}$ |
|---|---|---|---|---|---|
| Red | Minimum | -0.0487 | -0.0325 | -0.0627 | -0.1531 |
| | Maximum | 0.2279 | 0.1127 | 0.0447 | 0.0000 |
| | Range | 0.2766 | 0.1452 | 0.1074 | 0.1531 |
| Green | Minimum | -0.0567 | -0.0887 | 0.0000 | -0.1453 |
| | Maximum | 0.0325 | 0.0000 | 0.0769 | 0.0733 |
| | Range | 0.0892 | 0.0887 | 0.0769 | 0.2186 |
| Blue | Minimum | -0.1062 | -0.1448 | 0.0000 | -0.1349 |
| | Maximum | 0.0243 | 0.0000 | 0.0700 | 0.0501 |
| | Range | 0.1305 | 0.1448 | 0.0700 | 0.1850 |

Due to the improved colour reaction of the 5 g $L^{-1}$ AuNP-chitosan suspension, compared to lower concentrations and the AuNP-rGO suspension, subsequent colour development experiments (stability and solution) utilised the 5 g $L^{-1}$ AuNP-chitosan suspension alone.

### 4.3.2 AuNP-chitosan Stability

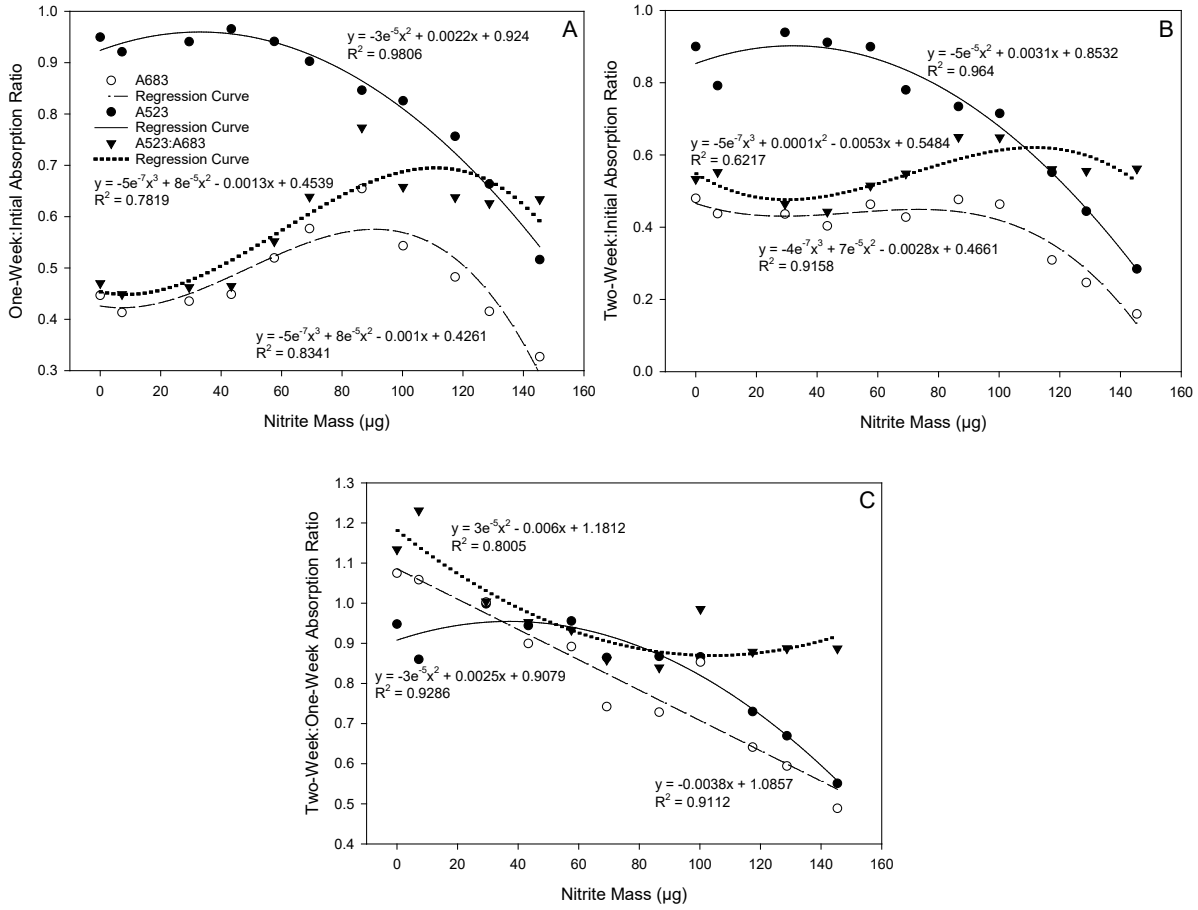


Figure 4.7: Stability of 5 g $L^{-1}$ chitosan stabilised Au nanoparticles (AuNP-chitosan) suspensions determined by UV-vis at 523 and 683 nm, and the 683:523 nm ratio compared to the initial 5 g $L^{-1}$ AuNP-chitosan suspensions (Figure 4.4C). Stability was determined as the ratio of these components for (A) one-week after initial analysis, (B) two-weeks after the initial analysis, and (C) three-weeks after the initial analysis.

The colour development continued after the initial analysis (Figure 4.7). The absorption ratio of one week, two weeks and three weeks after initial analysis to the initial analysis are < 1 for all components (red 523 nm, blue 683 nm, and 683:523). The 523 nm ratio decreased as the nitrite mass increased, because the higher nitrite mass vials continued developing to a greater extent (blue shifting). One week after the initial analysis the lower nitrite mass vials began forming 'globules', the same colour as the suspension. The globules formed due to the agglomeration of chitosan and not the nanoparticles. The 'globules' were not significantly blue shifted, which would result from the precipitation of the AuNP-chitosan. The increased mass of nitrite appears to stabilise the AuNP suspension by reducing

the aggregation of the chitosan. The AuNP-rGO suspension and lower AuNP-chitosan provided much weaker curve fits (Figures not included).

### *4.3.3 AuNP-chitosan DGT Development and Solution Trials*

5 g $L^{-1}$ AuNP-chitosan suspensions, as presented above, were determined to be the optimal concentration for use within the liquid binding layer DGT. Subsequent solution trials of the assembled AuNP-chitosan DGT, therefore, utilised 1.5 mL of 5 g $L^{-1}$ AuNP-chitosan suspension per DGT as the liquid binding layer. Colour change within the liquid binding layer was achieved *in situ* during solution trials (Figures 4.8 and 4.9). The colour development was not rapid enough to meet the theoretical requirements of DGT, as development occurred over several days, for combination of the AuNP-chitosan DGT with the Fe(0) reducing layer (results presented below).

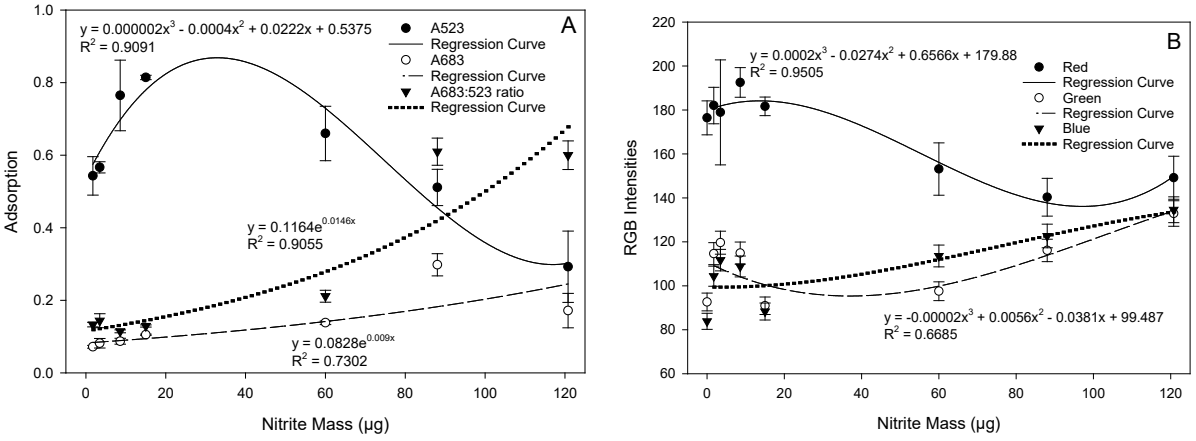


Figure 4.8: (A) UV-vis, and (B) RGB analyses of chitosan stabilised Au nanoparticles (AuNP-chitosan) DGT for laboratory deployments in synthetic solutions of various nitrite concentrations. Nitrite mass is the mass of nitrite within the binding layer. The same curve types were fitted as for the AuNP suspension data (Figures 4.4 and 4.5).

The AuNP-chitosan suspension colour change was clearly detectable visually after deployment (Figure 4.9A). The colour change was also clearly detectable in the DGT probes, after the material diffusion layer (MDL) was removed (Figure 4.9B). The blue shift due to the decrease in AuNP distance in the presence of nitrite was easily detectable visually (Figures 4.8A and B). The formation of AuNP-chitosan aggregates occurred at high nitrite (90 – 120 µg) masses (Figures 4.9A and B). AuNP-chitosan

aggregates formed on the dialysis membrane after deployments in high concentration nitrite solutions (Figure 4.9C).

Dilution of the AuNP-chitosan suspension occurred during solution deployments, the UV-vis (523 and 683 nm) ratio of AuNP-chitosan suspension in AuNP-DGT deployed in 0 mg $L^{-1}$ nitrite to the un-deployed AuNP-chitosan suspension were 0.69 and 1.01 respectively.

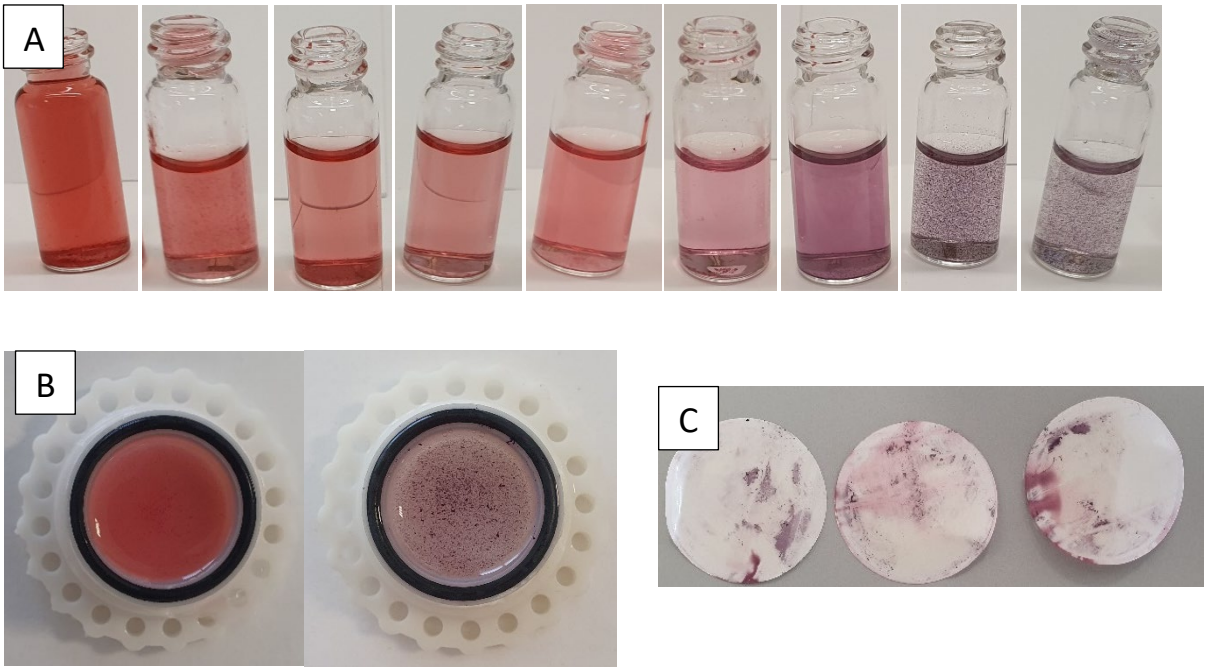


Figure 4.9: (A) Au nanoparticle suspension in 3D printed liquid binding layer DGT. (B) AuNP suspensions after deployment in liquid binding layer DGT in nitrite solutions (0 and 90 µg). (C) Formation of AuNP precipitates on the dialysis membranes where the nitrite mass in the binding layer was large (> 90 µg).

### *4.3.4 Nitrate Reduction and Diffusion Layer Properties*

Figure 10 shows the production of nitrite by the Fe(0)-p(AMPS/AMA) hydrogel. Reduction began immediately upon introduction of the Fe(0) hydrogel to the reaction vessel. Ammonia and ammonium production was determined experimentally (figure not shown), and lagged behind nitrite production by 60 minutes – in the absence of an A520E binding layer. A full nitrogen mass balance indicated $NO_x$ species were likely produced, beginning at approximately the same time as the ammonia and ammonium production. $NO_x$ species, however, were not determined experimentally. When an A520E

binding layer was included, removal of nitrite meant that further reduction to $NH_3/NH_4^+$ and gaseous species did not occur.

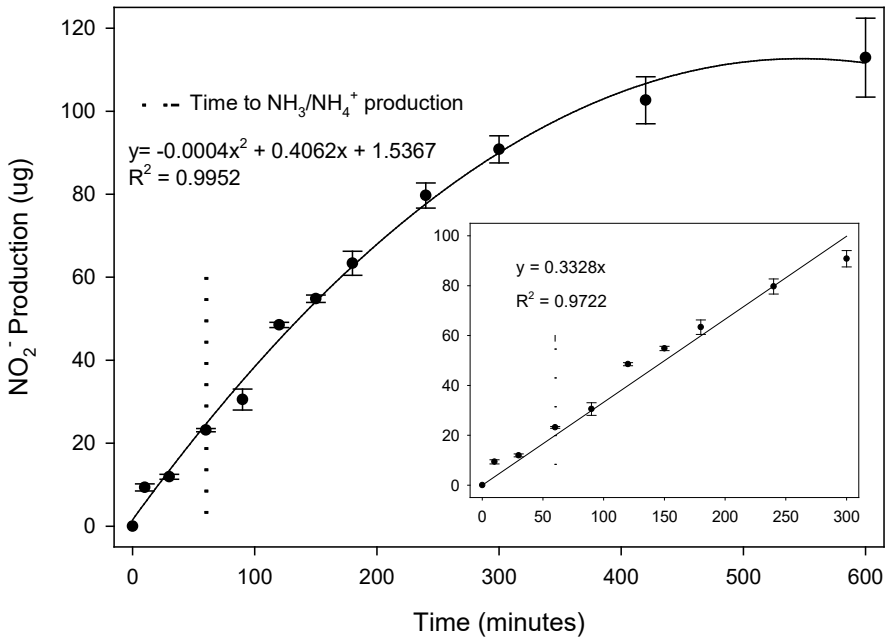


Figure 4.10: Nitrate reduction (nitrite production) with Fe(0) impregnated poly-2-acrylamido-2-methyl-1-propanesulfonic acid/acrylamide copolymer hydrogel (10 % AMPS), and inset of linear reduction.

The diffusion coefficients of nitrite and nitrate through the Fe(III)-p(AMPS/AMA) hydrogel were both 1.24 x $10^{-5}$ $cm^2$ $s^{-1}$ at 20.6 °C, temperature corrected to 25 °C they were 1.40 x $10^{-5}$ $cm^2$ $s^{-1}$. This is 95.8 % of the diffusion coefficient of nitrite through water at 25 °C (14.6 x $10^{-6}$ $cm^2$ $s^{-1}$) (Picioreanu et al., 1997). The thickness of the Fe(III)-p(AMPS/AMA) hydrogel after washing and swelling was 1.1 mm. The diffusion coefficients of nitrite and nitrate through the dialysis membrane were 4.65 x $10^{-6}$ $cm^2$ $s^{-1}$ at 21.9 °C and 4.56 x $10^{-6}$ $cm^2$ $s^{-1}$ at 20.4 °C, temperature corrected to 25 °C they were 5.05 x $10^{-6}$ $cm^2$ $s^{-1}$ and 5.15 x $10^{-6}$ $cm^2$ $s^{-1}$ respectively. This is 34.6 % and 35.4 % of the diffusion coefficient of nitrite through water at 25 °C. The thickness of the dialysis membrane after pre-treatment was 43 µm.

### *4.3.5 Formation of Au nanoparticles*

The formation of the AuNP-rGO and AuNP-chitosan composites were confirmed via FTIR and XRD (Figure 4.11). The broad and intense -OH stretch at 3380 $cm^{-1}$, strong C=O stretching at 1734 $cm^{-1}$, C=C conjugated ketone stretching at 1628 $cm^{-1}$, C-O phenol stretch at 1228 $cm^{-1}$, and C-O primary alcohol

stretch at 1058 $cm^{-1}$, present in sample 2 and not 1 (Figure 4.11A), are indicative of the formation graphite oxide from pure graphite (Emadi et al., 2017).

The rGO spectra is a combination of the chitosan and graphite oxide spectra (Emadi et al., 2017). The loss of the carboxylic acid C=O stretch at 1734 $cm^{-1}$ of the graphite oxide upon reaction with chitosan, and the presence of HN-CO stretching vibrations at 1648 $cm^{-1}$, support the formation of amide linkages between the NH and COOH groups of the chitosan and graphene oxide (Figures 4.2, and 4.11A) (Emadi et al., 2017). The intensity of the interaction of -OH groups of the graphene oxide and chitosan resulted in a more intense C-O primary alcohol stretch at 1093 $cm^{-1}$ for the rGO, compared to the stretch at 1058 $cm^{-1}$ for the graphite oxide (Emadi et al., 2017). The chitosan strong C-H stretch at 2880 $cm^{-1}$ was also present in the rGO, and persisted in the AuNP-chitosan and AuNP-rGO. The AuNP-chitosan and AuNP-rGO spectra were largely the same, and the intensity was diminished in comparison to the parent materials.

XRD analysis further confirmed the formation of the AuNP composites (Figure 4.11C) and precursors (Figure 4.11). A very strong peak at 9.8 ° and weak peak at 20 ° in the graphite oxide replaced the peaks present in the pure graphite. Chitosan provided a weak peak at 10.6 ° and a strong peak at 19.9 °. The reduced graphene oxide peaks were a combination of the graphite oxide and chitosan peaks (9.9 °, and 19.8 ° with shoulder at 21.8 °).

AuNP-rGO peaks at 38.0 °, 44.3 °, 64.5 ° and 77.5 °, and AuNP-chitosan peaks at 38.2 °, 44.4 °, 64.7 ° and 77.4 ° (Figure 4.11C) confirm the reduction of Au(III) to Au(0) (Ramasamy & Maliyekkal, 2014). They are indicative of the (111), (200), (220) and (311) planes of face centred cubic Au (Amanulla et al., 2017). The peaks at around 27 °, 32 °, 54 °, 57 °, 66 °, 73 ° and 75 ° correspond to NaCl (Ramasamy & Maliyekkal, 2014). The rGO peaks in the AuNP-rGO composite were significantly reduced in intensity. The chitosan peaks in the AuNP-chitosan composite largely disappeared (10.6 °), and the peak at 19.9 ° broadened and flattened from 17 ° to 25.6 °.

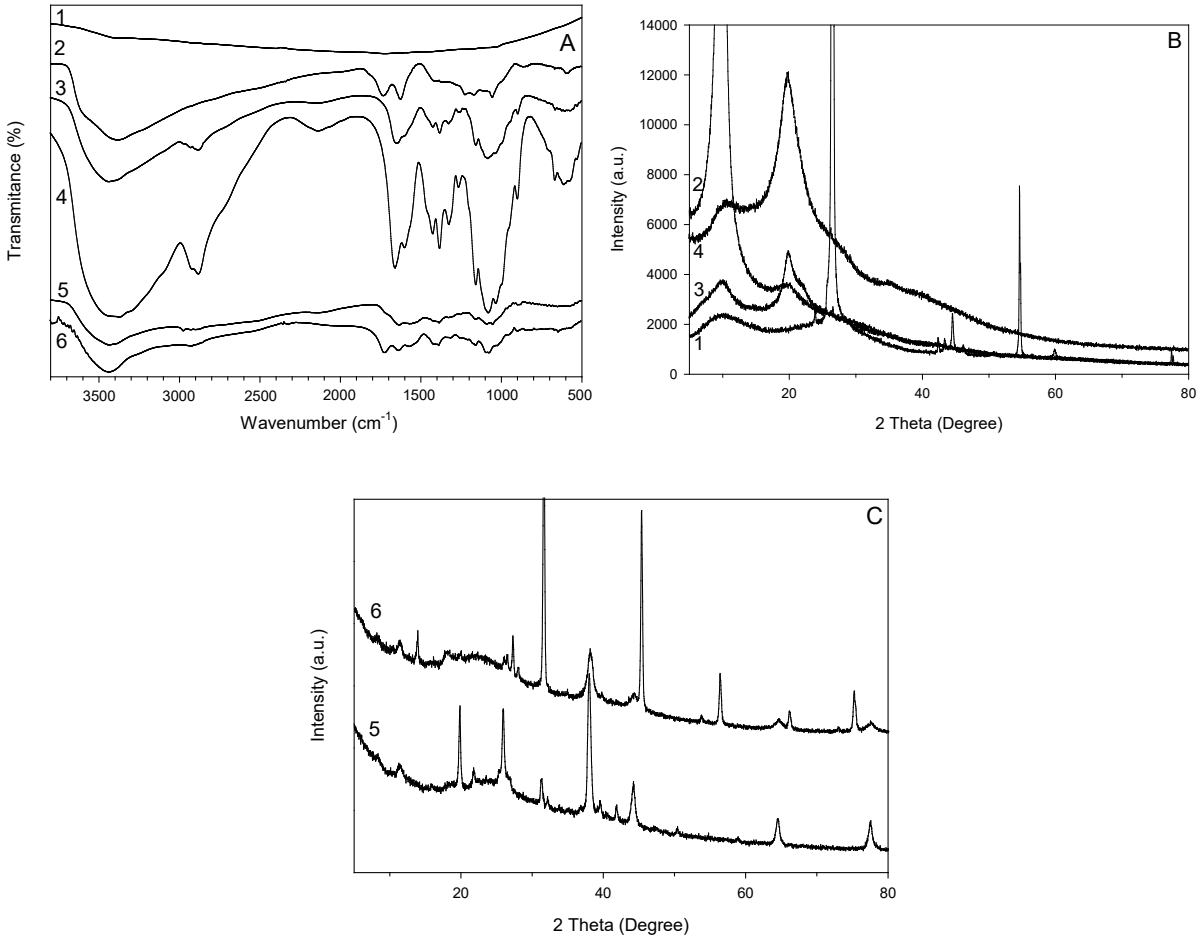


Figure 4.11: (A) Fourier-transform infrared chromatography, and (B) and (C) XRD: graphite (1), graphite oxide (2), reduced graphene oxide (3), chitosan (4), chitosan stabilised Au nanoparticles (5) and reduced graphene oxide supported Au nanoparticles (6). The spectra in (A) and (C) were artificially separated so the components were easily discernible, the relative transmittances and intensities were unchanged.

SEM imaging and elemental analysis (Figure 4.12) further confirmed the formation of the AuNP-chitosan and AuNP-rGO composites. The two-dimensional graphene oxide and irregular spherical chitosan were present in the AuNP-rGO (Figures 4.12A and C). The irregular spherical/globular chitosan structure was clearly visible in the AuNP-chitosan (Figure 4.12B). Elemental analysis (Figures 4.12E-F) of the bright areas in the back scattering images (Figures 4.12C-D) confirmed the presence of gold. It was considerably more difficult to find and analyse gold in the AuNP-chitosan composite, requiring much greater magnification, because the gold particles were much smaller than in the AuNP-rGO. This size difference resulted in different optical properties (Figure 4.3), due to the different surface plasmon resonance.

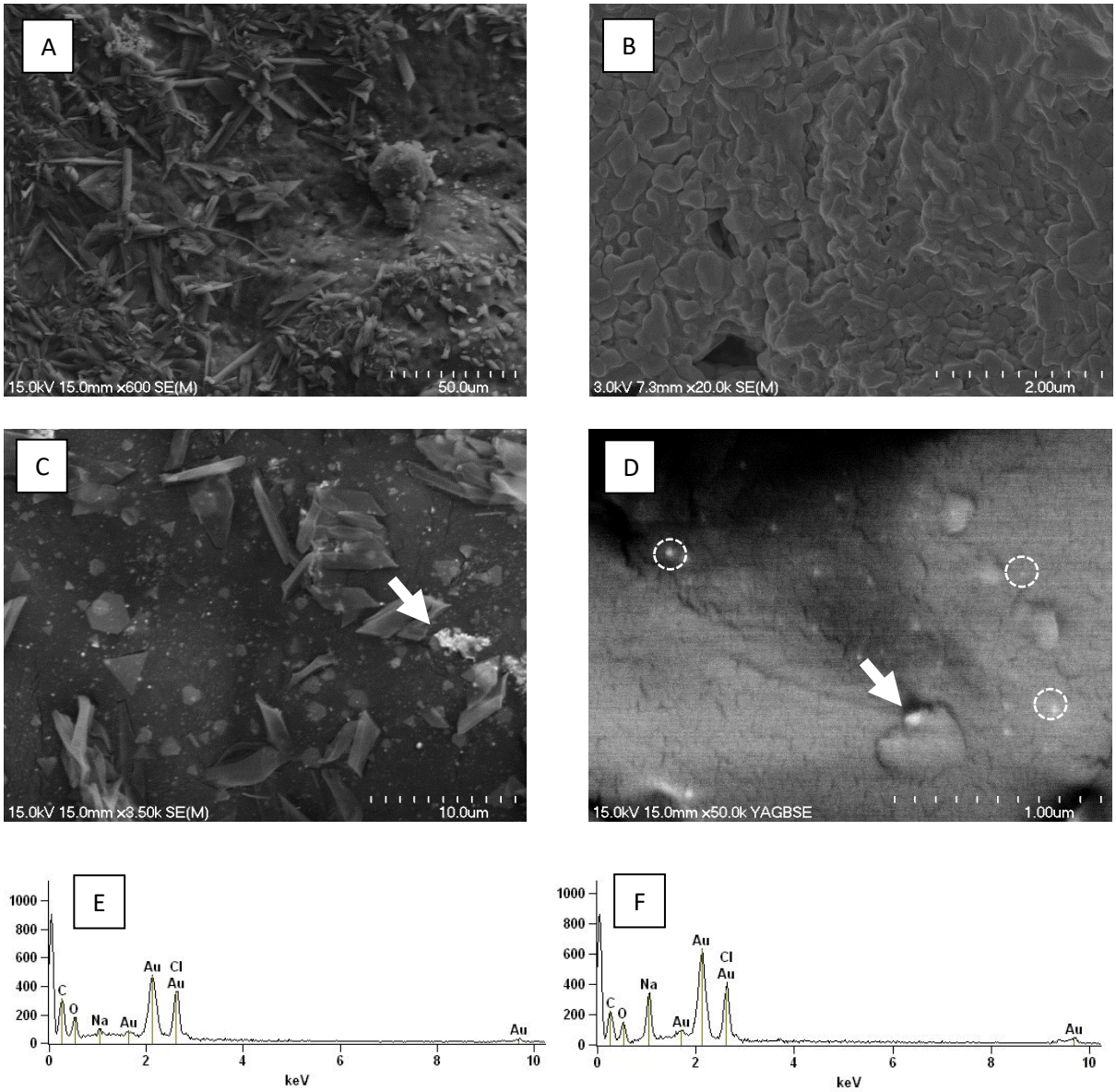


Figure 4.12: SEM images of reduced graphene oxide supported Au nanoparticles (AuNP-rGO) (A and C), and chitosan stabilised Au nanoparticles (AuNP-chitosan) (B and D). Elemental analysis of the marked spots of the AuNP-rGO (E) and AuNP-chitosan (F). Example AuNP circled in (D).

### *4.3.6 Fe p(AMA/AMPS) Hydrogel*

Iron impregnated hydrogels were successfully synthesised based on the method developed by Sahiner et al. (2010). The light areas in Figure 4.13 are the Fe particles suspended in and on the p(AMPS/AMA) hydrogel. Iron particles on the surface of the hydrogel are significantly larger than those within the polymeric network. The Fe particles are smaller in the hydrogels after reduction to Fe(0) and oxidation to Fe(III) by reaction with nitrate. The wrinkles in Figures 4.13B and D are likely due to the rapid drying and shrinking of the hydrogels.

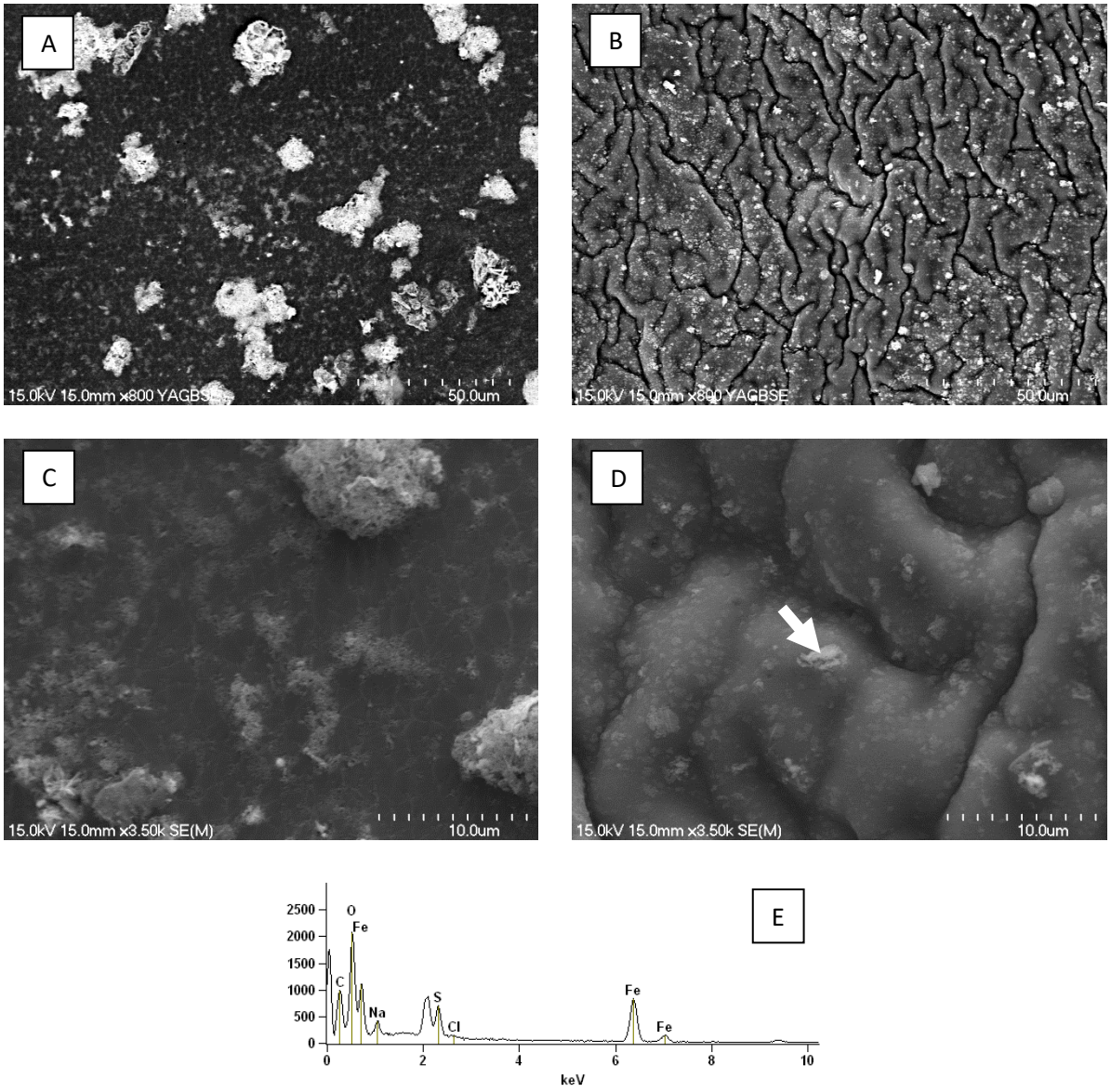


Figure 4.13: SEM images of iron impregnated p(AMA/AMPS) hydrogels. (A) and (C): hydrogels before iron reduction with $NaBH_4$. (B) and (D): hydrogels after reduction of nitrate to nitrite. (E) Elemental analysis of the site marked by the arrow in D.

## 4.4. Discussion

An AuNP-chitosan colourimetric technique was developed, and incorporated into a custom designed and 3D printed DGT probe, as a liquid binding layer. This approach provided quantitative nitrite masses between 0 – 145 µg. A poly-2-acrylamido-2-methyl-1-propanesulfonic acid/acrylamide (p(AMPS/AMA)) copolymer hydrogel was developed and impregnated with Fe(III) which was reduced to Fe(0) nanoparticles. The Fe(0)-p(AMPS/AMA) hydrogel was used to reduce nitrate to nitrite, for determination with the AuNP-chitosan suspension. Despite the success of the individual steps, there

are a number of challenges remaining (discussed below), such as resolving the insufficiently fast reaction rate of the AuNP-chitosan suspension so that DGT theory is met. When these challenges are overcome and the AuNP-chitosan and Fe(0) systems successfully combined, offer a new DGT that could quantitatively form colour *in situ* in response to nitrate in water bodies.

### *4.4.1 AuNP-chitosan DGT*

Colour change within the binding layer of the AuNP-chitosan DGT was achieved *in situ* in lab-based experiments, during deployment in nitrite solutions of various concentrations (0 – 1000 mg $L^{-1}$). The determined masses were significantly lower, however, than the expected masses. This was likely due to the dilution of the AuNP-chitosan suspension, and the rate of reaction of the AuNP-chitosan suspension not being rapid enough to meet the theoretical requirements of DGT (discussed below). The colour change was most easily discernible, via both UV-vis and RGB analysis, at nitrite masses greater than 40 µg, however, nitrite masses from 0 - 120 µg could be successfully determined.

Pre-concentration of the AuNP-chitosan suspension with small mass of nitrite (< 40 µg), prior to construction of the DGT, would make determination of low nitrite concentrations easier. The colour change was greatest above ~40 µg of nitrite, and it was difficult to visually discern differences in nitrite masses below ~40 µg (Figures 4.4 – 4.8). The presence of nitrite also appeared to stabilise the AuNP-chitosan suspension (discussed in section 4.4.2). High nitrite masses, however, appeared to be a potential issue for the deployment of AuNP-chitosan DGT due to the precipitation of the AuNP-chitosan on the dialysis membrane (Figure 4.9C).

Aggregation of the AuNP due to the presence of large masses of nitrite led to the precipitation of blue shifted AuNP on the dialysis membrane. As further discussed in section 4.4.3, this precipitation will affect the MDL thickness and present practical challenges for the field deployment of AuNP-chitosan DGT – although these affects were not examined in this study.

A DGT base for housing the AuNP suspension, and other liquid binding layers, was designed and 3D printed with total volume (excluding the volume created by extrusion of the rubber O-ring) of 2 mL

(Figure 4.9B). The AuNP-chitosan volume used in the DGT was 1.5 mL, the added volume meant that layering the dialysis membrane and other layers of the MDL was simple. Smaller volume probes were also constructed, but it was difficult to stop the AuNP suspension from being drawn out whilst the MDL was assembled. This meant that the AuNP-chitosan DGT needed to be deployed with the aperture window facing down, so that the AuNP-chitosan suspension was in full contact with the MDL. The base was designed to operate with the push-fit standard DGT solution probe cap. A screw on cap was also designed and tested, however the torsion force required to seal the dialysis membrane and rubber O-ring lead to tearing of the dialysis membrane.

The seal of the push-fit cap provided a strong seal, when combined with the low molecular weight cut-off dialysis membrane (< 15 kDa). The DGT remained sealed during vigorous shaking. There was, however, dilution of the AuNP-chitosan suspension during deployment, most clear in the decrease in the adsorption at 523 nm of the AuNP-chitosan suspension of DGT deployed in 0 mg $L^{-1}$ nitrite solution. The volume within the DGT did not change. The dilution was either due to leakages between the rubber O-ring and dialysis membrane, or diffusion of AuNP-chitosan particles through dialysis membrane. The dilution was likely a consequence of sonicating the AuNP-chitosan during the preparation of the suspension. Sonication has been reported as a method for the fragmentation of chitosan (Kasaai et al., 2008), producing smaller particles that could diffuse through the dialysis membrane. Formation of the AuNP-chitosan suspension in stronger solvent, instead of deionised water, may remove the need for sonication.

### *4.4.2 Colour Reaction*

Colour development occurred slowly, all samples were initially analysed seven days after the introduction of nitrite. Perceivable colour change did not occur until about four days. The colour change is induced by the shortening of the AuNP interparticle distance (Lee et al., 2008), in the presence of nitrite. Whether the AuNP-chitosan suspension meets the theoretical requirements for application in DGT, rapid and strong binding (Davison, 2016), is determined by the rate at which nitrite

is bound by to the AuNP-chitosan. Presently, colour development of the AuNP-chitosan suspension must occur after nitrite is bound, and nitrite must be bound strongly, to meet the theoretical requirements of DGT. It seems, however, that the binding of nitrite and the colour change is simultaneous, meaning that the binding of nitrite is not rapid. If this is correct, then the AuNP-chitosan DGT likely operate under Diffusional Equilibrium Theory (DET) and functionally similar to pore-water samplers, whereby the nitrite concentration in the binding layer is in equilibrium with the concentration of the bulk solution (Davison et al., 1991; Teasdale et al., 1995).

Coagulation of the AuNP-chitosan suspension occurred at low nitrite concentrations - likely due to the agglomeration of chitosan and not the nanoparticles. The coagulants were not significantly blue shifted, which would result from the precipitation of the AuNP-chitosan. Chitosan is soluble in acidic solutions (pH < 6), acids protonate the deacetylated units of chitosan, enabling the formation of thin chitosan coatings in solution (Pigaleva et al., 2014). Dissolved chitosan chains however, may preserve a degree of aggregation due to the presence of residual N-acetyl groups in the chitosan chain (Pigaleva et al., 2014). The deacetylated groups may also form intra and intermolecular bonds via hydrogen bonding (Pigaleva et al., 2014). This deterioration in the chitosan coating of the AuNP could lead to agglomeration (Pigaleva et al., 2014). The increased mass of nitrite, furthermore, appeared to stabilise the AuNP suspension, potentially by reducing the agglomeration of the chitosan. The formation of coagulants in deployed AuNP-DGT is a good and immediate test as to whether the DGT will provide quantitative data.

### *4.4.3 Advantages and Disadvantages*

Liquid binding phase DGT were pursued to retain the necessary mobility for the AuNP systems. Liquid binding phase DGT have been reported previously (Li et al., 2003; Liu et al., 2016); the system developed here builds on this previous work. Utilising a liquid binding phase DGT presents its own advantages and disadvantages compared to the standard hydrogel based DGT binding layers.

Standard DGT commonly utilise an analyte specific resin suspended in a polyacrylamide hydrogel as a binding layer (Davison, 2016). Suspension of AuNP in an APA network was also explored here. AuNP hydrogels were successfully produced via the hydrogel formation in particle suspension method, and analysed via UV-vis with altered plastic cuvettes. The AuNP hydrogels, however, did not produce a colour change in the presence of nitrite. This was likely due to the decreased mobility of the AuNP in the hydrogel framework, even though swelled APA gels are ~90 % water. The AuNP systems utilised were based on the aggregation mechanism, and the decreased mobility meant the inter-particle distance could not decrease in the presence of nitrite, necessary to illicit a colour change.

A potential advantage of the liquid binding phase DGT is that they may better meet the assumption that analyte concentration is zero, or negligibly small, at the diffusion layer (Davison & Zhang, 2012) – binding layer interface. As adsorption sites are occupied on the binding layer, target species would need to travel further into the binding layer to become bound, potentially extending the concentration gradient into the binding layer. If the AuNP-DGT are not absolutely fixed during deployment, the movement of DGT continually mixes the AuNP suspension, ensuring there are a greater number of binding sites at the diffusion layer/binding layer interface. Mixing of the AuNP suspension could also be diffusion driven. There is also no waste of potentially expensive reagents, unlike when cutting disks from sheets as with hydrogel binding layers – the specific volume of binding reagents/colour reagents can be pipetted into DGT base.

As previously reported, A520E-DGT were stable for several days and the binding layer can be dried before or after deployment and provide the same concentration (Corbett et al., 2019). This is an advantage of the standard nitrate-DGT over the AuNP systems. Colour development was a continuous gradual process, therefore the samples need to be analysed after a specific time period (seven days after the introduction of nitrite) or the samples calibrated against calibrations of the same age. The strongest calibrations, however, were produced after seven days, as the samples degenerated the colour and the suspensions became less stable. As discussed in section 4.4.2, coagulation of the

chitosan can occur if the samples are left for long periods before analysis or the AuNP could precipitate.

Coagulation will have practical implications for the deployment of AuNP-DGT. For example, if the deployment period is long, and/or nitrate concentration high, an AuNP-nitrite precipitate could form on the dialysis membrane as it did during the laboratory testing, extending the diffusion layer. Diffusive Gradients in Thin Films studies have reported biofouling on the membrane, where it meets bulk solution, which affected the analyte mass that diffused through to the binding layer and therefore the calculated concentration (Uher et al., 2012). This could potentially be overcome through the calculation of an effective diffusive boundary layer (DBL), whereby the effect the fouling has on the boundary layer is added to the DBL.

### *4.4.4 Formation of AuNP*

High molecular weight chitosan was used to ensure the final product was sufficiently large that it would not diffuse through the MDL. Although the dialysis membrane had a molecular weight cut-off of 15 kDa, and the chitosan used had a molecular weight of 150 kDa, dilution of the AuNP-chitosan suspension occurred when the AuNP-DGT were deployed in solution. As discussed above this was likely due to fragmentation of chitosan due to sonication (Kasaai et al., 2008). Dissolution, furthermore, of the high molecular weight chitosan required the addition of acid. HCl was chosen because the chloride would not interfere in the reaction. The addition of HCl to dissolve the chitosan necessitated the addition of $OH^-$ (from NaOH). The dissolution of chitosan requires increasingly acidic conditions as the molecular weight increases (Sogias et al., 2010), use of lower molecular weight chitosan may reduce the need for an acidic solvent and sonication of the AuNP-chitosan product, while still be sufficiently large that it cannot diffuse through the dialysis membrane.

### *4.4.5 Conclusion*

A new DGT system, based on a liquid binding layer containing a chitosan stabilised gold nanoparticle suspension, was tested for the colourimetric determination of nitrite.

A chitosan stabilised gold nanoparticle system was developed for the in-situ determination of nitrite, which was quantitative over a large nitrite concentration range. A Fe(0)-p(AMPS/AMA) hydrogel used as the diffusion layer, for the reduction of nitrate to nitrite, was also developed. Nitrate rapidly reduced to nitrite, the further reduction to $NH_3/NH_4^+$ and $NO_{x\ (g)}$ was avoided by the binding of nitrite to the binding layers. The diffusion characteristics were also determined. This work lays the foundations for the coupling of colourimetric techniques and DGT, for the infield quantitative determination of target species, such as nitrate.

Faster colour reaction rates would improve the ability of the colourimetric nitrate DGT to provide quantitative nitrate concentrations, by better meeting the theoretical requirement of DGT for rapid and strong anaylte binding to maintain the steady-state and concentration gradient (Davison, 2016). Alternative binding layers to the AuNP-chitosan system could be pursued, conversely methods for increasing the reaction rate of the AuNP-chitosan system, which may be preferable, given the specificity of the AuNP system for nitrite. Removing the need for reduction of nitrate to nitrite for the colourimetric determination within the binding layer, by development of a nitrate selective Au-nanoparticle for example, would simplify the preparation of the DGT system. Development of a nitrate specific rapid AuNP colour reaction is difficult due to the unreactive nature of nitrate, but it would remove the need for the Fe(0)-p(AMPS/AMA) hydrogel. The Fe(0)-p(AMPS/AMA) hydrogel can be difficult to handle due the high degree of water swelling and relatively poor mechanical stability in comparison to standard DGT APA hydrogels. Alternatively, incorporation of colourless or white reducing agents, such as nitrate-reductase or Zn(0), into the liquid binding layer would similarly overcome this.

## Funding

DairyNZ and the New Zealand Ministry for Primary Industries funded this study.

## Acknowledgements

We would like to acknowledge the financial support of DairyNZ and the Ministry for Primary Industries. We would also like to thank the late Professor Peter Teasdale for his guidance in moving towards liquid binding layers, and a special thank you to Jacob Shrubsall and Peter Jarman for their help with 3D printing.

## References


AHMED, E. M. (2015). Hydrogel: Preparation, characterization, and applications: A review. *Journal of Advanced Research, 6*(2), 105-121. doi:https://doi.org/10.1016/j.jare.2013.07.006

AMANULLA, B., PALANISAMY, S., CHEN, S.-M., CHIU, T.-W., VELUSAMY, V., HALL, J. M., CHEN, T.-W., & RAMARAJ, S. K. (2017). Selective Colorimetric Detection of Nitrite in Water using Chitosan Stabilized Gold Nanoparticles Decorated Reduced Graphene oxide. *Scientific Reports, 7*(1), 14182. doi:10.1038/s41598-017-14584-6

CAMPBELL, W. H. (1999). Nitrate Reductase Structure, Function and Regulation: Bridging the Gap between Biochemistry and Physiology. *Annual Review of Plant Physiology and Plant Molecular Biology, 50*(1), 277-303. doi:10.1146/annurev.arplant.50.1.277

CHEN, Q., CHEN, H., ZHU, L., & ZHENG, J. (2015a). Fundamentals of double network hydrogels. *Journal of Materials Chemistry B, 3*(18), 3654-3676. doi:10.1039/C5TB00123D

CHEN, W., CAO, F., ZHENG, W., TIAN, Y., XIANYU, Y., XU, P., ZHANG, W., WANG, Z., DENG, K., & JIANG, X. (2015b). Detection of the nanomolar level of total Cr[(III) and (VI)] by functionalized gold nanoparticles and a smartphone with the assistance of theoretical calculation models. *Nanoscale, 7*(5), 2042-2049. doi:10.1039/C4NR06726F

CHO, D.-W., SONG, H., SCHWARTZ, F. W., KIM, B., & JEON, B.-H. (2015). The role of magnetite nanoparticles in the reduction of nitrate in groundwater by zero-valent iron. *Chemosphere, 125*, 41-49. doi:https://doi.org/10.1016/j.chemosphere.2015.01.019

CORBETT, T. D. W., DOUGHERTY, H., MAXWELL, B., HARTLAND, A., HENDERSON, W., RYS, G. J., & SCHIPPER, L. A. (2019). Utility of 'Diffusive Gradients in Thin-Films' for the measurement of nitrate removal performance of denitrifying bioreactors. *Science of The Total Environment*, 135267. doi:https://doi.org/10.1016/j.scitotenv.2019.135267

DAS, J., & SARKAR, P. (2016). A new dipstick colorimetric sensor for detection of arsenate in drinking water. *Environmental Science: Water Research & Technology, 2*(4), 693-704. doi:https://doi.org/10.1039/C5EW00276A

DAVISON, W. (2016). *Diffusive Gradients in Thin-Films for Environmental Measurements*. Cambridge, UNITED KINGDOM: Cambridge University Press.

DAVISON, W., GRIME, G. W., MORGAN, J. A. W., & CLARKE, K. (1991). Distribution of dissolved iron in sediment pore waters at submillimetre resolution. *Nature, 352*(6333), 323-325. doi:10.1038/352323a0

DAVISON, W., & ZHANG, H. (2012). Progress in understanding the use of diffusive gradients in thin films (DGT) – back to basics. *Environmental Chemistry, 9*(1), 1-13. doi:https://doi.org/10.1071/EN11084

EMADI, F., AMINI, A., GHOLAMI, A., & GHASEMI, Y. (2017). Functionalized Graphene Oxide with Chitosan for Protein Nanocarriers to Protect against Enzymatic Cleavage and Retain Collagenase Activity. *Scientific Reports, 7*(1), 42258. doi:10.1038/srep42258

EPA, U. S. (1993). *Method 350.1: Nitrogen, Ammonia (Colorimetric, Automated Phenate)*. Cincinnati, OH Retrieved from https://www.epa.gov/esam/epa-method-3501-determination-ammonia-nitrogen-semi-automated-colorimetry

FANNING, J. C. (2000). The chemical reduction of nitrate in aqueous solution. *Coordination Chemistry Reviews, 199*(1), 159-179. doi:https://doi.org/10.1016/S0010-8545(99)00143-5

GALLOWAY, J. N., ABER, J. D., ERISMAN, J. W., SEITZINGER, S. P., HOWARTH, R. W., COWLING, E. B., & COSBY, B. J. (2003). The Nitrogen Cascade. *BioScience, 53*(4), 341-356. doi:10.1641/0006-3568(2003)053[0341:TNC]2.0.CO;2

GONG, J. P., KATSUYAMA, Y., KUROKAWA, T., & OSADA, Y. (2003). Double-Network Hydrogels with Extremely High Mechanical Strength. *Adv. Mater., 15*(14), 1155-1158. doi:10.1002/adma.200304907

GUNUPURU, R., MAITY, D., BHADU, G. R., CHAKRABORTY, A., SRIVASTAVA, D. N., & PAUL, P. (2014). Colorimetric detection of $Cu^{2+}$ and $Pb^{2+}$ ions using calix[4]arene functionalized gold nanoparticles. *Journal of Chemical Sciences, 126*(3), 627-635. doi:10.1007/s12039-014-0600-5

HUANG, J., BENNETT, W., TEASDALE, P. R., GARDINER, S., & WELSH, D. (2016a). Development and evaluation of the diffusive gradients in thin films technique for measuring nitrate in freshwaters. *Analytica Chimica Acta, 923*, 74-81. doi:10.1016/j.aca.2016.04.006

HUANG, J., BENNETT, W. W., WELSH, D. T., & TEASDALE, P. R. (2016b). Determining time-weighted average concentrations of nitrate and ammonium in freshwaters using DGT with ion exchange membrane-based binding layers. *Environmental Science: Processes & Impacts, 18*(12), 1530-1539. doi:10.1039/c6em00260a

IBRAHIM, M. H., XUE, Z., ABDU, H. I., SHINGER, M. I., IDRIS, A. M., EDRIS, M. M., SHAN, D., & LU, X. (2019). Sensitive and selective colorimetric nitrite ion assay using silver nanoparticles easily synthesized and stabilized by AHNDMS and functionalized with PABA. *Nanoscale Advances, 1*(3), 1207-1214. doi:10.1039/C8NA00146D

JAMSHIDI, H., & RABIEE, A. (2014). Synthesis and Characterization of Acrylamide-Based Anionic Copolymer and Investigation of Solution Properties. *Advances in Materials Science and Engineering, 2014*. doi:10.1155/2014/728675

KASAAI, M. R., ARUL, J., & CHARLET, G. (2008). Fragmentation of chitosan by ultrasonic irradiation. *Ultrasonics Sonochemistry, 15*(6), 1001-1008. doi:https://doi.org/10.1016/j.ultsonch.2008.04.005

KHALIL, I., JULKAPLI, N. M., YEHYE, W. A., BASIRUN, W. J., & BHARGAVA, S. K. (2016). Graphene-Gold Nanoparticles Hybrid-Synthesis, Functionalization, and Application in a Electrochemical and Surface-Enhanced Raman Scattering Biosensor. *Materials (Basel), 9*(6). doi:10.3390/ma9060406

KING, R. C., MULLIGAN, P. K., & STANSFIELD, W. D. (2013). Diffusion. In *A Dictionary of Genetics* (8 ed., pp. 122). Oxford: Oxford University Press.

LEE, J. H., WANG, Z., LIU, J., & LU, Y. (2008). Highly sensitive and selective colorimetric sensors for uranyl (UO2(2+)): development and comparison of labeled and label-free DNAzyme-gold nanoparticle systems. *J Am Chem Soc, 130*(43), 14217-14226. doi:10.1021/ja803607z

LI, W., TEASDALE, P. R., ZHANG, S., JOHN, R., & ZHAO, H. (2003). Application of a Poly(4-styrenesulfonate) Liquid Binding Layer for Measurement of $Cu^{2+}$ and $Cd^{2+}$ with the Diffusive Gradients in Thin-Films Technique. *Analytical Chemistry, 75*(11), 2578-2583. doi:10.1021/ac020658q

LIU, G., LU, M., HUANG, X., LI, T., & XU, D. (2018). Application of Gold-Nanoparticle Colorimetric Sensing to Rapid Food Safety Screening. *Sensors (Basel, Switzerland), 18*(12), 4166. doi:10.3390/s18124166

LIU, S., QIN, N., SONG, J., ZHANG, Y., CAI, W., ZHANG, H., WANG, G., & ZHAO, H. (2016). A nanoparticulate liquid binding phase based DGT device for aquatic arsenic measurement. *Talanta, 160*, 225-232. doi:https://doi.org/10.1016/j.talanta.2016.06.064

LIU, Y., & WANG, J. (2019). Reduction of nitrate by zero valent iron (ZVI)-based materials: A review. *Science of The Total Environment, 671*, 388-403. doi:https://doi.org/10.1016/j.scitotenv.2019.03.317

MAXWELL, B. M., BIRGAND, F., SMITH, B., & AVENI-DEFORGE, K. (2018). A small-volume multiplexed pumping system for automated, high-frequency water chemistry measurements in volume-limited applications. *Hydrology and Earth System Sciences, 22*(11), 5615-5628. doi:10.5194/hess-22-5615-2018

MORITA, E., & NAKAMURA, E. (2008). Reduction of Nitrate to Nitrite by Using Zinc Powder for Determination of Total Nitrogen in Sea Water. *Bunseki Kagaku, 57*(10), 777-781. doi:10.2116/bunsekikagaku.57.777

MURADOVA, G. G., GADJIEVA, S. R., DI PALMA, L., & VILARDI, G. (2016). Nitrates Removal by Bimetallic Nanoparticles in Water. *Chemical Engineering Transactions, 47*, 205-210. doi:10.3303/CET1647035

NYDAHL, F. (1976). On the optimum conditions for the reduction of nitrate to nitrite by cadmium. *Talanta, 23*(5), 349-357. doi:https://doi.org/10.1016/0039-9140(76)80047-1

PAREDES, J. I., VILLAR-RODIL, S., MARTÍNEZ-ALONSO, A., & TASCÓN, J. M. (2008). Graphene oxide dispersions in organic solvents. *Langmuir, 24*(19), 10560-10564. doi:10.1021/la801744a

PEREZ-CORONADO, A. M., CALVO, L., BAEZA, J. A., PALOMAR, J., LEFFERTS, L., RODRIGUEZ, J. J., & GILARRANZ, M. A. (2017). Selective Reduction of Nitrite to Nitrogen with Carbon-Supported Pd–AOT Nanoparticles. *Industrial & Engineering Chemistry Research, 56*(41), 11745-11754. doi:10.1021/acs.iecr.7b02944

PICIOREANU, C., LOOSDRECHT, M. C. M. V., & HEIJNEN, J. J. (1997). Modelling the effect of oxygen concentration on nitrite accumulation in a biofilm airlift suspension reactor. *Water Science and Technology, 36*(1), 147-156.

PIGALEVA, M. A., PORTNOV, I. V., RUDOV, A. A., BLAGODATSKIKH, I. V., GRIGORIEV, T. E., GALLYAMOV, M. O., & POTEMKIN, I. I. (2014). Stabilization of Chitosan Aggregates at the Nanoscale in Solutions in Carbonic Acid. *Macromolecules, 47*(16), 5749-5758. doi:10.1021/ma501169c

RAMASAMY, R. P., & MALIYEKKAL, S. M. (2014). Formation of gold nanoparticles upon chitosan leading to formation and collapse of gels. *New Journal of Chemistry, 38*(1), 63-69. doi:10.1039/C3NJ00603D

S˙LIWKA-KASZYŃSKA, M., KOT-WASIK, A., & NAMIEŚNIK, J. (2003). Preservation and Storage of Water Samples. *Critical Reviews in Environmental Science and Technology, 33*(1), 31-44. doi:10.1080/10643380390814442

SAHINER, N. (2013). Soft and flexible hydrogel templates of different sizes and various functionalities for metal nanoparticle preparation and their use in catalysis. *Progress in Polymer Science, 38*(9), 1329-1356. doi:https://doi.org/10.1016/j.progpolymsci.2013.06.004

SAHINER, N., OZAY, H., OZAY, O., & AKTAS, N. (2010). A soft hydrogel reactor for cobalt nanoparticle preparation and use in the reduction of nitrophenols. *Applied Catalysis B: Environmental, 101*(1), 137-143. doi:https://doi.org/10.1016/j.apcatb.2010.09.022

SCHNETGER, B., & LEHNERS, C. (2014). Determination of nitrate plus nitrite in small volume marine water samples using vanadium(III) chloride as a reduction agent. *Marine Chemistry, 160*, 91-98. doi:https://doi.org/10.1016/j.marchem.2014.01.010

SHENG, J. J. (2010). Polymer Flooding. In *Modern Chemical Enhanced Oil Recovery: Theory and Practice* (pp. 101-206). Burlington, MA, United States of America: Gulf Professional Publishing.

SOGIAS, I. A., KHUTORYANSKIY, V. V., & WILLIAMS, A. C. (2010). Exploring the Factors Affecting the Solubility of Chitosan in Water. *Macromolecular Chemistry and Physics, 211*(4), 426-433. doi:https://doi.org/10.1002/macp.200900385

SU, E., & OKAY, O. (2018). Hybrid cross-linked poly(2-acrylamido-2-methyl-1-propanesulfonic acid) hydrogels with tunable viscoelastic, mechanical and self-healing properties. *Reactive and Functional Polymers, 123*, 70-79. doi:https://doi.org/10.1016/j.reactfunctpolym.2017.12.009

SUTIRMAN, Z. A., SANAGI, M. M., ABD KARIM, K. J., & WAN IBRAHIM, W. A. (2016). Preparation of methacrylamide-functionalized crosslinked chitosan by free radical polymerization for the removal of lead ions. *Carbohydrate Polymers, 151*, 1091-1099. doi:https://doi.org/10.1016/j.carbpol.2016.06.076

TEASDALE, P. R., BATLEY, G. E., APTE, S. C., & WEBSTER, I. T. (1995). Pore water sampling with sediment peepers. *TrAC Trends in Analytical Chemistry, 14*(6), 250-256. doi:https://doi.org/10.1016/0165-9936(95)91617-2

THONIYOT, P., TAN, M. J., KARIM, A. A., YOUNG, D. J., & LOH, X. J. (2015). Nanoparticle-Hydrogel Composites: Concept, Design, and Applications of These Promising, Multi-Functional Materials. *Advanced science (Weinheim, Baden-Wurttemberg, Germany), 2*(1-2), 1400010-1400010. doi:10.1002/advs.201400010

TSOGAS, G. Z., KAPPI, F. A., VLESSIDIS, A. G., & GIOKAS, D. L. (2018). Recent Advances in Nanomaterial Probes for Optical Biothiol Sensing: A Review. *Analytical Letters, 51*(4), 443-468. doi:10.1080/00032719.2017.1329833

UHER, E., ZHANG, H., SANTOS, S., TUSSEAU-VUILLEMIN, M.-H., & GOURLAY-FRANCÉ, C. (2012). Impact of Biofouling on Diffusive Gradient in Thin Film Measurements in Water. *Analytical Chemistry, 84*(7), 3111-3118. doi:10.1021/ac2028535

YAN, N., CAPEZZUTO, F., LAVORGNA, M., BUONOCORE, G. G., TESCIONE, F., XIA, H., & AMBROSIO, L. (2016). Borate cross-linked graphene oxide–chitosan as robust and high gas barrier films. *Nanoscale, 8*(20), 10783-10791. doi:10.1039/C6NR00377J

YE, S., & FENG, J. (2016). The effect of sonication treatment of graphene oxide on the mechanical properties of the assembled films. *RSC Advances, 6*(46), 39681-39687. doi:10.1039/C6RA03996K

ZHANG, H., & DAVISON, W. (1995). Performance Characteristics of Diffusion Gradients in Thin Films for the in Situ Measurement of Trace Metals in Aqueous Solution. *Analytical Chemistry, 67*(19), 3391-3400. doi:10.1021/ac00115a005

ZHANG, Z., CHEN, Z., WANG, S., QU, C., & CHEN, L. (2014). On-Site Visual Detection of Hydrogen Sulfide in Air Based on Enhancing the Stability of Gold Nanoparticles. *ACS Applied Materials & Interfaces, 6*(9), 6300-6307. doi:10.1021/am500564w

ZHU, I., & GETTING, T. (2012). A review of nitrate reduction using inorganic materials. *Environmental Technology Reviews, 1*(1), 46-58. doi:10.1080/09593330.2012.706646

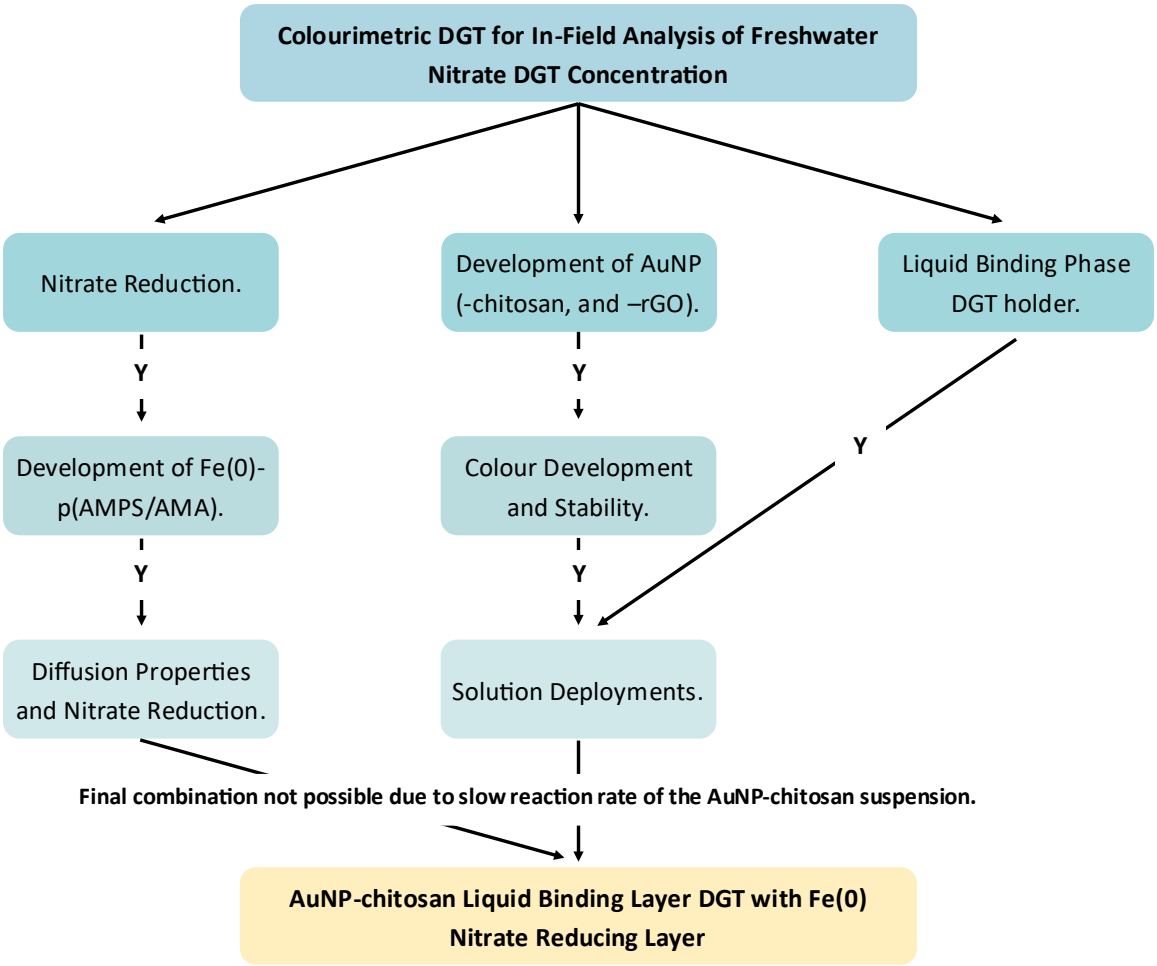


Figure 4.14: Research Schematic.

# Chapter 5 - Development of Bromide-Selective Diffusive Gradients in Thin-Films for the Measurement of Average Flow Rate of Streams.

*Adapted from:*

CORBETT, T. D. W., HARTLAND, A., HENDERSON, W., RYS, G. J. & SCHIPPER, L. A. 2021. Development of Bromide-Selective Diffusive Gradients in Thin-Films for the Measurement of Average Flow Rate of Streams. Science of the Total Environment.

## Highlights

- A novel bromide selective DGT ($Br^-$-DGT) was developed.
- The theory for using DGT for flow measurements was established.
- We developed a new method for quantitative water flow measurements using DGT.
- Flow rates were determined by combination of $Br^-$-DGT and the trace-dilution method.
- The novel $Br^-$-DGT provided quantitative bromide concentrations.

## Abstract

Diffusive Gradients in Thin-Films (DGT) have traditionally been used to measure time-weighted average concentration in water. We tested whether $Br^-$-DGT in combination with the trace-dilution flow rate method, could be used as a new approach for measuring water flow rate. A novel bromide selective DGT based on the Purolite Bromide Plus anion exchange resin ($Br^-$-DGT) was developed, which provided environmental bromide concentrations comparable to grab samples. The $Br^-$-DGT provided quantitative bromide concentrations at a range of pH, competing ion concentrations, and in synthetic natural solution. The uptake efficiency was 95.7 ± 3.4 %, and the elution efficiency was 95.5 ± 4.7 %. The absorption maximum/saturation point of each binding disk was 0.684 ± 0.001 mg. Bromide adsorption to the binding layer was linear to 44.1 % of the total binding capacity, 0.302 mg. The determined diffusion coefficient through the agarose cross-linked polyacrylamide (APA) hydrogels was 1.05 x $10^{-5}$ $cm^2$ $s^{-1}$ at 17.9 °C, temperature corrected to 25 °C was 1.29 x $10^{-5}$ $cm^2$ $s^{-1}$. Diffusive Gradients in Thin Films flow rates were between -14.7 and 6.50 % of the flow independently

monitored flow rate (weir). In comparison, grab sample flow rates diverged by 5.52 to 58.9 % from the weir flow rate.

## Graphical Abstract

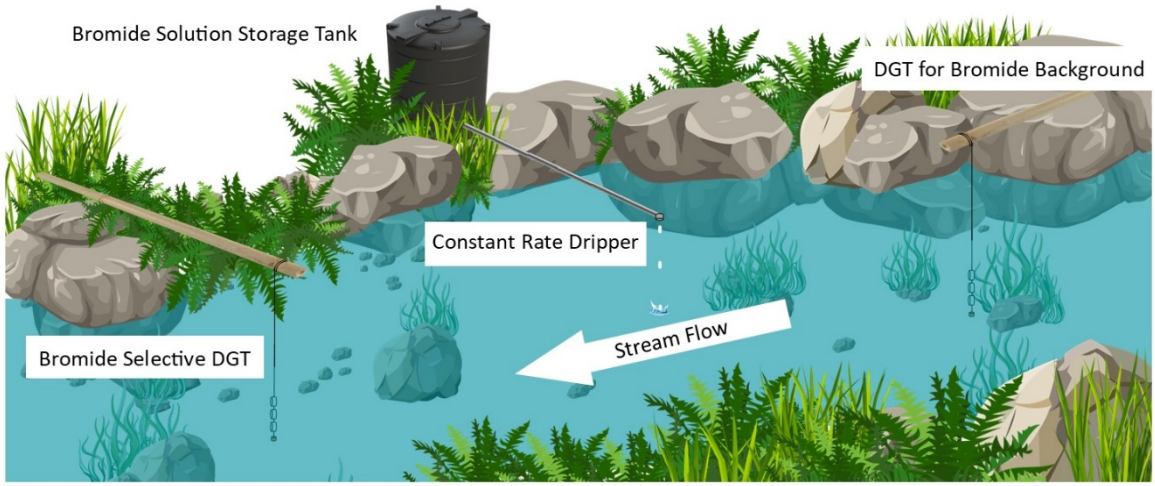


## 5.1. Introduction

Anthropogenic alterations of natural systems have affected local and global hydrological regimes, altering ecosystem responses (Vogel et al., 2015). Given the importance of fresh water systems to not only human wellbeing but also their supporting ecosystems and ecosystem processes, fresh water systems need to be monitored locally and globally (Karr, 1991). Numerous methods exist for the measurement of nutrient and contaminant concentrations in freshwater systems, ranging in expense, simplicity, and data quality - for example continuous automated monitoring/sampling, manual sampling, and passive sampling (Kianpoor Kalkhajeh et al., 2019). Similarly there are a multitude of methods for the measurement of flow rate, including, direct measurement, velocity-area, formed construction, and non-contact, each presenting challenges and advantages (Dobriyal et al., 2017).

Diffusive Gradients in Thin-Films (DGT) (Figure 5.1) was designed to be analyte-specific, and can provide quantitative concentration data at low concentrations (Panther et al., 2013; Zhang & Davison, 1995; Zhang et al., 1998). Diffusive Gradients in Thin Films are also capable of providing concentration measurements of nutrients comparable to high frequency grab sampling (Corbett et al., 2019; Huang

et al., 2016a). They overcome many of the limitations associated with grab sampling, such as the analytical requirements, and the expense of on-site monitoring equipment (Corbett et al., 2019; Maxwell et al., 2018).

DGT operate on the application of Fick's First Law (Zhang & Davison, 1995), whereby molecules move in the direction of decreasing concentration due to their random heat motion (King et al., 2013). A diffusive gel and membrane filter ensure that transport of analytes to a specific binding layer, which rapidly and strongly bound the analyte, was restricted to diffusion (Davison, 2016). Measurement of the accumulated mass enabled the calculation of the average concentration for the deployment period (Davison, 2016).

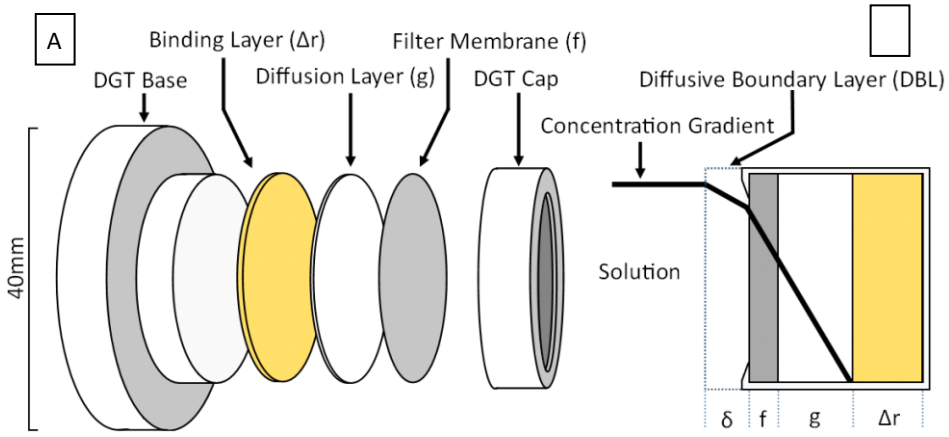


Figure 5.1: (A) Diffusive Gradient in Thin-films (DGT) solution probe exploded view (Corbett et al., 2019), and (B) cross-sectional view of the concentration gradient of bromide through the Diffusive Boundary Layer, and Material Diffusion Layer (Filter Membrane and Diffusion Layer).

DGT were originally designed for the measurement of trace metals (Zhang & Davison, 1995). Since then, DGT have been specifically designed for determining $NO_3^-$ and $PO_4^{3-}$, and have been shown to provide a useful measure of the concentrations of these major nutrient contaminants in water (Huang et al., 2016b; Zhang et al., 1998). Beyond concentration, it is important to consider the loading of nutrients in receiving waters (Pinckney et al., 2001). Loading is important because ecosystem responses can depend on the net export and import of nutrients, and is often expressed as tons of X per year by multiplying concentration by discharge or flow rate (Pinckney et al., 2001). The

measurement accuracy of these two variables and the frequency of the measurements determines the accuracy of the calculated loading rate (Pinckney et al., 2001). While DGT are well established for the measurement of environmental contaminants, we propose they can also be adapted for flow rate determination – as discussed in section 2.1.

A number of methods for determining flow exist, but each have a number of constraints. Direct measurement via the time volume method is only suitable for small narrow streams (Dobriyal et al., 2017). Formed constriction methods (weirs and flumes) are operationally difficult, expensive and their construction can alter hydrological regimes and local habitat (Bonacci et al., 2016). Non-contact measurement methods (remote sensing and particle image velocity) are also operationally difficult and expensive, and can have variable accuracy (Dobriyal et al., 2017). Velocity-area methods (float, dilution gauging, trajectory, current meters, acoustic doppler, and electromagnetic) vary in expense and accuracy, and the systems in which they can be applied (Dobriyal et al., 2017). Instantaneous tracer injection works well in steep and highly turbulent streams (Moore, 2005), however this approach is often thought to be of low accuracy and can cause environmental damage (Dobriyal et al., 2017). Constant-rate tracer injection has provided more accurate flow measurements at low flows (Moore, 2005).

Here we propose that a combination of constant-rate bromide injection coupled with downstream deployment of bromide-specific DGT can allow the calculation of time-weighted average flow rate, which accounts for flow rate changes due to episodic events. The theoretical basis was developed in the methods section (2.1). Briefly, the sum of the tracer concentration multiplied by the flow of the injection and the upstream (of the injection point) concentration multiplied by the upstream flow, equals the concentration multiplied by flow downstream. Diffusive Gradients in Thin-Films are robust, and when properly secured, can operate under various system conditions (Davison, 2016). In contrast, traditional measurement instrumentation can be damaged and water samples not collected due to

the risk to personnel safety (Pinckney et al., 2001). In loading events, the input of large analyte masses, are therefore missed or approximated to low accuracy (Pinckney et al., 2001).

Bromide ($Br^-$) is widely used as a tracer for water and solute tracer studies because it does not adsorb onto negatively charged soil particles and moves about as fast as water (Flury & Papritz, 1993). $Br^-$ has therefore been reported to act as a conservative tracer. It is however important to note that some tracer studies have reported uptake of $Br^-$ (< 10 %) by emergent plants (Parsons et al., 2004). Combined with the low natural background concentration, low toxicity to mammals, most freshwater organisms, and most plants, $Br^-$ is an ideal tracer (Flury & Papritz, 1993). To avoid the risk of chronic toxicity to the environment, the concentration of bromide should not exceed 1 mg $L^{-1}$ (Canton et al., 1983; Flury & Papritz, 1993). Toxicity studies of sodium bromide for algae (Scenedesmus pannonicus), crustaceans (Daphnia magna), and fish (Poecilia reticulata and Oryzias latipes), found the acute toxicity varied from 44 to 5800 mg $Br^-$ $L^{-1}$, and the no observed effect concentration in long-term studies to vary from 7.8 to 250 mg $Br^-$ $L^{-1}$ (Canton et al., 1983).

Development of a bromide-selective DGT for quantification of average flow rates represents a novel extension of the DGT technique, which have primarily been focussed on quantifying concentrations of specific analytes. The objectives of this study were to (i) develop a novel DGT selective for $Br^-$, and (ii) test whether these can be used to determine average flow rates when coupled with the tracer dilution method.

A bromide selective DGT could also provide an effective tool for bromide monitoring, particularly where concentrations may be environmentally harmful, such as reproduction, growth, behaviour and mortality of algae, crustaceans, and fish (Canton et al., 1983).

## 5.2. Methods

### *5.2.1 Theory*

DGT have not previously been utilised to determine flow rates. Figure 5.2 provides a schematic of a tracer experiment for determining flow rate. Instead of an instantaneous injection of bromide and measurement via grab sampling, bromide was added at a constant rate and concentration and was measured continuously by DGT.

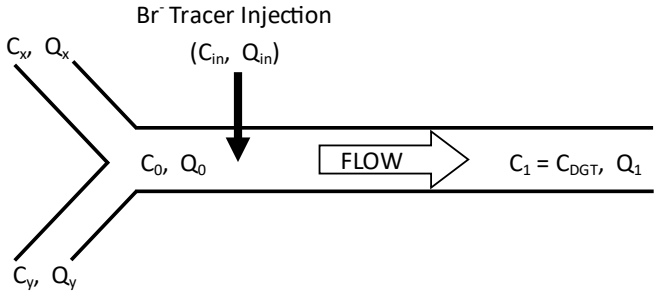


Figure 55.2**:** Schematic of the Bromide-DGT (Br-DGT) tracer experiment, and flow partitioning of stream branches (Equations 1 - 6). $C_0$, $C_{in}$, $C_1$, and $C_x$ and $C_y$ = concentration upstream of the tracer injection, bromide tracer injection, downstream of the tracer injection, and the branches of the steam (x and y). $Q_0$, $Q_{in}$, $Q_1$, and $Q_x$ and $Q_y$ = flow rates of upstream of the tracer injection, injection, downstream of the tracer injection point, and the branches of the steam (x and y) respectively.

When water with a flow rate of $Q_0$ (flow before tracer injection) with tracer concentration ($C_0$), and a tracer with concentration $C_{in}$ (tracer concentration) is injected with flow rate $Q_{in}$ (flow rate of tracer), the sum is the mixed flow rate $Q_1$ and concentration $C_1$ ($C_{DGT}$) downstream (Lee et al., 2007). Importantly this assumes complete mixing of the injected tracer, such that at the downstream measurement location the concentration is uniform (Lee et al., 2007), as shown in the following equations (Lee et al., 2007).

$$\boldsymbol{C_0 Q_0 + C_{in} Q_{in} = C_1 Q_1} \quad (1)$$

$$\boldsymbol{Q_0 + Q_{in} = Q_1} \quad (2)$$

By combining and rearranging these two equations, the following equation for $Q_0$ was obtained.

$$\boldsymbol{Q_0 = \frac{C_1 - C_{in}}{C_0 - C_1} \times Q_{in}} \quad (3)$$

Adapting the trace-dilution flow rate method for use with DGT requires three conditions. Firstly, $Q_{in}$ and $C_{in}$ must be constant. Diffusive Gradients in Thin Films deployment must occur after the bromide injection initiates and has begun flowing past the point of DGT deployment ($Q_1$). Lastly, the length of deployment (time) must be known. Diffusive Gradients in Thin Films provides time-weighted average concentration ($C_1$), the calculated flow rate ($Q_1$) was the time-weighted average flow. The contribution of the tracer injection to the total flow was so small it was effectively zero; hence, the flow at $Q_1$ could be treated as equal to $Q_0$.

An extension to determining the flow rate at a single point is the partitioning the contribution of tributaries to the total flow (Figure 5.2). To calculate the proportion of the flow that each branch of the stream contributed to the total flow in the main stream, $C_0$ and $Q_0$, and $C_{in}$ and $Q_{in}$ were treated as the concentration and flow of each branch ($C_x$, $C_y$, $Q_x$, and $Q_y$). The sum of the flow from the branches equals the total flow ($Q_1$). This yielded the following equations, for calculating the flow contributions of each branch feeding into the main stream.

$$\boldsymbol{C_x Q_x + C_y Q_y = C_0 Q_0} \tag{4}$$

$$\boldsymbol{Q_x = \frac{C_0 Q_0 - C_x Q_0}{C_y - C_x}} \tag{5}$$

$$\boldsymbol{Q_y = \frac{C_0 Q_0 - C_y Q_0}{C_x - C_y}} \tag{6}$$

### *5.2.2 General Procedures and $Br^-$-DGT Preparation*

Solutions were prepared with deionised water (18.2 MΩ). All equipment was washed in 10 % (v/v) HCl for a minimum of 24 hours, and thoroughly rinsed in deionised water. Experiments were conducted under clean laboratory conditions, and at least in triplicate. All reagents were sourced from Sigma Aldrich (Merck), New Zealand, unless stated otherwise. Materials (stakes, pegs, barrels, hose, nylon and rope) for deployments of bromide-DGT were sourced from local hardware stores, the constant rate drippers were produced by Aquadrip, Växjö, Sweden.

To our knowledge there were no reports of bromide selective DGT, hence a bromide selective DGT ($Br^-$-DGT) needed to be developed and tested. The following section details the preparation of the $Br^-$-DGT.

Gel solution, agarose cross-linked polyacrylamide (APA) diffusive gels, filter membranes, and anionic exchange binding resin impregnated binding hydrogels were prepared and stored using the same methods as stated in Corbett et al. (2019). Purolite Bromide Plus was dried, ground, and sieved to ≤90µm.

The background $Br^-$ mass for each deployment was determined, to ensure that any potential contamination was taken into account (Davison, 2016). The detection limit was calculated as three times the standard deviation of the background mass (Cai et al., 2017).

### *5.2.3 Uptake/Elution Efficiency and Saturation Point*

DGT relies on the binding layer having certain characteristics to provide quantitative concentration data. The uptake and elution efficiency define how well the binding resin adsorbs the analyte, and the recoverability of the bound mass (Davison, 2016). Saturation point, or adsorption maximum, is the total adsorbable mass and constrains the total deployment time. If the binding gel becomes saturated, it no longer adsorbs bromide, does not maintain the concentration gradient through the diffusive layer, and does not meet the theoretical requirements for the application of Fick's First Law to back calculate concentration (Davison, 2016).

Uptake efficiency was measured by placing resin disks in 10 mL bromide solutions (0.1-10 mg $L^{-1}$), prepared from 1000 mg $L^{-1}$ bromide solution from NaBr, and agitated for 24 hours on a shaker plate. Then the resin disks were transferred into fresh containers and eluted in 4 mL of 2 mol $L^{-1}$ NaCl for 24 hours, and finally diluted to 10 mL. Bromide was measured as described below. Uptake efficiency was calculated as percentage of bromide removed from solution, while elution efficiency was calculated as percentage of the bromide removed from solution during uptake, in the eluent removed from the resin (Huang et al., 2016b).

Saturation point was determined by placing resin disks in 10 mL of 1000 mg $L^{-1}$ bromide solution for 24 hours, and then eluted as stated above. The $Br^-$ mass present is greater than the binding disks were able to adsorb. The saturation point was taken as the total $Br^-$ mass present on the binding layer/removed from solution.

Previous research has found that the adsorption of target analytes is not linear to the saturation point (Corbett et al., 2019). Linear mass accumulation of the target analyte is necessary for DGT to provide quantitative concentrations (Davison, 2016). Adsorption isotherm experiments were performed to determine the adsorption of bromide through time, as binding sites are occupied. Bromide binding hydrogels were deployed in 50 mL of 100 mg $Br^-$ $L^{-1}$, from NaBr. NaCl (0.001 mol $L^{-1}$) was used as an ionic stabiliser. 1 mL samples were taken for 6 hours, and the bromide concentration analysed via ion chromatography, discussed in section 2.7.

### *5.2.4 Diffusion Coefficient*

The diffusion coefficient for bromide through the APA diffusive layer and filter membrane was previously undefined, and was required for concentration calculations. The diffusion coefficient was measured via diffusion cell (area = 3.46 $cm^2$), detailed below. The diffusion coefficient was confirmed by deploying sets of four bromide-DGT with material diffusion layer (MDL) thicknesses of 0.015, 0.055, 0.079 and 0.095 mm for 12, 18 and 24 hours in a synthetic bromide solution of known concentration (15 mg $Br^-$ $L^{-1}$). pH for both methods was ~6. Deployment of gels with different MDL thicknesses enabled calculation of the diffusive boundary layer – the area of solution at the MDL solution interface with decreased concentration in relation to the rest of solution (Davison, 2016), see below.

The high concentration chamber of the diffusion cell contained 130 mL of 80 mg $L^{-1}$ bromide; the low concentration chamber contained 130 mL of deionised water at time zero. NaCl (0.001 mol $L^{-1}$) was used as an ionic stabiliser. Subsamples (1 mL) were taken from both chambers hourly for 12 hours. The diffusion coefficient measured using the diaphragm diffusion cell was calculated using the following equation.

$$J = \frac{M}{A_p t} = \frac{D_g C}{\delta_g} \quad (7)$$

Where J = flux (mg $cm^{-2}$ $s^{-1}$), M = mass (mg), $A_p$ = diffusion window area ($cm^2$), t = time (s), $D_g$ = diffusion coefficient through gel ($cm^2$ $s^{-1}$), c = concentration (mg $cm^{-3}$), and $\delta_g$ = thickness of hydrogel (cm) (Davison, 2016).

The bromide concentration was analysed when each set of gels were removed. The concentration determined by DGT ($C_{DGT}$) was expected to be the same as $C_{solution}$ (Davison, 2016), after the elution factor and background gel mass were applied. The relationship between the accumulated mass and $C_{solution}$ provided a calibration curve with the following slope equation, where $A_{eff}$ = effective area due to lateral diffusion ($cm^2$), t = time/length of deployment (s), $D^{mdl}$, $D^w$ = material diffusion layer and water diffusion coefficients respectively ($cm^2$ $s^{-1}$), and $\delta^{mdl}$, $\delta^{dbl}$ = material diffusion layer and diffusive boundary layer thicknesses respectively (cm) (Davison, 2016).

$$Slope = A_{eff} t \left( \frac{D_{mdl} D_w}{\delta_{mdl} D_w + \delta_{dbl} D_{mdl}} \right) \quad (8)$$

Diffusion coefficients through the polyethersulfone filter membrane and APA diffusion layer are indistinguishable (Davison, 2016), as such they were treated as the same for bromide. Temperature was monitored throughout using temperature loggers; to temperature-correct the diffusion coefficients using the following equation (T = temperature; $D_T$ = diffusion coefficient at temperature T; $D_{25}$ = diffusion coefficient at 25°C) (Davison, 2016).

$$log D_T = \frac{1.37023(T - 25) + 0.000836(T - 25)^2}{109 + T} + log \frac{D_{25}(273 + T)}{298} \quad (9)$$

### *5.2.5 Ionic Strength, pH and Competing Ion Effects*

For the $Br^-$ selective DGT to provide environmental concentrations they needed to be capable of providing quantitative bromide concentrations at a range of solution pH and in the presence of

competing ions. For laboratory testing, temperature, pH, and conductivity were measured using an Xplorer GLX (PASCO, Washington, United States).

Firstly, DGT sets with different material diffusion layer thicknesses (0.055, 0.079 and 0.09 cm) were deployed in 8 L of 10 mg $L^{-1}$ bromide and 0.002 mol $L^{-1}$ NaCl solutions (pH = 3.5, 5.0, 7.0, 8.5) for 48 hours. Deploying in a large volume and at a relatively high concentration ensures the bromide mass adsorbed to the binding layer does not measurably decrease the overall bromide concentration. 1 mol $L^{-1}$ NaOH and HCl were used to adjust the pH.

Secondly, to determine the effect of competing ions on $C_{DGT}$, DGT sets of three different MDL thicknesses were deployed in bromide solutions (10 mg $L^{-1}$) containing one of $HCO_3^-$, $SO_4^{2-}$, $H_2PO_4^-$, $Cl^-$ and $NO_3^-$ (5 and 50 mg $L^{-1}$) from $NaHCO_3$, $Na_2SO_4$, $KH_2PO_4$, NaCl and $NaNO_3$, for 48 hours. These concentrations were chosen as they represent reasonable and high concentrations of possible competing ions in freshwater bodies (Cole & Prairie, 2014; Organisation, 2017; Reddy, 2020).

To determine the effect of ionic strength on bromide concentrations determined by DGT, DGT sets of three different MDL thicknesses were deployed in bromide solutions (10 mg $L^{-1}$) with varying ionic strengths. The solutions contained varying concentrations of NaCl (0.00001 mol $L^{-1}$ to 0.1 mol $L^{-1}$), to alter the ionic strength/conductivity.

Lastly, to ensure bromide selective DGT could provide quantitative concentrations in freshwater, they were also deployed in quadruplicate (MDL = 0.015, 0.055, 0.079, and 0.095 cm) in 8 L of soft synthetic freshwater, as prepared in Smith et al. (2002). Three stock solutions were prepared. Solution 1 was 500 mL of 1000 mg $Br^-$ $L^{-1}$, from NaBr. Solution 2 was 100 mL of 5.699 mg $L^{-1}$ $MgCl_2$, 17.50 mg $L^{-1}$ $CaCl_2.6H_2O$, and 3.542 $Ca(NO_3)_2.4H_2O$ (Smith et al., 2002). Solution 3 was 100 mL of 16.33 mg $L^{-1}$ $Na_2SO_4$, 2.502 mg $L^{-1}$ $KHCO_3$, and 1.678 mg $L^{-1}$ $NaHCO_3$ (Smith et al., 2002). From 8 L of deionised water (18.2 mΩ) appropriate volumes were removed so that when spiked with solution 1 (to provide $Br^-$ concentrations from 0.2 to 10 mg $L^{-1}$) and solutions 2 and 3 (8 mL each) the total volume remained 8 L. $CaCO_3$ 85.10 mg was then added and dissolved, before solutions 1-3 were added. The solution

compositions and order of combination ensured insoluble solids were not formed upon mixing. Temperature was logged throughout.

Previous research has reported the semi-quantitative adsorption of sulfate to the Purolite A520E nitrate specific binding layer (Corbett et al., 2019). It was expected, therefore, that nitrate and sulfate would adsorb to the Purolite Bromide Plus binding layer. To investigate if the DGT concentrations of nitrate and sulfate were quantitative, their bound masses were determined and the CDGT were compared to the solution concentrations determined via grab sampling. The nitrate and sulfate diffusion coefficients through APA hydrogels used in this study were 1.46 x $10^{-5}$ $cm^2$ $s^{-1}$ and 9.83 x $10^{-6}$ ± 0.35 x $10^{-6}$ $cm^2$ $s^{-1}$ at 25 °C respectively (Hanousek et al., 2016; Huang et al., 2016a).

### *5.2.6 DGT Deployment*

After development of the $Br^-$-DGT, they were deployed at multiple points along Mangaharakeke Stream, Hamilton, New Zealand (Figure 5.3A). Diffusive Gradients in Thin Films were deployed at six sites prior to running the tracer experiments to determine the background bromide concentration. During the first tracer study $Br^-$-DGT were deployed at sites 3, 4, and 5. During the second tracer study DGT were deployed at all six sites. Sites 4 and 5 were ~17 m and ~40 m downstream of the tracer injection respectively. Diffusive Gradients in Thin Films were deployed upstream (~10 m) of the injection point (site 3) to determine the bromide concentration before the injection point and to ensure there was no diffusion upstream, as well as determine the background concentration. Calculation of the distance to achieve complete tracer mixing is detailed in the supplementary material, the DGT were deployed well beyond the minimum distance of 3.6 m (Dingham, 1993; Kilpatrick & Cobb, 1985). Well within the distance to the Br--DGT deployment sites, which were ~17 and ~40 m downstream.

Each set consisted of four DGT with different MDL thicknesses (0.015, 0055, 0.079 and 0.95 cm), to provide replicates and calculate the diffusive boundary layer (discussed later). Bromide (46.2 g $L^{-1}$, from NaBr) was added at (6 L $h^{-1}$ for deployment 1 and 3.8 L $h^{-1}$ for deployment 2) from a reservoir

using pressure regulated drippers (Aquadrip, Växjö, Sweden). Bromide was added for 1 hour before the DGT were deployed, to ensure the tracer bromide was flowing past the downstream DGT locations.

Tracer study DGT probes were deployed for 12 hours, to ensure the total bromide mass and volume did not exceed the regulated values for tracer volume and mass (10 kilograms of salt or 100 litres of salt solution). Separate grab samples were taken at three intervals at each site - DGT deployment and removal, and halfway through the deployment. Background DGT were deployed for 24 hours. Grab samples were taken at DGT deployment and upon removal, at each location, during the background deployment. Temperature was logged at each deployment location using temperature iButtons (Thermochron, Wisconsin, USA). The Waikato Regional Council, as part of their freshwater monitoring network, independently monitored flow via a weir at site 5 (Waikato Regional Council, 2021). The rating curve, determined via manual velocity area gauging is provided in the supplementary information (Supplementary Material - Figure 5.7).

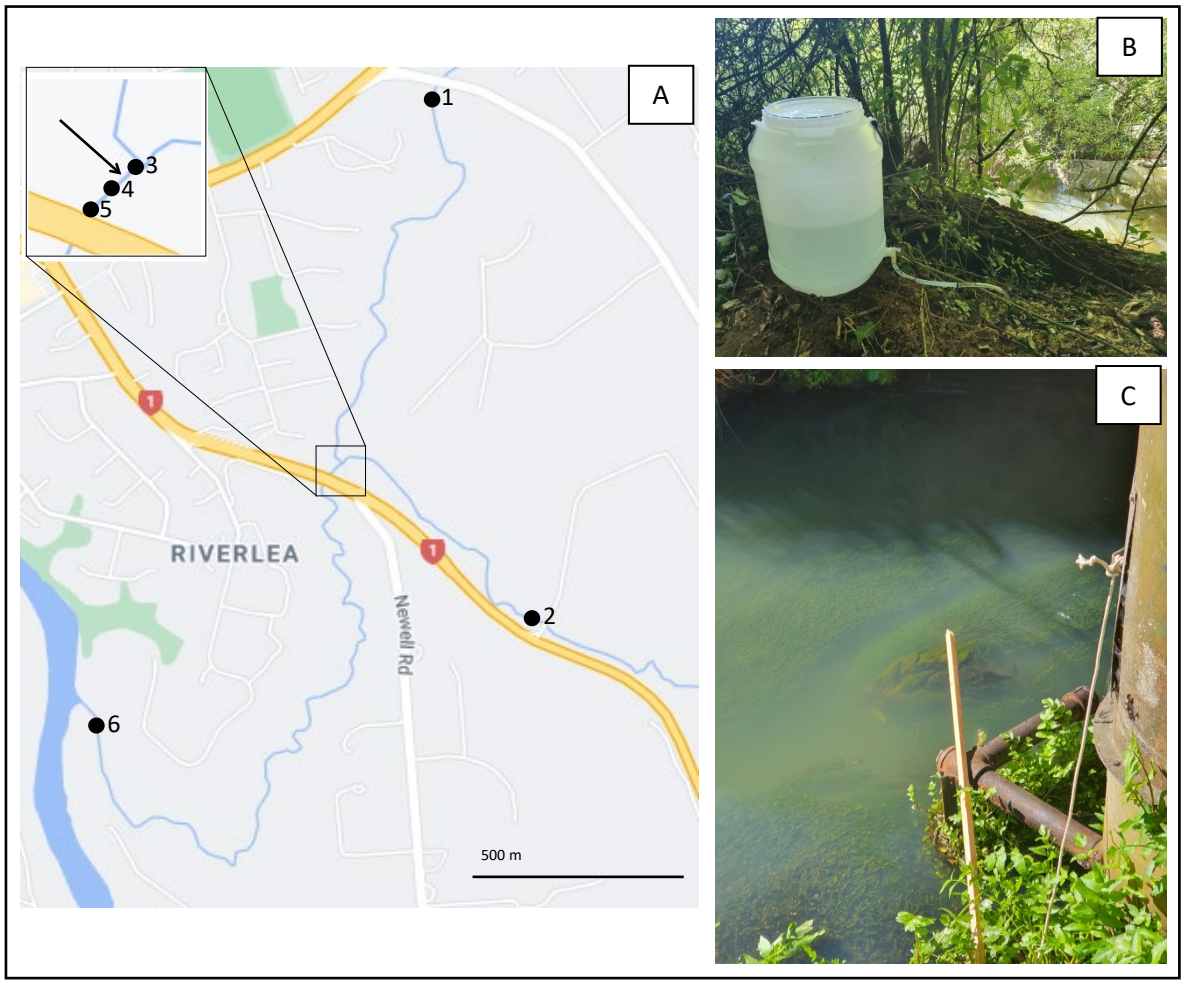


Figure 5.3 (A) Map of Mangaharakeke Stream (-37.80611, 175.33046) deployments, and numbered DGT (circles) and tracer injection (arrow) locations. (B) Image of the bromide injection. (C) A DGT deployment (site 5). Full site details provided in the supplementary material.

### *5.2.7 Analysis*

DGT were analysed as previously reported (Corbett et al., 2019), briefly, eluted DGT samples (eluent was 4 mL of 2 mol $L^{-1}$ NaCl) and grab samples were analysed alongside commercial anion standards (Dionex Seven Anion Standard) using a Dionex ICS-200 Ion Chromatograph (Dionex, California, United States) and a gradient concentration method.

Concentration was converted to mass after elution and application of the elution factor, to give the total mass accumulated, M (mg) – and inserted into the full DGT equation, below.

$$C_{DGT} = \frac{M}{A_{eff}t}\left(\frac{\Delta g_{gel}}{D_{gel}} + \frac{\Delta_f}{D_f} + \frac{\delta}{D_w}\right) \quad (10)$$

Where, $C_{DGT}$ = DGT concentration (mg $cm^{-3}$); t = length of deployment (s); $D_{gel}$, $D_f$, $D_w$ = diffusion coefficients for the diffusive gel and filter membrane respectively ($cm^2$ $s^{-1}$); Δg, Δf = thickness of diffusive gel and filter membrane respectively (cm); and, δ = thickness of the diffusive boundary layer (Davison, 2016).

The errors bars in the figures are the standard deviation (a), calculated using the following equation, where b, c and d are the standard deviation of the components. For example, for the calculation of the standard deviation of the solution and DGT concentration ratio, b, c, and d were the concentration determined by DGT and grab sampling, and the diffusion coefficient respectively.

$$a = \sqrt{b^2 + c^2 + d^2 \ldots} \quad (11)$$

### *5.2.8 Diffusive Boundary Layer*

The diffusive boundary layer is an important component of the full DGT concentration equation. It represents the area of solution at the aperture window with reduced bromide concentration in relation to the rest of solution (Corbett et al., 2019; Davison, 2016). The inverse of the accumulated mass, minus the background mass, was plotted against the combined gel and filter membrane thickness, the slope and intercept of the least squared equations were combined to give the equation below for DBL thickness (δ) (Zhang et al., 1998).

$$\delta = \frac{yD_w}{sD_{mdl}} \quad (12)$$

Where, $D_{mdl}$ = material diffusion layer diffusion coefficient, y= y intercept, s = slope (Davison, 2016).

## 5.3. Results

### *5.3.1 Field Deployments*

Table 5.1: Flow rates calculated using DGT and grab sampling calculated using equation 3, versus the independently determined flow (Weir Flow). *Note: the percentage difference of DGT and grab sampling to the independently determined (*weir*) flow is bracketed.*

| Deployment | Site | Weir Flow ($m^3 s^{-1}$) | $Br^-$-DGT ($m^3 s^{-1}$) | Grab Sampling ($m^3 s^{-1}$) |
|---|---|---|---|---|
| 1 | 4 | 0.665 | 0.666 | 0.702 |
| | | | *(0.23 %)* | (*5.52 %)* |
| | 5 | 0.665 | 0.708 | 0.764 |
| | | | *(6.50 %)* | (*14.8 %)* |
| 2 | 4 | 0.615 | 0.525 | 0.978 |
| | | | *(-14.7 %)* | *(58.9 %)* |
| | 5 | 0.615 | 0.643 | 0.734 |
| | | | *(4.41 %)* | *(19.3 %)* |

Data from the $Br^-$-DGT resulted in flow rate calculations generally within 6.5 % of the independently monitored weir flow rate (Waikato Regional Council, 2021), except at deployment 2 site 4 (-14.7 %) (Table 5.1), when combined with the trace-dilution flow rate method. Diffusive Gradients in Thin Films provided flow rates closer to the weir flow than grab sampling, which were up to 58.9 % greater than the weir flow rate (Table 5.1). The weir-based flow during the field deployments fluctuated throughout the tracer injection experiments by about 0.015 $m^3 s^{-1}$ (Figure 5.4A).

The bromide-selective DGT provided bromide concentrations closely matching the grab sample concentrations (Figure 5.4B). The background concentrations at each site were between 0.05 and 0.08 mg $L^{-1}$, the concentrations at sites 4 and 5 during the tracer studies were up to ~0.2 mg $L^{-1}$ (Figure 5.4B).

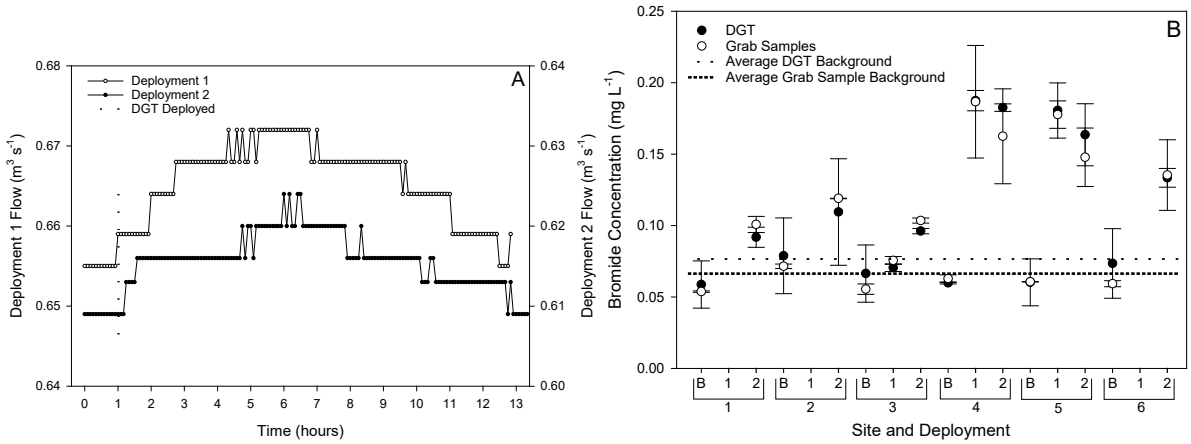


Figure 5.4 (A) Independently monitored weir flow regimes for DGT tracer studies. (B) DGT and grab sampling determined concentrations with standard deviations at all sites (1 to 6) for the background (B) and tracer deployments (1 and 2).

### *5.3.2 Flow Partitioning*

The contribution of the branches of the Mangaharakeke Stream to the total flow were calculated for the background DGT deployment, using the independently determined flow rate, and tracer deployment 2 using both the weir and the DGT derived flow rates. It was presumed that anion concentrations were constant from sites 1 and 2 to sites 3, 4, and 5 (downstream of the intersection) (Figure 5.3). The sum of the flows and concentrations from each branch equalled the flow downstream of their intersection.

The $Br^-$-DGT derived flow contributions from both stream branches, were similar to the flow rates determined via grab sampling, for the background deployment (Table 5.2). For the background deployment, the weir flow rate was used as the total flow rate, to partition the contributions of the feeder streams (from sites 1 and 2).

$Br^-$-DGT derived total flow and the weir-based total flow rate were used to compare the partitioning of flow contributions using DGT, for the second tracer deployment. The weir flow was used alone for partitioning via grab sampling. The $Br^-$-DGT provided contributing flow rates similar to those calculated using the independently measured flow as the total flow (Table 5.2). Flow partitioning, for the background and second tracer deployments, suggest that the bulk of the flow (60 to 85 %) originates

from the southern branch (site 2) of the Mangaharakeke Stream (Table 5.2). Diffusive Gradients in Thin Films were not deployed for flow partitioning for the first tracer study.

Table 5.2: Contributing flow rates from sites 1 and 2, calculated using the average flow rate for all anions measured ($Br^-$, $Cl^-$, $NO_3^-$, $SO_4^{2-}$, and $PO_4^{3-}$), and bromide DGT ($Br^-$-DGT)using equations 5 and 6. *$Br^-$-DGT[1] – total flow was DGT derived. $Br^-$-DGT[2] – total flow was weir-based flow.*

| Deployment | Site | Flow Rate Method ($m^3 s^{-1}$) | | |
|---|---|---|---|---|
| | | **$Br^-$-DGT[1]** | **$Br^-$-DGT[2]** | **Anion Average** |
| 2 | 1 | 0.156 | 0.149 | 0.188 |
| | 2 | 0.487 | 0.466 | 0.497 |
| | 5 (sum) | 0.643 | 0.615 | 0.615 |
| B | 1 | | 0.306 | 0.284 |
| | 2 | | 0.466 | 0.488 |
| | 5 (Sum) | | 0.772 | 0.772 |

### *5.3.3 Synthetic Freshwater Test of $Br^-$DGT*

Laboratory validation of the $Br^-$-DGT, before in-field deployments could begin, involved the deployment of DGT in synthetic freshwater, evaluation of the pH and competing ion effects on $C_{DGT}$, determination of the binding characteristics, and the diffusion coefficient of bromide through the material diffusion layer. The results of which are reported in the following sections.

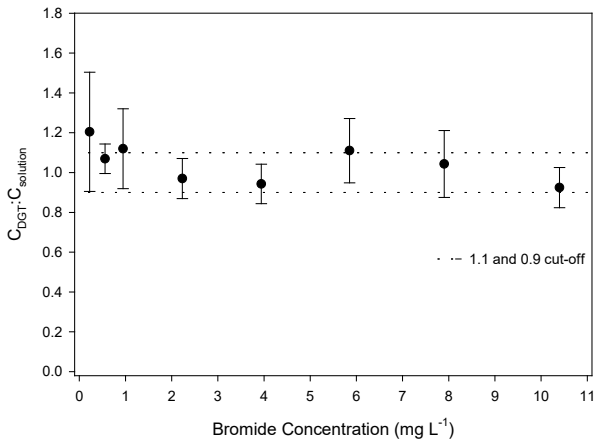


Figure 5.5 Ratio of bromide concentration determined by DGT to grab sampling when deployed in a synthetic natural solution.

The $Br^-$-DGT provided quantitative bromide concentrations in synthetic soft freshwater solution (Figure 5.5). As seen in Figure 5.5, the mean ratio of the bromide concentration determined by DGT to grab sampling sits near 1 concentrations above 0.25 mg $L^{-1}$ bromide. The 0.9 to 1.1 window is widely used in the DGT literature as the metric to establish whether the DGT provide quantitative concentration data for the target analyte (Cai et al., 2017; Huang et al., 2016a; Price et al., 2013).

### 5.3.4 Ionic Strength, pH and Competing Ion Effects

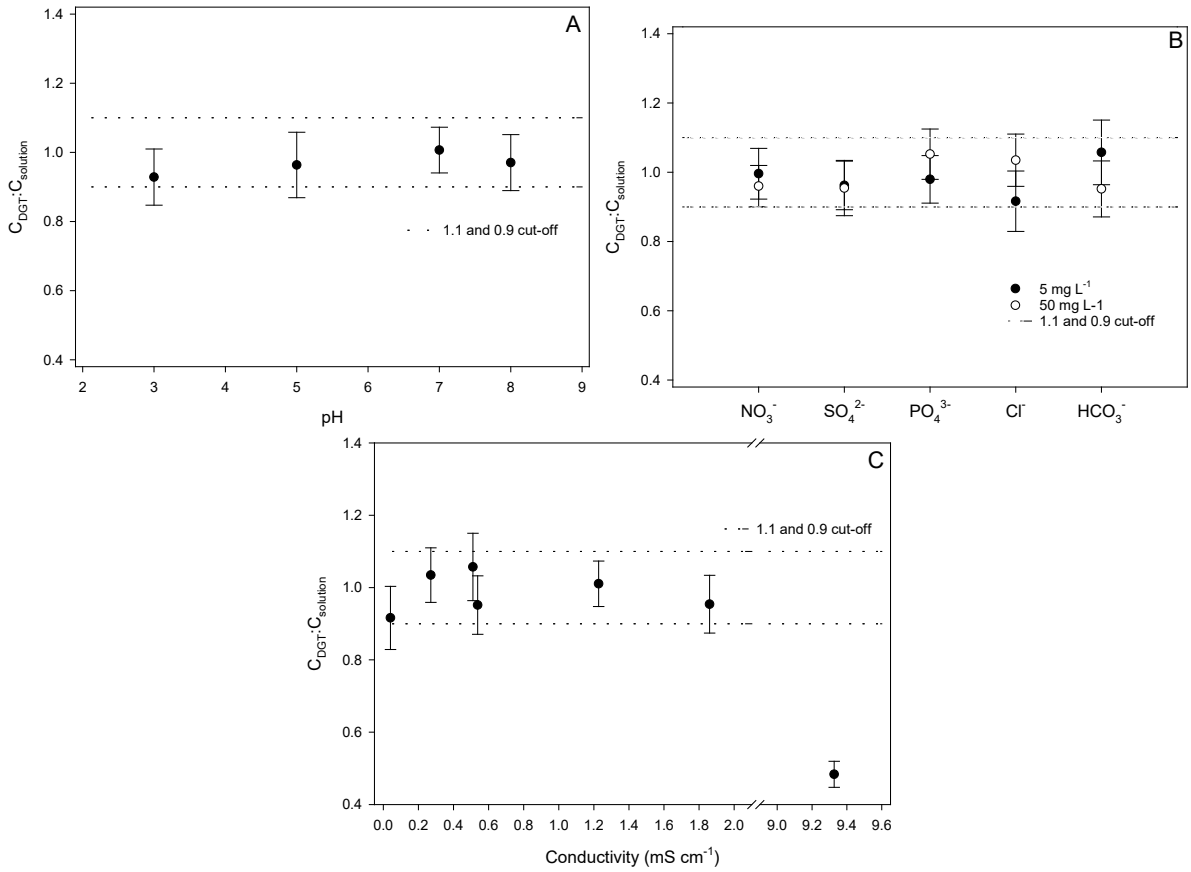


Figure 5.6: Ratio of bromide concentration determined by DGT to grab sampling at (A) various pH, (B) 5 and 50 mg $L^{-1}$ of nitrate, sulfate, phosphate, bicarbonate and chloride, and (C) various conductivities over 48 hour deployments.

The $Br^-$-DGT provided quantitative bromide concentrations at a range of pH, potential competing anion concentrations (nitrate, sulfate, phosphate, chloride, and bicarbonate) ranging from low to high values (5 and 50 mg $L^{-1}$), and conductivities (0.041 to 1.86 mS $cm^{-1}$). As seen in Figure 5.6, the mean ratio of the bromide concentration determined by DGT to grab sampling sits within the 0.9 to 1.1 window for all pH and competing ions analysed, and for conductivities < 1.9 mS $cm^{-1}$.

The binding resin also adsorbed nitrate and sulfate, and phosphate during field experiments (Supplementary Material - Figure 5.10). Unlike sulfate and nitrate, phosphate was not adsorbed during the laboratory testing (Supplementary Material - Figure 5.10). Carbonate was not adsorbed in either the field or laboratory experiments (Supplementary Material - Figure 5.10). The calculated DGT concentrations of nitrate were generally significantly higher than the concentrations determined via

grab sampling (except 50 mg $L^{-1}$ $NO_3^-$), and hence had large DGT to grab sampling ratios ($C_{DGT}$:$C_{solution}$ > 5.7) (Supplementary Material - Figure 5.10). In contrast, the calculated $C_{DGT}$ for sulfate was well below the concentration of the solution with ratios between 0.19 and 0.62, but were > 40 for the first tracer field study (Supplementary Material - Figure 5.10). The phosphate $C_{DGT}$ to $C_{solution}$ ratios were between 0 and 1.2 for field deployed DGT. The background mass of nitrate, and sulfate on the $Br^-$-DGT were 0.0724 ± 0.0050, and 0.0751 ± 0.0279 mg respectively, for all deployments. The background phosphate on the binding resin was immeasurable. There was no carbonate adsorption to the $Br^-$-DGT. Chloride adsorption data was not available because NaCl was used to elute the bound bromide – an alternative elution procedure would be required to analyse chloride adsorption.

### *5.3.5 Binding Gel Properties*

The background bromide mass was measured for each set of Bromide Plus DGT ($Br^-$-DGT) gels made. The background bromide mass of the gels used for determination of the diffusion coefficient, and pH and competing ion effects was 0.0213 mg, with standard deviation of 0.0027 mg, which provided a detection limit of 0.0081 mg (STD x 3).

The uptake efficiency was 95.7 ± 3.4 %, while the elution efficiency was 95.5 ± 4.7 %. The saturation point/adsorption maximum was 0.684 ± 0.001 mg. Bromide adsorption to the binding layer was linear to 0.302 mg $Br^-$, which was 44.1 % of the total binding capacity (Supplementary Material - Figure 5.9).

### *5.3.6 Diffusion Coefficient*

The diffusion coefficient was determined by deploying sets of DGT with different material diffusion layer thicknesses, and removing at set intervals, and was confirmed using a diffusion cell. The diffusion coefficient through the APA hydrogel was 1.05 x $10^{-5}$ $cm^2$ $s^{-1}$ at 17.9 °C, which temperature corrects to 1.29 x $10^{-5}$ $cm^2$ $s^{-1}$ at 25 °C. This was 62.1 % of the value of the diffusion coefficient of bromide through water at 25 °C (2.08 x $10^{-5}$ $cm^2$ $s^{-1}$) (Vanysek, 2003).

## 5.4. Discussion

A method for the determination of flow rates using DGT was established by the development of a bromide selective DGT method, and in combination with the tracer-dilution flow rate methodology. Flow rates determined using the bromide selective DGT were generally within 6.5 % of the weir flow rate. In contrast, flow rates determined via grab sampling ranged from -14.7 to 58.9 % of the weir flow. This initially required the development of bromide specific DGT, which involved the determination of the binding characteristics to the binding layer, the diffusion coefficient through the material diffusion layer, and the effects of pH and competing ion concentrations on $C_{DGT}$ – fully discussed below. Discussion of the efficacy of the developed $Br^-$-DGT follows the discussion of the flow rate determination using the $Br^-$-DGT and constant rate injection method.

### *5.4.1 Bromide Concentration and Flow Rates*

The development of a DGT method for the determination of flow rates is a novel extension of the DGT technique. The injection of bromide at a known concentration and flow rate, combined with a newly developed bromide selective DGT, enabled the calculation of the average flow rate. The flow rates determined via DGT were within 6.5 % of the weir flow rate, this was significantly better than the grab sampling flow rates which overestimated the flow by 5.42 % to 58.9 % (Table 5.1).

It is unsurprising that DGT provided more accurate flow rates, compared to grab sampling. Diffusive Gradients in Thin Films constantly accumulate the target analyte over the deployment period (Davison, 2016). Diffusive Gradients in Thin Films are therefore able to account for temporal changes in concentration, in this study due to changes in flow, and outperformed grab sampling which provide instantaneous spot measurements (Corbett et al., 2019; Davison, 2016). The ability of DGT to integrate the changes in concentration due to fluctuations in flow over the deployment period, meant that the DGT-derived flow rates were more accurate than the (infrequent) grab sampling derived flow rates (Table 5.1).

Although the flow rates were relatively consistent, 0.655 to 0.672 $m^3 s^{-1}$ in deployment 1 and 0.609 to 0.624 $m^3 s^{-1}$ in deployment 2 (Figure 5.4A), grab sampling was not able to accurately account for the changes in flow, unlike DGT. Bromide concentrations measured via DGT and grab sampling were similar for all deployments and sites. The marginal difference in average concentrations determined via DGT compared to grab sampling accounted for the accuracy of the derived flow rates. Theoretically, DGT would outperform grab sampling to a greater extent as the variability in flow rate increased, because grab sampling would capture even less of the change in tracer concentration due to the changes in flow rate.

### *5.4.2 Flow Rate Partitioning*

Establishment of the efficacy of DGT for determining flow rates enabled the extension of the methodology to differentiate the flow contributions of both branches feeding into the Mangaharakeke Stream (sites 1 and 2) (Figure 5.3).

Bromide selective DGT were used to determine the background bromide concentrations along both branches feeding into the Mangaharakeke Stream, sites 1 and 2 (Figure 5.3). The sum of the concentration and flow equalled the concentration and flow in the main stream body (Equation 1), enabling the calculation (Equations 5 and 6) of the contributions of both branches to the total flow (Table 5.2). During the background deployments, grab sampling and DGT were used to calculate the contributions of each branch to the total flow, which was independently measured. For the second tracer study, DGT were also used to the calculate total flow and each branch's contribution, and compared to the weir flow (Table 5.2). Site 2 provided the bulk of the flow compared to site 1 (Table 5.2).

These calculations were based on the assumption that there were no significant inputs between sites 1 and 2, and their intersection. There were likely flow inputs between sites 1 and 2, and the intersection – future bromide DGT deployments for measuring the contribution of feeder streams should be closer to the intersection for this assumption to be more accurate.

This method for partitioning flow could be extended up a catchment from a flow monitoring site, such as the bromide tracer-injection site, to determine the changes in flow along a stream and the inputs from other feeder streams. Bromide was perhaps the most appropriate of the common anions for this because it behaves as a conservative tracer (Parsons et al., 2004), and because it moves about as fast as the carrying waters (Flury & Papritz, 1993).

The implications of using DGT to determine and partition flow rates of streams and their tributaries, are that they could enable the calculation of nutrient loading and loading contribution from tributaries. This could help the targeting of nutrient mitigation strategies, as not only concentration would be known, but load also. This targeted approach to interventions has the potential to have greater downstream consequences, because ecosystem responses can depend on load (Pinckney et al., 2001).

### *5.4.3 Strengths and Weaknesses*

The major strength of DGT is their ability to provide accurate analyte concentrations, with considerably less on-site time and operational expense compared to other monitoring methods, such as high frequency grab sampling and automated multiplexed pumping systems (Corbett et al., 2019). This was further evidenced in this study, where DGT provided more accurate flow rates than grab sampling when coupled with the constant-rate tracer injection method. As discussed above, this was because DGT continuously adsorb the target analyte over the deployment period, providing a time weighted average concentration (Davison, 2016). The DGT were inexpensive, and deployment and removal required a few minutes on-site, rather than the number of hours involved in high frequency grab sampling for example. As previously reported, DGT reduce the number of samples for analysis compared to high frequency grab sampling methods (Corbett et al., 2019).

The bromide-DGT and constant rate injection combined method also presents advantages to other flow rate methods. Formed construction methods (weirs and flumes) can be expensive and operationally difficult, and their construction can alter hydrological regimes and local habitat (Bonacci

et al., 2016). Alternative methods such as remote sensing are also operationally difficult and expensive, and variable in accuracy (Dobriyal et al., 2017). The DGT flow method is operationally simple, inexpensive, and as discussed is capable of providing accurate stream flow rates.

Constant rate tracer injection flow rate methods have been reported to provide more accurate flow measurements than instantaneous injection methods (Moore, 2005). As we have shown, when combined with DGT the constant rate tracer injection method provided more accurate data with less on-site time, than when combined with grab sampling.

Instantaneous injection methods are an alternative approach that provide a snap shot of the flow rate. In contrast, constant rate tracer injection flow rate methodologies provide flow rates over a longer measurement period. Tracer injection generally involves the addition of a high volume/mass of a salt or dye tracer (Moore, 2005), this approach can be of low accuracy and cause environmental damage (Dobriyal et al., 2017). Diffusive Gradients in Thin Films constantly accumulate the target analyte, pre-concentrating the target analyte. As such, DGT reduce the total tracer salt mass required at any one time for accurate determination of concentration. This can be taken advantage of to ensure that the tracer concentration remains well below environmentally toxic levels.

The constraint of any tracer dilution method is the quantity of salt required to raise the concentration of a stream or river to levels that provide accurate derived flows. While DGT may be able to decrease the quantity of salt required, the mass of salt was still relatively large. Local regulations also limit the total volume and mass of tracer that can be added, combined these limit the length of deployment and the size of the stream or river measureable. This likely means that the method as developed here would not be suitable for determining the flow rate of large rivers due to the dilution of the salt tracer.

A further challenge was that the bromide selective DGT adsorbed other anions (nitrate, sulfate, and phosphate) (Supplementary Material - Figure 5.10). The adsorption of competing ions could potentially decrease the possible length of deployment – discussed in the following section. This was not an issue during our study because of the relatively short 12 and 24 h deployments. The

concentrations of these anions measured using the bromide selective DGT were not, however, quantitative during field or laboratory experiments. Other specific DGT are required if nutrient loading was to be calculated using DGT.

For longer deployments other challenges, such as the formation of bio-films on the filter membrane have been reported (Feng et al., 2016; Uher et al., 2012). The biofilms altered the diffusive path-length, and biased the accumulation of some analytes (Uher et al., 2012). Biofouling was not an issue for this study, because the deployment period was not sufficient for films to form.

The $Br^-$-DGT also provides a tool for the environmental monitoring of bromide in systems where bromide pollution may be an issue. The largest natural source of bromide is the ocean, and due to the low natural abundance of bromide in earth materials, the bromide present in terrestrial ecosystems is assumed to be derived from seaborne aerosols (Flury & Papritz, 1993). There are, however, numerous potential anthropogenic sources. Until the mid-1980s bromide was used as a fuel additive, bromide is widely used in flame retardants, methyl bromide is used as a pesticide, and brominated substances have been widely used for water treatment, and in the gas, oil and photography industries (Vainikka & Hupa, 2012). Natural gas extraction via hydraulic fracturing has also been reported to produce brines of high halide concentration (Parker et al., 2014).

### *5.4.4 Validation of the Bromide Plus DGT ($Br^-$-DGT)*

Laboratory validation experiments confirmed that the $Br^-$-DGT are capable of providing quantitative bromide concentrations, and should be able to provide time weighted average flow rate when coupled with a continuous trace injection method.

The performance of the $Br^-$-DGT in synthetic soft freshwater was examined, by deploying DGT in synthetic freshwater spiked with different masses of bromide. The $C_{DGT}$ to $C_{solution}$ ratio of 0.92 to 1.12 between 0.5 and 104 mg $Br^-$ $L^{-1}$ (1.20 at 0.22 mg $Br^-$ $L^{-1}$) suggested the $Br^-$-DGTs were capable of providing quantitative bromide concentrations in freshwaters. Supporting their use in freshwater systems. Importantly the $Br^-$-DGTs were quantitative when deployed in solutions with bromide

concentrations < 1 mg $L^{-1}$, used for the tracer-flow field experiments. Field deployments of the $Br^-$-DGTs, furthermore, accurately determined the background bromide concentration in the Mangaharakeke Stream, when compared to grab sampling.

### *5.4.5 Ionic Strength, pH and Competing Ion Effects*

The effect of pH on the DGT bromide concentration was examined (Figure 5.6A) at a range of pH that could be expected in natural systems. The $C_{DGT}$ to $C_{solution}$ ratio were within 0.9 to 1.1 ratio cut-offs, suggesting the $Br^-$-DGTs operated independently of pH between 3.0 and 8.0.

The effect of ionic strength on the DGT bromide concentration was examined (Figure 5.6C) by deploying $Br^-$-DGT in solutions with a range of conductivities. The $C_{DGT}$ to $C_{solution}$ ratio were between 0.9 to 1.1 for conductivities between 0.041 and 1.9 mS $cm^{-1}$, however, at high conductivities (9.3 mS $cm^{-1}$) the $C_{DGT}$ to $C_{solution}$ ratio was ~0.5. The wide range of conductivities over which the Br--DGT provided quantitative bromide concentrations suggests they are suitable for determining bromide in most freshwaters (< 1.5 mS $cm^{-1}$) (ANZECC, 2000), however they are not suitable for deployment in highly saline environments.

Bromide adsorption to the Bromide Plus resin was driven by ionic exchange and hence determination of the effects of major potential competing anions (5 to 50 mg $L^{-1}$ of either $Cl^-$, $NO_3^-$, $PO_4^{3-}$, $SO_4^{2-}$, and $HCO_3^-$) was important (Figure 5.6B). It is unlikely higher concentrations of the ions would be encountered in freshwaters, excluding geothermal streams where $SO_4^{2-}$ concentrations could be higher due in part to increased dissolution due to higher temperatures (Gude, 2018). NaCl (2 mol $L^{-1}$) was used to elute the binding gels, similarly to the nitrate selective A520E-DGT method (Huang et al., 2016a). As such, deployment of the $Br^-$-DGT is also likely restricted to freshwater (Huang et al., 2016a). The $C_{DGT}$ to $C_{solution}$ ratio was 0.92 to 1.05, well within 0.9 to 1.1 ratio cut-offs. This suggests the $Br^-$-DGTs operated independently of competing ion concentration, further supporting the use of $Br^-$-DGTs for determination of bromide concentration in freshwater systems.

Interestingly, the $Br^-$-DGTs adsorbed nitrate and sulfate in the field deployment, synthetic natural solution and competing ion experiments (Supplementary Material - Figure 5.10). $Br^-$-DGT also adsorbed phosphate in the field experiments (Supplementary Material - Figure 5.10). Adsorption of the competing ions was not quantitative. Adsorption of competing ions to the ion exchange resin is not surprising, since, semi-quantitative sulfate adsorption to the A520E nitrate DGT has previously been reported (Corbett et al., 2019).

Competing ion adsorption has practical implications for the deployment of $Br^-$-DGT. Adsorption of competing ions could reduce the total binding capacity, and therefore the potential length of deployment, for bromide by occupying binding sites on the resin, unless adsorbed ions exchange for bromide preferentially. The quantitative adsorption of bromide suggests this was the case, however further investigation is required. The deployment of $Br^-$-DGT should be restricted to freshwater systems until further efficacy studies in systems with high competing ion concentration can be conducted (e.g. nutrient mitigation, saline, and geothermal systems).

### *5.4.6 Uptake and Elution Efficiencies*

Reproducible uptake and elution efficiencies are crucial to the precision and accuracy of DGT (Zhang & Davison, 1995). The uptake needed to be rapid and strong for the application of Fick's First Law of Diffusion. Rapid and strong uptake ensures the free bromide concentration at the diffusive layer/binding layer interface is zero, maintaining the concentration gradient through the material diffusion layer. The recoverability of the bound mass needs to be high and consistent to ensure the error in the mass used to determine $C_{DGT}$ and subsequently the error in $C_{DGT}$ is low. The uptake (95.7 ± 3.4 %) and elution (95.5 ± 4.7 %) efficiencies met these requirements – supporting the use of $Br^-$-DGTs for the quantitative determination of bromide concentrations.

### *5.4.7 Binding Layer Adsorption*

The saturation point/adsorption maximum was 0.684 ± 0.001 mg. This is comparable to previously reported adsorption maximum of anionic exchange resins for nitrate 1.03 ± 0.01 mg (Corbett et al.,

2019). The reduction in the deviation in the saturation point is either due to the intrinsic binding capacity of the each resin (Purolite Bromide Plus and A520E), or to slight differences in the binding gel preparation (same mass of resin, different sizes). Although both share the same polymer structure (macroporous polystyrene cross-linked with divinylbenzene) and reported capacity, the functional groups differ – Purolite A520E functional group was a quaternary ammonium, the Bromide Plus functional group was undisclosed (Purolite, 2021). The Bromide Plus was ground to at least 90 µm, whereas the A520E was ground to at least 125 µm, 4 g of resin was used in both binding layer preparation methods (Corbett et al., 2019). The extra grinding should have increased the surface area and binding capacity as more sites are readily available, however, it may also have resulted in the loss of functional groups.

Bromide adsorption to the bromide-specific binding layer was linear to 0.301 mg, which was 44.1 % of the adsorption maximum/saturation point. This is similar to the 55 % reported for nitrate-specific A520E DGT (Corbett et al., 2019). As discussed above, the difference was likely due to the difference in functional groups.

Linear accumulation of bromide to the binding layer was necessary to meet the requirements of DGT and provide quantitative bromide concentrations (Davison, 2016). The binding sites on the binding layer were occupied as mass was accumulated, which lead to adsorption of bromide diverging from linearity. It follows that the bromide masses accumulated on binding resin should not exceed 0.301 mg for the bromide-selective DGT to provide quantitative bromide concentrations. Deployment lengths should be sufficiently short that 0.301 mg is not exceeded. The mass of all deployed DGT in this study were well below the 0.301 mg cut-off, because the deployment lengths were short and solution concentrations were low.

The background mass (0.0213 ± 0.0027 mg) was consistent and provided a low limit of detection (0.0081 mg $Br^-$). A low limit of detection is a requirement for the accurate determination of concentration when the adsorbed mass on the binding layer is low. A low bromide mass may be a

result of low solution concentration, short experiment duration, a large DBL due to poor solution mixing/low flow, or a low diffusion coefficient due to low temperatures.

### *5.4.8 Diffusion Coefficient*

The diffusion coefficient of bromide through the APA hydrogels was 62.1 % of the value of the diffusion coefficient of bromide through water at 25 °C. This is considerably lower than the diffusion coefficients of other anions through the APA diffusive gel compared to water – nitrate (97 %), sulfate (91 %) and phosphate (99 %) (Hanousek et al., 2016; Huang et al., 2016a; Zhang et al., 1998). This highlights the necessity for each laboratory using DGT to confirm the diffusive properties of the analytes being measured, as recommended by Davison (2016). Accurate determination of the diffusion coefficient is fundamental to the accuracy of the concentration determined by DGT (Davison, 2016). This is because the diffusion coefficient depends on the swelling characteristics of the hydrogels used - a less swollen hydrogel network results in a more restrictive diffusive pathway and lower diffusion coefficient. The degree of swelling is dependent on the monomers and the relative concentrations used, the polymerisation method used, and the degree of cross-linking (Ahmed, 2015). The time for polymerisation depends on, but is not limited to, the temperature and redox initiator molarity (Ahmed, 2015) – 45 °C , and TEMED (25 µL) and ammonia peroxidisulfate (75 µL of 10 % m/v) in this study. Variations in these factors will result in different hydrogel properties (Ahmed, 2015), which will affect the diffusion coefficient.

### *5.4.9 Conclusions*

A bromide-selective DGT was developed and combined with the trace-dilution flow method. This proved capable of providing quantitative environmental bromide concentrations, and flow rates. The theoretical basis for using DGT to determine flow rates was established. The technique was expanded to provide approximations of the contribution of different parts of a catchment to the downstream flow, expanding the applicability of DGT for environmental flow measurements.

## Funding

The University of Waikato, DairyNZ and the New Zealand Ministry for Primary Industries funded this study.

## Acknowledgements

We would like to acknowledge the financial support of The University of Waikato, DairyNZ and the Ministry for Primary Industries; Purolite for the Bromide Plus anionic exchange resin; and The Waikato Regional Council for the weir-based flow data. Adam Hartland was also supported by a Rutherford Discovery Fellowship award [grant number: RDF-UOW1601]. Special thanks to Jacob Shrubsall and Tiffany Bale for their invaluable help with the fieldwork.

# References


AHMED, E. M. (2015). Hydrogel: Preparation, characterization, and applications: A review. *Journal of Advanced Research, 6*(2), 105-121. doi:https://doi.org/10.1016/j.jare.2013.07.006

ANZECC. (2000). *Australian and New Zealand Guidelines for Fresh and Marine Water Quality*. Canberra: Australian and New Zealand Environment and Conservation Council/Agriculture and Resource Management Council of Australia and New Zealand

BONACCI, O., BUZJAK, N., & ROJE-BONACCI, T. (2016). Changes in hydrological regime caused by human intervention in karst: the case of the Rumin Springs. *Hydrological Sciences Journal, 61*(13), 2387-2398. doi:10.1080/02626667.2015.1111518

CAI, C., WILLIAMS, P. N., LI, H., DAVISON, W., WEI, T.-J., LUO, J., ZHU, Y.-G., & ZHANG, H. (2017). Development and Application of the Diffusive Gradients in Thin Films Technique for the Measurement of Nitrate in Soils. *Analytical Chemistry, 89*(2), 1178-1184. doi:10.1021/acs.analchem.6b03609

CANTON, J. H., WESTER, P. W., & MATHIJSSEN-SPIEKMAN, E. A. M. (1983). Study on the toxicity of sodium bromide to different freshwater organisms. *Food and Chemical Toxicology, 21*(4), 369-378. doi:https://doi.org/10.1016/0278-6915(83)90090-X

COLE, J. J., & PRAIRIE, Y. T. (2014). Dissolved $CO_2$ in Freshwater Systems. In *Reference Module in Earth Systems and Environmental Sciences*: Elsevier.

CORBETT, T. D. W., DOUGHERTY, H., MAXWELL, B., HARTLAND, A., HENDERSON, W., RYS, G. J., & SCHIPPER, L. A. (2019). Utility of 'Diffusive Gradients in Thin-Films' for the measurement of nitrate removal performance of denitrifying bioreactors. *Science of The Total Environment*, 135267. doi:https://doi.org/10.1016/j.scitotenv.2019.135267

COUNCIL, W. R. (2021). Waikato Regional Council - River Flow at Dreadnought. Retrieved from http://riverlevelsmap.waikatoregion.govt.nz/cgi-bin/hydwebserver.cgi/points/details?point=815&catchment=17

DAVISON, W. (2016). *Diffusive Gradients in Thin-Films for Environmental Measurements*. Cambridge, UNITED KINGDOM: Cambridge University Press.

DINGHAM, S. L. (1993). *Physical Hydrology*. New York: Macmillan College Publishing.

DOBRIYAL, P., BADOLA, R., TUBOI, C., & HUSSAIN, S. A. (2017). A review of methods for monitoring streamflow for sustainable water resource management. *Applied Water Science, 7*(6), 2617-2628. doi:10.1007/s13201-016-0488-y

FENG, Z., ZHU, P., FAN, H., PIAO, S., XU, L., & SUN, T. (2016). Effect of Biofilm on Passive Sampling of Dissolved Orthophosphate Using the Diffusive Gradients in Thin Films Technique. *Analytical Chemistry, 88*(13), 6836-6843. doi:10.1021/acs.analchem.6b01392

FLURY, M., & PAPRITZ, A. (1993). Bromide in the Natural Environment: Occurrence and Toxicity. *Journal of Environmental Quality, 22*(4), 747-758. doi:10.2134/jeq1993.00472425002200040017x

GUDE, V. G. (2018). Chapter 4 - Geothermal Source for Water Desalination—Challenges and Opportunities. In V. G. Gude (Ed.), *Renewable Energy Powered Desalination Handbook* (pp. 141-176): Butterworth-Heinemann.

HANOUSEK, O., MASON, S., SANTNER, J., CHOWDHURY, M. M. A., BERGER, T. W., & PROHASKA, T. (2016). Novel diffusive gradients in thin films technique to assess labile sulfate in soil. *Analytical and bioanalytical chemistry, 408*(24), 6759-6767. doi:10.1007/s00216-016-9801-8

HUANG, J., BENNETT, W., TEASDALE, P. R., GARDINER, S., & WELSH, D. (2016a). Development and evaluation of the diffusive gradients in thin films technique for measuring nitrate in freshwaters. *Analytica Chimica Acta, 923*, 74-81. doi:10.1016/j.aca.2016.04.006

HUANG, J., BENNETT, W. W., WELSH, D. T., & TEASDALE, P. R. (2016b). Determining time-weighted average concentrations of nitrate and ammonium in freshwaters using DGT with ion exchange membrane-based binding layers. *Environmental Science: Processes & Impacts, 18*(12), 1530-1539. doi:10.1039/c6em00260a

KARR, J. R. (1991). Biological Integrity: A Long-Neglected Aspect of Water Resource Management. *1*(1), 66-84. doi:10.2307/1941848

KIANPOOR KALKHAJEH, Y., JABBARIAN AMIRI, B., HUANG, B., HENAREH KHALYANI, A., HU, W., GAO, H., & THOMSON, M. L. (2019). Methods for Sample Collection, Storage, and Analysis of Freshwater Phosphorus. *Water, 11*(9), 1889.

KILPATRICK, F. A., & COBB, E. D. (1985). Measurement of Discharge Using Tracers. In *Techniques of Water-Resources Investigations* (Vol. 3, pp. 1-91). Washington, DC: U.S. Geological Survey.

KING, R. C., MULLIGAN, P. K., & STANSFIELD, W. D. (2013). Diffusion. In *A Dictionary of Genetics* (8 ed., pp. 122). Oxford: Oxford University Press.

LEE, S.-K., CHUNG, S.-C., & PARK, S.-K. (2007). Chemical Tracer Method for Measurement of Flow Rates in Closed Conduits. *Journal of Nuclear Science and Technology, 44*(11), 1467-1473. doi:10.1080/18811248.2007.9711394

MAXWELL, B. M., BIRGAND, F., SMITH, B., & AVENI-DEFORGE, K. (2018). A small-volume multiplexed pumping system for automated, high-frequency water chemistry measurements in volume-limited applications. *Hydrology and Earth System Sciences, 22*(11), 5615-5628. doi:10.5194/hess-22-5615-2018

MOORE, R. D. (2005). Slug Injection Using Salt in Solution. *Streamline Watershed Management Bulletin, 8*(2), 1-6.

ORGANISATION, W. H. (2017). *Guidelines for Drinking-Water Quality* (4 ed.). Geneva, Switzerland: World Health Organization.

PANTHER, J. G., STEWART, R. R., TEASDALE, P. R., BENNETT, W. W., WELSH, D. T., & ZHAO, H. (2013). Titanium dioxide-based DGT for measuring dissolved As(V), V(V), Sb(V), Mo(VI) and W(VI) in water. *Talanta, 105*, 80-86. doi:https://doi.org/10.1016/j.talanta.2012.11.070

PARKER, K. M., ZENG, T., HARKNESS, J., VENGOSH, A., & MITCH, W. A. (2014). Enhanced Formation of Disinfection Byproducts in Shale Gas Wastewater-Impacted Drinking Water Supplies. *Environmental Science & Technology, 48*(19), 11161-11169. doi:10.1021/es5028184

PARSONS, D. F., HAYASHI, M., & VAN DER KAMP, G. (2004). Infiltration and solute transport under a seasonal wetland: bromide tracer experiments in Saskatoon, Canada. *Hydrological Processes, 18*(11), 2011-2027. doi:10.1002/hyp.1345

PINCKNEY, J. L., PAERL, H. W., TESTER, P., & RICHARDSON, T. L. (2001). The role of nutrient loading and eutrophication in estuarine ecology. *Environmental health perspectives, 109 Suppl 5*(Suppl 5), 699-706. doi:10.1289/ehp.01109s5699

PRICE, H. L., TEASDALE, P. R., & JOLLEY, D. F. (2013). An evaluation of ferrihydrite- and Metsorb™-DGT techniques for measuring oxyanion species (As, Se, V, P): Effective capacity, competition and diffusion coefficients. *Analytica Chimica Acta, 803*, 56-65. doi:https://doi.org/10.1016/j.aca.2013.07.001

PUROLITE. (2021). Strong Base Anion Ion Exchange Resins. Retrieved from https://www.purolite.com/product-type/ion-exchange-resin-strong-base-anion

REDDY, P. (2020). *Resource Management (National Environmental Standards for Freshwater) Regulations 2020*. Wellington: Parliamentary Counsel Office.

SMITH, E. J., DAVISON, W., & HAMILTON-TAYLOR, J. (2002). Methods for preparing synthetic freshwaters. *Water Research, 36*(5), 1286-1296. doi:https://doi.org/10.1016/S0043-1354(01)00341-4

UHER, E., ZHANG, H., SANTOS, S., TUSSEAU-VUILLEMIN, M.-H., & GOURLAY-FRANCÉ, C. (2012). Impact of Biofouling on Diffusive Gradient in Thin Film Measurements in Water. *Analytical Chemistry, 84*(7), 3111-3118. doi:10.1021/ac2028535

VAINIKKA, P., & HUPA, M. (2012). Review on bromine in solid fuels – Part 2: Anthropogenic occurrence. *Fuel, 94*, 34-51. doi:https://doi.org/10.1016/j.fuel.2011.11.021

VANYSEK, P. (2003). Ionic Conductivity and Diffusion at Infinite Dilution. In D. R. Lide (Ed.), *CRC Handbook of Chemistry and Physics* (84 ed., pp. 95-97). London: CRC Press.

VOGEL, R. M., LALL, U., CAI, X., RAJAGOPALAN, B., WEISKEL, P. K., HOOPER, R. P., & MATALAS, N. C. (2015). Hydrology: The interdisciplinary science of water. *51*(6), 4409-4430. doi:10.1002/2015wr017049

ZHANG, H., & DAVISON, W. (1995). Performance Characteristics of Diffusion Gradients in Thin Films for the in Situ Measurement of Trace Metals in Aqueous Solution. *Analytical Chemistry, 67*(19), 3391-3400. doi:10.1021/ac00115a005

ZHANG, H., DAVISON, W., GADI, R., & KOBAYASHI, T. (1998). In situ measurement of dissolved phosphorus in natural waters using DGT. *Analytica Chimica Acta, 370*(1), 29-38. doi:https://doi.org/10.1016/S0003-2670(98)00250-5

## Supplementary Material

Determination of complete mixing distance was calculated using the following equation (Dingham, 1993; F.A. Kilpatrick, 1985):

$$L_{mix} = k_{mix} \frac{CX^2}{g^{1/2}Y} \qquad L_{mix} = 0.140 \times \frac{0.05 \times 10^2}{9.8^{1/2} \times 0.5} = 3.6 \text{ m}$$

Where $L_{mix}$ = the length to complete mixing (m), $k_{mix}$ = the mixing coefficient, C = Chézy's constant, X = the average reach width (m); g = gravitational acceleration ($m^2s^{-1}$), and Y = average reach depth (m) (Dingham, 1993; F.A. Kilpatrick, 1985).

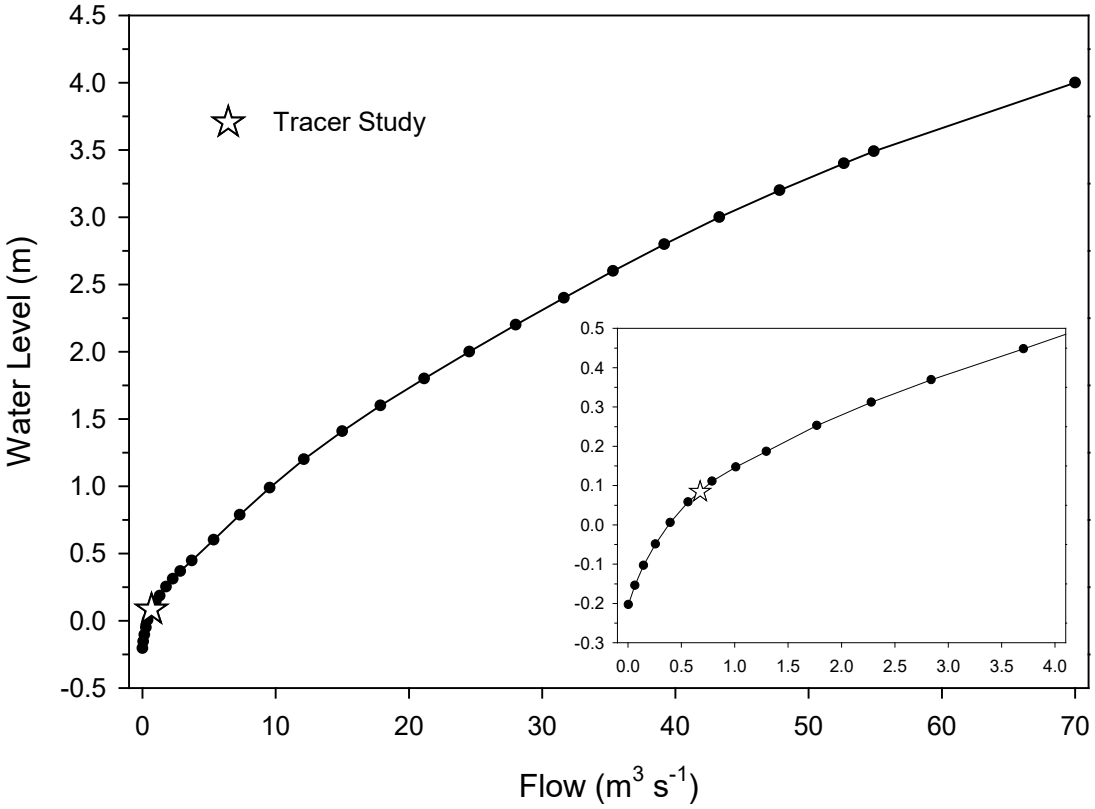


Figure 5.7: Rating Curve for Independent Monitoring Station (Waikato Regional Council, 2021), with low flow section enlargement provided. Star indicates the region where the tracer study fell.

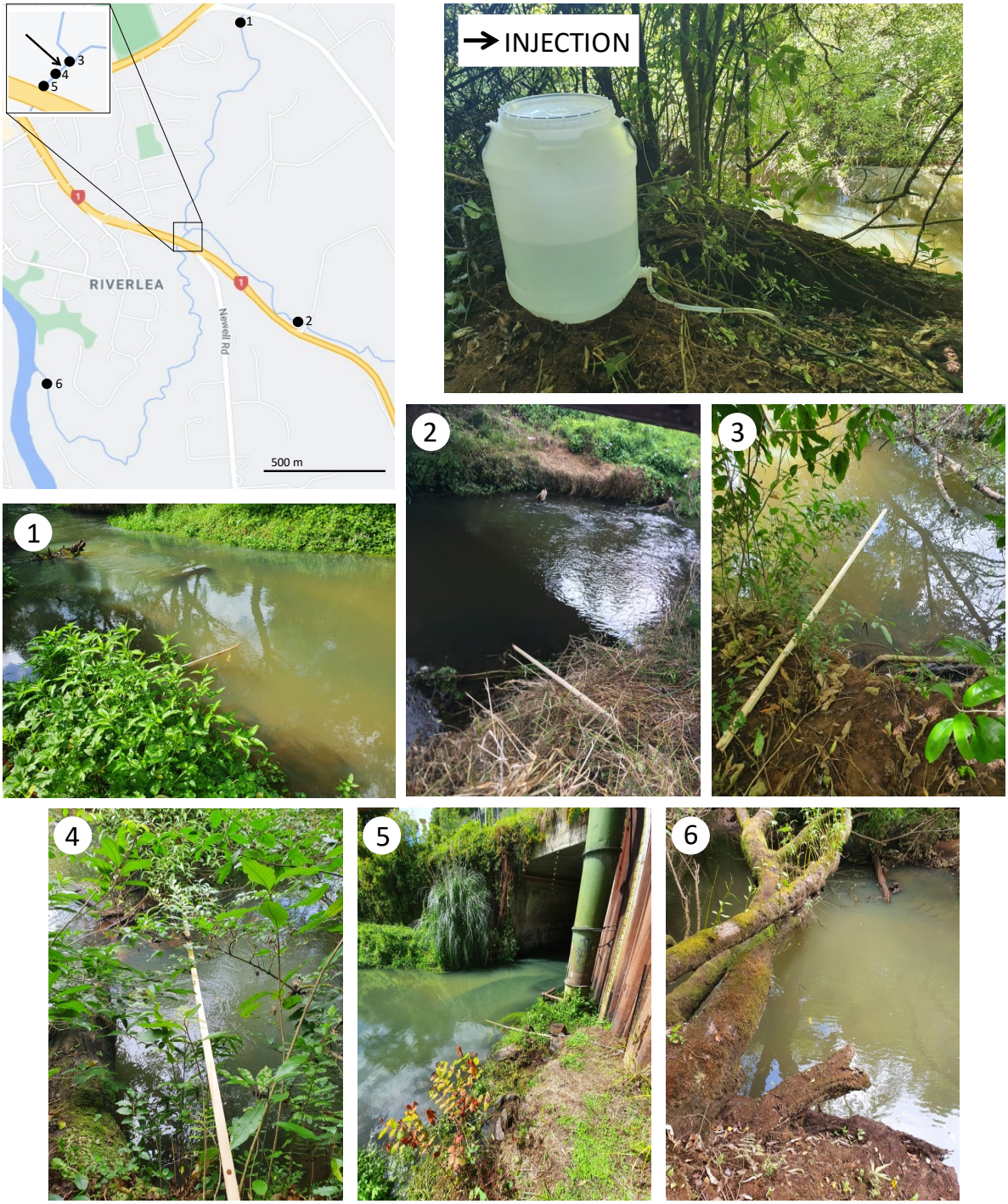


Figure 5.8: Images of the all deployment locations and tracer injection.

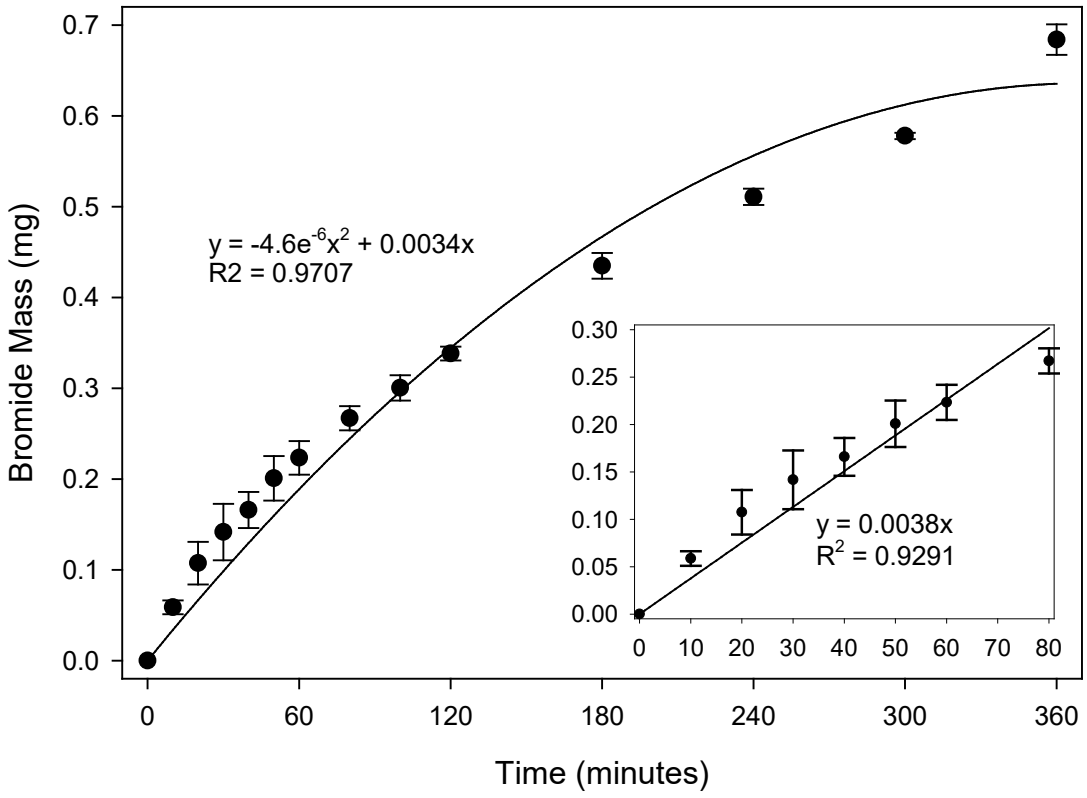


Figure 5.9: Adsorption Isotherm of bromide to the bromide-specific binding layer.

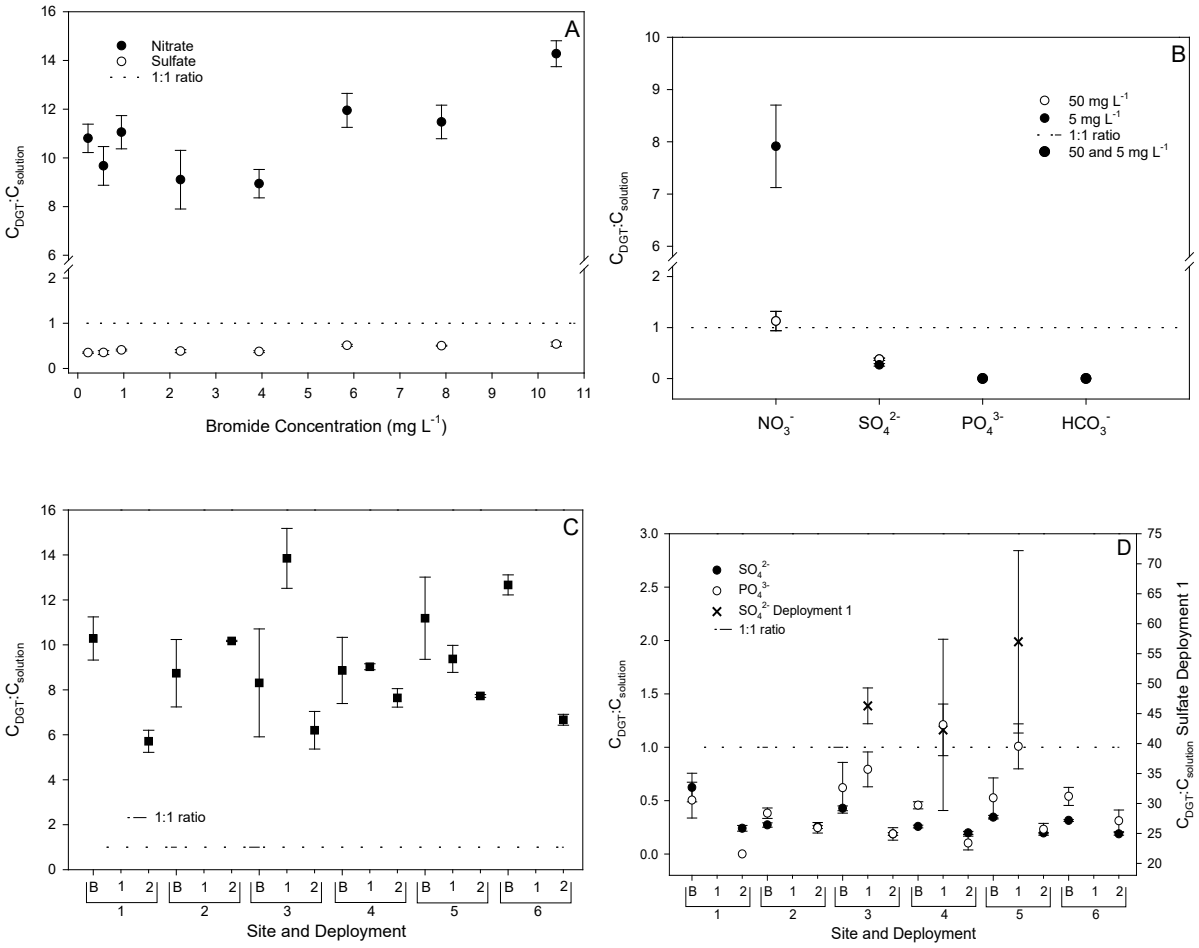


Figure 5.10: Ratio of DGT determined concentration of adsorbed competing ions to grab sample concentrations for the (A) synthetic natural solution, (B) competing ion experiments, (C) nitrate concentrations for the field deployments (48 hours), and (D) sulfate and phosphate concentrations for the field deployments (12 hours).

# Chapter 6 - The Temperature and Flow Dependence of Nitrate Concentration and Load Estimates based on Diffusive Gradients in Thin-Films.

*Under Review at Journal of Environmental Quality:*

CORBETT, T. D. W., HARTLAND, A., HENDERSON, W., RYS, G. J. & SCHIPPER, L. A. 2021. The Temperature and Flow Dependence of Nitrate Concentration and Load Estimates based on Diffusive Gradients in Thin-Films. Journal of Environmental Quality.

## Core Ideas

- DGT nitrate loadings were compared to the loads calculated using high/low frequency sampling.
- Bias in DGT loads approached 30 % as flow/concentration correlation approached -1 / 1.
- Increased correlation between temperature and concentration increased DGT concentration bias.

## Abstract

Concentrations determined using Diffusive Gradients in Thin-Films (DGT) have been used to derive time-averaged loads in streams and rivers. Diffusive Gradients in Thin Films, however, provide time-weighted average concentrations that assume the independence of concentration and flow. Additionally, dynamic and coordinated changes in temperature, flow, and concentration, are potential sources of bias in concentration and load calculations. We modelled scenarios in which temperature and flow were correlated to varying degrees with nitrate concentration, and evaluated the consequences for DGT nitrate concentration and load calculations. As the correlation between solution flow and concentration moved towards 1 and -1, the nitrate load determined by DGT either over or underestimated the actual load by as much as 30 %. In DGT-based load estimates, the degree of potential bias should be assessed, and the concentration-flow relation characterised. As the correlation of analyte concentration and temperature approached 1 and -1, the deviation of the concentration determined by DGT ($C_{DGT}$) from the actual concentration increased. In most cases, this

bias was less than 2 %, however, if the changes in concentration and temperature were large (~10 mg $L^{-1}$ and ~10 °C) the bias exceeded 5 %. Concentration and temperature are unlikely to be perfectly or strongly correlated or anti-correlated in natural systems and thus should not affect the accuracy of DGT concentration calculations in most circumstances. The more uncorrelated solution temperature, flow and concentration, the closer DGT derived nitrate concentration and load were to the actual solution concentration and load.

## 6.1. Introduction

Diffusive Gradients in Thin-Films (DGT) were developed for the passive *in situ* determination of analyte concentrations in solution and soil (Panther et al., 2010; Zhang & Davison, 1995; Zhang et al., 1998). Diffusive Gradients in Thin Films have been developed for a wide range of analytes (inorganic and organic) based on hydrogel-supported resins and commercially available membranes (Huang et al., 2016c; Panther et al., 2013; Zhang & Davison, 1995; Zhang et al., 1998). More recently, development of alternative binding layers, such as liquid binding layers, has further extended the DGT technique (Li et al., 2003; Liu et al., 2016).

The development of DGT was founded on application of Fick's First Law of Diffusion (Zhang & Davison, 1995), which describes the tendency of molecules to move from high to low concentration areas due to their random heat motion (King et al., 2013). Increases in temperature increase the molecules' random heat motion, and therefore the rate of diffusion. Conversely, decreases in temperature decrease the rate of diffusion. Diffusive Gradients in Thin Films passively accumulate the target analyte on the specific binding layer, the transport to which is restricted to diffusion by the material diffusion layer (MDL) (Davison, 2016). The rapid and strong adsorption of the target analyte maintains the concentration gradient through the material diffusion layer (MDL) (Davison, 2016). The elution and measurement of the accumulated mass enables the calculation of the time-weighted average concentration (Davison, 2016).

DGT are theoretically capable of accounting for changes in temperature, and are flow independent if the diffusive boundary layer is included in the DGT equation (Eq. 1) (Davison, 2016). Accurate measurement of temperature is necessary for the accurate determination of the analyte diffusion coefficient (Eq. 2) (Davison, 2016), a key component of the $C_{DGT}$ equation. There is an underlying assumption that there is no correlation between temperature and concentration in the water body. To our knowledge, however, there has been no investigation of how the DGT-determined concentration changes as solution concentration and temperature co-vary.

DGT have also been used to calculate analyte loading although this is not common practice (Corbett et al., 2019; Søndergaard et al., 2014). The use of passive samplers, including macro-organisms, for determining loading is more widely tested to varying degrees of success (Audet et al., 2014; Müller et al., 2008; Søndergaard et al., 2014), however, to our knowledge this is the first time the term DGT load has been used. Given the growth in the use of DGT it is pertinent to raise potential issues with using DGT to determine loads, to avoid potential misuse. The importance of correlation between solution flow and concentration and the extent to which it affects loads determined by DGT has also not been investigated. Loading, calculated as the product of concentration and flow rate, is important because ecosystem responses depend on the total export and import of nutrients, not concentration alone (Pinckney et al., 2001).

We hypothesised that the degree of correlation and the degree of variability in concentration, temperature, and flow would potentially bias the DGT concentration and subsequent load calculations. For example, we evaluated the effect on $C_{DGT,}$ if solution temperature and concentration both linearly increase by ~ 10 °C and 10 mg $L^{-1}$ over 24 hours. While this is extreme, we wanted to provide an insight as to what the bias could be, to identify sensible operational environments. This study focused on a theoretical investigation into these effects. We also sought to highlight the challenges of using DGT for determining nutrient loading, when combined with methods for measuring flow rate.

## 6.2. Methods

Two different modelling scenarios were investigated. Firstly, we examined the effect of rapid and large concentration and temperature changes, with varying degrees of correlation, on $C_{DGT}$. Secondly, we explored the effect of concentration and flow fluctuation, with varying degrees of correlation, on DGT derived loads compared to high and low frequency grab sampling. Correlation was defined as the Pearson Product-Moment Correlation. Modelling was performed in Excel 2016 (Microsoft, Washington, USA).

While nitrate analysis via DGT is a relatively new addition to the DGT analytical portfolio, there is a growing body of evidence to the efficacy of using DGT to determine nitrate concentrations in freshwater and soils (Cai et al., 2017; Corbett et al., 2019; Huang et al., 2016a; Huang et al., 2016b; Huang et al., 2016c; Ren et al., 2020). Our access to high frequency nitrate concentration and flow data, with coupled successful DGT deployments, enabled the confirmation of the modelled load data with real DGT data.

### *6.2.1 Temperature and Concentration*

For DGT to provide quantitative environmental concentrations and loads, DGT must be responsive to both rapid changes in concentration and temperature. Temperature controls the diffusion coefficients, a fundamental component of the DGT equation (Eq. 1).

$$\boldsymbol{C_{DGT} = \frac{M.\Delta g}{D.A.t}} \quad (1)$$

Where, $C_{DGT}$ = DGT concentration (mg $cm^{-3}$); M = analyte mass on binding layer (mg); A = area of diffusion ($cm^2$); t = length of deployment (s); D = diffusion coefficient through the material diffusion layer ($cm^2$ $s^{-1}$); and, Δg = the thickness of the material diffusion layer (Davison, 2016; Zhang & Davison, 1995).

Diffusion coefficients for numerous trace metals, anions, oxyanions, and organic molecules have been determined and reported for the standard material diffusion layer (MDL) (Davison, 2016; Hanousek et

al., 2016; Huang et al., 2016a; Zhang & Davison, 1995; Zhang et al., 1998). The MDL consists of an agarose cross-linked polyacrylamide hydrogel of various thicknesses and a polyether sulfone filter membrane (Davison, 2016). The MDL diffusion coefficients for specific analytes are generally reported for the temperatures at which they were determined and temperature corrected to 25 °C (Davison, 2016). The diffusion coefficient of nitrate used in this study was 1.46 x $10^{-5}$ $cm^2$ $s^{-1}$ at 25 °C (Huang et al., 2016a). For DGT deployments, as in this study, the diffusion coefficients must be temperature corrected to the average temperature for the DGT deployment using the following equation, where, T = temperature; $D_T$ = diffusion coefficient at temperature T; $D_{25}$ = diffusion coefficient at 25 °C (Davison, 2016).

$$\boldsymbol{logD_T = \frac{1.37023(T-25)+0.000836(T-25)^2}{109+T} + log\frac{D_{25}(273+T)}{298}} \quad (2)$$

Here, we modelled the responsiveness of DGT and the inherent bias due to rapid and slow concentration and temperature changes of solution over 48 hours using theoretical systems where there were both large and small concentration and temperature changes. Field deployment periods of 18 to 48 hours have been reported for A520E nitrate specific DGT (Corbett et al., 2019; Huang et al., 2016a), 48 hour deployment period were chosen for this study because it is the upper limit of successfully reported field deployments.

Solution parameters were generated for each run in hourly increments, to enable the calculation of the time-weighted average solution concentration and temperature. The average solution concentration and temperature for each time period was used to calculate the mass flux to the DGT binding layer (Eq. 2), by rearranging Eq. 1. The diffusion coefficient was calculated using the average temperature for each hour.

$$\boldsymbol{M = \frac{\frac{(C_{t_n}+C_{t_{n+1}})}{2}.D_{\left(\frac{(T_n+T_{n+1})}{2}\right)}.A.t}{\Delta g}} \quad (3)$$

Where, M = mass for the hour time period (mg); $C_{tn}$ and $C_{tn+1}$ = solution concentration at the beginning and end of the hour respectively (mg $cm^{-3}$); $D_{(Tn.../2)}$ = diffusion coefficient ($cm^2$ $s^{-1}$), for the average temperature over the hour, temperature corrected using Eq. 2; $(T_n+T_{n+1})/2$ = average temperature of the hour which was inserted into Eq. 2, $T_n$ and $T_{n+1}$ are the temperatures at the beginning and end of the hour respectively (°C); A = area of diffusion (3.1416 $cm^2$); t = length of time (3600 s); and, Δg = thickness of the material diffusion layer (0.095 cm). The standard material diffusion layer (MDL) thickness was utilised (Davison, 2016). Calculations to determine the effect of changes in MDL thickness were not performed, because, as discussed later, it was presumed steady state was reached immediately, which negates the effects of the rate of response to solution concentration changes based on MDL thickness.

The DGT concentration was calculated using Eq. 1, however the mass (M) component equal to the sum of the masses for each time period calculated using Eq. 3. The percentage difference (%difference) of the DGT concentration ($C_{DGT}$) form the solution concentration ($C_{solution}$) was calculated using Eq. 4. $C_{solution}$ was the time-weighted average concentration of the solution.

$$\%\ \boldsymbol{difference} = \frac{\boldsymbol{C_{DGT} - C_{solution}}}{\boldsymbol{C_{solution}}} . \mathbf{100} \quad (4)$$

The correlation of solution temperature and concentration were varied between 1, 0 and -1. The concentrations in scenario one used were 1 to 10.6, 5.8, 0.58, and 0.1 to 1.06 mg $NO_3^-$-N $L^{-1}$. The associated temperatures were 10 to 22, 16, 10 to 12.4, and 11.2 °C. These regimes were combined such that concentration and/or temperature increased and decreased linearly, or were held constant over the modelled deployment period (Figure 6.1A). In the second scenario, either one or both of concentration and temperature cycled through the same regimes (Figure 6.1B). Changes in concentration and temperature within each run increased or decreased linearly, i.e. the change between each hour period was the same, to simplify the calculation of the time-weighted average solution concentrations and temperatures.

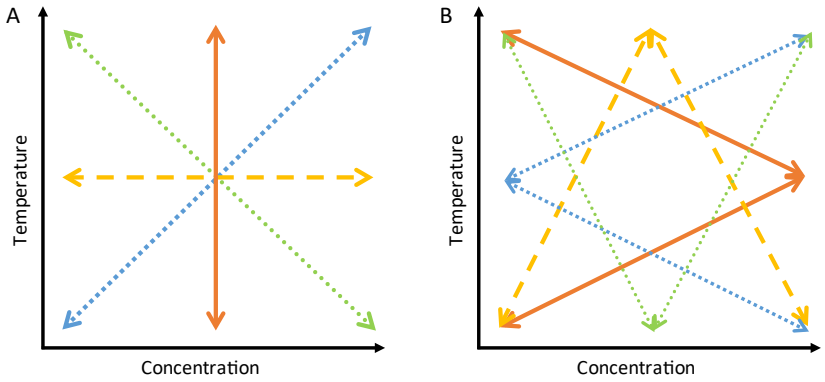


Figure 6.1: Diagrams of (A) scenario one and (B) scenario two models. Not all variants within each scenario are included. The arrows denote the change in temperature and concentration through time.

### *6.2.2 Flow, Concentration and Load*

The accuracy of load calculations are dependent on the accuracy of both flow and concentration measurements (Pinckney et al., 2001). Here, the efficacy of using DGT for determining the load was modelled using nitrate concentration and flow data measured over 1 month from a denitrifying bioreactor (Corbett et al., 2019; Maxwell et al., 2018). The bioreactor data was used because it provided a data set with pronounced variations in concentration and flow, and the high frequency of sampling enabled an accurate calculation of the load. Nitrate concentrations were determined by grab sampling at 30 and 60-minute intervals, while flow measurements were independently measured at the same interval (Corbett et al., 2019; Maxwell et al., 2018). Denitrifying bioreactors are anaerobic carbon rich systems, designed to support the microbial transformation of excess nitrate to $N_2$ (g) (Addy et al., 2016; Rivett et al., 2008; Schipper et al., 2010). Diffusive Gradients in Thin Films have been successfully been deployed in bioreactors, providing quantitative nitrate concentrations when compared to high frequency grab samples (Corbett et al., 2019).

The model created was compared to the real data from DGT deployments in the bioreactor (Corbett et al., 2019), to confirm the differences of the DGT determined load to the 'actual' load. High frequency nitrate concentration measurements in the bioreactor were made using an automated multiplexed pumping system and UV-vis field spectrophotometer coupled system (MPS-UV Vis)

(Maxwell et al., 2018). The in-field measurements made via UV-vis were calibrated via regular grab samples (Maxwell et al., 2018). Comprehensive testing of the efficacy of the system ensured the degree of uncertainty, due to matrix effects for example, was minimal (Maxwell et al., 2018). The accuracy and frequency of the measurements provided a nitrate concentration data set that should closely describe the real nature of the system, and was thus used to represent the 'actual' solution values. The diffusive boundary layer was accounted for by deploying three DGT with different material diffusive layer thicknesses, in the inlet and outlet chambers, and the three centre wells (Corbett et al., 2019).

The modelled load data were generated by rearranging the flow and concentration regimes as measured in the bioreactor. The average concentration and flow, remained constant, but the flow and concentration values were redistributed to provide flow and concentration regimes of varying correlation (1 to -1). The 'actual' load was determined by summing the load (flow x concentration x time) for each time interval. The DGT determined load was calculated in a similar fashion, except the concentration used at each time interval was the average concentration ($C_{DGT}$), the load for each time interval was summed and compared against the 'actual' load. The percentage difference (%difference) was determined using the following equation. .

$$\%\,\boldsymbol{difference} = \frac{\boldsymbol{Load_{DGT} - Load_{actual}}}{\boldsymbol{Load_{actual}}}.\mathbf{100} \quad (5)$$

In standard regulatory measurement regimes, grab samples are taken monthly or fortnightly (Kronvang & Bruhn, 1996; Moatar & Meybeck, 2005; Tulagi, 2019). To represent this, each concentration data point was taken individually to represent the concentration for the month period, and as for the DGT calculated load the low frequency grab sampling concentration was used to determine the load for each time interval. Total nitrate-N was determined by multiplying load by time.

For the purposes of modelling, it was assumed that when solution concentration changed, the steady state between the DGT and bulk solution was reached immediately. This is unlikely to be true, particularly as the MDL thickness increases, because of the time it takes for analyte to diffuse through

the MDL. This effect becomes negligible, however, where the change in concentration occurs gradually over hour timescales (Davison, 2016). The time to reach steady state, and the associated percentage error have been investigated (Eq. 6) (Davison & Zhang, 2012).

$$\boldsymbol{Percentage\ error} = \frac{\boldsymbol{g^2}}{\boldsymbol{6D}} . \frac{\boldsymbol{100}}{\boldsymbol{T}} \tag{6}$$

Where, g = MDL thickness (cm), D = temperature corrected diffusion coefficient ($cm^2\ s^{-1}$) and T = deployment time (s). The transient period, the period before steady state is met (Lehto et al., 2006), is generally associated with the deployment of the DGT and not concentration changes during the deployment. It is recommended that DGT deployments are sufficiently long that the associated error has little or no meaningful effect on the calculated DGT concentration (Davison, 2016). This approach implicitly assumes that changes are gradual such that the steady state is reached quickly and does not affect $C_{DGT}$. This is not an unreasonable assumption, because as previously shown, DGT are able to account for rapid changes in nitrate concentration, providing concentration data that closely matches very high frequency grab sampling concentrations (Corbett et al., 2019). The decision to exclude the time to steady state, in this exercise, was made to simplify the model, excluding other factors that may make the effects of solution temperature and concentration indistinguishable. To empirically justify disregarding the transient periods the percentage error in the average concentrations was calculated. The errors were applied to the average DGT concentrations as detailed in Eq. 7, and the load calculations were re-run with higher and lower concentration for each flow regime. The percentage error in the load bias (% ELB) due to the transient period was then calculated using Eq. 8. Where $C_{DGT\ error}$ = the upper and lower DGT concentrations after the percentage error is applied; and $Load_{DGT\ error}$ = the load calculated using $C_{DGT\ error}$.

$$\boldsymbol{C_{DGT\ error}} = \boldsymbol{C_{DGT}} \pm \frac{\boldsymbol{Percentage\ Error}}{\boldsymbol{100}} . \boldsymbol{C_{DGT}} \tag{7}$$

$$\%\ \boldsymbol{ELB} = \frac{\boldsymbol{Load_{DGT\ error}} - \boldsymbol{Load_{DGT}}}{\boldsymbol{Load_{DGT}}} . \boldsymbol{100} \tag{8}$$

## 6.3. Results

### *6.3.1 Temperature and Concentration*

Temperature modelling showed that large rapid increases and decreases in concentration and temperature, whether correlated or anti-correlated (1 and -1 correlation), produced the largest difference (3 to 7.3 %) between the DGT determined concentration and solution concentration determined by high frequency grab sampling (Table 6.1). All other permutations, outlined in the methods section, produced very small differences between 2 and -2 %.

Table 6.1**:** Summary of the differences of concentrations determined by Diffusive Gradients in Thin-Films (DGT) to the actual concentration determined by high frequency grab sampling, when temperature and concentration completely correlate ($R^2$ = 1) and anti-correlate ($R^2$ = -1). *Note: all values are not reported, only those with differences ≥ 2 and -2 %.*

| **Temperature** (°C) | **Concentration** (mg $L^{-1}$) | **Correlation** ($R^2$) | $\frac{C_{DGT} - C_{solution}}{C_{solution}} \times 100$ (%) |
|---|---|---|---|
| Increasing (10 to 22) | Increasing (1 to 10.6) | 1 | 5.3 |
| Increasing (10 to 22) | Decreasing (10.6 to 1) | -1 | -4.7 |
| Decreasing (22 to 10) | Increasing (1 to 10.6) | -1 | -4.7 |
| Decreasing (22 to 10) | Decreasing (10.6 to 1) | 1 | 5.3 |
| Cycling (10 to 22) | Cycling (1 to 10.6) | 1 | 7.3 |
| Cycling (22 to 10) | Cycling (1 to 10.6) | -1 | -3 |

### 6.3.2 Flow, Concentration, and Load

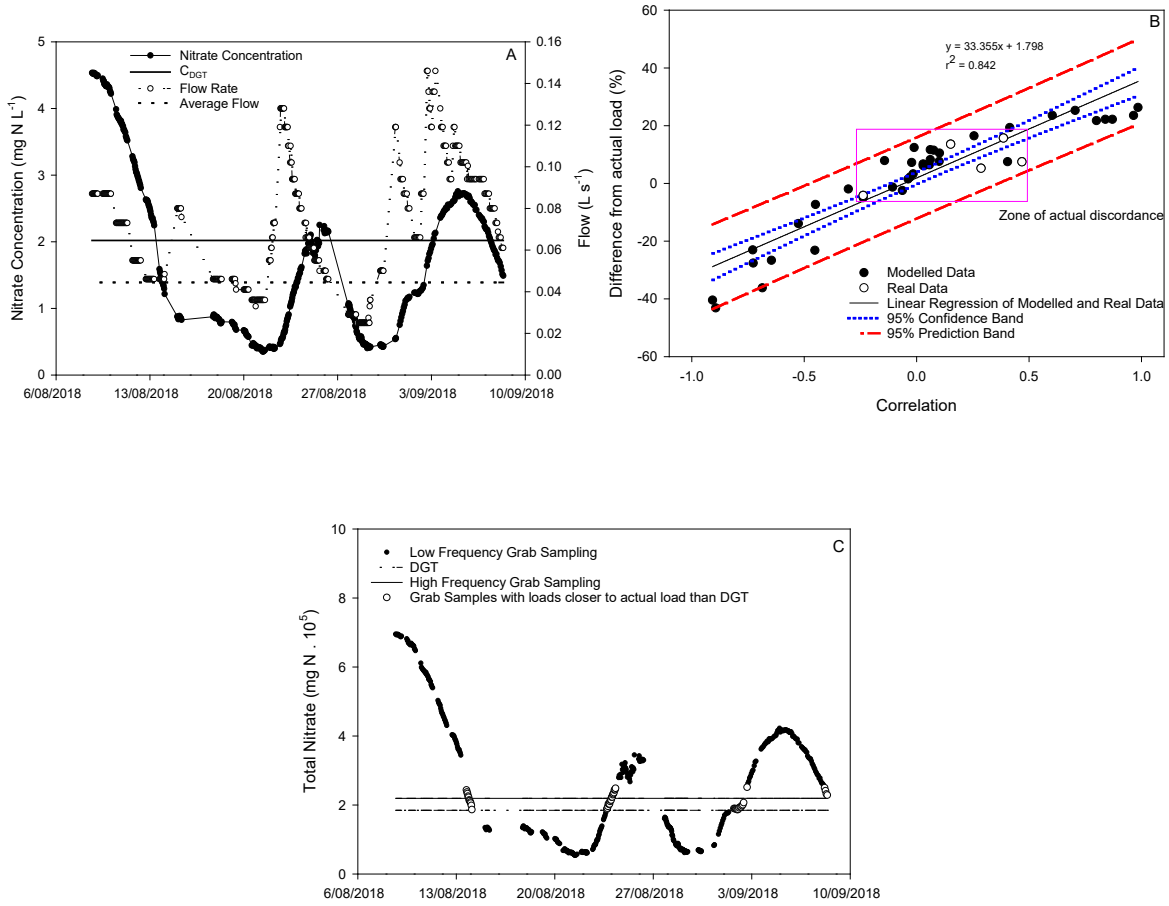


Figure 6.2: (A) Measured nitrate concentration and flow rate hydrograph for the modelled period, where DGT concentration ($C_{DGT}$) and DGT flow ($Flow_{DGT}$) = DGT/average concentration and flow respectively. (B) The difference in total nitrate-N determined by high frequency grab sampling (actual) and DGT, for real flow/concentration regimes and modelled load data (redistributed real nitrate concentration and flow data). (C) Total nitrate-N for loads determined by infrequent grab sampling when projected for the whole month, versus DGT and high frequency grab sampling. Grab samples that provided total nitrate-N values closer to the actual than DGT, or equal to DGT were circled.

Over the one month analysis period, both flow and concentration varied by an order of magnitude (Figure 6.2A), from 0.025 to 0.146 L $s^{-1}$ and 4.53 to 0.35 mg N $L^{-1}$, respectively. As the correlation between flow and concentration moved towards 1 and -1, the total nitrate-N (mg N) calculated by DGT moved away from the actual total nitrate-N, calculated from high frequency flow and concentration data, i.e. the percentage difference in calculated load from actual increased (Figure

6.2B). The error in the calculated DGT load due to the transient period, the time before steady state was reached, in the modelled data was < 0.1 %.

The number of individual spot samples (grab samples) which allowed calculation of loads equivalent to, or better than DGT, i.e. closer to the actual determined by high frequency grab sampling and flow measurements, was relatively small - 45 out of 447 samples (Figure 6.2C). While this represents ~10 % of the samples, they were not randomly distributed through time and fell within short windows of time. The total sampling time was 734.3 hours. The total sampling time which provided loads equivalent to DGT or closer to the actual load than DGT was 51.9 hours, equivalent to 7.1 % of the sampling time. These sampling times predominantly occurred between late afternoon and very early morning.

## 6.4. Discussion

Through modelling scenarios of varying degrees of correlation between concentration and other field variables (flow and temperature) we showed that temperature fluctuations produce little effect on the concentration determined by DGT. In contrast, as the correlation between flow and concentration approached 1 and -1, load calculations determined by DGT overestimated or underestimated the actual load by up to 30 %.

The determined conclusions drawn here likely translate to other DGT methods. This should be confirmed with other analytes, such as phosphate and transition metals (e.g. Cd, and As), however, this requires it the creation of a high frequency concentration and flow data set with coupled DGT deployments.

### *6.4.1 Flow, Concentration and Load*

DGT were designed to determine time-weighted average analyte concentration independent of solution flow (Davison, 2016). Solution flow/mixing, in part, determines the diffusive boundary layer (DBL), the area of solution at the DGT window with decreased concentration relative to the rest of solution. The full DGT equation incorporates the DBL, maintaining the flow independence of $C_{DGT}$.

Diffusive Gradients in Thin Films, therefore, do not capture the degree of correlation between flow and concentration. When using DGT to calculate load, furthermore, the correlation of analyte concentration to flow was important for determining the accuracy of calculated loadings (Figure 6.2B). The greater the correlation or anti-correlation, the greater the potential bias, as large as 30 %, in the DGT determined load (Figure 6.2B). Conversely, the bias will reduce as the flow and concentration become uncorrelated (Figure 6.2B). This may not be an issue in perturbed systems where chemostasis has been observed for anthropogenic nitrate, due to the release of legacy stored nitrate at a constant concentration, resulting from long-term, distributed land application from fertiliser, effluent, nitrogen fixation, and atmospheric deposition (Basu et al., 2010; Duncan et al., 2017; Musolff et al., 2015; Thompson et al., 2011).

The accuracy of load calculations are determined by the measurement accuracy and frequency of both flow and concentration measurements (Pinckney et al., 2001). The standard approach adopted by monitoring authorities is to monitor and log water flow continuously, and take fortnightly or monthly grab samples for concentration measurements (Tulagi, 2019). The infrequency of sampling is unlikely to provide accurate nutrient loads, particularly in fluctuating systems such as the system used in this study (Figure 6.2A). The accuracy of the mean concentration values over time and therefore loads, determined by grab sampling, when extrapolated to the whole month were low. For example, in the system measured and modelled in this study ~ 90 % of grab samples would not estimate $NO_3^-$-N loads within 16 % of the actual load (Figure 6.2C). This error of grab sampling estimates was greater than the error in the load estimate based on DGT (16 %) – which decreased to < 10 % if load is calculated as $C_{DGT}$ multiplied by the flow for each time interval (30 or 60 minutes) instead of the average flow.

The timing and frequency of manual grab sampling required to provide loadings closer to the actual load than DGT were also impractical, being between late afternoon/evening and early morning. The impracticality of the sampling timings may not be the case in other systems, but unless high frequency sampling or passive long-term sampling is undertaken, the extent to which load is under or

overestimated could not be known. The uncertainty of the extent of the divergence from the actual load reinforces the need for measurement accuracy of both flow and concentration.

If using infrequent grab sampling to calculate long-term loading, the risk of over or underestimating the actual load increases, furthermore it is not possible to know whether the load is over or underestimated and to what extent. Using DGT to measure concentration, and subsequently calculate load, over a month period was an improvement upon standard monitoring practices (continuous flow and infrequent grab sampling) (Figure 6.2C).

DGT have been shown to be capable of providing accurate time-weighted nitrate concentrations in highly variable denitrifying bioreactor systems, when compared to hourly grab sampling (Corbett et al., 2019). Diffusive Gradients in Thin Films therefore have the potential to resolve one of the major challenges facing monitoring authorities, and individuals – affordable and accurate determination of average nutrient concentration in water bodies. It is critical, however, that the correlation between flow and concentration is known before load estimates are made to avoid potential bias when correlation approaches 1 and -1.

### *6.4.2 Temperature and Concentration*

A fundamental variable component of DGT is the temperature dependence of diffusion. We used a theoretical scenario of temperature and concentration correlation to investigate the difference between $C_{DGT}$ and $C_{solution}$ (the actual concentration of the solution). Temperature and concentration were varied in order to achieve correlation coefficients from 1 to -1. Variation of temperature and concentration was large or small, and rapid or slow.

For the most part, temperature caused little difference between $C_{DGT}$ and $C_{solution}$, particularly when the concentration and temperature varied little and slowly irrespective of correlation (Table 6.1). $C_{DGT}$ diverged from $C_{solution}$ most in scenarios with large and rapid temperature changes with correlations approaching 1 and -1 (Table 6.1). Diffusive Gradients in Thin Films field deployments generally require the measurement of temperature, so that the diffusion coefficient can be appropriately corrected –

but often temperature is only measured at DGT deployment and removal (Davison, 2016; Huang et al., 2016a). In isothermal or near isothermal systems, even if there is significant concentration variation it seems that constant temperature monitoring is not necessary (Table 6.1). In systems where temperature varies significantly it should be monitored throughout, regardless of the correlation to concentration. For example, large rivers have enough water mass such that the temperature does not rapidly fluctuate. In contrast, small streams may experience large and rapid diurnal temperature fluctuations. If the temperature is not accurately determined, $C_{DGT}$ may differ significantly from $C_{solution}$.

DGT provides time-weighted average analyte concentration by integrating short-term analyte concentration changes over the deployment period (Davison, 2016). Diffusive Gradients in Thin Films therefore provides an improvement of the standard infrequent grab sampling methodology, by taking into account the changes in analyte concentration. Monitoring temperature throughout the DGT deployment, similarly, provides improved DGT derived concentrations.

If DGT are to be used by monitoring authorities and the general public it may be impractical and too expensive to monitor temperature continuously at each deployment site. Understanding the characteristics of the deployment site, such as flow and daylight exposure, will help determine whether temperature needs to be monitored throughout.

### *6.4.3 Conclusions and Implications*

The divergence of the DGT derived load from the actual load has implications for the use of DGT for contaminant monitoring. Diffusive Gradients in Thin Films are likely not capable of providing accurate loadings in systems where concentration and flow are more tightly linked. For example, high correlation of nitrate concentration to flow has been reported, due to snowmelt and after rainfall events (Lucey & Goolsby, 1993; Perrot et al., 2014; Wang et al., 2015). In large rivers and streams this may not be an issue, as the river volume could moderate the effects of any flash events.

Finally, the divergence of $C_{DGT}$ from the actual concentration, with high correlation/anti-correlation of concentration and temperature, is less likely to hinder the field deployments of DGT. Even in the most

extreme cases where concentration and temperature co-vary by more than 10 °C and 10 mg $L^{-1}$, the bias was only ~ 7 %.

DGT concentration and load calculations approached the actual solution concentration and load as temperature and concentration, and flow and concentration were more uncorrelated. Solution temperature and concentration covariance produced little effect on the concentration determined by DGT. In contrast, as flow and concentration became more correlated and anti-correlated the DGT derived load diverged by up to 30 % from the actual load, which is problematic if DGT are used to determined analyte loadings.

## Funding

DairyNZ and the New Zealand Ministry for Primary Industries funded this study.

## Acknowledgements

We would like to acknowledge the support of The University of Waikato and the financial support of DairyNZ and the Ministry for Primary Industries. The views expressed in this paper are those of the authors and do not necessarily reflect the views or policies of DairyNZ or the Ministry for Primary Industries.

## References


ADDY, K., GOLD, A. J., CHRISTIANSON, L. E., DAVID, M. B., SCHIPPER, L. A., & RATIGAN, N. A. (2016). Denitrifying Bioreactors for Nitrate Removal: A Meta-Analysis. *Journal of Environmental Quality, 45*(3), 873-881. doi:10.2134/jeq2015.07.0399

AUDET, J., MARTINSEN, L., HASLER, B., DE JONGE, H., KARYDI, E., OVESEN, N. B., & KRONVANG, B. (2014). Comparison of sampling methodologies for nutrient monitoring in streams: uncertainties, costs and implications for mitigation. *Hydrol. Earth Syst. Sci., 18*(11), 4721-4731. doi:10.5194/hess-18-4721-2014

BASU, N. B., DESTOUNI, G., JAWITZ, J. W., THOMPSON, S. E., LOUKINOVA, N. V., DARRACQ, A., ZANARDO, S., YAEGER, M., SIVAPALAN, M., RINALDO, A., & RAO, P. S. C. (2010). Nutrient loads exported from managed catchments reveal emergent biogeochemical stationarity. *37*(23). doi:https://doi.org/10.1029/2010GL045168

CAI, C., WILLIAMS, P. N., LI, H., DAVISON, W., WEI, T.-J., LUO, J., ZHU, Y.-G., & ZHANG, H. (2017). Development and Application of the Diffusive Gradients in Thin Films Technique for the Measurement of Nitrate in Soils. *Analytical Chemistry, 89*(2), 1178-1184. doi:10.1021/acs.analchem.6b03609

CORBETT, T. D. W., DOUGHERTY, H., MAXWELL, B., HARTLAND, A., HENDERSON, W., RYS, G. J., & SCHIPPER, L. A. (2019). Utility of 'Diffusive Gradients in Thin-Films' for the measurement of nitrate removal performance of denitrifying bioreactors. *Science of The Total Environment*, 135267. doi:https://doi.org/10.1016/j.scitotenv.2019.135267

DAVISON, W. (2016). *Diffusive Gradients in Thin-Films for Environmental Measurements*. Cambridge, UNITED KINGDOM: Cambridge University Press.

DAVISON, W., & ZHANG, H. (2012). Progress in understanding the use of diffusive gradients in thin films (DGT) – back to basics. *Environmental Chemistry, 9*(1), 1-13. doi:https://doi.org/10.1071/EN11084

DUNCAN, J. M., WELTY, C., KEMPER, J. T., GROFFMAN, P. M., & BAND, L. E. (2017). Dynamics of nitrate concentration-discharge patterns in an urban watershed. *53*(8), 7349-7365. doi:https://doi.org/10.1002/2017WR020500

HANOUSEK, O., MASON, S., SANTNER, J., CHOWDHURY, M. M. A., BERGER, T. W., & PROHASKA, T. (2016). Novel diffusive gradients in thin films technique to assess labile sulfate in soil. *Analytical and bioanalytical chemistry, 408*(24), 6759-6767. doi:10.1007/s00216-016-9801-8

HUANG, J., BENNETT, W., TEASDALE, P. R., GARDINER, S., & WELSH, D. (2016a). Development and evaluation of the diffusive gradients in thin films technique for measuring nitrate in freshwaters. *Analytica Chimica Acta, 923*, 74-81. doi:10.1016/j.aca.2016.04.006

HUANG, J., BENNETT, W. W., WELSH, D. T., LI, T., & TEASDALE, P. R. (2016b). "Diffusive Gradients in Thin Films" Techniques Provide Representative Time-Weighted Average Measurements of Inorganic Nutrients in Dynamic Freshwater Systems. *Environmental Science & Technology, 50*(24), 13446-13454. doi:10.1021/acs.est.6b02949

HUANG, J., BENNETT, W. W., WELSH, D. T., & TEASDALE, P. R. (2016c). Determining time-weighted average concentrations of nitrate and ammonium in freshwaters using DGT with ion

exchange membrane-based binding layers. *Environmental Science: Processes & Impacts, 18*(12), 1530-1539. doi:10.1039/c6em00260a

KING, R. C., MULLIGAN, P. K., & STANSFIELD, W. D. (2013). Diffusion. In *A Dictionary of Genetics* (8 ed., pp. 122). Oxford: Oxford University Press.

KRONVANG, B., & BRUHN, A. J. (1996). Choice of sampling strategy and estimation method for calculating nitrogen and phosphorus transport in small lowland streams. *10*(11), 1483-1501. doi:https://doi.org/10.1002/(SICI)1099-1085(199611)10:11<1483::AID-HYP386>3.0.CO;2-Y

LEHTO, N. J., DAVISON, W., ZHANG, H., & TYCH, W. (2006). An Evaluation of DGT Performance Using a Dynamic Numerical Model. *Environmental Science & Technology, 40*(20), 6368-6376. doi:10.1021/es061215x

LI, W., TEASDALE, P. R., ZHANG, S., JOHN, R., & ZHAO, H. (2003). Application of a Poly(4-styrenesulfonate) Liquid Binding Layer for Measurement of $Cu^{2+}$ and $Cd^{2+}$ with the Diffusive Gradients in Thin-Films Technique. *Analytical Chemistry, 75*(11), 2578-2583. doi:10.1021/ac020658q

LIU, S., QIN, N., SONG, J., ZHANG, Y., CAI, W., ZHANG, H., WANG, G., & ZHAO, H. (2016). A nanoparticulate liquid binding phase based DGT device for aquatic arsenic measurement. *Talanta, 160*, 225-232. doi:https://doi.org/10.1016/j.talanta.2016.06.064

LUCEY, K. J., & GOOLSBY, D. A. (1993). Effects of Climatic Variations over 11 Years on Nitrate-Nitrogen Concentrations in the Raccoon River, Iowa. *22*(1), 38-46. doi:https://doi.org/10.2134/jeq1993.00472425002200010005x

MAXWELL, B. M., BIRGAND, F., SMITH, B., & AVENI-DEFORGE, K. (2018). A small-volume multiplexed pumping system for automated, high-frequency water chemistry measurements in volume-limited applications. *Hydrology and Earth System Sciences, 22*(11), 5615-5628. doi:10.5194/hess-22-5615-2018

MOATAR, F., & MEYBECK, M. (2005). Compared performances of different algorithms for estimating annual nutrient loads discharged by the eutrophic River Loire. *19*(2), 429-444. doi:https://doi.org/10.1002/hyp.5541

MÜLLER, B., STIERLI, R., & GÄCHTER, R. (2008). A low-tech, low-cost passive sampler for the long-term monitoring of phosphate loads in rivers and streams. *Journal of Environmental Monitoring, 10*(7), 817-820. doi:10.1039/B806465B

MUSOLFF, A., SCHMIDT, C., SELLE, B., & FLECKENSTEIN, J. H. (2015). Catchment controls on solute export. *Advances in Water Resources, 86*, 133-146. doi:https://doi.org/10.1016/j.advwatres.2015.09.026

PANTHER, J. G., STEWART, R. R., TEASDALE, P. R., BENNETT, W. W., WELSH, D. T., & ZHAO, H. (2013). Titanium dioxide-based DGT for measuring dissolved As(V), V(V), Sb(V), Mo(VI) and W(VI) in water. *Talanta, 105*, 80-86. doi:https://doi.org/10.1016/j.talanta.2012.11.070

PANTHER, J. G., TEASDALE, P. R., BENNETT, W. W., WELSH, D. T., & ZHAO, H. (2010). Titanium Dioxide-Based DGT Technique for In Situ Measurement of Dissolved Reactive Phosphorus in Fresh and Marine Waters. *Environmental Science & Technology, 44*(24), 9419-9424. doi:10.1021/es1027713

PERROT, D., MOLOTCH, N. P., WILLIAMS, M. W., JEPSEN, S. M., & SICKMAN, J. O. (2014). Relationships between stream nitrate concentration and spatially distributed snowmelt in high-elevation catchments of the western U.S. *50*(11), 8694-8713. doi:https://doi.org/10.1002/2013WR015243

PINCKNEY, J. L., PAERL, H. W., TESTER, P., & RICHARDSON, T. L. (2001). The role of nutrient loading and eutrophication in estuarine ecology. *Environmental health perspectives, 109 Suppl 5*(Suppl 5), 699-706. doi:10.1289/ehp.01109s5699

REN, M., DING, S., SHI, D., ZHONG, Z., CAO, J., YANG, L., TSANG, D. C. W., WANG, D., ZHAO, D., & WANG, Y. (2020). A new DGT technique comprised in a hybrid sensor for the simultaneous measurement of ammonium, nitrate, phosphorus and dissolved oxygen. *Science of The Total Environment, 725*, 138447. doi:https://doi.org/10.1016/j.scitotenv.2020.138447

RIVETT, M. O., BUSS, S. R., MORGAN, P., SMITH, J. W. N., & BEMMENT, C. D. (2008). Nitrate attenuation in groundwater: A review of biogeochemical controlling processes. *Water Research, 42*(16), 4215-4232. doi:https://doi.org/10.1016/j.watres.2008.07.020

SCHIPPER, L., ROBERTSON, W., GOLD, A., JAYNES, D. B., & C. CAMERON, S. (2010). Denitrifying Bioreactors — An Approach for Reducing Nitrate Loads to Receiving Waters. *Ecological Engineering, 36*, 1532-1543. doi:10.1016/j.ecoleng.2010.04.008

SØNDERGAARD, J., BACH, L., & GUSTAVSON, K. (2014). Measuring bioavailable metals using diffusive gradients in thin films (DGT) and transplanted seaweed *(Fucus vesiculosus)*, blue mussels *(Mytilus edulis)* and sea snails *(Littorina saxatilis)* suspended from monitoring buoys near a former lead–zinc mine in West Greenland. *Marine Pollution Bulletin, 78*(1), 102-109. doi:https://doi.org/10.1016/j.marpolbul.2013.10.054

THOMPSON, S. E., BASU, N. B., LASCURAIN JR., J., AUBENEAU, A., & RAO, P. S. C. (2011). Relative dominance of hydrologic versus biogeochemical factors on solute export across impact gradients. *47*(10). doi:https://doi.org/10.1029/2010WR009605

TULAGI, A. (2019). *Waikato River water quality monitoring programme: Data report 2017*. (12603454). Hamilton, New Zealand: Waikato Regional Council

WANG, H., GAO, J.-E., LI, X.-H., ZHANG, S.-L., & WANG, H.-J. (2015). Nitrate Accumulation and Leaching in Surface and Ground Water Based on Simulated Rainfall Experiments. *PLOS ONE, 10*(8), e0136274. doi:10.1371/journal.pone.0136274

ZHANG, H., & DAVISON, W. (1995). Performance Characteristics of Diffusion Gradients in Thin Films for the in Situ Measurement of Trace Metals in Aqueous Solution. *Analytical Chemistry, 67*(19), 3391-3400. doi:10.1021/ac00115a005

ZHANG, H., DAVISON, W., GADI, R., & KOBAYASHI, T. (1998). In situ measurement of dissolved phosphorus in natural waters using DGT. *Analytica Chimica Acta, 370*(1), 29-38. doi:https://doi.org/10.1016/S0003-2670(98)00250-5

# Chapter 7 - Summary, Conclusions and Recommendations

## 7.1 Summary and Conclusions

The following section summarised the conclusions of each individual study, linking them back to the objectives of this research project (Figure 7.1). In the process demonstrating how each study alone, and the research project as a whole, improves our understanding of DGT and resolves some of the key monitoring issues facing regulators, researchers, and the community.

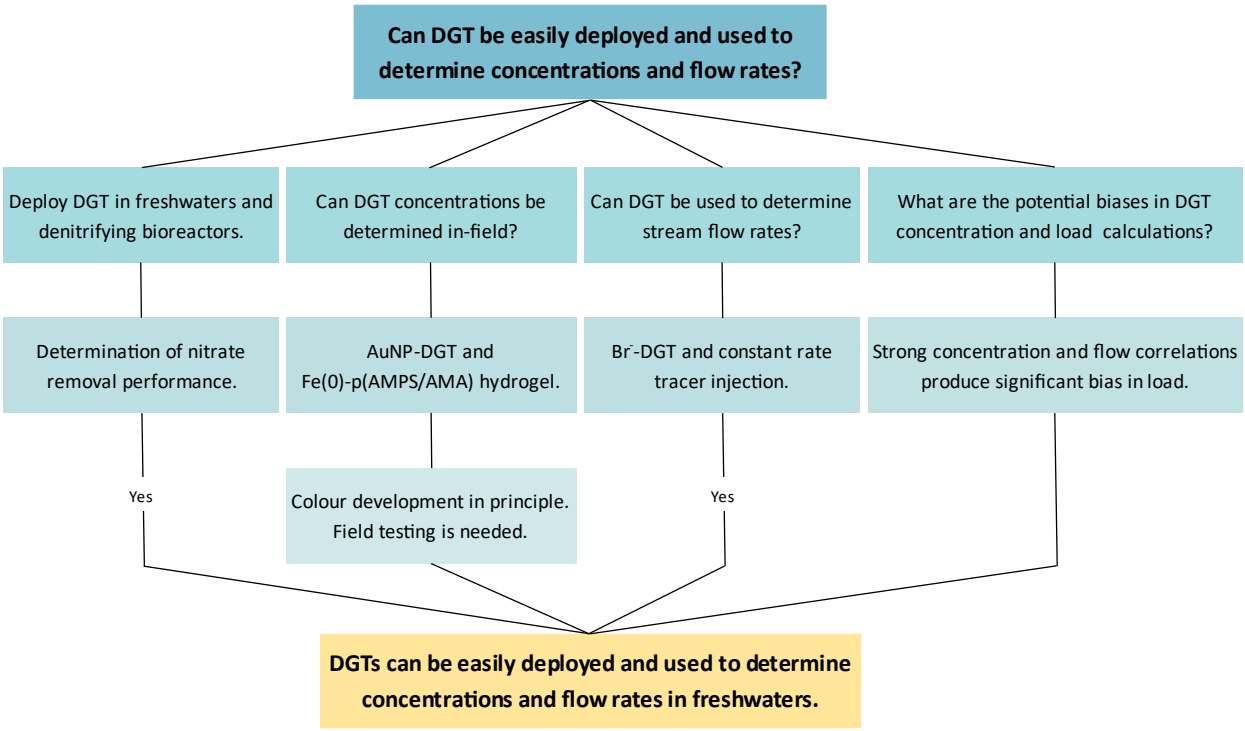


Figure 7.1: PhD Schematic.

### *7.1.1 Utility of DGT for Measuring Nitrate in Freshwaters and Mitigation Strategies*

The first study of this research project focused on establishing the utility of nitrate-DGT for environmental monitoring in New Zealand. The National Policy Statement for Freshwater Management states the need for widespread and constant monitoring of waterways (Government, 2020), however, current methods are either too expensive or cannot provide the necessary data. Using DGT to measure nitrate concentrations in the chemically and physically challenging denitrifying

bioreactor systems successfully demonstrates the utility and efficacy of nitrate-specific DGT (A520E-DGT) (Corbett et al., 2019). The main conclusions of this study were (Corbett et al., 2019):

- DGT were successful deployed along two different denitrifying bioreactor systems, one treating agricultural run-off and the other treating effluent and grey-water from a commercial facility, in the centre wells, and inlet and outlet structures;
- The $NO_3^-$ concentrations determined via DGT were in strong agreement with the high frequency grab sampling concentrations, while concentration determined via low frequency grab sampling missed the temporal fluctuations in $NO_3^-$;
- DGT more easily accounted for the temporal variation in $NO_3^-$ than both grab sampling methods, because as passive samplers DGT were essentially set-and-forget while grab sampling required considerable on-site time to take the required number of samples, which also increased the number of samples for analysis and therefore analysis costs;
- DGT enabled the determination of bioreactor performance via calculation of average nitrate removal rates, which were between 1.2 and 30.8 g N $m^{-3}$ $d^{-1}$ for the two bioreactors; and
- The ability of A520E-DGT to determine $NO_3^-$ concentrations in the chemically (high concentrations of potentially competing species) and physically (low flow and poor mixing) bioreactor systems demonstrated that nitrate-specific DGT provided a low cost, accurate, and easy-to-use method for monitoring $NO_3^-$.

As discussed in the following section, continued studies utilising DGT for nitrate monitoring will be needed to provide a sufficient body of evidence required for regulatory authorities to consider using DGT. As outlined by the National Policy Statement for Freshwater Management, there is significant need for tools to meet the enable the widespread monitoring required to improve the health of our waterways. Current methods are generally limited by the need for laboratory analysis, expensive on-site equipment, or low accuracy (Corbett et al., 2019). The democratisation of water quality

monitoring, furthermore, requires the development of DGT which do not require laboratory analysis such that the general public can perform quantitative analyses.

### *7.1.2 Colourimetric DGT*

The second study sought to incorporate colour reagents into the DGT binding layer specific such that in-field analysis of nitrate-DGT could be performed. The main conclusions of this study were (Chapter 4):

- An chitosan-stabilised Au nanoparticle suspension, with molecular weight > 150 kDa, was developed for the colourimetric determination of nitrite, providing quantitative concentrations (0 to 1000 mg $L^{-1}$) and masses (0 to 145 µg);
- A DGT probe was designed and 3D printed (3D images in appendix 1), which could be used with the standard DGT solution probe caps and dialysis membrane (molecular weight cut-off < 15 kDa), to house the AuNP-chitosan suspension for deployments in solution;
- An Fe(0) impregnated poly-2-acrylamido-2-methyl-1-propanesulfonic acid/acrylamide copolymer hydrogel Fe(0)-p(AMPS/AMA) was developed for the reduction of nitrate to nitrite, which produced a total nitrite mass of ~110 µg;
- The Fe(0)-p(AMPS/AMA) was produced by hydrating a synthesised poly-2-acrylamido-2-methyl-1-propanesulfonic acid/acrylamide copolymer hydrogel (p(AMPS/AMA)) (10 % AMPS, and 90 % AMA) with an Fe(III) solution to form an Fe(III)-p(AMPS/AMA) hydrogel, which was then treated with $NaBH_4$ to form an Fe(0)-p(AMPS/AMA) hydrogel;
- The AuNP liquid binding layer DGT provided distinct colour changes when deployed in synthetic nitrite solutions of varying concentrations (0 – 1000 mg $L^{-1}$), however, they operated more as Diffusive Equilibrium Theory (DET) due to the slow reaction rate of the AuNP-chitosan suspension; and,

- The slow reaction rate of the AuNP-chitosan also prohibited the combination with the Fe(0) reducing hydrogel, because, the uptake of nitrite was not sufficiently rapid stop further reduction of nitrite to $NH_3/NH_4^+$ $_{(aq)}$ and $NO_{(x)}$ $_{(g)}$ species.

Incorporation of colour reagents and reductants into DGT represents a novel approach to the extension of the DGT methodology. Determination of concentrations alone, however, do not necessarily provide the whole picture (as discussed in Chapters 2, 5 and 6). Loading can determine the ecosystem response (Pinckney et al., 2001).

### *7.1.3 $Br^-$-DGT Development and Flow Rate Measurement*

Study three focussed on the development of a bromide-selective DGT ($Br^-$-DGT) and the combination with the constant-rate trace dilution method, for the determination of bromide concentrations and stream flow rates. The main conclusions of study three were (Corbett et al., 2021a):

- A novel bromide-specific DGT ($Br^-$-DGT) which provided quantitative bromide concentrations at a range of pH and competing ion concentrations was developed, based on the Purolite Bromide Plus anion exchange resin;
- Key DGT parameters were quantified, such as uptake (95.7 ± 3.4 %) and elution (95.5 ± 4.7 %), adsorption maximum (0.684 ± 0.001 mg), and the diffusion coefficient of bromide through the APA diffusion layer (1.29 x $10^{-5}$ $cm^2$ $s^{-1}$ at 25 °C);
- The theory for using DGT to measure flow was established, and quantitative infield flow measurements were made at stream using the $Br^-$-DGT when combined with the constant-rate trace-dilution flow rate method;
- The $Br^-$-DGT flow rates were between -14.7 and 6.50 % of the flow independently monitored flow rate (weir), in comparison, grab sample flow rates diverged by 5.52 to 58.9 % from the weir flow rate; and,
- Measurement of background bromide concentrations enabled the calculation of the contributions of tributaries to the total flow at the measurement point, this could enable the

calculation of flows and loads up a catchment from a flow monitoring site when combined with other DGT (e.g. nitrate or phosphate DGT), which could aid in the targeting of mitigation strategies.

Development of a bromide-selective DGT, and the combination with the constant-rate trace dilution method, are novel extensions of the DGT methodology. Diffusive Gradients in Thin Films, for the first time, can be used to determine analyte concentration, stream flow, and therefore analyte loading. There are numerous implications of using DGT to determine flow rates and concentrations, chiefly, DGT can potentially be used to partition concentration and load contributions within a catchment. Providing an easy-to-use, affordable and accurate tool for the targeting of mitigation strategies. Utilising DGT to determine loads, however, requires an understanding of the potential sources of bias in DGT concentration and load calculations.

### *7.1.4 Potential Sources of Bias in DGT Concentration and Load Calculations*

Study four utilised a modelling approach to understand the effects of the covariance of temperature and concentration on the DGT determined concentration, and covariance of flow and concentration on the DGT determined nitrate load, compared to the actual stream concentration and load. The DGT method is theoretically flow independent if the diffusive boundary layer is accounted for, and if the temperature is accurately measured so that the analyte diffusion coefficients can be accurately calculated (Davison, 2016). The main conclusions were (Corbett et al., 2021b):

- The effects of varied correlation of concentration and temperature, as they changed dynamically, on the DGT determined concentration were modelled, yielding biases generally less than 5 % even as the correlation approached 1 and -1;
- The effects of dynamic changes in flow and concentration, with correlations between -1 and 1, on the DGT determined concentration were modelled and compared to the actual load, yielding biases approaching 30 % as the correlation approached -1 and 1;

- Flow and concentration correlations between -0.2 and 0.1 resulted in biases in the modelled loads less than 5 %; and,
- The bias in DGT determined load is potentially problematic if DGT are to be used to determine analyte loadings. The nature of the system needs to be understood before embarking on using DGT to determine loads, DGT are likely not capable of providing accurate loads where concentration and flow are large and more tightly linked (e.g. due to snowmelt or rainfall).

Modelling the effects of dynamic changes in concentration, flow and temperature, with varying degrees of correlation, on DGT determined loads and concentrations had previously not been explored. Generally, irrespective of the relationship between concentration and temperature, DGT are capable of providing accurate nitrate concentrations. Diffusive Gradients in Thin Films are also capable of providing accurate nitrate loads, if concentration and flow are not highly correlated. An acceptable correlation, whereby the potential bias is < 10 %, is likely between -0.35 and 0.25. Concentration and flow correlation is unlikely problematic in most cases, however, understanding of the system prior to using DGT for load calculations is best practice.

### *7.1.5 Thesis Aims*

The aims of this thesis were to illustrate the utility of nitrate-DGT as a monitoring tool, and the expansion of the DGT methodology to increase the number of potential uses and users. Each research chapter of this thesis addresses a different component of these aims. Importantly when considered together these chapters provide solutions to some of the challenges for the widespread adoption of DGT. Deploying DGT in the chemically and physically challenging denitrifying bioreactors comprehensively demonstrated that the A520E nitrate-specific DGT are a capable and useful tool for monitoring nitrate concentrations, and for determining the performance of nutrient mitigation strategies. Development of the colourimetric liquid binding layers and reducing hydrogels/diffusive layers, lay the foundations for a quantitative nitrate-specific DGT that can be analysed easily infield. It also creates a framework for the development of colourimetric DGT specific for other analytes.

Development of the bromide selective DGT, and combination with the constant tracer method, enables DGT to be utilised for determining flow rates and therefore analyte loading. Loading is a key determinant of potential ecological damage. Finally, understanding the limitations and the relationships of key components for using DGT for environmental monitoring (flow, temperature, concentration, and load) draws attention to the considerations required for using DGT for environmental monitoring.

## 7.2 Recommendations and Future Research

DGT have shown they can overcome many of the methodological limitations of other nutrient measurement techniques, and provide affordable and accurate data more easily, however, their use remains limited to researchers. To encourage the uptake of DGT by regulators and the general public, testing and validation within large-scale monitoring regimes of a range of aquatic systems could be undertaken. This monitoring approach should include stakeholders, such as Iwi, farmers, and regional councils. These studies could also include user driven monitoring programmes to ascertain the limitations and challenges that they face, to establish clear user protocols. In the New Zealand context, work is also required to create space for the use of DGT in the Resource Management Act.

### *7.2.1 Improving Colour Development in DGT*

Incorporation of colourimetric reagents into the DGT methodology was achieved, through the development of an AuNP-chitosan liquid binding layer. As discussed above, the slow rate of reaction, however, meant the AuNP-chitosan DGT operated more as a DET. Increasing the reaction rate of the colour reagents is the primary obstacle to the successful development of colourimetric DGT for infield determination of nitrate, and other analytes. Nitrate to nitrite reduction was achieved within the Fe(0) reducing gel, there are however, further opportunities to improve the efficacy of the developed nitrate colourimetric DGT. Further research opportunities include:

- There are numerous requirements of any colourimetric method for incorporation into a DGT binding layer, these include: selectivity for the target analyte(s); quantitative over a range of

solution pH, conductivity, and temperatures; stability; visually determinable colour change over a large range of analyte masses; and, a fast reaction rate, so that the steady-state is maintained through the diffusion layer. Catalysts could be explored to improve the reaction rate of the AuNP-chitosan system developed here. Determining the reaction kinetics/reaction order would help in the further development of the AuNP-chitosan method, and in the development of alternative methods.

- Development of a 'one-pot' liquid binding layer, which includes the colour reagent and the reducing agent, could overcome many of the issues arising from the variable concentration gradients of nitrate and nitrite within the diffusive layers. Reduction of nitrate to nitrite creates a concentration gradient through the first layers of the diffusion layer, which may trend to zero as nitrate is rapidly reduced within the Fe(0)-hydrogel reducing layer. Traditionally the binding layer drives the concentration gradient of the determined analyte, however, in effect the reducing hydrogel acts as the nitrate binding layer. The nitrite concentration increases in the reducing layer, and decreases to zero as it diffuses to and is bound by the binding layer, creating another concentration gradient. This may make it difficult to determine nitrate concentrations, because the nitrite masses in the binding layer are the product of two concentration gradients.
- Development of a 'one-pot' liquid binding layer has important implications for the reductant used. Transition metals such as Cd, Co, V, Fe, Cu and Zn, are traditionally used to reduce nitrate (Hydes & Hill, 1985; Morita & Nakamura, 2008; Nydahl, 1976), alternative methods have also involved nitrate reductase (Campbell, 1999). There are numerous important considerations to take into account when selecting the reductant, including the particle size, stability, toxicity, specificity, colour, and matrix effects. Use of the transition metals will also require binding to, or immobilisation on a polymer to exceed the molecular weight cut-off of the dialysis membrane. Zn or nitrate reductase are likely the better options due to the colour and toxicity of other potential reductants.

- Luminescent and fluorescent bio-marking (Bakker et al., 2019; Stepanenko et al., 2008) of nitrate reducers or nitrate reductase, and incorporation into the binding layer could remove the need for colour reagents. This represents a significant change in approach, moving away from the current inorganic chemistry driven development, to biochemical based methods.
- Development of nitrate specific nanoparticles (Daniel et al., 2009), alternatively, could remove the necessity for the reducing diffusive layer altogether. As discussed above, however, the rate of reaction any alternative colour reagents must be sufficiently fast for the developed system to operate as a DGT not a DET.
- The successful development of a colourimetric DGT requires deployment of the DGT in a range of natural systems (stream, lakes, mitigation strategies). As described above, this could be inclusive of stakeholders, and take into account the limitations and challenges of the standard nitrate-specific DGT identified by stakeholders.

Colourimetric determination of nutrients and contaminants holds considerable promise for enabling the general public to monitor their local systems independently, affordably and accurately. As such, the development of systems for phosphate, ammonia, organic contaminants, and specific trace metals could be addressed. Colourimetric DGT for the determination of phosphate, for example, does not require the reduction of phosphate and could proceed via an altered molybdenum blue method.

### *7.2.2 Use of DGT to Determine Flow Rates*

Determination of the efficacy of the $Br^-$-DGT and constant-rate tracer injection flow method in other freshwater bodies, and mitigation strategies could be assessed. For example, increased dilution of the bromide tracer in larger rivers may result in immeasurable increases in the bromide concentration. Alternative tracers and binding layers could also be assessed. The development of highly sensitive organics-DGT present an interesting alternative, when combined with newly developed DNA tracers.

### *7.2.3 Potential Biases*

Further field and laboratory studies are also required, to determine the extent to which, and the systems in which it is significant, concentration, temperature and flow correlation affects DGT calculated concentration and loads. This would require the deployment of DGT alongside high frequency samplers, or considerable on-site time to achieve the necessary resolution for comparisons via manual grab sampling. Achieving analyte concentrations of varying correlations to flow may be difficult, and could include the incorporation of the tracer dilution method to create highly correlated flow and concentration systems.

Overall, there are numerous opportunities for the future development of DGT, for the determination of nutrient concentrations, stream flow, loadings, mitigation strategy performance, and the widespread use by the public and regulatory authorities.

# References


BAKKER, K. M., ROCKE, T. E., OSORIO, J. E., ABBOTT, R. C., TELLO, C., CARRERA, J. E., VALDERRAMA, W., SHIVA, C., FALCON, N., & STREICKER, D. G. (2019). Fluorescent biomarkers demonstrate prospects for spreadable vaccines to control disease transmission in wild bats. *Nature Ecology & Evolution, 3*(12), 1697-1704. doi:10.1038/s41559-019-1032-x

CAMPBELL, W. H. (1999). Nitrate Reductase Structure, Function and Regulation: Bridging the Gap between Biochemistry and Physiology. *Annual Review of Plant Physiology and Plant Molecular Biology, 50*(1), 277-303. doi:10.1146/annurev.arplant.50.1.277

CORBETT, T. D. W., DOUGHERTY, H., MAXWELL, B., HARTLAND, A., HENDERSON, W., RYS, G. J., & SCHIPPER, L. A. (2019). Utility of 'Diffusive Gradients in Thin-Films' for the measurement of nitrate removal performance of denitrifying bioreactors. *Science of The Total Environment*, 135267. doi:https://doi.org/10.1016/j.scitotenv.2019.135267

CORBETT, T. D. W., HARTLAND, A., HENDERSON, W., RYS, G. J., & SCHIPPER, L. A. (2021a). Development of Bromide-Selective Diffusive Gradients in Thin-Films for the Measurement of Average Flow Rate of Streams. *Science of The Total Environment*.

CORBETT, T. D. W., HARTLAND, A., HENDERSON, W., RYS, G. J., & SCHIPPER, L. A. (2021b). The Temperature and Flow Dependence of Nitrate Concentration and Load Estimates based on Diffusive Gradients in Thin-Films. *Journal of Environmental Quality (Under Review)*.

DANIEL, W. L., HAN, M. S., LEE, J.-S., & MIRKIN, C. A. (2009). Colorimetric Nitrite and Nitrate Detection with Gold Nanoparticle Probes and Kinetic End Points. *J Am Chem Soc, 131*(18), 6362-6363. doi:10.1021/ja901609k

DAVISON, W. (2016). *Diffusive Gradients in Thin-Films for Environmental Measurements*. Cambridge, UNITED KINGDOM: Cambridge University Press.

GOVERNMENT, N. Z. (2020). *National Policy Statement for Freshwater Management 2020*. Wellington: Minister for the Environment.

HYDES, D. J., & HILL, N. C. (1985). Determination of nitrate in seawater: Nitrate to nitrite reduction with copper-cadmium alloy. *Estuarine, Coastal and Shelf Science, 21*(1), 127-130. doi:https://doi.org/10.1016/0272-7714(85)90011-3

MORITA, E., & NAKAMURA, E. (2008). Reduction of Nitrate to Nitrite by Using Zinc Powder for Determination of Total Nitrogen in Sea Water. *Bunseki Kagaku, 57*(10), 777-781. doi:10.2116/bunsekikagaku.57.777

NYDAHL, F. (1976). On the optimum conditions for the reduction of nitrate to nitrite by cadmium. *Talanta, 23*(5), 349-357. doi:https://doi.org/10.1016/0039-9140(76)80047-1

PINCKNEY, J. L., PAERL, H. W., TESTER, P., & RICHARDSON, T. L. (2001). The role of nutrient loading and eutrophication in estuarine ecology. *Environmental health perspectives, 109 Suppl 5*(Suppl 5), 699-706. doi:10.1289/ehp.01109s5699

STEPANENKO, O. V., VERKHUSHA, V. V., KUZNETSOVA, I. M., UVERSKY, V. N., & TUROVEROV, K. K. (2008). Fluorescent proteins as biomarkers and biosensors: throwing color lights on molecular and cellular processes. *Curr Protein Pept Sci, 9*(4), 338-369. doi:10.2174/138920308785132668

# Appendices

## Appendix A – Liquid DGT 3D Model

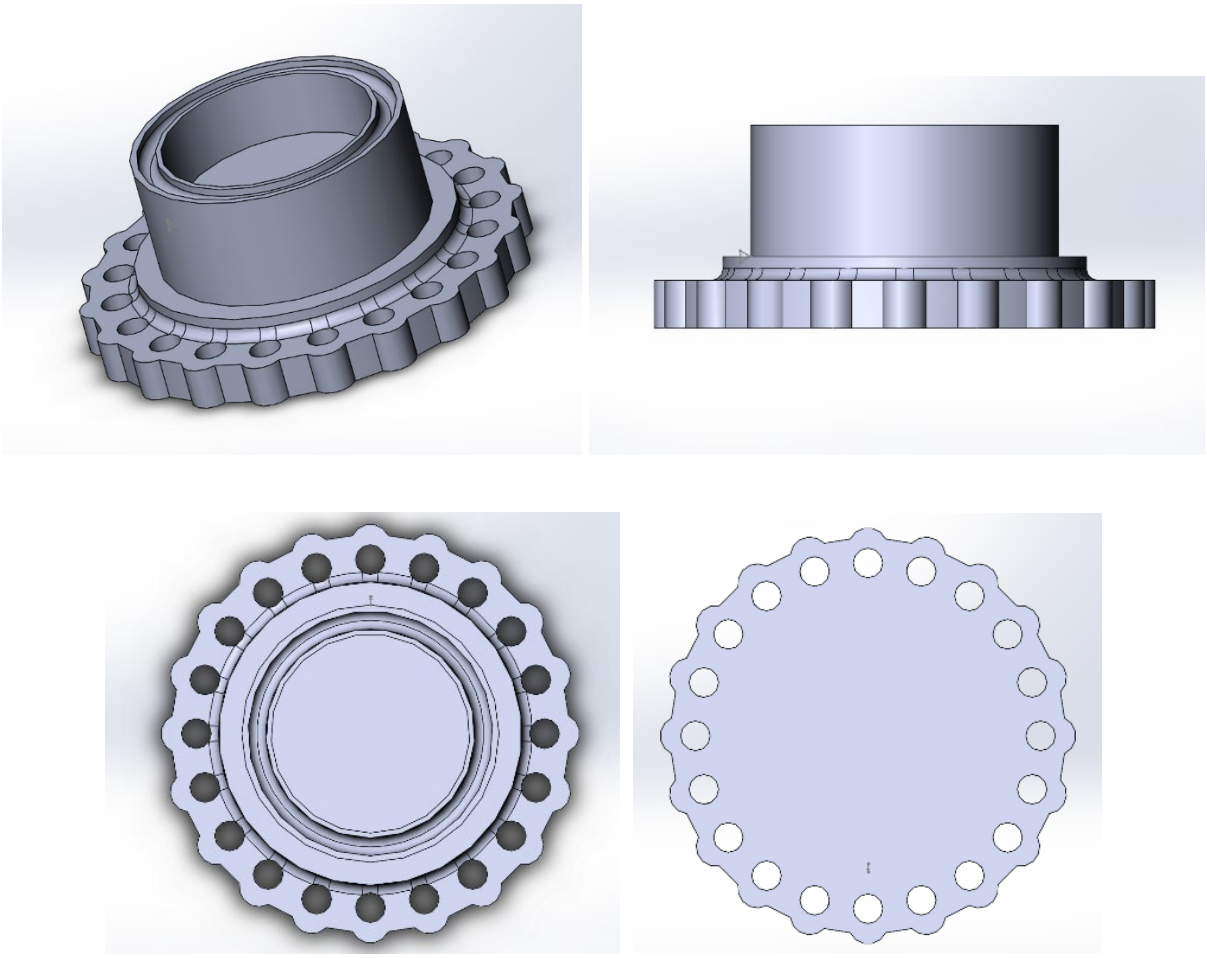

Figure A0.1: 3-dimensional model of the liquid binding phase Diffusive Gradients in Thin-Films solution probe base.

The liquid binding phase DGT were designed to hold 2 mL of liquid, and for the standard push fit DGT cap. A rubber O-ring fits in the outer groove, which seals the liquid binding layer when the dialysis membrane is pushed against it by the cap and material diffusion layer. A twist on cap was designed to make the unit more easily reusable, however, the torsion force applied to seal the liquid layer ripped the dialysis membrane. Twist DGT may be more appropriate for standard hydrogel based DGT.

# Appendix B – Co-Authorship Forms

THE UNIVERSITY OF WAIKATO

## Co-Authorship Form

Postgraduate Studies Office
Student and Academic Services Division
Wahanga Rēhinga Mataurange Akonga
The University of Waikato
Private Bag 3105
Hamilton 3240, New Zealand
Phone +64 7 838 4439
Website http://www.waikato.ac.nz/sasd/postgraduate/

This form is to accompany the submission of any PhD that contains research reported in published or unpublished co-authored work. **Please include one copy of this form for each co-authored work.** Completed forms should be included in your appendices for all the copies of your thesis submitted for examination and library deposit (including digital deposit).

Please indicate the chapter/section/pages of this thesis that are extracted from a co-authored work and give the title and publication details or details of submission of the co-authored work.

Utility of 'Diffusive Gradients in Thin-Films' for the measurement of nitrate removal performance of denitrifying bioreactors

| | |
|---|---|
| Nature of contribution by PhD candidate | Collaboration on project conception, data collection, analysis, interpretation, and manuscript writing |
| Extent of contribution by PhD candidate (%) | 90 |

**CO-AUTHORS**

| Name | Nature of Contribution |
|---|---|
| Louis Schipper | Collaboration on project conception, analysis and interpretation, and manuscript editing |
| Adam Hartland | Collaboration on project conception, analysis and interpretation, and manuscript editing |
| Bill Henderson | Collaboration on analysis and interpretation, and manuscript editing |
| Gerald Rys | Collaboration on analysis and interpretation, and manuscript editing |
| Hannah Dougherty | Data collection, and manuscript editing |
| Bryan Maxwell | Data collection, and manuscript editing |

### Certification by Co-Authors

The undersigned hereby certify that:

- the above statement correctly reflects the nature and extent of the PhD candidate's contribution to this work, and the nature of the contribution of each of the co-authors; and

| Name | Signature | Date |
|---|---|---|
| Louis Schipper | L A Schipper | 29/3/21 |
| Adam Hartland | A Hartland | 30/4/21 |
| Bill Henderson | W. Henderson | 30/4/21 |
| Gerald Rys | G Rys | 30/4/2021 |
| Hannah Dougherty | Hannah Dougherty | 30/04/2021 |
| Bryan Maxwell | Bryan Maxwell | 30/04/2021 |

THE UNIVERSITY OF WAIKATO

# Co-Authorship Form

Postgraduate Studies Office
Student and Academic Services Division
Wahanga Ratonga Mataurange Akonga
The University of Waikato
Private Bag 3105
Hamilton 3240, New Zealand
Phone +64 7 838 4439
Website: http://www.waikato.ac.nz/sasd/postgraduate/

This form is to accompany the submission of any PhD that contains research reported in published or unpublished co-authored work. **Please include one copy of this form for each co-authored work.** Completed forms should be included in your appendices for all the copies of your thesis submitted for examination and library deposit (including digital deposit).

Please indicate the chapter/section/pages of this thesis that are extracted from a co-authored work and give the title and publication details or details of submission of the co-authored work.

The Temperature and Flow Dependence of Nutrient Concentration and Load Estimates based on Diffusive Gradients in Thin-Films.

| | |
|---|---|
| Nature of contribution by PhD candidate | Collaboration on project conception, data collection, analysis, interpretation, and manuscript writing |
| Extent of contribution by PhD candidate (%) | 90 |

## CO-AUTHORS

| Name | Nature of Contribution |
|---|---|
| Louis Schipper | Collaboration on project conception, analysis and interpretation, and manuscript editing |
| Adam Hartland | Collaboration on project conception, analysis and interpretation, and manuscript editing |
| Bill Henderson | Collaboration on analysis and interpretation, and manuscript editing |
| Gerald Rys | Collaboration on analysis and interpretation, and manuscript editing |
| | |
| | |

## Certification by Co-Authors

The undersigned hereby certify that:

- the above statement correctly reflects the nature and extent of the PhD candidate's contribution to this work, and the nature of the contribution of each of the co-authors; and

| Name | Signature | Date |
|---|---|---|
| Louis Schipper | L A Schipper | 29/3/21 |
| Adam Hartland | A Hartland | 30/4/21 |
| Bill Henderson | W Henderson | 30/4/21 |
| Gerald Rys | G Rys | 30/4/2021 |
| | | |
| | | |

THE UNIVERSITY OF WAIKATO

# Co-Authorship Form

Postgraduate Studies Office
Student and Academic Services Division
*Waharoa Ratonga Matauranga Akonga*
The University of Waikato
Private Bag 3105
Hamilton 3240, New Zealand
Phone +64 7 838 4439
Website http://www.waikato.ac.nz/sasd/postgraduate/

This form is to accompany the submission of any PhD that contains research reported in published or unpublished co-authored work. **Please include one copy of this form for each co-authored work.** Completed forms should be included in your appendices for all the copies of your thesis submitted for examination and library deposit (including digital deposit).

Please indicate the chapter/section/pages of this thesis that are extracted from a co-authored work and give the title and publication details or details of submission of the co-authored work.

Development of Bromide-Selective Diffusive Gradients in Thin-Films for the Measurement of Average Flow Rate of Streams.

| | |
|---|---|
| Nature of contribution by PhD candidate | Collaboration on project conception, data collection, analysis, interpretation, and manuscript writing |
| Extent of contribution by PhD candidate (%) | 90 |

## CO-AUTHORS

| Name | Nature of Contribution |
|---|---|
| Louis Schipper | Collaboration on project conception, analysis and interpretation, and manuscript editing |
| Adam Hartland | Collaboration on project conception, analysis and interpretation, and manuscript editing |
| Bill Henderson | Collaboration on analysis and interpretation, and manuscript editing |
| Gerald Rys | Collaboration on analysis and interpretation, and manuscript editing |
| | |
| | |

### Certification by Co-Authors

The undersigned hereby certify that:

- the above statement correctly reflects the nature and extent of the PhD candidate's contribution to this work, and the nature of the contribution of each of the co-authors; and

| Name | Signature | Date |
|---|---|---|
| Louis Schipper | L A Schipper. | 29/3/21 |
| Adam Hartland | A Hartland | 30/4/21 |
| Bill Henderson | W. Hen | 30/4/21 |
| Gerald Rys | G Rys | 30/4/2021 |
| | | |
| | | |

THE UNIVERSITY OF WAIKATO

Postgraduate Studies Office
Student and Academic Services Division
Waharoa Rangahau Maturanga Akonga
The University of Waikato
Private Bag 3105
Hamilton 3240, New Zealand
Phone +64 7 838 4439
Website http://www.waikato.ac.nz/sasd/postgraduate/

# Co-Authorship Form

This form is to accompany the submission of any PhD that contains research reported in published or unpublished co-authored work. **Please include one copy of this form for each co-authored work.** Completed forms should be included in your appendices for all the copies of your thesis submitted for examination and library deposit (including digital deposit).

Please indicate the chapter/section/pages of this thesis that are extracted from a co-authored work and give the title and publication details or details of submission of the co-authored work.

Incorporation of Zero-Valent Metal Reductants and Gold Nanoparticles into Hydrogel Networks for Colourimetric DGT Nitrate Determination

| | |
|---|---|
| Nature of contribution by PhD candidate | Collaboration on project conception, data collection, analysis, interpretation, and manuscript writing |
| Extent of contribution by PhD candidate (%) | 90 |

## CO-AUTHORS

| Name | Nature of Contribution |
|---|---|
| Louis Schipper | Collaboration on project conception, analysis and interpretation, and manuscript editing |
| Adam Hartland | Collaboration on project conception, analysis and interpretation, and manuscript editing |
| Bill Henderson | Collaboration on project conception, analysis and interpretation, and manuscript editing |
| Gerald Rys | Collaboration on analysis and interpretation, and manuscript editing |
| | |
| | |

## Certification by Co-Authors

The undersigned hereby certify that:

- the above statement correctly reflects the nature and extent of the PhD candidate's contribution to this work, and the nature of the contribution of each of the co-authors; and

| Name | Signature | Date |
|---|---|---|
| Louis Schipper | L A Schipper | 29/3/21 |
| Adam Hartland | | 30/4/21 |
| Bill Henderson | | 30/4/21 |
| Gerald Rys | G Rys | 30/4/2021 |
| | | |
| | | |

# Appendix C – Copyright Authorisation

Authorisation was sought for the republication of figures and artwork.

| Thesis Page Number | Details | Date Permission Requested | Permission granted for digital thesis and date |
|---|---|---|---|
| 15 | Figure 2.2B Bioreactor treating agricultural runoff (Corbett et al., 2019). Diffusive Gradients in Thin Films were deployed at both bioreactors in study 1. The inlet and outlet chambers, and wells where DGT were deployed and grab samples taken are numbered (Corbett et al., 2019).<br><br>Permission is not required for publication in my thesis, because I am the author. | 16/11/2021 | Yes<br>16/11/2021 |
| 18 | Figure 2.4A Exploded Diffusive Gradient in Thin-Films (DGT) piston assembly schematic (Corbett et al., 2019).<br><br>Permission is not required for publication in my thesis, because I am the author. | 16/11/2021 | Yes<br>16/11/2021 |
| 15 | Figure 2.2A: Denitrifying bioreactor schematic.<br><br>RAMBAGS, F., TANNER, C. C., STOTT, R., & SCHIPPER, L. A. (2016). Faecal Bacteria, Bacteriophage, and Nutrient Reductions in a Full-Scale Denitrifying Woodchip Bioreactor. Journal of Environmental Quality, 45(3), 847-854. doi:10.2134/jeq2015.06.0326<br><br>Authorisation provided by journal, and author. | 16/11/2021 | Yes<br>16/11/2021 |
| 16 | Figure 2.3: Potential sites and approaches for enhancing denitrification to reduce nitrogen movement along the nitrogen cascade.<br><br>SCHIPPER, L. A., GOLD, A. J., & DAVIDSON, E. A. (2010). Managing denitrification in human-dominated landscapes. Ecological Engineering, 36(11), 1503-1506. doi:https://doi.org/10.1016/j.ecoleng.2010.07.027<br><br>Authorisation provided by journal, and author. | 16/11/2021 | Yes<br>16/11/2021 |